The Karoo sand sea in changing climates: Early Jurassic interdune lakes and erg dynamics in southern Africa

Howard Vincent Head

A thesis submitted to the Faculty of Science, University of Cape Town, in fulfilment of the requirements for the degree of Doctor of Philosophy

October 2022

Supervisor: Associate Professor Emese Bordy

Declaration

I declare that this thesis is my own original work, and where aided, it has been acknowledged as such. It is being submitted for the Degree of Doctor of Philosophy to the University of Cape Town, Faculty of Science and has not yet been previously submitted to any other university or academic institution.

_____

7th day of October

Abstract

Aeolian systems have a particular sensitivity to climate change, and where these are preserved in the geological record, they can provide insights into palaeo-climatic drivers of erg dynamics through time. This thesis investigates the sedimentary geology of the southern extension of a vast ancient desert system that was active over Pangaea and formed part of one of the largest known sand seas in Earth's history. The Lower Jurassic Clarens Formation in the main Karoo Basin of southern Africa has been interpreted as an aeolian succession that is dominated by massive sandstones in the lower and upper parts of the unit, whereas large-scale cross-bedded sandstones are mostly associated with its middle part. Lenticular mudstones and sandstones with ripple marks, ripple cross-lamination, horizontal lamination and desiccation cracks have also been reported from the lower and upper parts of the succession. Based on the stratigraphic distribution of the sedimentary facies, the formation is informally subdivided into 3 zones that seem to reflect a wet-dry-wet climate megacycle. To date, the age of the formation is based on a very small detrital zircon dataset, the bio- and chronostratigraphy of the conformably underlying Elliot Formation and the radioisotopic dates of Drakensberg Group basalts that are conformably overlying the Clarens Formation. Thus far, few investigations have targeted the evolution of this Early Jurassic fluvio-lacustrine-aeolian system, and the origin of massive sandstone facies that dominates parts of the formation. Therefore, this study re-evaluates the origin and basinal distribution of the sedimentary facies, and the spatiotemporal controls on erg development during the deposition of the Clarens Formation. Moreover, this study provides the first robust chronostratigraphic framework and provenance history for this iconic Early Jurassic aeolian system of southwestern Gondwana.

The wet-dry-wet climate megacycle is not only corroborated herein, but using maximum depositional ages from detrital zircons, these climatic changes are now better dated. The results show a Late Sinemurian wet phase, an larly Pliensbachian dry phase and a late Pliensbachian wet phase during Clarens times. Newly documented field evidence shows that ponds and large lakes co-existed with aeolian dunes, with sand sheets, loess plains and fluvial systems having been established downwind. The size of the late Sinemurian ponds and lakes were controlled by their proximity to the erg margin, such that small ponds developed close to the erg centre, and large lakes were established along the erg margin. By the Early Pliensbachian, an intensification of the arid conditions led to the increased availability of sediments for aeolian entrainment, resulting in expansion of the erg eastward. Wet conditions ensued once again in the Late Pliensbachian, and lead to the contraction of the erg and expansion of loess plains with seasonally wet interdunes. Sediment, mostly supplied from the west, was overwhelmingly recycled from pre-existing, Karoo-age deposits and sedimentary rocks associated with the Pan-African orogeny, although evidence for some non-sedimentary and young, syn-Clarens sources are also present. The youngest zircon population show subtle temporal and spatial trends that can be used as proxies for the erg development. The late Sinemurian signal is identified in the lower zone in the south of the basin and is incorporated in subsequent zones in the central and northern parts of the basin, suggesting that, although the main wind direction was from the west northwest, the basin was filled from south to north. This newly established temporal framework of the wet-dry-wet climate cycle in the Clarens Formation corresponds well with the palaeoclimatic trends interpreted for the Tethyan margin of Gondwana, signifying that this may have been a global trend in the Early Jurassic.

Acknowledgements

"If I have seen further, it is by standing on the shoulders of giants" Sir Isaac Newton.

This endeavour would not have been possible without the support, encouragement, and sheer determination of my supervisor, family, and friends throughout my PhD journey. To this end, I thank my supervisor, Emese Bordy, for the continued support and encouragement along the way, especially when things seemed the most difficult. Thank you for believing that I could achieve this goal, even when I doubted myself.

Secondly, I thank my family and friends for keeping me sane during what I can only describe as an emotional voyage of self-discovery; for never asking the oftentimes unanswerable questions about "when will you finish", "why are you in the field again" or about the so-called "dinosaur sand" as opposed to "diamond sand". My eternal gratitude to my parents and brother, Pepler, for never wavering in their belief in me and my dreams, and Megan, who is my inspiration in all things geological.

I also thank my sedimentary research group colleagues, who have become my academic family. Mieng, Akhil, Rob, Claire, Riyaad, Chad, Lara and Yambi, I can never express how glad I am that you were all part of this journey. Thank you for driving 50 000 km with me, for climbing many mountains with me, for many lively conversations and for all the fun and thrilling moments we can laugh about now. I am grateful for the assistance and guidance in geochronology related work by Laura Bracciali and Robert Bohlar.

Thank you also to many others who have played their part in my success: Andrea, Carel, Mollie and Stephan. A big thank you to the department support staff who were always willing to help: Khensani, Ivan, John, Diffy, Johnathan, Rene, Nathalie and Elretha. Lastly, I thank the various farm owners who graciously allowed us to conduct field work on their land, and the many people we encountered on our trips into Lesotho, for making the field work extra interesting.

Research components of this project were supported by the following funding bodies:

- National Research Foundation (NRF) African Origins Programme (AOP)
- Geological Society of South Africa: Research, Education, and Investment Fund (REI Fund)
- Geological Society of America: GSSA-El-Baz Research Grant
- Palaeontological Scientific Trust (PAST) Student Research Grant
- Society for Sedimentary Geology (SEPM) Student Research Grant

I am grateful for personal financial support and bursary funding from:

- GENUS (NRF-DST Centre of Excellence in Palaeosciences): 2020–2022
- University of Cape Town: Vice-Chancellor Scholarship 2019–2020

Table of Contents

Chapter 1. Introduction

1.1 Motivation and aims

Globally, the Jurassic period is punctuated by the wide-spread appearance of thick aeolian successions which have been extensively studied, especially in North America (e.g., Kocurek and Dott, 1983; Blakey *et al*., 1988; Dickinson and Gehrels, 2003; Loope *et al*., 2004; Rodriguez-Lopez *et al*., 2014; Hasiotis *et al.,* 2021) and South America (e.g., Scherer and Lavina, 2005; Scherer and Goldberg, 2007; Scherer *et al.,* 2007). These Jurassic aeolian systems developed under the influence of active trade wind belts linked to sub-tropical, high-pressure systems over large continental landmasses (Rodriguez-Lopez *et al*., 2014). Within southwestern Gondwana, such vast erg systems also developed during the Early Jurassic as part of an aridification trend (Bordy *et al*., 2004, 2020), the culmination of which is represented by the youngest sedimentary unit within the Karoo Supergroup: the Clarens Formation. Sedimentary rocks in the Clarens Formation have been interpreted to be mainly aeolian in origin, Early Jurassic in age, and thus characterizing a period in Earth's history that followed the end-Triassic mass extinction event (du Toit, 1905; Haughton, 1924; Stockley, 1947; Beukes, 1969, 1970; Johnson, 1976; Eriksson, 1981, 1986; Holzförster, 2007; Bordy, 2008; Bordy and Head, 2018; Bordy *et al*., 2020). Correlated Lower Jurassic units appear throughout southern Africa, such as the Etjo Formation in Namibia, the Forest Sandstone in Zimbabwe, and the Tseung and Bodibeng Sandstones in Botswana (Visser, 1984; Smith *et al*., 1993; Holzförster *et al*., 1999; Bordy and Head, 2018). In addition, Lower Jurassic aeolianites also appear in South America (e.g., Parana Basin - Milani *et al*., 1998), North America (Glen Canyon Group – Rodrigues-Lopez *et al*., 2014; and references therein), and China (Santai Formation - Xu *et al*., 2013,2021; and references therein). For these reasons, the preserved sedimentary record of the Clarens Formation is significant for understanding the ecological impact of the end-Triassic biotic crisis, and how the environment and life in it bounced back and evolved not only in southwestern Gondwana, but also in Pangaea at large in the Early Jurassic.

Characteristically, the Clarens Formation forms steep cliffs across southern Africa that are cream, pink to buff in colour with caves and rock shelters at the base of the cliffs. A conformable, transitional basal contact exists with the Elliot Formation, in which maroon sandstones to mudstones are often interbedded with cream, pink- to buff-coloured sandstones (Van Eeden, 1937; Stockley, 1947; Beukes, 1970; Johnson, 1976; Erkisson, 1981, 1986; Bordy *et al*., 2004; Bordy and Head, 2018, Van dijk and Erisskon, 2021). An upper conformable contact with the overlying Drakensberg Group is also observed, in which, mostly in the lower part, sandstone interbeds also occur (Duncan et al., 1997; Moulin *et al*., 2017; Brody *et al*., 2021). The thickness of the Clarens Formation varies from 10 to 300 meters in places whereas 150 m is a good average representation throughout the outcrop area in southern Africa. The age assessment of the Clarens Formation is mostly grounded in the existing bio- and chronostratigraphy of the underlying upper Elliot Formation (Hettangian-Sinemurian) and radio isotopic dates from the overlying lower Drakensberg Group (Pliensbachian – e.g., du Toit, 1905; Haughton, 1924; Duncan *et al*., 1997; Knoll, 2005; McPhee *et al*., 2017; Moulin *et al*., 2011; Svensen *et al*., 2012; Moulin *et al*., 2017; Bordy and Head 2018; Rademan, 2018; Abrahams, 2020; Bordy *et al*., 2020, 2021). Direct age assessment of the unit is extremely

limited to-date due to the lack of primary markers such as volcanic ash throughout the Clarens Formation depositional succession (e.g., Bordy *et al*., 2020)

Overall, massive to large-scale, cross-bedded, medium- to very fine-grained, silty sandstones are prevalent throughout the succession (Beukes, 1970; Eriksson, 1981, 1986; Bordy and Head, 2018). Sandstones are quartz-rich, felspathic wackes and minor arkosic arenites that were mostly recycled from pre-Clarens sedimentary rocks (Beukes, 1969, 1970; Johnson, 1976; Eriksson, 1981, 1986; Eriksson *et al*., 1994). Since the grain size of the massive, silty sandstones is consistent with that of loess, these massive rocks have been interpreted as loessic in origin (Beukes, 1970; Johnson, 1976). Their alternative interpretations include the destruction of primary stratification features either during rainstorms due to rainwater percolation (Beukes, 1969, 1970) or mass movement processes (e.g., dune slumping - Eriksson, 1981, 1986). The large-scale, cross-bedded sandstones have been consistently interpreted as ancient migrating dunes in the vast aeolian system, swept by a strong west-to-east wind regime (Beukes, 1969, 1970; Johnson, 1976; Eriksson, 1981, 1986; Bordy and Head, 2018). Other, subordinate sedimentary facies associations have been documented as thin, lenticular layers that are prominent in the basal and upper part of the Clarens Formation. These include sandstones with ripple-cross lamination, ripple marks, and horizontal lamination as well as massive to laminated mudstones. These basal and upper facies associations have been associated with fluvio-lacustrine processes (Beukes, 1969, 1970; Bordy and Head, 2018; Bordy *et al*., 2021), and their stratigraphic distribution allows for the tripartite subdivision of the Clarens Formation. Of these three informal zones, the middle zone, with prominent large-scale, cross-bedded sandstones, occurs between the lower and upper zones, where massive sandstones dominate, and lenticular sandstones and mudstones are frequently observed. This regional tripartite zonation also led to the interpretation of climatic megacycles that shifted from wet to arid and then back to wet conditions during Clarens times (Beukes, 1969, 1970; Bordy and Head, 2018).

In addition to the massive, lenticular and the large-scale, cross-bedded sandstones, Eriksson (1981, 1986) also documented fine-grained sandstones with horizontal lamination, convolute lamination, and thin horizontal bedding as well as medium- to coarse-grained, trough to planar cross-bedded sandstones in the eastern, southeastern, and northwestern outcrop areas. These facies associations were shown to reflect sedimentary process in sheetflows and braided wadi channels on a distal alluvial fan that were prevalent east of the basin (Eriksson, 1981, 1986). This prompted the interpretation that wet-dry facies distribution in the Clarens Formation is not only due to temporal climatic shifts, but also due to spatial changes with the east and southeast of the outcrop areas reflecting a wet desert setting, whereas the north and northwest region being attributable to dry desert conditions.

Despite these decades-old interpretations of the sedimentology of the Clarens Formation, the intricate nature of the fluvio-lacustrine processes in the broader aeolian setting as well as the dust fall processes in the case of the massive sandstones remain unaccounted. Furthermore, the current provenance interpretations for the Clarens Formation are based on a localised outcrop area in the KwaZulu Natal Drakensberg region and thus without a systematic regional study of the source

terrains, the Clarens provenance history remains incomplete. The age assessment of the unit is also largely limited to a relative age derived from evidence in over- and underlying successions. This overall Sinemurian to Pliensbachian age of the Clarens Formation is not nuanced enough to determine potential age variations in the sediment supply dynamics across the Clarens Formation outcrop area.

Aims of this doctoral thesis:

Considering that the sedimentary characteristics of the Clarens Formation require further investigation, this study focuses on the sedimentary facies analysis of the Lower Jurassic Clarens Formation in the main Karoo Basin (MKB) of southern Africa to:

1) Assess the facies characteristics of the Clarens Formation to reconstruct, at high resolution, the palaeogeography of these fluvial-lacustrine systems and their distribution within the aeolian environment..

2) Evaluate, on variable time scales, the sedimentary processes (palaeo-flow, wind-patterns, etc.) that generated the complex sedimentary architecture of this stratigraphic unit.

3) Assess the spatiotemporal development of the Clarens Formation aeolianites via detrital zircon LA-ICP-MS analysis to build a firmer chronostratigraphic framework and refine its sedimentary provenance.

4) Contextualise the regional climate cycles within the global climate trends during the Early Jurassic.

1.2 Thesis structure

Each individual chapter in this doctoral thesis represents an independent body of work in the format of standard academic manuscripts and allows for the detailed investigation of a specific aspect of the Clarens Formation as listed in the above aims. Therefore, Chapters 2 throuhg 5 each have their own abstract, introduction, geological background, methods, results, discussion, conclusion, and references. Chapter 2 presents the documentation and interpretation of the spatiotemporal distribution of lenticular sandstones and mudstones in the Clarens Formation. Given the limited understanding of these fluvio-lacustrine deposits, this chapter documents the variety of lacustrine deposits in the Clarens Formation from three case studies in main Karoo Basin. Chapter 3 examines the spatiotemporal distribution of the massive sandstones that dominate the Clarens Formation and accounts for the sedimentological genesis of such facies in aeolian settings. Chapter 4 details the facies architecture of the Clarens Formation to explain the regional spatiotemporal trends in erg development, whereas Chapter 5 analyses the sediment provenance and age of the Clarens Formation. Combined, these four core chapters allow the formulation of a regional perspective on the Clarens Formation within southwestern Gondwana and its global context during the Early Jurassic.

1.3 References

Abrahams, M. 2020. Evaluation of tridactyl theropod tracks in southern Africa: quantitative morphometric analysis across the Triassic–Jurassic boundary. Unpublished doctoral thesis, University of Cape Town. 208 pp Available: http://hdl.handle.net/11427/32436

Beukes, N.J. 1969. Die sedimentologie van die Etage Holkranssandsteen, sisteem Karoo. Unpublished MSc dissertation, University of the Orange Free State, Bloemfontein, 138 pp. Available: http://hdl.handle.net/11660/7671

Beukes, N.J. 1970. Stratigraphy and sedimentology of the Cave Sandstone stage, Karoo System. In: S.H. Haughton (Ed), Proceedings and papers of the 2nd Gondwana symposium. *Council for Scientific and Industrial Research,* Pretoria: 321–341.

Blakey, R.C. Peterson, F. and Kocurek, G. 1988. Synthesis of late Paleozoic and Mesozoic eolian deposits of the Western Interior of the United States. *Sedimentary Geology*, 56(1-4): 3–125. DOI: 10.1016/0037-0738(88)90050-4

Bordy, E.M., Hancox, P.J. and Rubidge, B.S. 2004. Basin development during the deposition of the Elliot Formation (Late Triassic-Early Jurassic), Karoo Supergroup, South Africa. *South African Journal of Geology*, 107(3): 397-412. DOI: 10.2113/107.3.397

Bordy, E.M. and Head. H.V. 2018. Lithostratigraphy of the Clarens Formation (Stormberg Group, Karoo Supergroup), South Africa. *South African Journal of Geology*, 121: 119–130. DOI: 10.25131/sajg.121.0009

Bordy, E.M., Rampersadh, A., Abrahams, M., Lockley, M.G. and Head, H.V. 2020. Tracking the Pliensbachian–Toarcian Karoo firewalkers: Trackways of quadruped and biped dinosaurs and mammaliaforms. *PLOS one*, 15(1): e0226847. DOI: 10.1371/journal.pone.0226847

Bordy, E.M., Haupt, T.N. and Head, H.V. 2021. Karoo lava-fed deltas and a petrified forest from the Lower Jurassic of southern Gondwana. *Palaeogeography, Palaeoclimatology, Palaeoecology*, 575: 110484. DOI: 10.1016/j.palaeo.2021.110484

Dickinson, W.R. and Gehrels, G.E. 2003. U–Pb ages of detrital zircons from Permian and Jurassic eolian sandstones of the Colorado Plateau, USA: paleogeographic implications. *Sedimentary Geology*, 163(1-2): 29–66. DOI: 10.1016/S0037-0738(03)00158-1

Duncan, R. A., Hooper, P. R., Rehacek, J., Marsh, J. S. and Duncan, A. R. 1997. The timing and duration of the Karoo igneous event, southern Gondwana. *Journal of Geophysical Research*, 102: 18127–18138. DOI: 10.1029/97JB00972

du Toit, A.L. 1905. Geological survey of the division of Aliwal North, Herschel, Barkly East and part of Wodehouse: *Annual Report of the Geological Commission of the Cape of Good Hope*. 71–181.

Eriksson, P.G. 1981. A palaeoenvironmental analysis of the Clarens Formation in the Natal Drakensberg. *Transactions of the Geological Society of South Africa*, 84: 7–17.

Eriksson, P.G. 1986. Aeolian dune and alluvial fan deposits in the Clarens Formation of the Natal Drakensberg. *Transactions of the Geological Society of South Africa*, 89: 389–393.

Eriksson, P.G., McCourt, S. and Snyman, C.P. 1994. A note on the petrography of upper Karoo sandstones in the Natal Drakensberg: implications for the Clarens Formation palaeoenvironment. *South African Journal of Geology*, 97(1): 101–106.

Hasiotis, S.T., Chan, M.A. and Parrish, J.T. 2021. Defining bounding surfaces within and between eolian and non-eolian deposits, Lower Jurassic Navajo Sandstone, Moab Area, Utah, USA: Implications for subdividing erg system strata. *Journal of Sedimentary Research*, 91(12): 1275–1304. DOI: https://doi.org/10.2110/jsr.2021.027

Haughton, S.H. 1924. The Fauna and stratigraphy of the Stormberg Series. *Annals of the South African Museum*, 8: 1–517.

Holzförster, F., Stollhofen, H. and Stanistreet, I.G. 1999. Lithostratigraphy and depositional environments in the Waterberg-Erongo area, central Namibia, and correlation with the main

Karoo Basin, South Africa. *Journal of African Earth Sciences*, 29(1): 105-123. DOI: 10.1016/S0899-5362(99)00083-4

Holzförster, F. 2007. Lithology and depositional environments of the Lower Jurassic Clarens Formation in the eastern Cape, South Africa. *South African Journal of Geology*, 110(4): 543–560. DOI: 10.2113/gssajg.110.4.543

Johnson, M.R. 1976. Stratigraphy and sedimentology of the Cape and Karoo Sequences in the eastern Cape Province. Unpublished doctoral thesis, Rhodes University, Grahamstown, South Africa, 336pp. Available: http://hdl.handle.net/10962/d1005617

Knoll, F. 2005. The tetrapod fauna of the Upper Elliot and Clarens formations in the main Karoo Basin (South Africa and Lesotho). *Bulletin de la Société géologique de France*, 176(1): 81–91. DOI: 10.2113/176.1.81

Kocurek, G. and Dott, R.H. 1983. Jurassic paleogeography and paleoclimate of the central and southern Rocky Mountains region, In *Mesozoic Paleogeography of the West-Central United States, Rocky Mountain Paleogeography Symposium 2*. M.W. Reynolds and E.D. Dolly (Eds). SEPM, 101–149.

Loope, D.B., Eisenberg, L., Waiss, E., Nelson, E. P. and Erslev, E. A. 2004. Navajo sand sea of near-equatorial Pangea: Tropical westerlies, slumps, and giant stromatolites. Field Trips in the Southern Rocky Mountains, USA: *Geological Society of America Field Guide*, 5: 1-13.

McPhee, B., Bordy, E., Sciscio, L. and Choiniere, J. 2017. The sauropodomorph biostratigraphy of the Elliot Formation of southern Africa: Tracking the evolution of Sauropodomorpha across the Triassic–Jurassic boundary. *Acta Palaeontologica Polonica*, 62(3): 441–465.

Milani, E.J., Araujo, L.M., Cupertino, J.A., Faccini, U.F. and Scherer, C.M. 1998. Sequences and stratigraphic hierarchy of the Parana Basin (Ordovician Cretaceous), Southern Brazil. *Série Científica*, 29.

Moulin, M., Fluteau, F., Courtillot, V., Marsh, J., Delpech, G., Quidelleur, X., Gérard, M. and Jay, A.E. 2011. An attempt to constrain the age, duration, and eruptive history of the Karoo flood basalt: Naude's Nek section (South Africa). *Journal of Geophysical Research: Solid Earth*, 116(B07403). DOI: 10.1029/2011JB008210

Moulin, M., Fluteau, F., Courtillot, V., Marsh, J., Delpech, G., Quidelleur, X. and Gérard, M. 2017. Eruptive history of the Karoo lava flows and their impact on early Jurassic environmental change. *Journal of Geophysical Research: Solid Earth*, 122(2): 738–772. DOI: 10.1002/2016JB013354

Rademan, Z. 2018. Radiometric dating and stratigraphic reassessment of the Elliot and Clarens formations; near Maphutseng and Moyeni, Kingdom of Lesotho, southern Africa. Unpublished MSc dissertation, Stellenbosch University. 181 pp. Available: http://hdl.handle.net/10019.1/104888

Rodríguez-López, J.P., Clemmensen, L.B., Lancaster, N., Mountney, N.P. and Veiga, G.D. 2014. Archean to Recent aeolian sand systems and their sedimentary record: current understanding and future prospects. *Sedimentology*, 61(6): 1487–1534. DOI: 10.1111/sed.12123

Scherer, C.M. and Lavina, E.L., 2005. Sedimentary cycles and facies architecture of aeolian–fluvial strata of the Upper Jurassic Guará Formation, Southern Brazil. Sedimentology, 52(6), pp.1323-1341. DOI: https://doi.org/10.1111/j.1365-3091.2005.00746.x

Scherer, C.M. and Goldberg, K. 2007. Palaeowind patterns during the latest Jurassic–earliest Cretaceous in Gondwana: evidence from aeolian cross-strata of the Botucatu Formation, Brazil. *Palaeogeography, Palaeoclimatology, Palaeoecology*, 250(1-4): 89-100. DOI: https://doi.org/10.1016/j.palaeo.2007.02.018

Scherer, C.M., Lavina, E.L., Dias Filho, D.C., Oliveira, F.M., Bongiolo, D.E. and Aguiar, E.S. 2007. Stratigraphy and facies architecture of the fluvial–aeolian–lacustrine Sergi Formation (Upper

Jurassic), Recôncavo Basin, Brazil. *Sedimentary Geology*, 194(3-4): 169-193. DOI: https://doi.org/10.1016/j.sedgeo.2006.06.002

Smith, R.M.H., Eriksson, P.G. and Botha, W.J. 1993. A review of the stratigraphy and sedimentary environments of the Karoo-aged basins of Southern Africa. *Journal of African Earth Sciences*, 16(1–2): 143–169. DOI: 10.1016/0899-5362(93)90164-L

Stockley, G.M. 1947. The Geology of Basutoland. *Geological Magazine*, 77(6): 444–460.

Svensen, H., Corfu, F., Polteau, S., Hammer, Ø. and Planke, S. 2012. Rapid magma emplacement in the Karoo large Igneous Province. *Earth Planetary Science Letters*, 325–326: 1–9. DOI: 10.1016/j.epsl.2012.01.015

Van Eeden, O.R. 1937. The geology of the country around Bethlehem and Kestell, with special reference to oil indications. *Memoirs of the Geological Survey of South Africa*. 33: 68.

van Dijk, D.E. and Eriksson, P.G. 2021. Bipedal leaping Jurassic vertebrates in Southern Africa: proposed new ichnotaxon and inferred palaeoenvironment. *Transactions of the Royal Society of South Africa*: 76(3): 235–245. DOI: 10.1080/0035919X.2021.1964104

Visser, J.N.J. 1984. A review of the Stormberg Group and Drakensberg volcanics in southern Africa. *Palaeontologia Africana*, 25: 5–27.

Xu, H., Liu, Y. Q., Kuang, H.W., Liu, Y.X., Peng, N., Dong, C., Xue, P. L., Xu, J.L., Chen, J. and Liu, H. 2013. Sedimentology, palaeogeography and palaeoecology of the Late Jurassic-Early Cretaceous eolian sands in North China. *Journal of Palaeogeography*, 15(1): 11–30.

Xu, H., Liu, Y., Kuang, H., Peng, N., Xu, K. and Chen, J. 2021. Diverse preserved dinosaur footprint assemblage from Jurassic–Cretaceous transition eolian dune deposits of western Shandong Province, China. *Cretaceous Research*, 121: 104733. DOI: 10.1016/j.cretres.2020.104733

Chapter 2.

Dynamics of an Early Jurassic aeolian system: evidence from the interdunal pond and lake deposits in the Clarens Formation of southern Africa

Abstract

The Sinemurian to Pliensbachian Clarens Formation has a well-established aeolian origin and an exceptional lithological homogeneity across the main Karoo Basin of southern Africa. Within the predominantly aeolian deposits, strata of lacustrine origin have also been identified, yet the detailed spatiotemporal evaluation of these facies and the interaction of the aeolian, fluvial, and lacustrine processes that led to their formation have not been investigated. In this study, three pluvial facies have been identified that reflect the development of ponds and lakes amongst aeolian dunes and sand sheets of the Clarens erg system. The pond deposits in the northern part of the basin are restricted to interdune hollows within, at the time, actively climbing aeolian system. A high sediment availability and high wind speeds limited the space available for these ponds to expand into lakes. Moreover, migrating dunes in this climbing system outpaced the water-table rise which promoted the formation of discontinuous lenses of the pluvial facies, typical in erg centre settings. Lacustrine deposits in the southern part of the basin show the development of both spatially isolated lakes, where flooding was controlled by groundwater flow, and more extensive lakes, where flooding was related to both groundwater flow and flood-induced hyperconcentrated flows. The development of candidate composite surfaces along the erg margin resulted in the expansion of interdunes and formation of interdunal lakes that were preserved in an exceptionally large (up to 50 m) thickness. Lacking desiccation features in the pluvial facies suggests that the lakes formed in uninterrupted humid climate phases. Relative to the northern part of the basin, the lacustrine facies in the south, with its more significant thickness and lateral extent, shows that here, the basin was characterized by both a longer-term humid phase and a higher relative subsidence. Ultimately, the pluvial facies in the Clarens Formation are an indication for an aeolian depositional area that was subjected to repeated and prolonged pluvial episodes that promoted the establishment of localised ecosystems in an otherwise harsh environment in this part of southwestern Gondwana in the Early Jurassic.

2.1. Introduction

Aeolian systems, in particular interdune areas of ergs, show an exceptional sensitivity to climate change. Moreover, decoding ancient fluvial and lacustrine processes in such aeolian settings is key for unravelling basin dynamics, which are primarily driven by climatic and tectonic processes. Such interdunal lakes and ponds are typically shallow and have short lifespans. Lacustrine deposits within the aeolian Clarens Formation of the main Karoo Basin have been attributed to the development of playas in this Early Jurassic aeolian setting of southwestern Gondwana (e.g., Beukes 1969, 1970; Eriksson 1981, 1986; Bordy and Catuneanu, 2001; Bordy and Head, 2018). The occurrence of these lake deposits in the lower and upper parts of the Clarens Formation has led to the informal division of the Clarens Formation succession in the main Karoo Basin (MKB; Figure 2.1) into three zones, where the middle zone reflects more arid conditions relative to the lower and upper zones (Beukes, 1969; 1970; Bordy and Head, 2018). These three zones are thought to represent wet-to-dry climatic

shifts during the Clarens Formation depositional episode from the Sinemurian to the Pliensbachian (e.g., Beukes 1969, 1970; Eriksson 1981, 1986; Bordy *et al*., 2020a). Despite the limited identification of these lacustrine deposits several decades ago, their in-depth facies description, basin-wide mapping and evaluation with respect to the fluvial-lacustrine interaction in the Clarens Formation remain undocumented. In addition to addressing these aspects of the Clarens Formation, this study also aims to describe the lacustrine facies at three new study sites (Figure 2.1) and assess the importance of the aeolian-fluvial-lacustrine interactions within the context of climatic changes in this Early Jurassic aeolian system.

2.2. Geological background

The Sinemurian to Pliensbachian Clarens Formation represents the youngest sedimentary unit within the Karoo Supergroup of southern Africa (Figure 2.1; Bordy and Head, 2018). The Clarens Formation has a conformable, transitional lower contact with the Elliot Formation and a conformable upper contact with the overlying flood basalts of the Drakensberg Group (Beukes, 1969, 1970; Johnson, 1976; Eriksson, 1981, 1986; Bordy and Head; 2018; Bordy *et al*., 2021 – Figure 2.1). Typical thickness ranges of 90 to 150 m appear to be a good representation throughout the basin, despite extreme localised thickness variations that occur, whereas the succession is absent in parts of the basin (du Toit, 1905, 1918; Johnson, 1976). The Clarens Formation comprises thick to very thick white, cream, pink to buff-coloured medium- to very fine-grained sandstones that are characteristically massive or preserve large-scale cross-bedding (Beukes, 1969, 1970; Bordy and Head, 2018). These characteristics gave rise to its interpretation as an overall aeolian sedimentary succession, while the occurrence of various lenticular mudstones and sandstones have been linked to ephemeral fluvial to lacustrine processes during episodic wet phases in this ancient desert setting (du Toit, 1905, 1918; Beukes, 1969, 1970; Johnson, 1976; Eriksson, 1979, 1981, 1986; Bordy and Catuneanu, 2002; Holzförster, 2007; Bordy *et al*., 2008; Bordy, 2009; Bordy and Head; 2018; Van Dijk and Eriksson, 2021; Bordy *et al*., 2021). These deposits were documented as being concentrated towards the lower and upper parts of the succession within the MKB, and based on this distribution, Beukes (1969, 1970) provided an informal tripartite division of the Clarens Formation into a middle zone that is dominated by large-scale, cross-bedded sandstones, and which is bounded by lower and upper zones that are dominated by massive sandstones. In addition to the tripartite stratigraphic division, Eriksson (1981, 1986) offered evidence for spatial domains in the Clarens Formation, which comprise a wet outer erg in the east, southeast, and northeast, as well as a dry inner erg in the central and western regions of the outcrop area.

Although the lenticular mudstone and sandstone deposits of the Clarens Formation lack detailed sedimentologic assessments to-date, these beds are associated with various vertebrate and invertebrate body and trace fossils as summarized in Bordy *et al*. (2020a), Viglietti *et al*. (2020), and Mukaddam *et al*. (2021). This paleontological heritage is exclusively continental biota and includes freshwater fish (*Semionotus capensis*; *Endemichthys likoeli*; *Daedalichthys formosa*), freshwater branchiopod crustaceans ("conchostracans"), crocodylomorphs (*Notochampsa istedana; Sphenosuchus acutus*), ornithischians (*Heterdontosaurus tucki*; *Lycorhinus angustidens*), sauropodomorphs (*Massospondylus carinatus*; *Ngwevu intloko*), cynodonts (*Tritylodontoides maximux*; *Pachygenelus monus*; *Diarthrognathus broomi*; *Tritheledon riconoi*), *mamaliaformes (Erythrotherium parringtoni),* sphenodontia (*Clevosaurus* sp.), termite nests, vertebrate tracks, plant impressions and, fossil wood. The diverse fossil record of the Clarens Formation is the ultimate

evidence for wetter conditions and thriving localised ecosystems within this overall desert setting. Furthermore, evidence from the sedimentary interbeds within the overlying Karoo continental flood basalts (lower Drakensberg Group – Figure 2.1) suggests that these ecosystems remained active beyond the initiation of volcanic activities in the Karoo-Ferrar Large Igneous Province (Moulin *et al.*, 2017; Bordy *et al.*, 2020b, 2021).

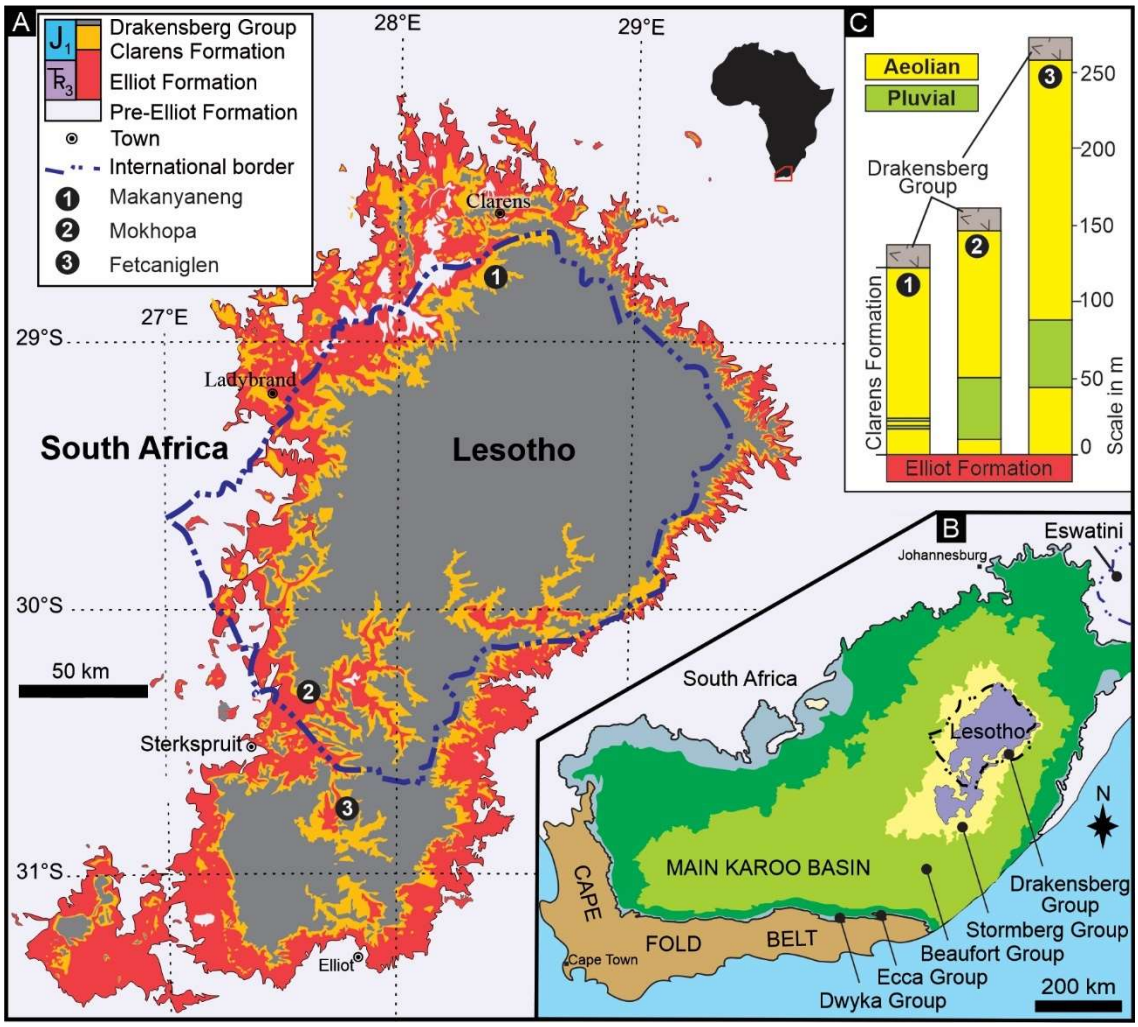

Figure 2.1: Location and geological context of the study sites. **A**. Simplified geological map of the upper Stormberg Group (Karoo Supergroup) showing the three study locations in the Sinemurian-Pliensbachian Clarens Formation. **B**. Map of the main Karoo Basin in South Africa and Lesotho. **C**. Simplified stratigraphic logs at the three study sites.

2.3. Methods

Data was collected at three study sites within the Clarens Formation where lacustrine deposits were interpreted from outcrop-based sedimentary observations in the main Karoo Basin (MKB) in South Africa and Lesotho (Figure 2.1). The GPS coordinates of the study sites can be found in Appendix 1. Documenting the grain size, sedimentary structures, lithology, composition and under- and over-lying facies contact types enabled the classification of the sedimentary facies along with the compilation of detailed centimetre-scale sedimentary logs. In addition, panels showing the lateral facies association were constructed by overlapping digital field images. These outcrop maps capture the temporal and spatial distribution of facies and facies association arrangements, which are dependent on external forcing factors that affect sedimentation (Kocurek and Havholm, 1993; Mountney and Thompson, 2002; Mountney and Jagger, 2004; Mountney, 2006; Al-Masrahy and Mountney, 2015; Hasiotis *et al*., 2021). The spatial relationships of larger scale facies associations were reconstructed by mapping prominent sedimentary features on satellite imagery using Google Earth Pro software. This approach is based on the well-known facies analysis method outlined by Miall (1996) for the evaluation of sedimentary basins. The use of sedimentary facies codes utilised in this study were based on that of do Amarante *et al.* (2019) adapted from Miall (1996), where an aeolian process is denoted by a letter 'e' at the end of a code. Palaeocurrent measurements were taken from foreset dip directions of large-sale cross-bedded sandstones (High and Picard, 1974; Miall, 1974; Dasgupta, 2002) to understand and reconstruct the dominant wind regimes, sediment pathways and source dynamics (Miall, 2016) across southwestern Gondwana during the Early Jurassic.

2.4. Sedimentary facies and their associations

The lithofacies in the lower Clarens Formation were grouped into 16 sedimentary facies (Table 2.1) and three sedimentary facies associations (FA; Table 2.2). Four of the facies in this study (Table 2.1) are similar to sedimentary facies of the Natal Drakensberg region that were identified by Eriksson (1981, 1986). In Eriksson's scheme, Facies 1 comprises fine-grained, laminated, and convoluted sandstones that are frequently interbedded with very fine-grained sandstones and mudstones, which has been interpreted as sediments of playa lakes, associated with wadi channels and sheetflood deposits. Facies 2 exhibits medium- to coarse-grained cross-bedded sandstones attributed to desert flooding processes in braided wadi channels and sheet flows, whereas Facies 3 is composed of massive sandstones linked to mass movement processes. Lastly, Facies 4 comprises very fine-grained sandstones that exhibit large-scale, planar cross-bedding, interpreted as deposits of migrating dunes (Eriksson, 1981, 1986).

2.4.1. Facies Association 1 (FA1)

Description: This facies association is characterised by laterally extensive sandstone bodies with fine- to medium-grain sizes and large-scale cross-bedding (Ste). It ranges in thickness from 1 to 2 m, where stacked sets are between 2 and 10 m in thickness, but can be as thick as 35 m. These sandstones exhibit sharp upper and lower surfaces that are planar or slightly undulating. Sandstones are white to pale orange in colour. Internal stratification shows laminated sands interbedding with 3–5 cm thick, massive sands. In places, low-angle cross-bedding is associated with the large-scale cross-bedding.

Interpretation: The large-scale cross-bedding composed of interbedded laminations and sandstone wedges indicate typical grain-fall and grain-flow processes and suggests that Facies Association 1 is the result of migrating dunes (Hunter, 1977). 154 paleocurrent measurements (Appendix 2) from the large-scale, cross-bedded sandstones suggests a consistent wind regime with the main current direction from west to east (main vector direction: 110°; consistency ratio: 0.8). Low-angle cross-bedding associated with large-scale cross-bedding is interpreted as dune plinth deposits, or the fill of dune hollows (Kocurek and Havholm, 1993).

Table 2.1: Interdunal lacustrine and aeolian deposits common in the lower and upper Clarens Formation. This facies table is based on observations made during this study as well as four lithofacies described by Eriksson (1981, 1986).

Code	Lithofacies	Description	Interpretation
Ste	Large-scale cross-bedded sandstone	Fine- to medium-grained; thick to very thick beds; Corresponds to Facies 4 of Eriksson (1981, 1986)	Aeolian dune deposits
Sle	Low-angle cross-bedded and horizontally laminated sandstone	Fine- to medium-grained; thick to very thick beds	Aeolian sand sheets or dune plinth deposits
Sse	Massive sandstone associated with an aeolian process	Very fine- to fine-grained; thick to very thick beds; Corresponds to Facies 3 of Eriksson (1981, 1986).	Loess or structureless aeolian dune deposits.
Sae	Wavy laminated sandstone	Fine-grained, medium beds	Adhesion process, dry sand adheres to damp surface
Sm	Massive sandstone	Fine- to medium grained; medium to thick beds	Hyperconcentrated flows or dune slumping process
Sh	Horizontally laminated sandstone	Fine- to medium-grained; medium to thick beds	Flood deposition, upper flow regime
Sl	low-angle cross-bedding,	Fine- to medium-grained sandstones; (associated with Sh); medium to thick beds	Flood deposition, upper flow regime
Shi	Hummocky cross-stratified sandstone	Fine-grained; thin beds	Storm wave deposits in large lakes
Sr	Ripple cross-laminated sandstones or ripple marked surfaces	Asymmetrical (i), symmetrical (ii) and interference (iii) ripples and cross-lamination in thin to very thin beds	Unidirectional current (i), bidirectional wave action (ii) in a low energy environment or changing hydrodynamic conditions (iii)
Smc	Mudstone clast conglomerate	Rip-up mudstone clasts in massive sandstone	Rapid, erosive high-energy flow
Fl	Laminated mudstone	Thin to thick beds; Corresponds to Facies 1 of Eriksson (1981, 1986)	Suspension settling from water column of aqueous current or wind derived very fine sediments into a lake
Fm	Massive mudstone	Thin to thick beds Corresponds to Facies 1 of Eriksson (1981, 1986)	As Fl above, but bioturbated
MISS	Wrinkle and roll-up structures, microbial surface textures	MISS associated with abiotic deformation structures usually on sandstone bedding planes	Development of microbial mats along sandstone substrates, subsequent mechanical deformation

Cc	Charcoal	Charcoal in massive sandstone	See section 4.2
S	Siderite nodules	Small, spherical nodules Larger layered nodules	See section 4.3
Ds	Desiccation cracks	Associated with Sr	Drying of the substrate

Table 2.2. Summary of the facies associations (FAs) of the lower and upper Clarens Formation, including the internal facies compositions (see Table 2.1), sediment transport processes and interpretations (see text for details).

Facies Association		Characteristic Facies	Sediment Transport Process	Interpretation
FA 1		Ste, Sle that can be traced to Ste	Migrating dunes	Aeolian dune deposits
FA 2		Sle	Migrating sand sheets	Aeolian sand sheet deposits
FA3	**FA3 (general)**	Fl, Fm, Sm, Sh, Sl,	Suspension settling of silt and wind-blown silt into pond or lake	Pond and lake deposits
	FA3A	Fl, Sae, Sr, Ds	Suspension settling of silt in water column and wind-blown silt	Pond deposit
	FA3B	Fl, Fm, Sm, Sr, Sae, MISS	Suspension settling of silt in water column and wind-blown silt	Lake deposits
	FA3C	Fl, Fm, Sm, Sh, Sl, Sr, Shi, MISS, Cc, S	Suspension settling of silt and wind-blown silt; Flood induced hyperconcentrated flows	Lake and flood related flow deposits

2.4.2. Facies Association 2 (FA2)

Description: This facies association is dominated by laterally extensive, horizontally laminated to low-angle, cross-bedded (Sl), fine- to medium-grained, tabular sandstones with thicknesses of 1 to 1.5 m. The low-angle, cross bedded sandstones appear as laminae that are interbedded with sandstone wedges. Where exposed, the beds occur across the entire length of the outcrop that can range from several 10s to 100s m. Upper bedding contacts are sharp, whereas lower bedding contacts tend to undulate.

Interpretation: The horizontal and low-angle cross-bedding that characterises this facies association represents deposition of aeolian sand sheets that form by the migration of wind ripples along distinct interdunal surfaces that result in low-angle stratification with almost no visibly preserved forests (Hunter, 1977; Kocurek and Dott, 1981; Hasiotis *et al.*, 2021). Ripple foreset laminae are often not preserved due to the homogeneity of the grainsize associated with aeolian deposits (Mountney, 2006). The sandstones wedges suggest that the internal arrangement is the result of climbing translatent ripple stratification (Kocurek, 1991) as these wind ripples migrated through the interdune. In a scenario where the depositional surface is damp or wet, the result may be planar wind ripple stratification (Kocurek and Nielson, 1986). Aeolian sand sheets largely develop because of conditions that are not conducive for dune construction. These may reflect a negative sand budget as sand sheets could represent reworking of sand dunes during deflationary stages of erg

development (Mountney, 2006), however, their presence has also been linked to a reduced sediment availability related to flooding of interdunal areas (Kocurek and Nielson, 1986).

2.4.3. Facies Association 3 (FA3)

This facies association comprises laminated (Fl) and massive (Fm) siltstones that are interbedded with massive sandstones (Sm), wavy laminated sandstones (Sae), horizontally laminated sandstones (Sh) and low-angle, cross-bedded sandstones (Sle) to various degrees. Laminated and massive siltstones are either lenticular when associated with wavy laminated sandstone (Sae) or laterally extensive when associated with massive, horizontally laminated and low-angle, cross-bedded sandstones. In addition, sandstone bedding planes preserve ripple marks, microbial surface textures, and wrinkle structures. This facies association is subdivided into three subfacies associations that each reflect the interaction of aeolian, fluvial, and lacustrine processes in different proportions.

2.4.3. 1. Facies Association 3A: Makanyaneng type (FA3A)

Description: The Makanyaneng site is located in the north of Lesotho, close to the town of Butha-Buthe (Figure 2.1). Here, Facies Association 3A (Figures 2.2A, 2.3, 2.4) consists of a lenticular, laminated sandy siltstone (Fl, Figure 2.3E) unit that is roughly 1 m thick and 30 m in lateral extent having concostrachans preserved within (Figure 2.3E inset). Overlying the siltstones are two fine-grained, lenticular, 0.5-m-thick sandstone beds that are dominated by wavy lamination (Sae; Figure 2.3G). These wavy-laminated sandstones laterally taper out in a down-wind direction and have a close spatial relationship with an overlying large-scale, cross-bedded sandstone (Figure 2.4). The position of Facies Association 3A within the overall Makanyaneng stratigraphy is shown in Figure 2.2A. These beds are bound by, and laterally terminate onto, large-scale cross-beds, which indicate a palaeowind direction from west to east (Figures 2.3A, 2.4). The outcrop is oriented parallel to the paleo-wind direction. The sandstone surface that underlies the sandy siltstones preserves ripple marks (Figure 2.3B), mud cracks (Figure 2.3C), and poorly exposed adhesion structures (Figure 2.3D). Moreover, the ripple marked surface has a sharp contact with the grain-fall lamination of the underlying large-scale, aeolian cross-beds (Figure 2.3F) and a slope that gradually shallows towards the horizontally laminated siltstones (Figure 2.3A). At least two of these surfaces can be observed at the Makanyaneng site. Within the wavy-laminated sandstone (Sae), a fluid escape structure is also recorded (Figure 2.3H).

Interpretation: Facies Association 3A consist of laminated mudstone (Fl) and wavy laminated sandstone (Sae) that represents damp to wet interdunal conditions in which an isolated pond developed (Kocurek, 1981; Kocurek and Fielder, 1982, Mountney, 2006). Initially, the interdune surface was damp, and adhesion processes dominated, however, after the onset of wet conditions, marked by the ripple marks, the accumulation of laminated siltstone dominated. More specifically, shallow streams flowing down dune stoss slopes possibly reworked the dune sands as indicated by the ripple marks. These damp to wet sediments subsequently dried and cracked up as indicated by desiccation cracks on an inclined surface dipping towards the laminated siltstone. The latter accumulated from suspension in the interdune pond. No evidence for drying of the interdune pond can be observed, suggesting that the water table remained close to the interdune surface as the pond silted up.

Interdunal pond margins were moist enough for adhesion processes (i.e., for dry sand to adhere to a damp surfaces) to occur as suggested by the presence of the wavy lamination in the two overlying

sandstone beds (Kocurek, 1981; Kocurek and fielder, 1982; Hummel and Kocurek, 1984). Water escape structures in the wavy-laminated sandstone indicate that the eastward migrating large-scale aeolian dunes quickly encroached upon the silted-up interdune area, which was still damp. The close spatial relationship of the wavy lamination and dune toesets (Figure 2.4) could be interpreted as a damp interdune adhesion lamination, whereas the wavy laminations may represent an extension of the dune toesets (Hummel and Kocurek, 1984).

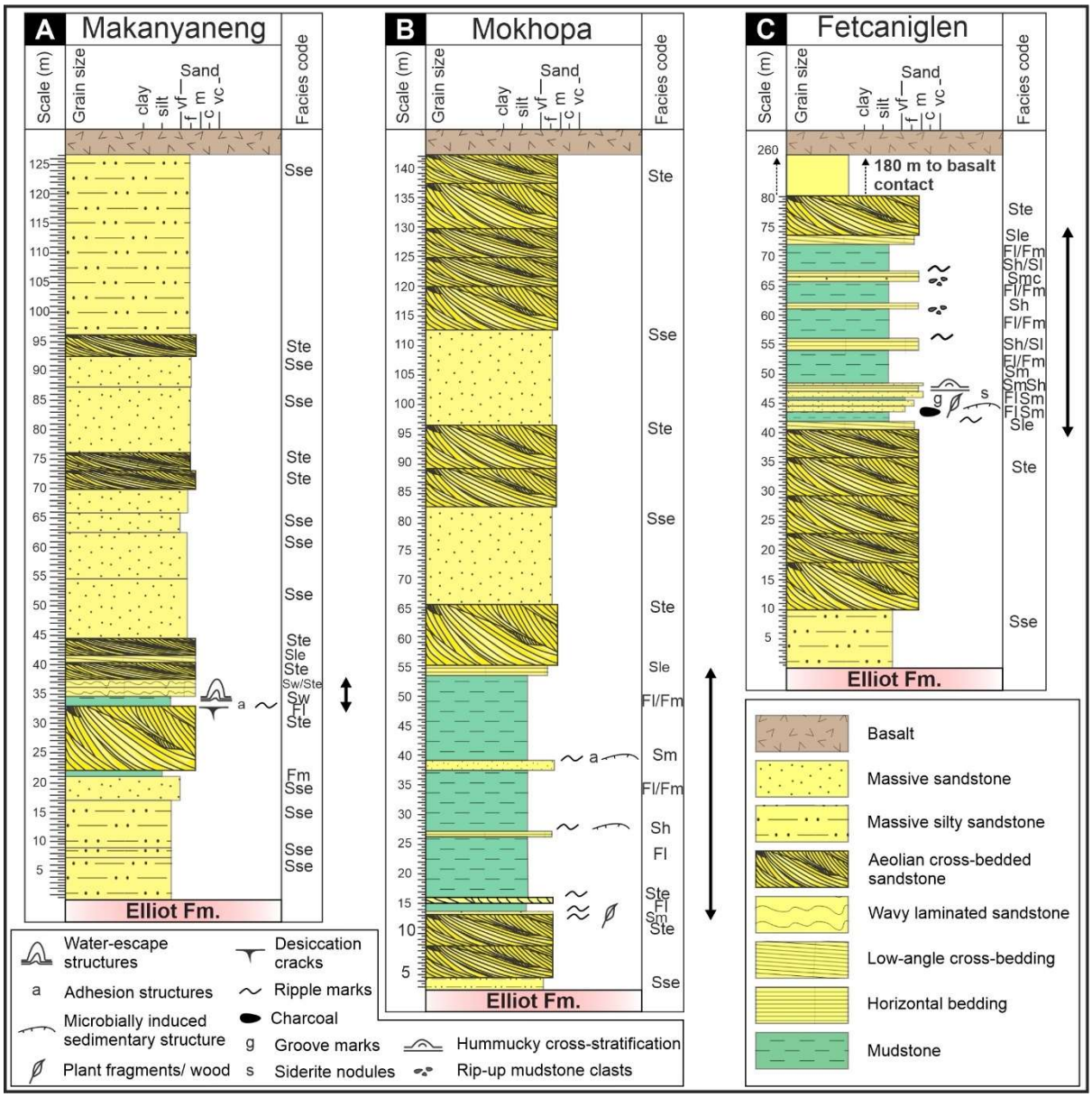

Figure 2.2: Sedimentary logs of Facies Associations 3A, Ab and 3C at the three study sites (for location in the basin, see Figure 2.1). Black double headed arrows demarcate the various Facies Associations within the overall aeolian succession at these study sites. For facies codes, see Table 2.1.

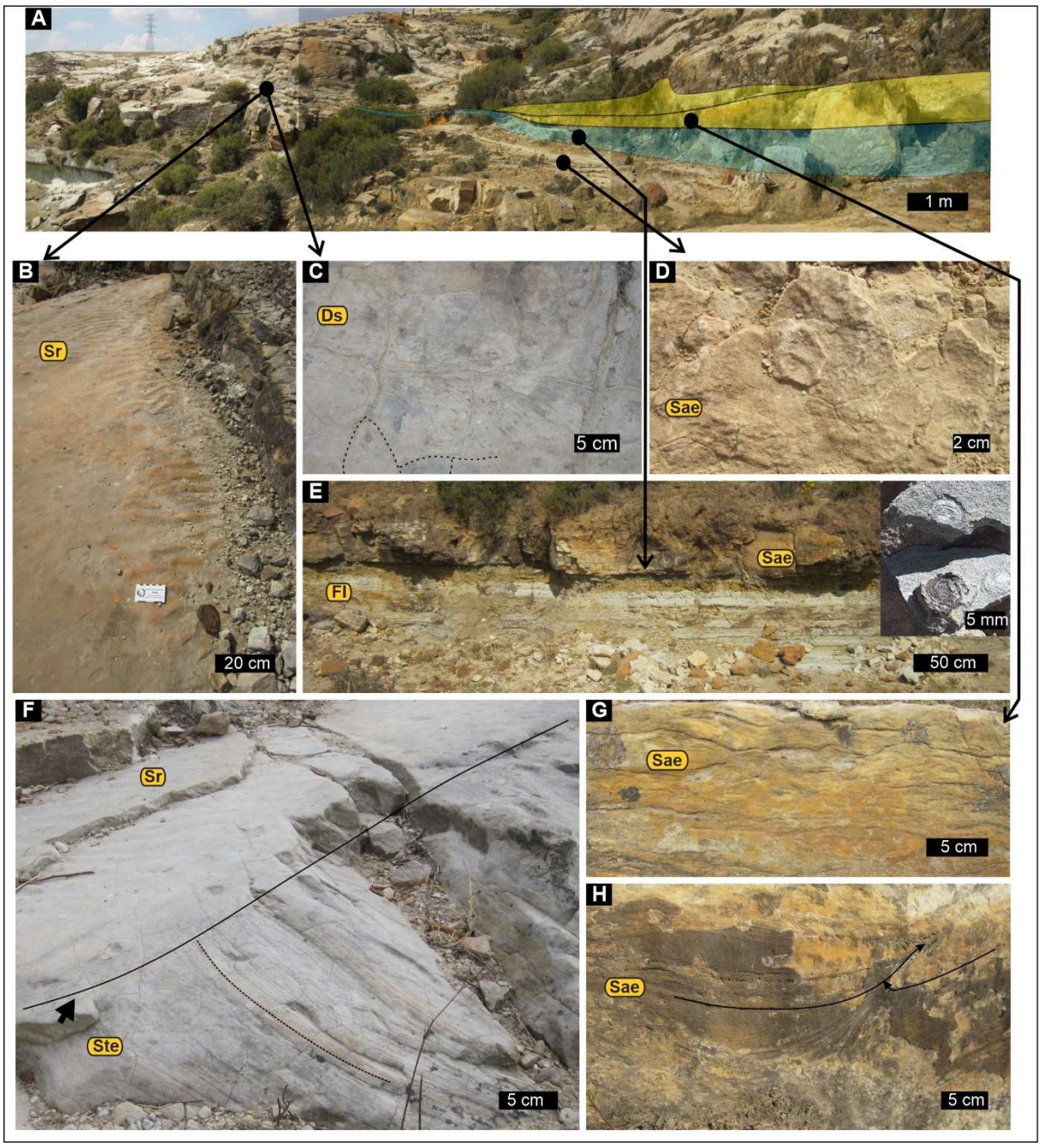

Figure 2.3: Sedimentary features at the Makanyaneng pond site. **A**. Overview of the outcrop oriented parallel to wind transport direction (E-W). **B**. Ripple marked surface along dune stoss slope. **C**. Desiccation cracks along dune stoss slope associated with ripple marks in B. **D**. Poorly preserved adhesion structures. **E**. Laminated siltstones containing conchostracans (inset). **F**. Ripple marked inclined surface has a sharp contact (black arrow) with underlying large-scale aeolian cross-bedding. **G**. Wavy lamination. **H**. Water-escape structure within the wavy-laminated sandstone in G. For facies codes, see Table 2.1.

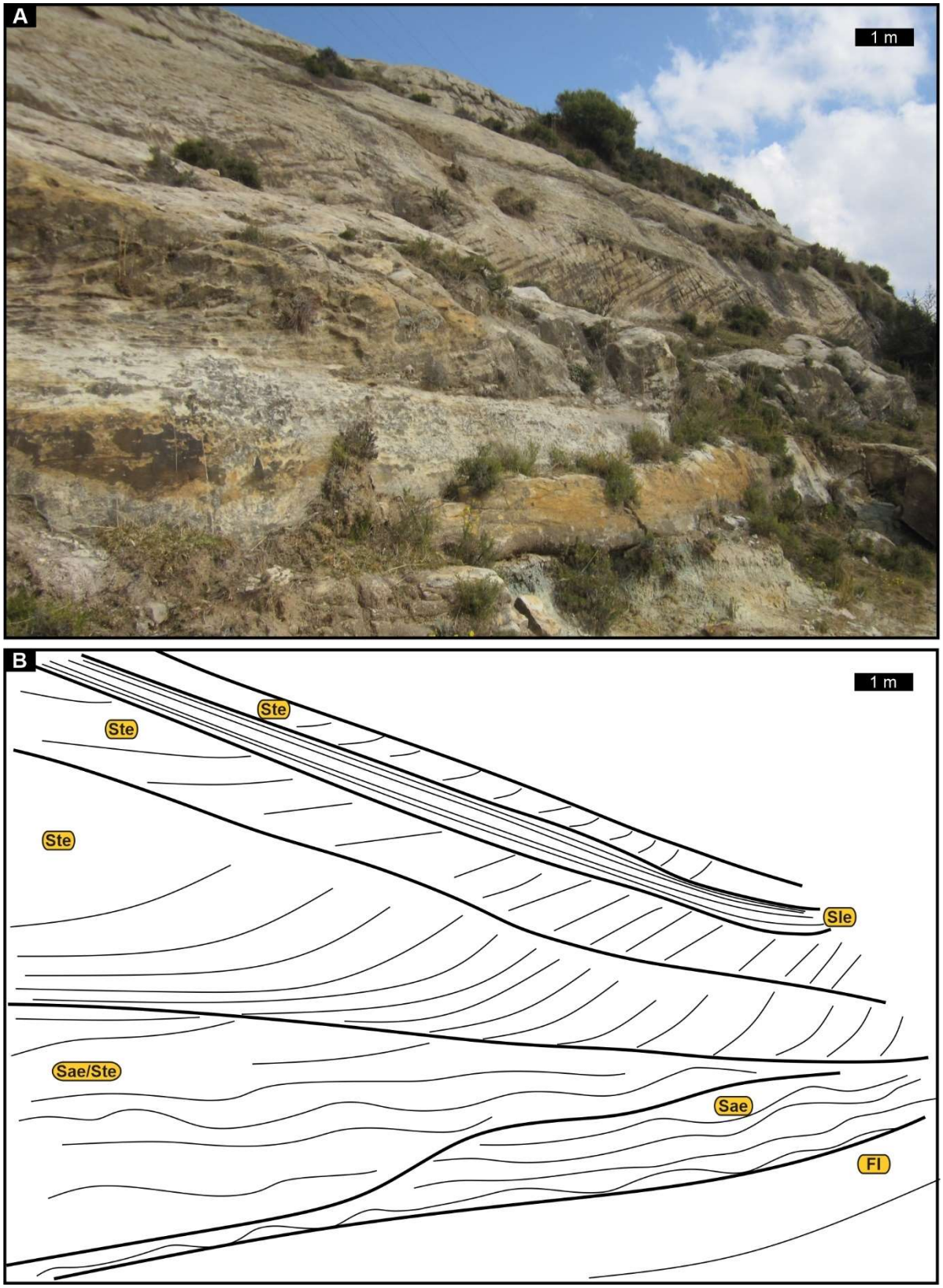

Figure 2.4: Facies Associon 1 interbedded with Facies Association 3A at the Makanyaneng site. **A**. Outcrop. **B**. Interpretative outline of B. For facies codes, see Table 2.1.

2.4.4.2. Facies Association 3B : Mokhopa type (FA3B)

Description: The Mokhopa site is located in southwestern Lesotho, close to the town of Quthing (Figure 2.1). Here, Facies Association 3B (Figures 2.2B, 2.5, 2.6, 2.7) is dominated by green to maroon sandy siltstones that are horizontally laminated (Fl; Figures 2.5E, 2.6C) and interbedded with two, fine-grained sandstone beds that are either massive (Sm; Figure 2.6C) or horizontally laminated (Sh; Figure 2.2B). The ~ 40-m-thick facies association (Figure 2.7A, B) can be traced for ~ 500 m laterally, after which it pinches out completely (Figure 2.7A, B). Facies Association 3B is exposed in an outcrop that is oriented N-S, perpendicular to the overall paleo-wind direction which was from west to east.

At the base, the siltstones are bound by prominent large-scale, cross-bedded sandstones (Ste; Figure 2.5B) that are interbedded with ~ 50-cm-thick, massive, fine- to medium-grained, lenticular sandstones (Figure 2.6D). The upper contact of the siltstones is defined by a laterally continuous, tabular, fine-grained, horizontally laminated (Sh) to low-angle, cross-bedded (Sle) sandstone. The overlying, ~ 1.5-m-thick sandstones are succeeded by large-scale, aeolian cross-bedded, fine- to medium-grained sandstones (Ste). On the bedding plane of the surface that represents the base to the siltstones, cross-bedded sandstones preserve both straight crested and linguoid ripples along with interference ripples (Figure 2.5A, C). Interbedded with the siltstones, the sandstones comprise lenticular, fine-grained, massive (Sm) and horizontally laminated sandstones (Sh) that are 1 and 1.5 m thick, respectively. Interbedding of the massive sandstones become more frequent laterally, towards the margins of the siltstones (Figure 2.6C). When exposed, the surface of the sandstone lenses dips at a slight angle towards the siltstones and preserve symmetrical ripple marks (Sr, Figure 2.5D), wrinkle structures – microbially induced sedimentary structures (MISS; Figure 2.6A), microbial matt roll-up structures (Figure 2.12B), ex-situ petrified tree trunks (Figures 2.2 and 2.5D) and adhesion structures (Sae; Fig. 2.6B).

Interpretation: The association of laminated siltstone (Fl), horizontally laminated sandstone (Sh) and massive sandstone (Sm) sandwiched between large-scale, aeolian cross-bedded sandstones suggests deposition in a wet interdune area that allowed the establishment of a lake with a diameter of at least 500 m. During the initiation of wet conditions, small interdune areas were inundated as evidenced by the ripple marks. Deposition within shallow streams that were influenced by both current-generated and wind-driven wave action took place as indicated by interference ripples, which show multiple ripple orientations. These complex interference ripple sets resulted from a multi-phase formation driven by changing hydrodynamic conditions, when flood waters recede and expose channel margins that refract the current. These refracted waves subsequently partially overprint the primary ripple sets formed by the current and both ripple orientations are then preserved (Picard and High, 1970; 1973; Bordy *et al*., 2020b). In addition, the appearance of both straight crested and linguoid ripples in close proximity, suggests the development of interdunal streams of varying energy. The massive lenticular sandstone associated with the dune strata underlying Facies Association 3B suggests mass movement processes that reworked the aeolian dunes and led to the formation of an extensive low relief interdunal surface (Hummel and Kocurek, 1983; Langford and Chan, 1988; 1989; Langford, 1989). Alternatively, these massive beds could also indicate the occurrence of sand sheets where the primary stratification is not preserved, or dust fall processes that is well known to form massive deposits (Smalley and Krinsley, 1978; Smalley and Smalley, 1983; Pye and Tsoar, 1987; Tsoar and Pye, 1989; Johnson, 1993; Pye, 1995).

Inundation of the entire interdune area is suggested by the appearance of extensive laminated siltstones on top of this interdune surface. These siltstones continued to be deposited in the

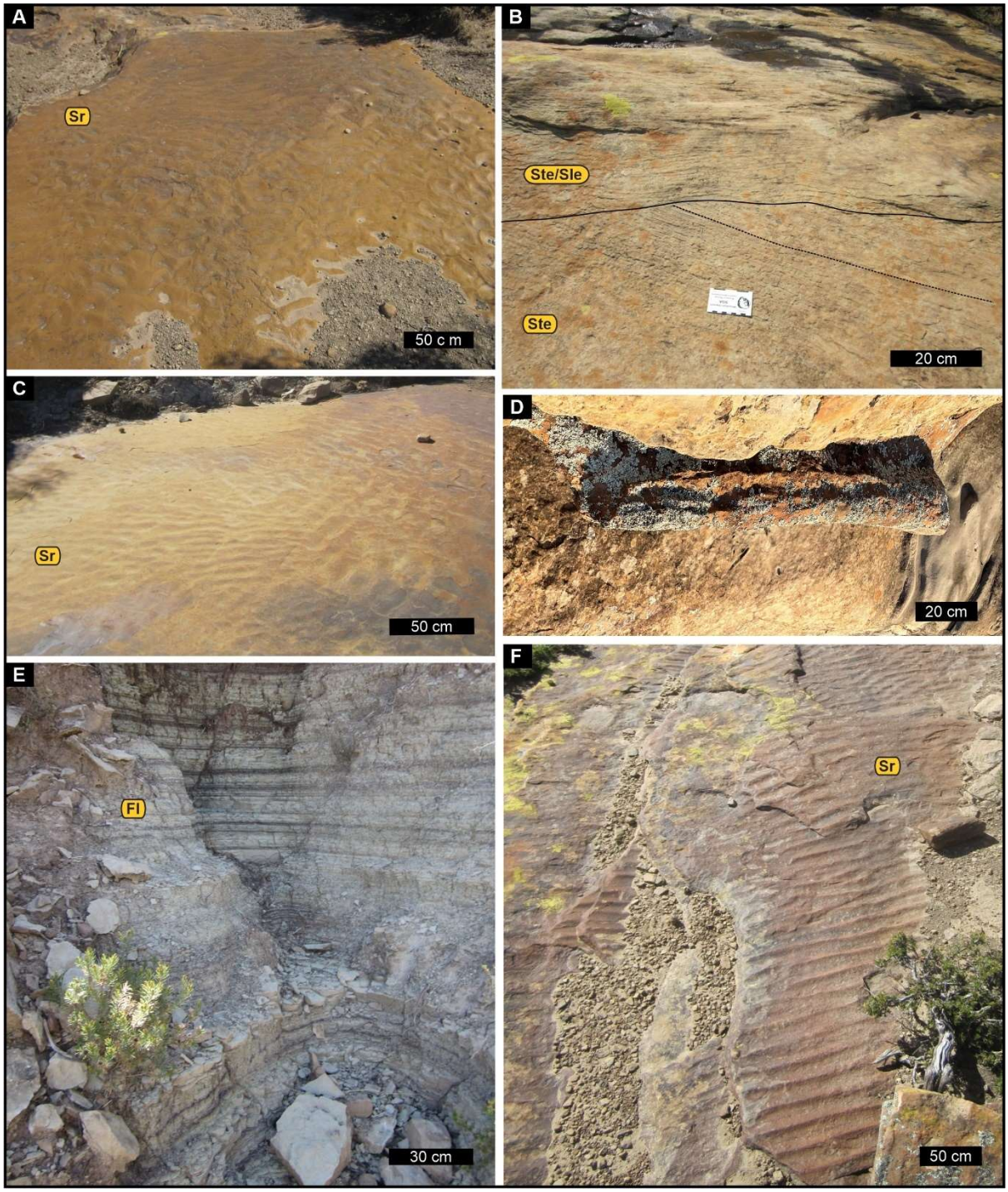

Figure 2.5: Sedimentary features of the Mokhopa site. **A**. Straight crested and linguoid ripples. **B**. Aeolian cross-bedding found below the lacustrine siltstones (not in image). **C**. Interference ripples. **D**. Ex-situ petrified tree trunk in massive sandstones. **E**. Laminated sandy siltstones. **F**. Stacked, inclined, sandstones with symmetrical (wave) ripple marks on bedding planes. For facies codes, see Table 2.1.

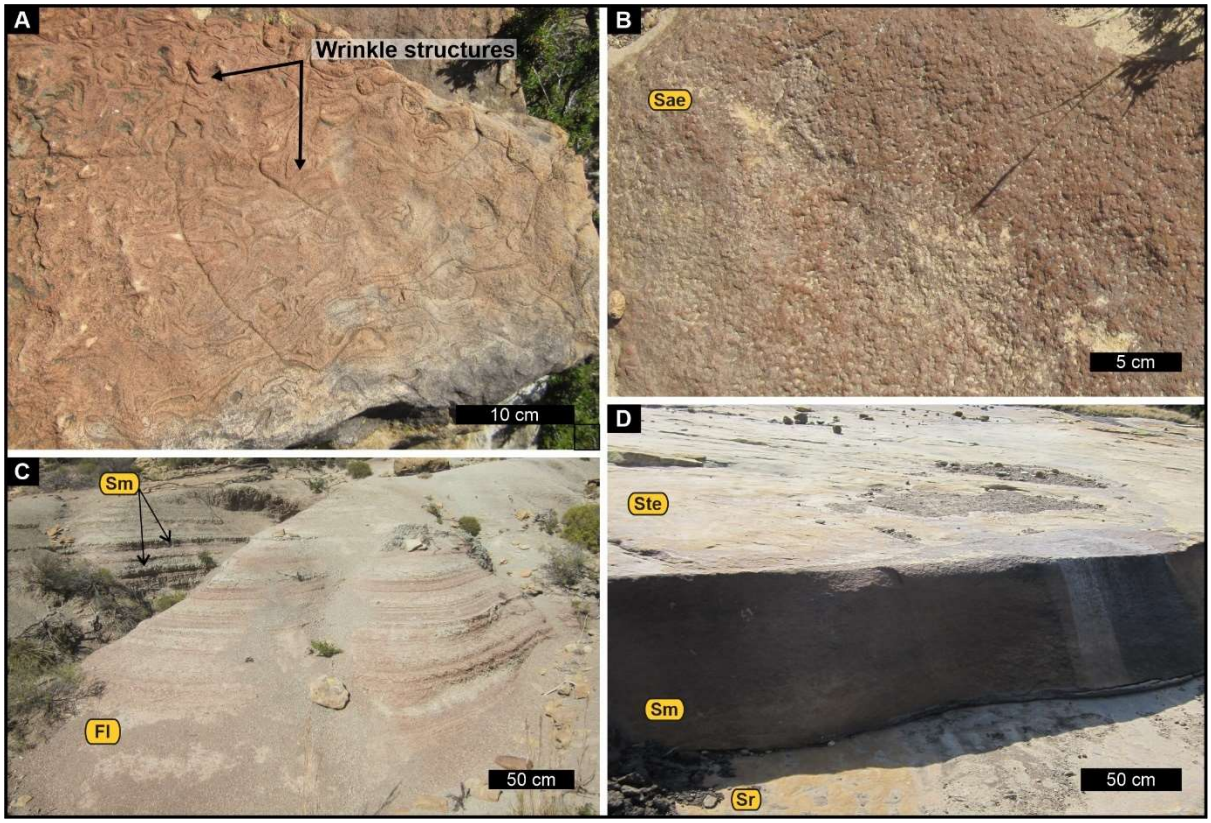

Figure 2.6: Sedimentary features at the Mokhopa site (continued). **A**. Wrinkle structures. **B**. Adhesion structures. **C**. Interbedded laminated siltstones and massive sandstones. **D**. Massive sandstone underlain by a ripple marked sandstone and overlain by aeolian cross-bedded sandstone. For facies codes, see Table 2.1.

Mokhopa interdunal lake for a prolonged period without drying out as implied by the lack of subaerial exposure features (e.g., desiccation cracks, raindrop impressions, vertebrate tracks). Short-lived traction currents were active, and continuously infiltrated the lake as suggested by the interbedded sandstone lenses that preserved stacked symmetrical ripple marked surfaces, MISS, and adhesion structures. These are collectively indicative of dynamic interdune lake margins and a spatially migrating (i.e., transgressing and regressing) lake shoreline as dictated by the alternating damp and wet conditions (Ahlbrandt and Fryberger, 1981; Kocurek, 1981; Kocurek and fielder, 1982; Hummel and Kocurek, 1983; Langford, 1989; Mountney and Russell, 2009). The inclined surfaces that dip towards the siltstones suggests that these areas were topographically higher than the interdune surface (Langford, 1989). The lack of drying features may suggest that the interdunes were continuously flooded, and this in turn suggests that the water table was located above the interdune surface. The overlying low-angle, cross-bedded sandstone could represent either an aeolian sand sheet indicating subsequent dry terrestrial conditions, or dune plinth deposits as dunes migrated over the interdune deposit (Kocurek and Havholm, 1993).

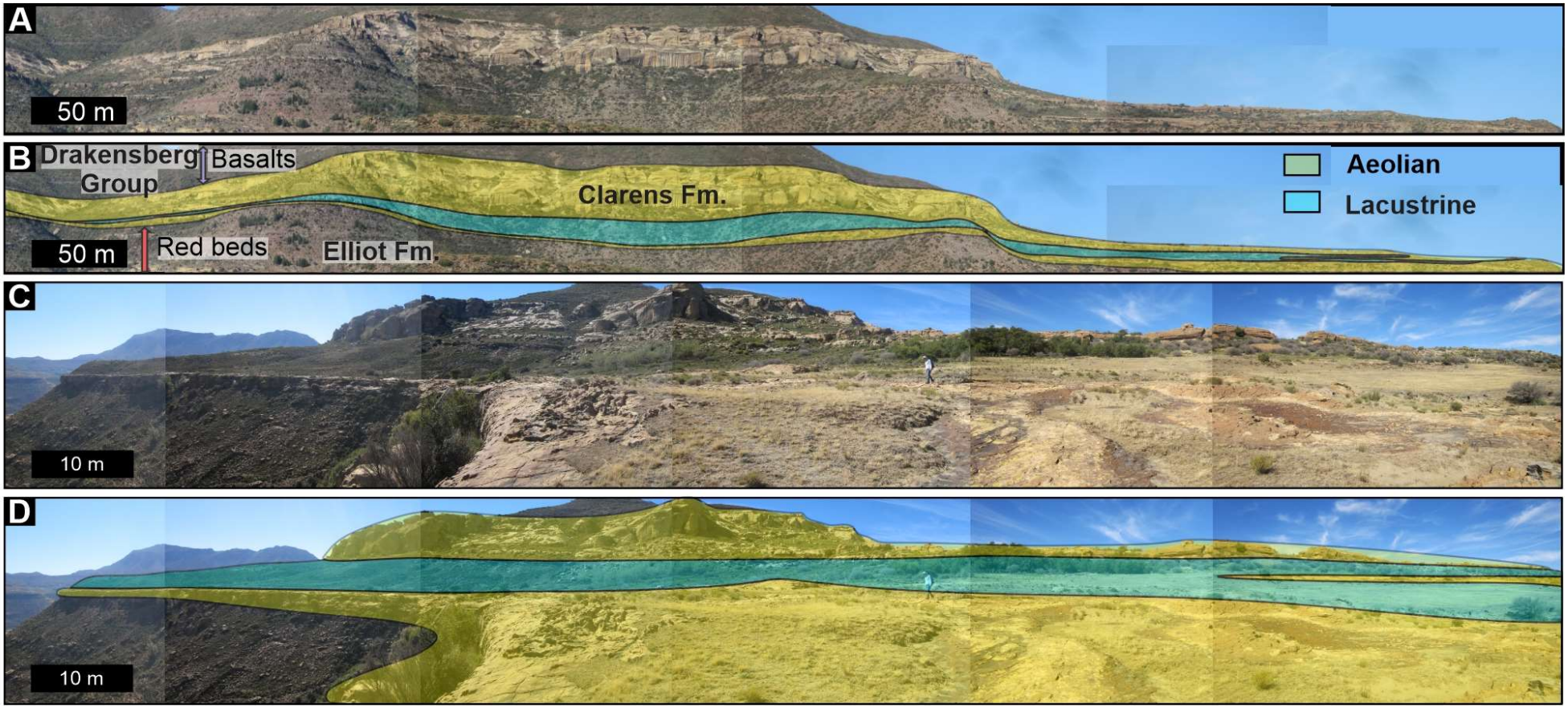

Figure 2.7: Mokhopa outcrop overview, oriented N-S. **A**. Overview of the entire outcrop. **B**. Interpretative facies overlays indicating stratigraphic context. **C**. Overview from the south. **D**. Interpretative facies overlay of C.

2.4.4.3 Facies Association 3C: Fetcaniglen type (FA3C)

Description: The Fetcaniglen lake site is located along the Lundeans Nek road, close to the town of Barkly East in the Eastern Cape, South Africa (Figure 2.1). Here, Facies Association 3C is composed of siltstone and four, fine- to medium-grained sandstone units (Figures 2.2C, 8). These four interbedded sandstones, being more competent than the siltstones, are prominent features throughout hill sides in the area, resulting in a terraced landscape, and thus are easily mappable. Facies Association 3C is bound at the base by low-angle, cross-bedded, laterally extensive tabular sandstones that overly aeolian dune strata (Figures 2.1A, 2.9B). At the top, Facies Association 3C is bound by horizontal to low-angle, cross-bedded sandstones (Figure 2.1A).

The siltstones of Facies Association 3C are laterally extensive, massive (Fm) to laminated (Fl) and their thickness ranges between 0.2 to 2 m. The laterally extensive, tabular, and mostly massive sandstone bodies have sharp lower contacts, and are 0.3 to 1.5-m-thick (Figure 2.2C). Moreover, sandstones with horizontal (Sh) to low-angle, cross-bedding (Sl; Figure 2.10A) are also preserved in the upper parts of Facies Association 3 C (Figure 2.2C). Hummocky cross-stratification in a ~ 15-cm-thick bed is also present within a tabular sandstone and is sandwiched between two thick massive sandstone beds (Figure 2.9EF). Load casts (Figure 2.9D) along lower bedding planes, and rip-up mudstone-clast conglomerates (Figure 2.10B) in the lower part of the beds can be relatively common, and so are ripple marks (Figure 2.9A) along upper bedding planes. In addition, sandstone bedding planes also preserve drag marks (Figure 2.9C), wrinkle structures and microbial mat textures (Figure 2.12 A, D, E), which are identified as MISS. In some of the thinner massive sandstones, wood fragment impressions (Figure 2.10E) and meso- and micro-charcoal (Figure 2.10C, D) were identified based on the criteria of Scott *et al*. (2010; e.g., lustrous sheen, black streak, brittleness). In addition, the microcharcoal appears as black laths, distributed among fine-grained sand to silt particles, with the cellular structure still intact (Figure 2.10C).

The Fetcaniglen lake site also contains a horizon with carbonate nodules identified as siderite based on its dark brown colour. Two different types of siderite concretions are present. Type 1 concretions are small, roughly 2-3 cm in diameter, spherical bodies that are common along the upper bedding plane of a sandstone layer that also preserves a microbially induced surface texture (Figure 2.12E) and within thicker sandstone beds. Type 2 concretions are larger, 5 – 10 cm in diameter, ellipsoidal bodies that internally show a continuation of primary layering of the host, mostly 5 cm-thick sandstones (Figures 2.12 C). The layering is horizontal in the centre part of the nodule and slightly curved in outer layers. In addition, surrounding upper and lower sedimentary strata also show deformation around the concretion (Figure 2.12C).

Within the same overall stratigraphic interval, roughly 1.6 km northeast of the main study site, 0.5-m-thick, fine- to medium-grained, wavy-laminated sandstones (Sae) and massive sandstones (Sm) are observed and are sandwiched between large-scale, aeolian cross-bedded sandstones (Ste) that preserve an array of sedimentary structures on their upper bedding planes. These range from symmetrical ripple marks with a resting trace that may resemble *Lockeia* (Figure 2.11E), adhesion structures (Figure 2.11D), wavy lamination (Figure 2.11B), runzel marks (Figure 2.11A), dendritic rill marks (Figure 2.11A), and ichnofossils of possible snail trail or flying trace origin (Hasiotis *et al.,* 2012; Hasiotis, 2006 - Figure 2.11C). The latter is presents as a shallow thin trail, roughly 3 mm in uniform diameter having a length of 30 cm. The combination of various crossing loops and sinuous lines give it an irregular curvilinear shape.

Interpretation: The association of laminated siltstones (Fl), massive sandstone (Sm), horizontally laminated sandstone (Sh), and low-angle cross-bedded sandstones (Sl) are indicative of a wet interdune setting that preserved the sediments of both lacustrine and fluvial flood related processes. The appearance of horizontal bedding to low-angle cross-bedded sandstones (Sle) in Facies Association 3C is interpreted as dry interdune sand sheets. Given the extent (up to 8 km) and thickness (~ 50 m) of Facies Association 3C at the Fetcaniglen site, low-angle cross-bedded sandstones (Sle) most likely reflect the development of aeolian sand sheets on an extensive interdunal plain (Kocurek, 1981). Sand sheets usually develop where conditions for aeolian dune formation is lacking due to limited dry sand supply (Kocurek and Lancaster, 1999). Moreover, their formation has been linked to flooding that flattens the dune topography and reworks dunes into sheets of sand (Kocurek and Nielson, 1986; Lancaster, 1989). The onset of flooding is therefore associated with the development of sand sheets at the Fetcaniglen site.

Thick, laterally extensive laminated siltstones without any desiccation cracks suggests the rise of the water table above the surface of the interdunal plain and thus the establishment of a lake system that was ~ 8 km in diameter (Figure 2.8A). Massive sandstones within the laminated siltstones indicates that sediments, brought by running water, entered the lake body during flooding events. Moreover, the lack of desiccation features suggest that the area remained flooded for a prolonged period. Hummocky cross-stratification is associated with the occurrence of surface storm waves (Harms, 1979; Morsilli and Pomar, 2012) and have been identified in lakes with depths between 1 and 2 m (Duke, 1986; Greenwood and Sherman, 1986) and even up to 20 m (Eyles and Clark, 1986, Morsilli and Pomar, 2012). Transported debris that dragged and scraped the substrate on the lake floor is evidenced by abundant drag marks on the upper bedding planes of sandstones along with the preservation of microbial surface textures that show deformation along drag grooves. The combination of these features and the lack of desiccation structures not only suggest that the area was permanently flooded, but also that the shallow lake that occupied it was subject to periods of low sedimentation rates (Nofke *et al* 2001; Davies *et al*., 2107). In addition, the preservation of tool mark, drag marks and microbial surface textures as well as the load casts collectively suggests that the episodic depositional events that generated currents in the lake were not always erosive, and that their sediments passively and rapidly blanketed the lake floor.

The presence of ripple cross-lamination and ripple marked surfaces on the bedding planes of interbedded sandstones suggest the weakening of the flow strength within the lake basin to such a degree that low energy features could form and eventually suspension settling took over as the water table remained above the interdune surface. In this interpretation, these sandstones are the result of short-lived, high-energy flood events that typically result in horizontal layering in sandstones with sheet-like geometries (Mckee *et al*., 1966, Langford and Chan, 1989). The symmetrical ripple marks found 1.6 km away from the main site (Figures 2.8, 2.11E) suggest that gentle, oscillatory currents were active along the lake shore. The occurrence of wavy laminated sandstone indicates that here, winds were actively depositing sand onto damp surfaces (Kocurek, 1981; Kocurek and Fielder, 1982; Hummel and Kocurek, 1984). Dendritic rill marks have been observed in aeolian environments in association with slumping of dunes (Picard and High, 1973) and thus these rill marks may indicate the continuous reworking of dunes along the lake margin, together with massive sandstones that also suggest mass movement processes such as dune slumping. The possible snail trail or fly traces, together with the other biogenic structures (e.g., plant fossils, MISS), show that the lake was able to support a fairly diverse biota (for their interpretation, see the Discussion). It should be noted that the siltstones could not be traced into the interpreted lake margin setting (location I on Figure 2.8), and for this reason could also represent an isolated damp to wet interdune that was coeval but spatially isolated of the Fetcaniglen lake.

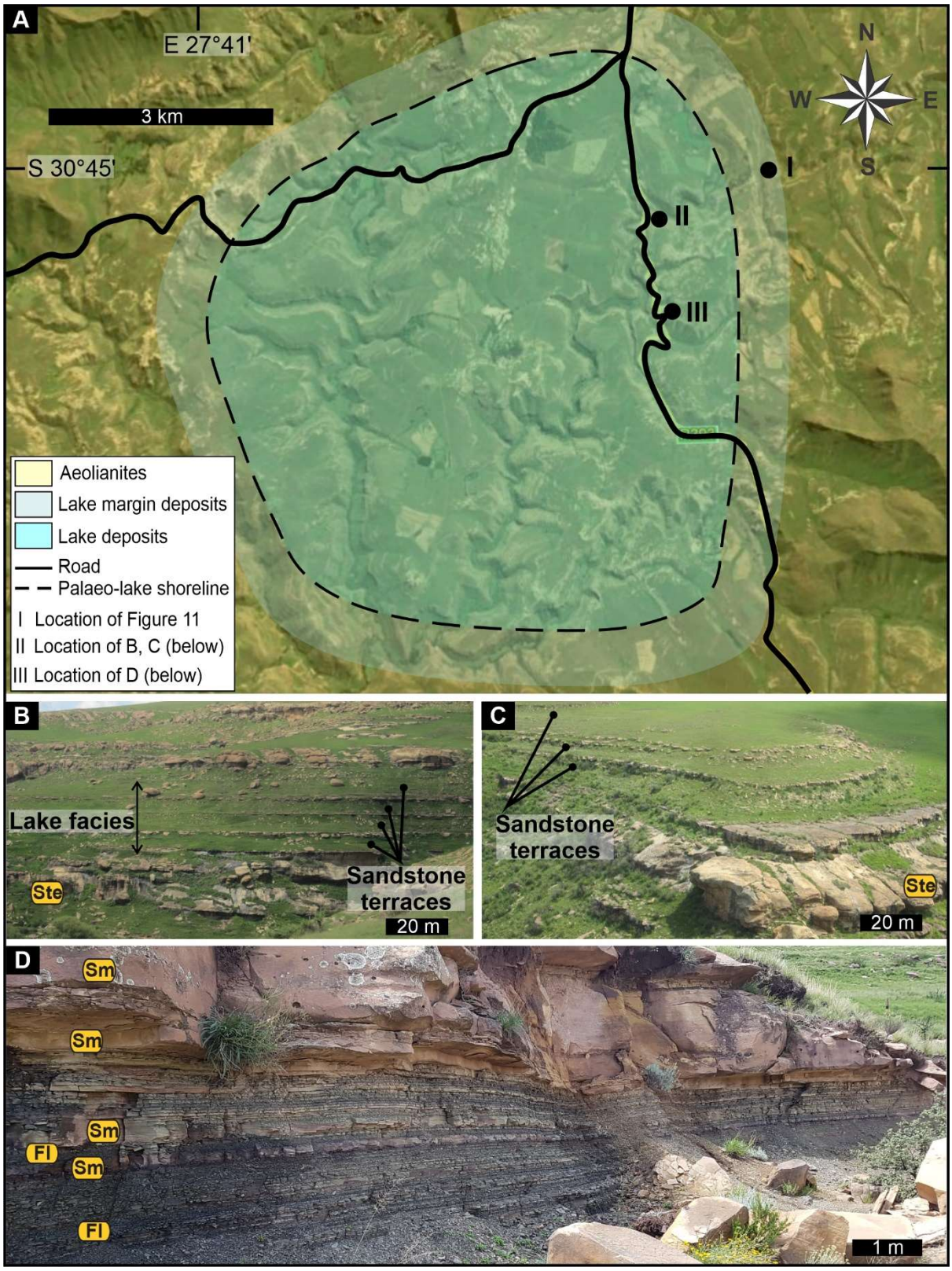

Figure 2.8: Large-scale facies relationships at the Fetcaniglen lake site. **A**. Facies map show the position of images B, C and D as well as Figure 2.11. **B**. Outcrop of Facies Association 3C looking east. **C**. Outcrop of Facies Association 3C, looking west. **D**. Close-up view of the interbedded sandstones

and siltstones within Facies Association 3C. For facies codes, see Table 2.1. Base map from Google Earth**.**

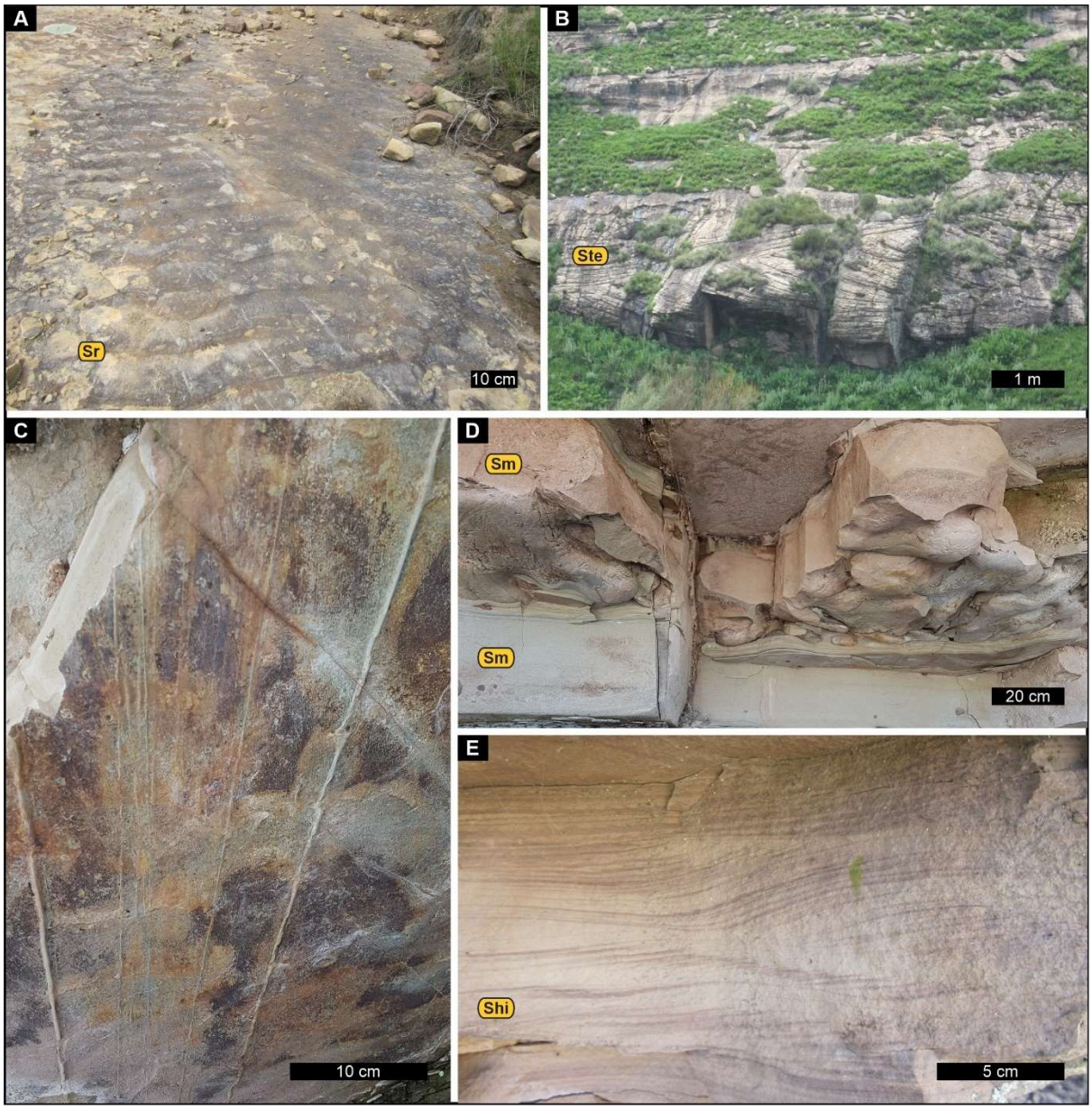

Figure 2.9: Sedimentary features at the Fetcaniglen lake site. **A**. Ripple marks found at the base of the siltstones. **B**. Large-scale aeolian cross-bedding. **C**. Drag mark casts on the lower bedding plane of a sandstone. **D**. Load casts at the base of a massive sandstone. **E**. Hummocky cross-stratification.

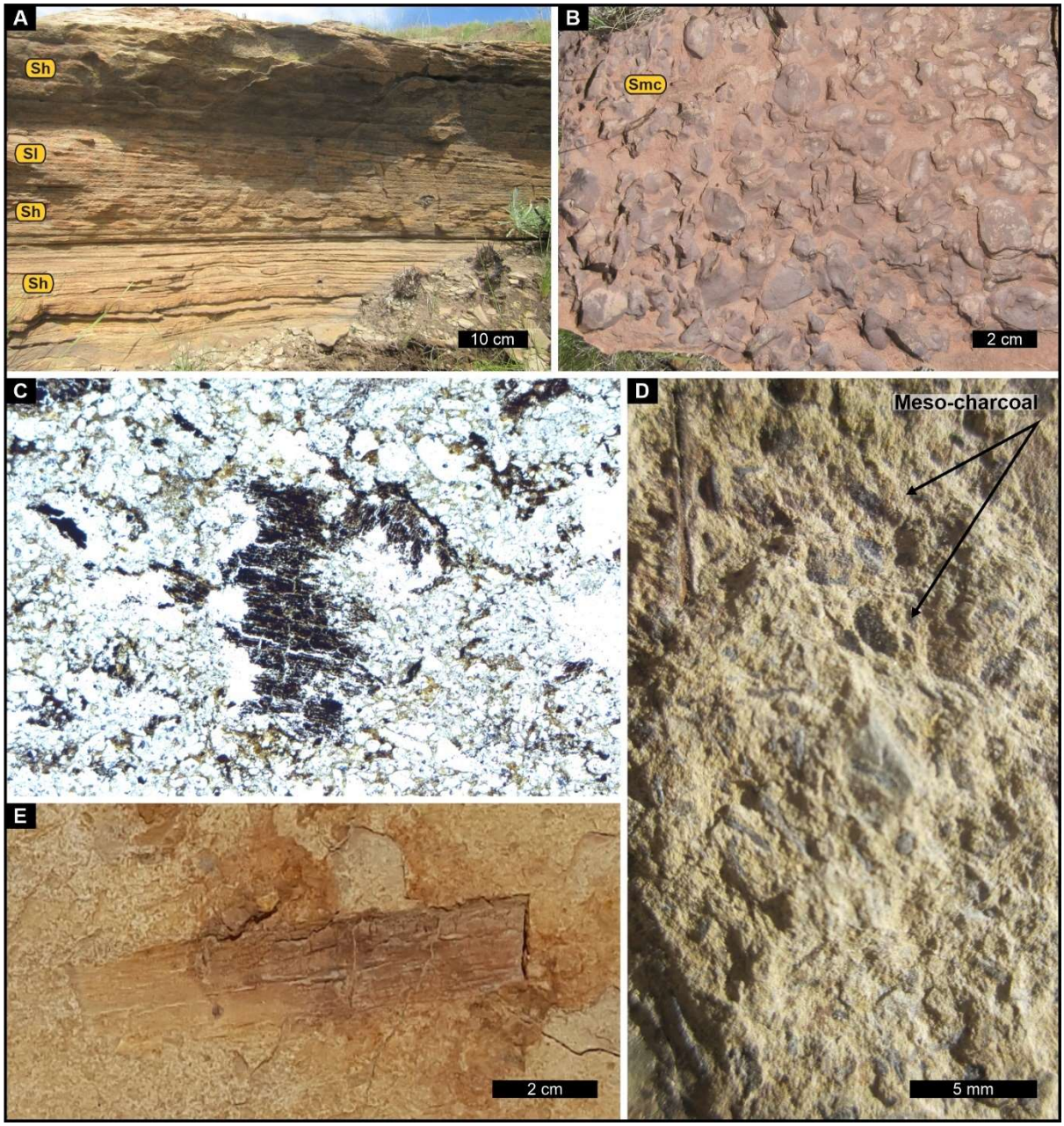

Figure 2.10: Sedimentary features at the Fetcaniglen lake site (continued). **A**. Sandstone with horizontal lamination and low-angle cross-bedding. **B**. Intraformational rip-up mudstone clast conglomerate. **C**. Photomicrograph of micro-charcoal with lath-shaped cellular structures. **D**. Massive sandstone containing both plant fragments and meso-charcoal. **E**. Plant impression with cellular structures. For facies codes, see Table 2.1.

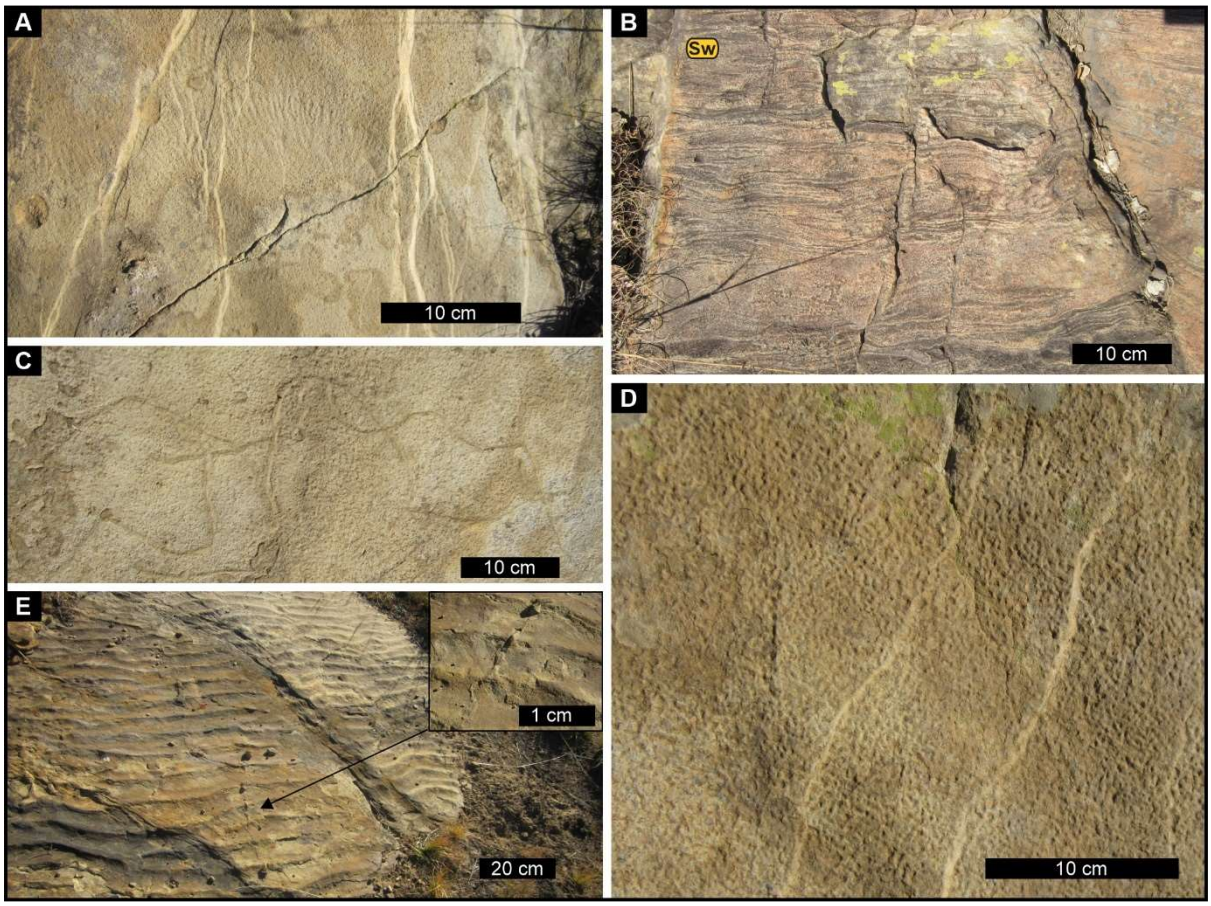

Figure 2.11: Sedimentary structures observed north-east of the study site (location of this site is marked as I on Figure 2.8). **A**. Runzel marks and dendritic rill marks. **B**. Wavy lamination. **C**. Ichnofossils interpreted as locomotion trace of possible snail trail or flying traces. **D**. Adhesion structures. **E**. Symmetrical ripple marks. Note the distinct resting trace in the foreground that resembles *Lockeia* isp. – see inset. For facies codes, see Table 2.1.

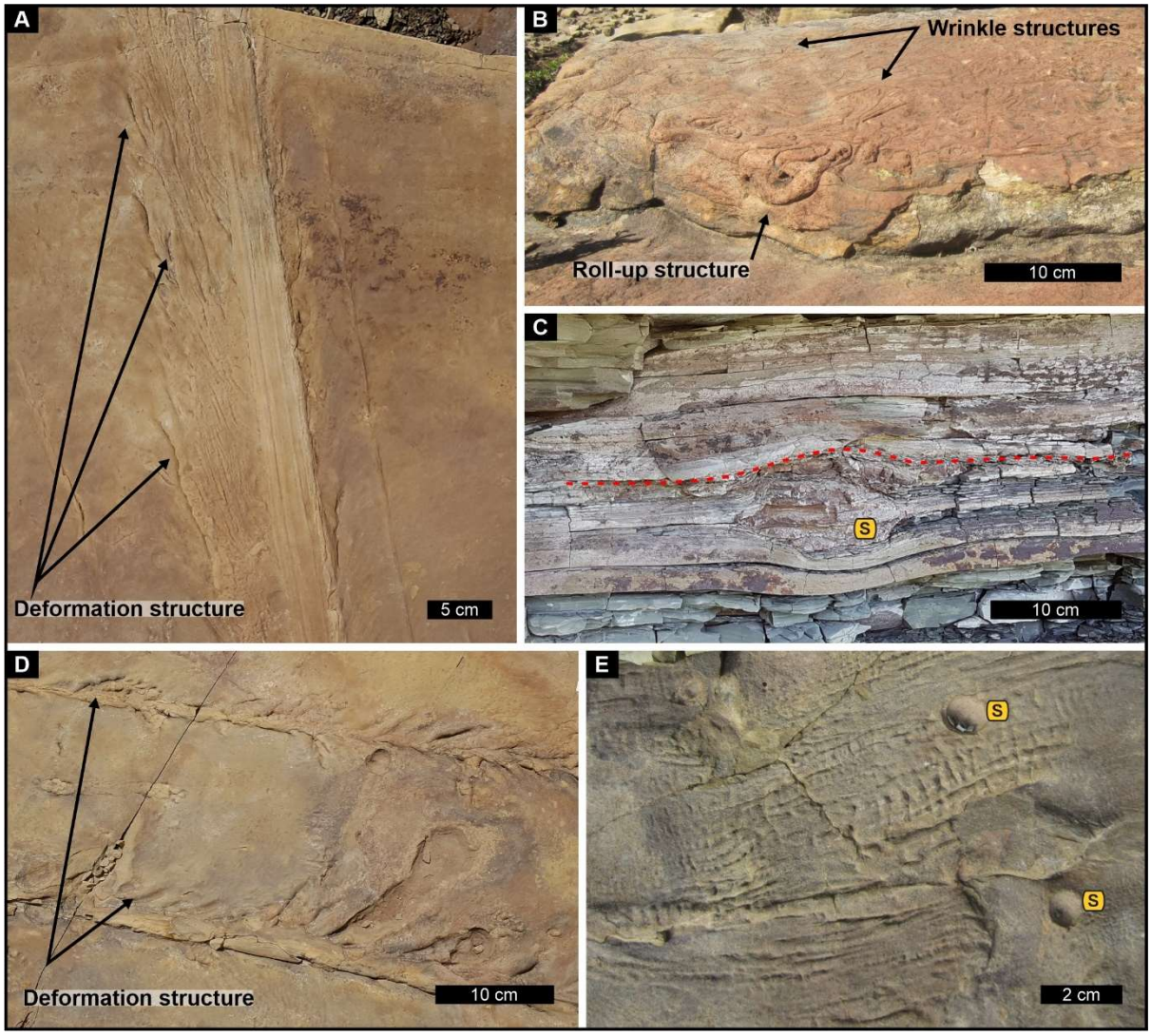

Figure 2.12: Microbially induced sedimentary structures (MISS) and siderite nodules (S). **A**. Drag marks with deformation. **B**. Mat roll-up structure with wrinkle structures on top (as seen in Figure 2.6 A). **C**. Siderite nodule (upper deformation indicated by red dashed line). **D**. Drag mark casts on the base of sandstone showing deformation of the substrate. **E**. Microbially induced sedimentary structure that resembles *Microcoleus* sp. Note the siderite nodules (S).

2.5. Discussion

2.5.1. Palaeoenvironmental implications of key sedimentary structures in the lake deposits

2.5.1.1. Microbially induced sedimentary structures (MISS)

The identification of MISS within the geological record is complex as biotic and abiotic processes can lead to the preservation of morphological features that are sometimes indistinguishable (Davies *et al*., 2016). However, by contextualising the surface textures and providing detailed descriptions, the presence or absence of microbial activity can be inferred with a reasonable level of certainty. Due to

the uncertainty related to a MISS diagnosis, Davies *et al*. (2016) developed a classification scheme for suspected MISS structures. Their objective naming approach allows for the uncertainty to be directly related to the classification. Wehrmann *et al*. (2011) described microbial mats in a Triassic siliciclastic playa environment and attributes the appearance of detached pieces of the microbial mats to frequent reworking. In the inland saline lakes of Spain (Geurrero *et al*., 1994), cohesive and thick mats are found in areas where sediments are permanently covered by water. These microbial mats occur in very specific conditions within the depositional environment, characterised by a substrate of quartz-rich, fine-grained sand with moderate hydraulic energy (Guerrero *et al*., 1994; Noffke, 2010), all of which are associated with deposits of the interdunal lakes of the Clarens Formation.

Given these parameters, the probable preservation of MISS within the lake deposits of the Clarens Formation is based on the following criteria. Firstly, the surface textures at the Fetcaniglen lake site shows distinct deformation structures that are indicative of cohesive sediment behaviour. These deformation structures are associated with ripple marks that occur within stacked sandstones and are mostly observed in interdune or saline playa deposits (Schieber *et al*., 2007). The destruction features may be suggestive of desiccation, although no other evidence is apparent for drying.

Secondly, the surface texture identified at the Fetcaniglen site closely resembles that of *Microcoleus* sp. and has been identified in modern inland saline lakes and deserts (Geurrero and de Wit, 1992; Belnap, 2005). Furthermore, what appears as a chevron-like structure differs from the classical chevron mark (see Reineck, 1980 and references therein) by retaining a linear groove cast throughout. This suggests that the chevron-like structure is a result of deformation of a cohesive surface by means of drag marks. For these reasons, surface textures described occurring in interdunal sandstones of the Clarens Formation can be classified as 'Ba' (i.e., Similar form to modern MISS; structures indicating hydrodynamics conditions of deposition) in the classification scheme of Davies *et al*. (2016), which implies a putative MISS classification with a relatively high likelihood of having a MISS origin.

The development of primary sedimentary surface textures takes place during stages of stasis of the sedimentary system, and the time required for these microbial mats to grow during these periods are particularly important for the development of microbial surface textures (Gerdes, 2010; Davies *et al*., 2017). During these periods of stasis, microbial mats are subjected to various morphological changes brought on by responses to environmental factors, growth, decay, and degradation. This would imply that during the development of MISS surface textures within the Fetcaniglen lake site, the lake was subjected to periods of stasis, where little to no sedimentation or erosion was taking place. In addition, to be preserved and enter the geological record, the subsequent sedimentation event must be of relatively low energy to prevent the destruction of the surface texture. All in all, the preservation of MISS at the Mokhopa and Fetcaniglen sites suggests that substrate conditions within the lakes were episodically conducive to the development of microbial mats and that the lakes were shallow and calm (subjected to moderate hydraulic energy) between flooding episodes.

2.5.1.2. Charcoal

The co-occurrence of plant fragments (phytoliths) with meso- and micro-charcoal within Facies Association 3C (Fetcaniglen type) suggests that these particles experienced very little transport from a nearby source (Scott *et al*., 2000, Scott, 2010). The charcoal is associated with a structureless sandstone, which could indicate a mass movement process, such as a hyperconcentrated flow into the interdune during a storm flooding event (e.g., Muir *et al*., 2015). Of greater significance is the

overall implication that the presence of charcoal has for the palaeo-environment. The formation of wildfires is mostly associated with the interplay of climate and weather conditions that control the availability of fuel, fuel moisture, and the provision of an ignition source (Tooth *et al*., 2009; Muir *et al*., 2015; Bordy *et al*., 2018). With this in mind, for the occurrence of wildfires within the Clarens Formation palaeo-environment, enough biomass had to be available, along with associated storm events that triggered the wildfires. Given the overall palaeo-environment interpreted as a desert sand sea, the occurrence of large quantities of biomass is not typically expected, but long-lived wet interdunal lakes could have provided the ideal conditions to support localised palustrine wetland habitats as part of an overall lacustrine ecosystem. Therefore, the occurrence of the charcoal is an indication that, at least locally, sufficient biomass was available to sustain wildfires.

2.5.1.3. Siderite concretions

Type 2 siderite concretions (See section 3.4.3) are described by Sellez-Martinez (1996) as having formed by displacive growth during diagenesis, while the layer retained an adequate elasticity that would have made the deformation possible as the concretion grew. This implies a multi-stage growth pattern where the initial concretion continued to grow, while subsequent compaction deformed the under- and overlying strata relative to the rigid concretion (Raiswell, 1971; Marshall and Pirrie, 2013). Additional growth stages led to the preservation of the deformed layering within the overall concretion along with associated deformation of the surrounding sedimentary strata. The spherical shape of the Type 1 siderite concretion suggests a shallow burial depth with a low overburden pressure influencing compaction during cementation, which is a function of the sedimentation rate (Majewki, 2000).

Concretions have been associated with organic carbon bearing sediments as well as microbiological carbonate sources in the depth ranges where microbial processes occur (Raiswell, 2000), and where nucleation and cementation are believed to take place close to the sediment-water interface (Fisher *et al*., 1998; El Albani *et al*., 2001; Bondioli *et al*., 2015). These concretions only form where enough time is allowed for diffusion of ions through the sediment column and implies formation during phases of slower sedimentation rates (or hiatuses) (Majewski, 2000; Marshall and Pirrie, 2013). If similar conditions were at work during the formation of these concretions within the Fetcaniglen lake site, an early diagenetic origin can be assumed, and the appearance of both concretion types may imply that sedimentation rates fluctuated during the depositional history of the Fetcaniglen lake.

2.5.2. Palaeoenvironmental reconstruction of pluvial facies

Throughout the MKB (Figure 2.1), interdunal deposits are comparatively rare in the lower and upper Clarens Formation, mostly appearing associated with the development of damp and wet interdune conditions. These damp to wet interdune areas represents development of lacustrine conditions in response to various controlling parameters. The combined effect of aeolian sand availability, dune migration, and water-table fluctuation manifests in different ways resulting in preservation of a variety of interdune-dune architectural configurations that reveal controls driven by subsidence and climatic variation (Kocurek and Havholm, 1993; Carr-Crabaugh and Kocurek, 1998; Mountney and Thompson; 2002, Mountney, 2006; Mountney, 2012). Given these parameters that control deposition, the described interdunal ponds and lakes of the Clarens Formation can be assessed to define the interplay of these paraments that resulted in the formation of each specific interdunal

pond or lake. In our study, the classification of ponds and lakes are hinged on the relative scale of each type as compared to the other, and therefore, facies associated with pond interpretations have a relatively smaller scale as compared to the facies associated with lake interpretations.

The thin, lens-like architecture of FaciesAssociation 3A association at the Makanyaneng site (Figure 2.3, 2.13) suggests the development of wet interdunal conditions within an isolated depression like a pond, where interdunal space was severely restricted and controlled by migrating dunes (Deynoux *et al*., 1989; Mountney and Thompson, 2002). The restricted nature of the interdunes limited fluvial activity within the dune field to small ephemeral streams along dune slopes, and water from precipitation events would have been incorporated into the ground water through infiltration, allowing for sporadic water-table rise. A water-table situated close to the accumulation surface would have been very sensitive to climatic fluctuations, and even minor precipitation events would have resulted in a rapid water-table response (Tyler *et al*., 2006; Shaw and Bryant, 2011). Alternatively, the appearance of spatially limited damp to wet interdunes could represent an area where aeolian scour took place down to the water table, however, this would result in isolated deposit of this nature (Mountney and Jagger, 2004). At least two of these damp to wet interdunes were identified within the outcrop area of the Makanyaneng site, making the former more likely.

The close spatial relationship of dune toesets and wavy lamination suggests that active dune migration was concurrent with interdunal lake development and that a climbing dune system must have been active (Pulvertaft, 1985; Mountney and Thompson, 2002). High migration rates and fluctuating water-table responses resulted in the formation of lenses of damp and wet interdunes as dunes moved over and closed interdunal space. Similar conditions have been described by Mountney and Thompson (2002) for the Helsby Sandstone Formation (UK), where a rising water table intersected interdunal hollows that were spatially controlled by aeolian dune strata. Although similar in geometry and development, the Makanyaneng site does not exhibit evidence for episodic drying, which indicates that it was linked to a longer-term absolute water-table rise. In this case, a humid climatic phase, combined with a high sediment supply and strong winds played an active role in the continued development of wet aeolian conditions in an overall dry aeolian system (Clark and Rendell, 1998). The high sediment availability could stem from the position of the Makanyaneng site closer to the erg center. Overall, the Makanyaneng site reflects a progressive transition from damp to wet interdunal deposition, when a high water-table allowed for the accumulation of silt in a small shallow pond setting.

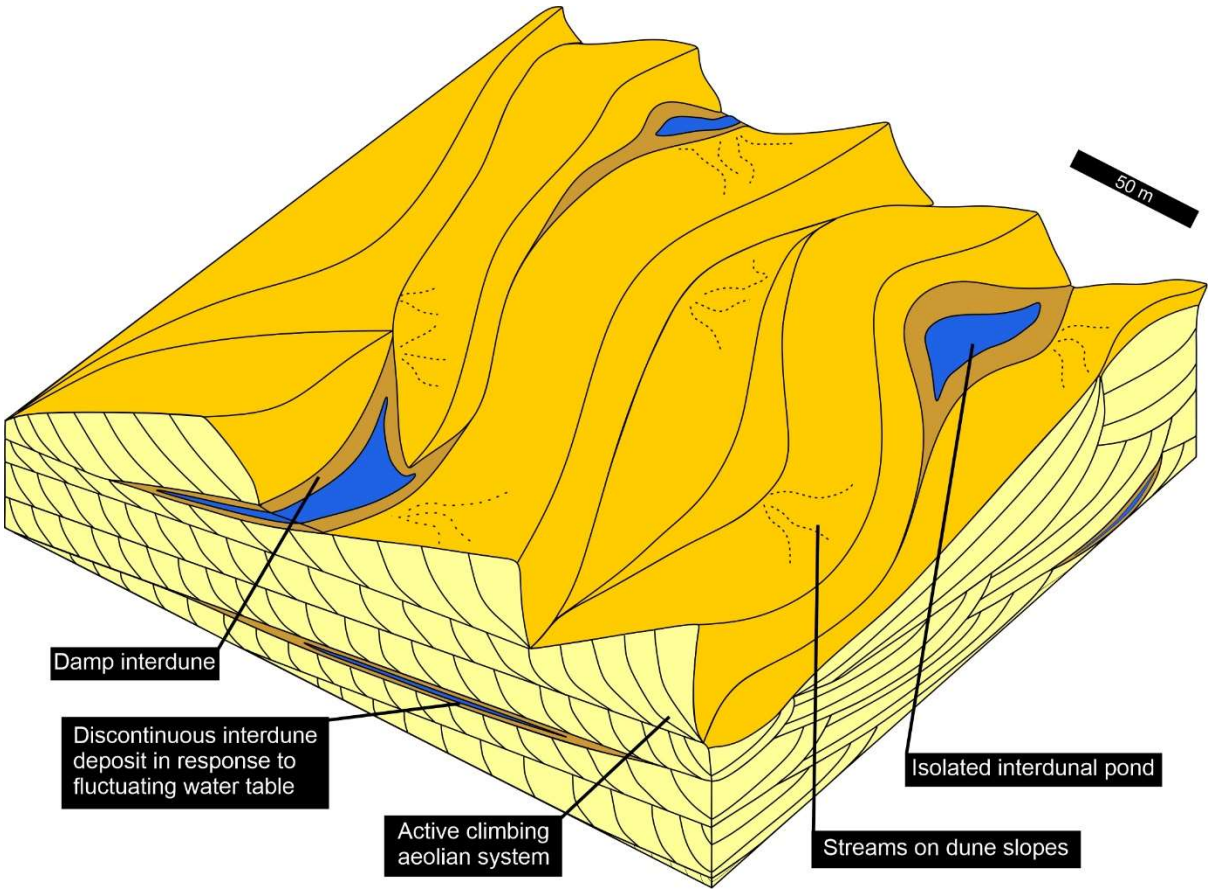

Figure 2.13: Palaeoenvironmental reconstruction of the interdunal ponds at the Makanyaneng site.

The Mokhopa site records a gradual rise in the water table expressed in the inundation of isolated interdunes (Figure 2.14). In cases where the water table fluctuates, periodic wetting and drying will be recorded, however, an overall absence of drying features for the Mokhopa site points to the development of a relatively long-lived shallow lake within the newly formed interdune, while still confined by surrounding dune strata. Flooding in the interdune resulted in flattening of the interdune area by eroding and reworking of dunes. The limited preservation of fluvial deposits suggests that interdune flooding can be ascribed to a rise in the groundwater. Where the water table and sediment supply are in equilibrium for extended periods of time, an interdunal expansion would be expected (Figure 2.14; Kocurek and Havholm, 1993). Moreover, the downwind perpendicular extent as well as the observed sedimentary features of the wet interdune recorded at the Mokhopa site suggest reorganisation of the dune field and eventual merging of isolated interdune ponds (Hummel and Kocurek, 1984; Langford, 1989; Mountney and Jagger, 2004; Mountney, 2012, Mckie, 2011).

This reflects similar conditions as described for the Cutler Formation and Cedar Mesa Sandstone in the USA (Langford and Chan, 1989; 1989; Mountney and Jagger, 2004), suggesting an aeolian-dominated erg margin (Mountney and Jagger, 2004) where isolated interdunes became locally connected to form a wet interdune corridor.

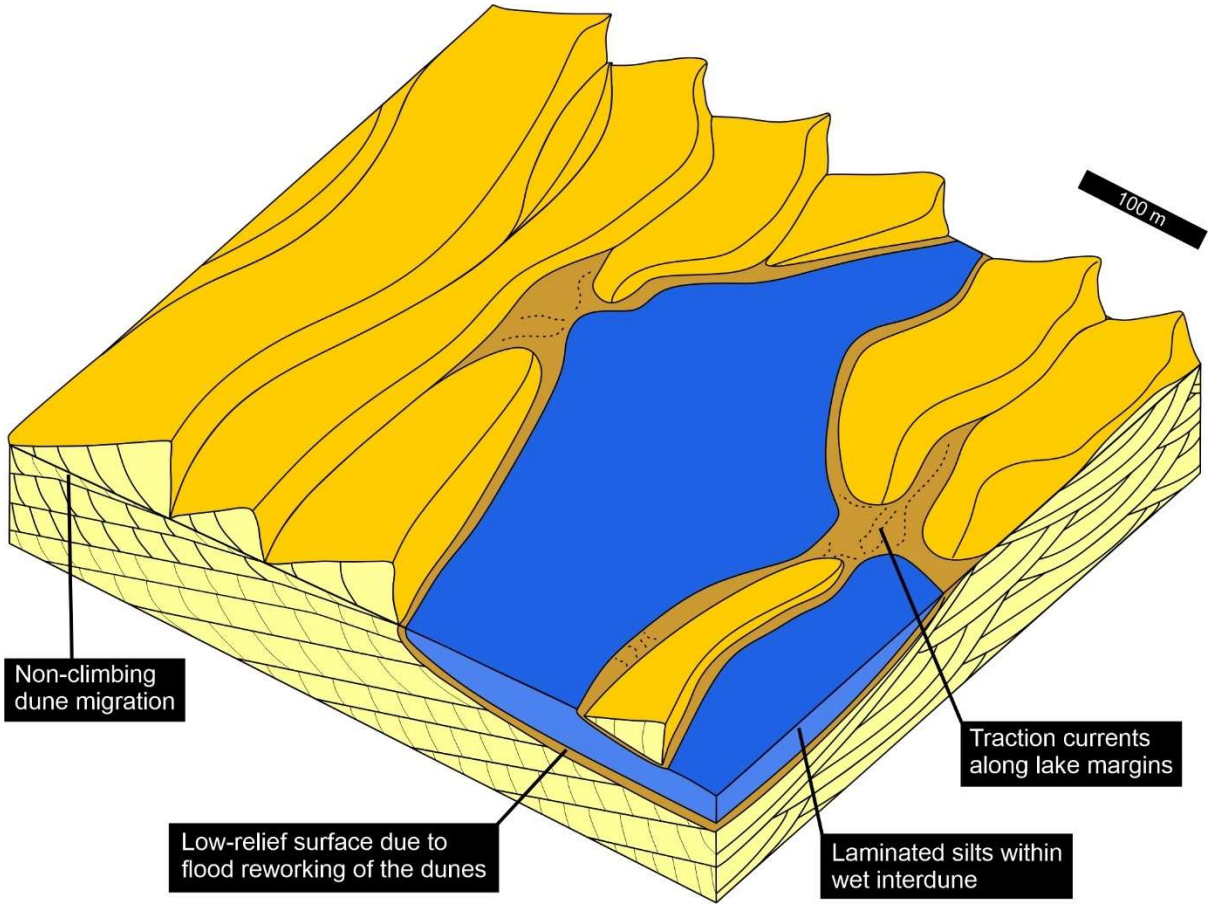

Figure 2.14: Palaeoenvironmental reconstruction of the interdunal lake at the Mokhopa site.

The Fetcaniglen site represents the largest interdune succession (both vertically and laterally) observed within the Clarens Formation so far. The development of such extensive interdune flats have been described by Wilson (1972) within compound draa, where these slow moving bedforms develop large interdunes (Ahlbrandt and Fryberger, 1981; Langford, 1989). The onset of wet conditions at the Fetcaniglen site is marked by the presence of aeolian sand sheets (Kocurek and Neilson, 1986; Langford, 1989; Hummel and Kocurek, 1994), which have been linked to flooding and in turn a limited sand availability due to moisture. This lack of sediment availability for aeolian transport allows for the wind to become undersaturated with regards to its carrying capacity, which results in the reworking of existing dunes to form sand sheets (Mountney and Thompson, 2002; Mountney, 2006). A similar occurrence has been described by Kocurek and Nielson (1986), where flooding promoted the development of sand sheets at Padre Island in Texas by reworking dunes and inhibiting dune formation. The development of wet conditions may have been linked to a rise in the water table, which ultimately led to the establishment of a lake when the water-table was situated persistently above the surface of the interdunal area.

Fluvial related flooding within the Fetcaniglen interdunal lake is linked to repeated large-scale flooding events that discharged water and sediment into the lake (Figure 2.15). Floods in aeolian setting are generally characterised by hyperconcentrated flows during extreme storm events (Svendsen *et al*., 2003; Gibling, 2006). Where these hyperconcentrated flows enter water bodies, subaqueous hyperconcentrated flows can occur (Mulder and Alexander, 2001), and result in the deposition of massive sand bodies, which may be deposited in stages of incremental build up (Major,

1997). Furthermore, during hyperconcentrated flows, hydroplaning can occur and inhibit erosion of basal sediments during these high velocity flows (Mohrig *et al*., 1998; Mulder and Alexander, 2001), which may explain the preservation of drag marks and deformed microbial surface textures along bedding planes.

In contrast, the occurrence of horizontal lamination and low-angle cross-bedded sandstones with basal rip-up mudstone-clast conglomerates that are found in the upper part of the Fetcaniglen site may represent more tractional flows during the waning stage of floods. The presence of ripple marks on the bedding plane also suggests progressive deceleration of flow conditions. Evaporites were not found within the Fetcaniglen site (or anywhere within the Clarens Formation), and this may be the result of the water sources combined with the mineralogy of the surrounding rocks, which play an important role in arid lake and overall groundwater chemistry (Rosen, 1994).

The absence of features indicative of drying (e.g., desiccation cracks) in the siltstones of the Fetcaniglen site suggests that the area was continuously flooded for relatively long time periods of unknown absolute duration. Organic rich layers, MISS, possible snail trail or flying traces, and charcoal point to the establishment of a local ecosystem along interdune margins that could only have come about in a relatively long-lived lake setting. The close spatial relationship of the siltstones and the aeolian dune beds, wavy-laminated, and massive strata suggests that the extent of the interdune area was controlled by actively migrating dunes (Langford and Chan, 1988; Mountney, 2012).

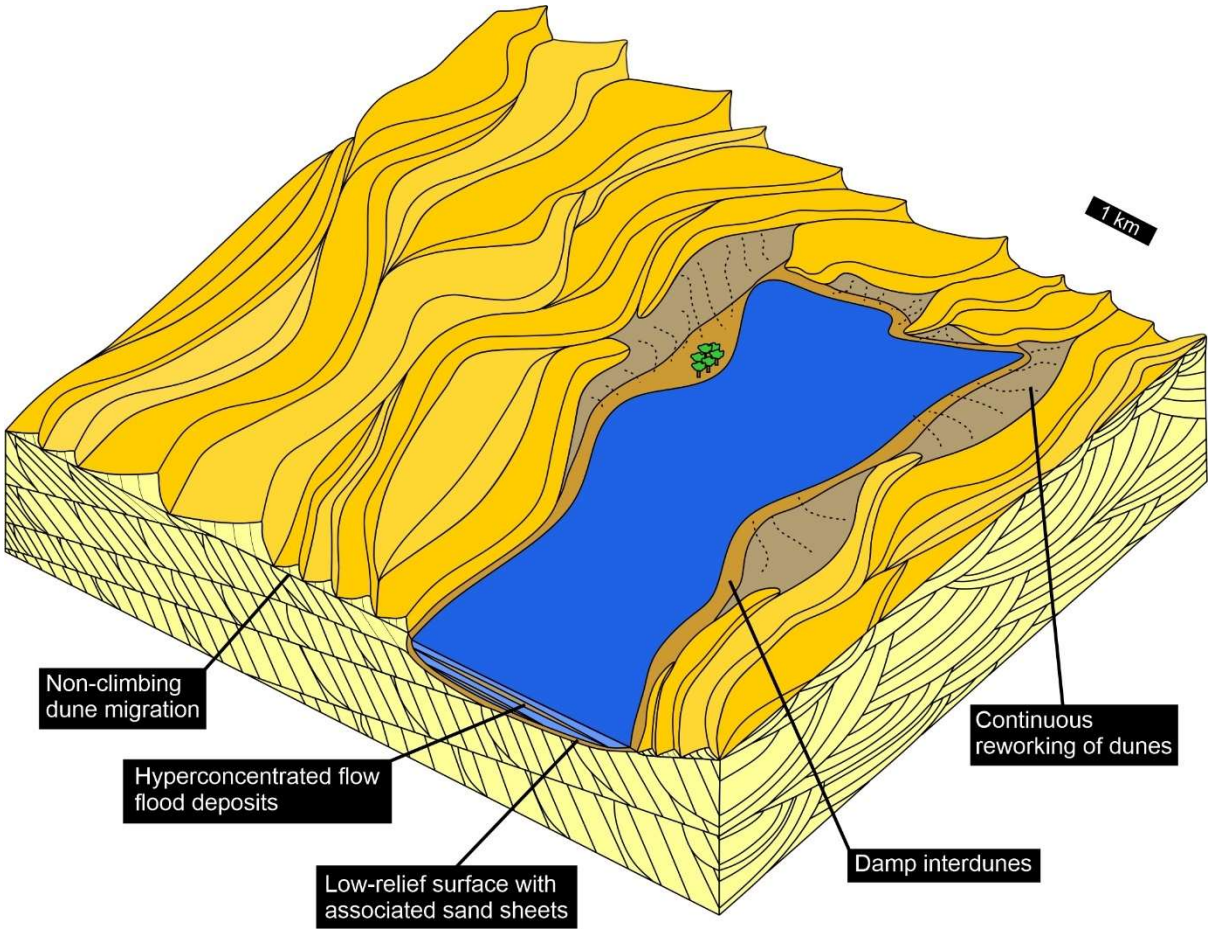

Figure 2.15: Palaeoenvironmental reconstruction of the interdunal lake at the Fetcaniglen site.

The expansion of interdunes is recorded at both the Mokhopa and Fetcaniglen sites, although at different scales. This process of formation whereby interdunal expansion occurs through reorganisation of the dune field by flooding has been described as flood surfaces from the Cutler Formation and Cedar Mesa Sandstone in the USA (Langford and Chan, 1988; 1989; Langford, 1989; Mountney and Jagger, 2004; composite surfaces of Hasiotis *et al*., 2021). These surfaces develop where a temporary change in the angle of climb to zero occur and interdunes become interconnected through non-climbing dune migration (Langford and Chan, 1988; Mountney and Jagger, 2004; Montney, 2012). These surfaces have characteristic planar dip, and result in the typical tabular geometry of wet interdune deposits, and interdunes that are filled by sediments related to repeated flooding (Langford and Chan, 1988). They are also characterised by the occurrence of flooding during active dune migration, and geometries that thicken laterally and vertically toward interdune centres, as observed for the Mokhopa site.

These composite surfaces described for the Cedar Mesa Sandstone are largely related to fluvial flooding along erg margins, however, Langford and Chan (1988) suggested that composite surfaces may also develop through lacustrine processes. In addition, composite surfaces become less frequent from the erg margin to the erg center. In the Clarens Formation, development of these candidate composite surfaces are, therefore, attributed to both surface water and groundwater flooding of interdunes that resulted in the formation of interdunal lakes in two ways. Firstly, flooding that is related to minimal fluvial activity, where the groundwater fluctuation was the primary control on the inundation of the interdune and reorganisation of the dune field. This is best seen at Mokhopa. The accumulated siltstone was a result of both suspension settling from the water column and wind-blown silt settling into a shallow lake (Howell and Mountney, 1997; Cohen, 2003). Secondly, flooding associated with frequent fluvial related flooding that brought water and sediment into the lakes. Onset of flooding of the Fetcaniglen site is also attributed to a rise in the groundwater level, however, the extent of the interdune area resulted in the development of flood-induced sand sheets during storms and the eventual formation of an interdunal lake (Figure 2.15). The interdune area expanded to such a degree that fluvial activity was able to rework dune sediments and subsequently deposited into the interdunal lake as hyperconcentrated flows. The similarity in grain size and composition of the lacustrine sandstones and the dune strata is evidence for localized fluvial processes. This is because sediments in aeolian-fluvial systems associated with episodic flooding that rework the aeolian bedforms typically show characteristics and compositions similar to the surrounding dunes (Al-Masrahy and Mountney, 2015).

Since accumulation of interdune deposits typically do not exceed a few meters (Loope, 1985; Paim and Scherer, 2005; Jones *et al.,* 2016), it needs to be considered that the Mokopha and Fetcaniglen lake deposits may not represent interdunal deposits, but rather independently developed lacustrine systems. These would have developed during periods of aeolian cessation that allowed for the accumulation of lacustrine deposits during a wet climatic phase and, therefore, the development of complex surfaces (Hasiotis *et al.,* 2021). However, given the evidence for dune field reorganisation for the Mokhopa site, the development of a composite surface seems more likely for Facies 3B. In contrast, the isolated nature of the lake margin processes at the Fetcaniglen site, combined with its scale, may suggests that, here, Facies 3B could also have development as a result of higher order bounding surfaces such as a complex surface.

2.5.3. Lakes in modern aeolian settings

For a lake to form, water and a topographically closed depression is required (Cohen, 2002). Within an erg setting, the topographically closed depression is formed by the effect of dune migration and erg construction that create interdune depressions, and such lakes are, therefore, the primary result of wind action (Cohen, 2002). These lakes are generally very shallow and short lived, because of the mobile dunes and high sand supply that rapidly fill the interdune depressions. They may be termed playa, however, terminology around this classification is ambiguous. For Rosen (1994), a playa classification is hinged on a set of conditions that define the geomorphic feature. Firstly, an intercontinental basin is required, secondly, for at least half of the year the water balance should be negative, and thirdly, the capillary fringe of the water-table must be such that evaporation will result in surface discharge. A similar description is given by Briere (2000), adding that these features are usually associated with evaporites. Furthermore, a definition of a playa lake is given where a feature is transitional between a playa and a lake on the bases that it is neither flooded nor dry for more than 75% of the time (Briere, 2000).

Given the lack of sedimentary features that are indicative of drying of the surface and no associated evaporite deposition for the described paleolakes of the Clarens Formation, the waterbodies reflect conditions more in line with what Briere (2000) defines as an ephemeral lake. These waterbodies form in various ways and may come about by: a) ponding of rainwater within interdune hollows, b) a rise of the local water-table brought on by long-term climate change and/or c) a temporary rise of the water-table as a result of flooding (Ward, 1988; Langford, 1989; Teller and Lancaster, 1990). For the described Clarens Formation palaeo-lakes, flooding was most likely linked to a long-term humid phase as the thickness and lack of drying features may represent sustained, long-lasting lacustrine deposition (Ahlbrand and Fryberger, 1981). While the internal architecture of a preserved accumulation is a reflection of the water-table, migration rate and sediment availability, the thickness of the various facies associations related to pluvial processes is controlled by the rate of accommodation space as a function of subsidence (Brookfield, 1977; Howell and Mountney, 1997, Mountney and Thompson, 2002; Scherer and Lavina, 2005). Moreover, differential subsidence may cause localised fluctuations in thicknesses as compared to a minimum thickness resulting from regional subsidence (Carr-Crabaugh and Kocurek, 1998). Therefore, the unusually high thickness of preserved lacustrine deposits seen at the Mokhopa and Fetcaniglen sites as compared to the Makanyaneng site may be a function of higher local subsidence rates in the southern part of the Clarens Basin (Howell and Mountney, 1997), although no evidence for local tectonic activity was observed. Alternatively, thick dune and interdune deposits can also be the result of high angles of climb in an aeolian system (Mountney and Jagger, 2004), however, composite surfaces (flood surfaces) have been shown to develop in temporarily non-climbing systems (Langford and Chan, 1988, Mountney and Jagger, 2004; Mountney, 2012).

Interdunal lakes described from the Namib Desert by Stanistreet and Stollhofen (2002) and Svendsen *et al*. (2003), originated from the damming effect of dunes in river courses, where ponds are formed by overbank flow during fluvial flooding into dune fields. Such interdunal lakes manifest as relatively thin mud interbeds or drapes within aeolian dune strata, which reflect their short-lived nature. Hyperconcentrated flows have been associated with these aeolian-fluvial settings where gravitational slumping is induced by flood waters that infiltrate permeable dune sand. Interdunal lakes were also described for the Nebraska Sand Hills in the USA (Ahlbrandt and Fryberger, 1981; Loope *et al.,* 1995), in which dune dammed palaeovalleys resulted in a high water-table, raising the water-table by an estimated 25 m. Loope *et al*. (1995) also noted the irregular thickness of facies related to lacustrine processes for the Nebraska Sand Hills lakes, along with a lack of evidence for

desiccation, which was attributed to Holocene climate variations, however, the secondary influence of the damming effect of dunes in the palaeovalleys allowed for locally complex water-table responses. This suggests that the water-table in arid areas may show localised variations owing to inherent controls. In addition, hyperconcentrated flows have also been described for the Nebraska Sand Hills (Sweeney and Loope, 2001) and have been linked to the occurrence of small-scale alluvial fans sourced from dune sand. Both the Nebraska Sand Hills and Namib Desert examples may be a modern analogue for the hyperconcentrated flows of the Fetcaniglen site, however, the hyperconcentrated flows discharged into a lake setting.

Modern interdunal lakes that may be likened to the isolated dune-controlled ponds and lakes of the Mokhopa and Makanyaneng sites, are the lakes of Inner Mongolia in China. Wang *et al.* (2016) described the occurrences of permanent interdunal lake bodies within the Badain Jaran desert, where two types of lakes are evident. Firstly, small, shallow elongated lakes that are seemingly controlled by aeolian deflation and blowouts, and secondly, large, deep oval-shaped lakes (Hofmann, 1996; Wang *et al*., 2016). These lakes are primarily constrained to the southern part of the desert. Microbial mats have also been observed within the littoral zone of the desert lakes. The preservation of lake sediments beyond the current lake limits suggests that lake levels fluctuated throughout the Holocene due to climate variability (Hofmann, 1996, Yang *et al*., 2003). During earlier phases of lake development, these saline lakes were filled with fresh to brackish water, and covered large areas (Hofmann, 1996; Yang *et al*., 2003), to such a degree that the current isolated lakes represented one laterally extensive lake body. Large-scale sand dunes spatially controlled the lateral extents of the lakes (Wang *et al*., 2015). Water sources are suggested to be controlled by rainfall variations within the desert (Yang *et al*., 2010, Wu *et al*., 2017; Yue *et al*., 2019), where substantial long-term precipitation infiltrated sand layers of the mega dunes and neighbouring mountains, recharging groundwater sources (Zhoa *et a*l., 2017; Wu *et al*., 2017; Yue *et al*., 2019). Repeated and extended periods of wet and dry climatic conditions have also been documented for the Lake Chad basin during the Miocene-Pliocene (Mousa *et al*., 2016), and the current Lake Chad represents a shallow terminal freshwater lake within the Sahara Desert (Sylvestre *et al*., 2018). The lake is fed by the Chari-Logone river and the lake levels have been shown to reflect changes in regional precipitation. In a similar way to the lakes of the Badain Jaran Desert and Lake Chad, the described palaeo-lakes of the Clarens Formation may have come about by a long-term climatic change to more humid conditions that controlled the water-table.

In addition, Loope and Rowe (2002) described the occurrence of pluvial episodes within the Navajo Sandstone in the USA, where groundwater recharge occurred through precipitation related to a change in climate. Locally, groundwater discharged into interdunal areas and led to the development of localised ecosystems. These pluvial episodes are identified by intervals of extensive bioturbation (Loope and Rowe, 2002; Melchor, 2015). Despite the lack of evidence for widespread bioturbation, the presence of facies related to lacustrine deposition in the Clarens Formation demonstrates that interdunes were locally inundated. Furthermore, the presence of possible snail trail or fly traces, plant impressions, petrified tree trunks, charcoal and biogenic structures suggest that a localised ecosystem developed during the deposition of the Fetcaniglen lake, which can, therefore, be linked to pluvial episodes such as those from the Navajo sandstone and the so-called Green Sahara Episodes (Larrasoana *et al.,* 2013) that caused the absolute water-table rise. The Development of these composite surfaces is also consistent with Eriksson's (1981, 1986) interpretation of prevalent wet aeolian system along the southern and eastern erg margins (See Eriksson, 1986)

The distinction between tectonic versus climatic control on water-table fluctuations may be difficult (Howell and Mountney, 1997), and as such, a relative or absolute water-table rise remains unclear for the Mohkopa site. The preservation of fluvial flood deposits and charcoal in the facies related to pluvial processes supports the occurrence of precipitation related to storm events and suggests an absolute water-table rise for the Fetcaniglen site (Kocurek and Havholm, 1993). Permanent lakes can come about within a closed basin that is subjected to a continued ground- and surface water flow (Cohen, 2003), and, therefore, their appearance in aeolian strata reflects an increase in relative humidity. Given the large thickness of Facies Associations 3B and 3C observed for both the Mokhopa and Fetcaniglen sites, it seems more probable that the water-table rise was due to the combined effect of local subsidence and a more humid climate that allowed for the water table to remain high for a prolonged period of time, locally creating additional accumulation and preservation space within the Clarens basin. Both the Mokhopa and Fetcaniglen sites may represent flooding closer to the erg margin (Figures 2.14, 2.15), where increased moisture limited sediment supply and allowed for the reorganisation of interdunes.In contrast, the Makanyaneng site may represent deposition within the erg center, where a fluctuating water-table resulted in a stacking pattern where damp and wet interdune elements formed discontinuous lenses amongst dune strata within a climbing dry aeolian system (Figure 2.13). Overall, the identification of these long-lived permanent lakes within the Clarens Formation is an indication that the overall aeolian system was subjected to prolonged and repeated periods of wet conditions possibly linked to pluvial episodes that allowed for the development of candidate composite- and complex surfaces (Flood surfaces).

2.6. Conclusions

This study details, for the first time, the complex fluvial-lacustrine interactions in the aeolian Clarens Formation. Three types of pluvial related facies were identified that are situated amongst aeolian dune and sand sheet facies, where the size and complexity of associated facies are dependent on the position of the depositional site relative to the erg margins along with the effect of the sediment availability. The first facies associations reflect a pond that was confined to interdune hollows whose lateral extent was severely restricted by migrating dunes. The thickness and extent of the pond facies suggest that this northern part of the basin was subjected to high-sediment availability and high-wind strength that allowed for migrating dunes to outpace water-table rise as the erg system climbed, typical of an erg centre. The second facies association is that of large-scale lakes in which flooding is related to groundwater flow, whereas the third one is represented by large-scale lakes, where flooding is associated with both groundwater flow and repeated flood-induced hyperconcentrated flows. The thickness of the large-scale lakes situated in the southern part of the basin is exceptional for such setting and indicates a lower sediment availability and larger interdune expansion typical of erg margins. Such extreme thicknesses of lake sediments point to a combination of a long-term humid phase and differential subsidence that played an active role in the accumulation and preservation of facies related to lacustrine processes in the aeolian Clarens Formation. The overall lack of desiccation features observed for these pluvial deposits imply that these were the effect of a long-term humid phase. Thriving local ecosystems developed in these ponds and lakes that were periodically subjected to high sedimentation rates linked to storm events with subsequent quiescence as suggested by the presence of hyperconcentrated flow deposits, MISS, plant impressions, charcoal, and siderite nodules. The Clarens basin was, therefore, episodically subjected to relatively long-lived wet conditions (pluvial episodes) in which ponds and lakes formed during the development of candidate composite surfaces closer to the erg margin.

2.7. References

Abrahams, M., Bordy, E.M. and Knoll, F. 2021. Hidden for one hundred years: a diverse theropod ichnoassemblage and cross-sectional tracks from the historic Early Jurassic Tsikoane ichnosite (Clarens Formation, northern Lesotho, southern Africa). *Historical Biology*, 33(10): 2504–519. DOI: 10.1080/08912963.2020.1810681

Ahlbrandt, T.S. and Fryberger, S.G. 1981. Sedimentary features and significance of interdune deposits. In *Recent and Ancient Nonmarine Depositional Environments: Models for Exploration*. F. G. Ethridge and R. M. Flores (Eds). SEPM Special Publications 31: 293–314. DOI: 10.2110/pec.81.31.0293

Al-Masrahy, M.A. and Mountney, N.P. 2015. A classification scheme for fluvial–aeolian system interaction in desert-margin settings. *Aeolian Research*, 17: 67–88. DOI: 10.1016/j.aeolia.2015.01.010

Belnap, J. 2005. CRUSTS: Biological. In *Encyclopedia of soils in the environment*. Hillel, D. (ed). Elsevier, 339–347.

Bamford, M.K. 2004. Diversity of the woody vegetation of Gondwanan Southern Africa. *Gondwana Research*, 7(1): 153–164. DOI: 10.1016/S1342-937X(05)70314-2

Beukes, N.J. 1969. Die sedimentologie van die Etage Holkranssandsteen, sisteem Karoo. Unpublished MSc dissertation, University of the Orange Free State, Bloemfontein, 138pp. Available: http://hdl.handle.net/11660/7671

Beukes, N.J. 1970. Stratigraphy and sedimentology of the Cave Sandstone stage, Karoo System. In: S.H. Haughton (Ed), Proceedings and papers of the 2nd Gondwana symposium. Council for Scientific and Industrial Research, Pretoria: 321–341.

Bondioli, J.G., Matos, S.A., Warren, L.V., Assine, M.L., Riccomini, C. and Simões, M.G. 2015. The interplay between event and background sedimentation and the origin of fossil-rich carbonate concretions: a case study in Permian rocks of the Paraná Basin, Brazil. *Lethaia*, 48: 522–539. DOI: 10.1111/let.12124

Bordy, E.M. 2008. Enigmatic trace fossils from the aeolian Lower Jurassic Clarens Formation, southern Africa. *Palaeontologia Electronica*, 11: 16A.

Bordy, E.M. and Catuneanu, O. 2002. Sedimentology and palaeontology of upper Karoo aeolian strata (Early Jurassic) in the Tuli Basin, South Africa. *Journal of African Earth Sciences,* 35(2): 301–314. DOI: 10.1016/S0899-5362(02)00103-3

Bordy, E.M., Bumby, A.J., Catuneanu, O. and Eriksson, P.G. 2009. Possible trace fossils of putative termite origin in the Lower Jurassic (Karoo Supergroup) of South Africa and Lesotho. *South African Journal of Science*, 105(9-10): 356–362.

Bordy, E.M. and Head. H.V. 2018. Lithostratigraphy of the Clarens Formation (Stormberg Group, Karoo Supergroup), South Africa. *South African Journal of Geology*, 121: 119–130. DOI: 10.25131/sajg.121.0009

Bordy, E.M., Bowen, D.A., Moore, J., Garnett, M.H. and Tsikos, H. 2018. A Holocene "Frozen Accident": Sediments of Extreme Paleofloods and Fires in the Bedrock-Confined Upper Huis River, Western Cape, South Africa. *Journal of Sedimentary Research*, 88: 696–716. DOI: 10.2110/jsr.2018.29

Bordy, E.M., Abrahams, M., Sharman, G.R., Viglietti P.A., Benson R.B.J., McPhee B.W., Barrett P.M., Sciscio, L., Condon, D., Mundil, R., Rademan, Z., Jinnah, Z., Clark, J.M., Suarez, C.A., Chapelle, K.E.J. and Choiniere J.N. 2020a. A chronostratigraphic framework for the upper Stromberg Group: implications for the Triassic-Jurassic boundary in southern Africa*. Earth-Science Reviews,* 203: 103120. DOI: 10.1016/j.earscirev.2020.103120

Bordy, E.M., Rampersadh, Abrahams, M., Lockley, M.G. and Head, H.V. 2020b. Tracking the Pliensbachian–Toarcian Karoo firewalkers: Trackways of quadruped and biped dinosaurs and mammaliaforms. *PloS ONE* 15(1): e0226847. DOI: 10.1371/journal.pone.0226847

Bordy, E.M., Haupt, T.N. and Head, H.V. 2021. Karoo lava-fed deltas and a petrified forest from the Lower Jurassic of southern Gondwana. *Palaeogeography, Palaeoclimatology, Palaeoecology*, 575: 110484. DOI: 10.1016/j.palaeo.2021.110484

Briere, P.R. 2000. Playa, playa lake, sabkha: Proposed definitions for old terms. *Journal of Arid Environments*, 45: 1–7. DOI: 10.1006/jare.2000.0633

Brookfield, M.E. 1977. The origin of bounding surfaces in ancient aeolian sandstones. *Sedimentology*, 24: 303–332. DOI: 10.1111/j.1365-3091.1977.tb00126.x

Broom, R. 1904. On a new crocodilian genus (Notochampsa) from the Upper Stormberg beds of South Africa. *Geological Magazine*, 1: 582–584. DOI: 10.1017/S0016756800124367

Broom, R. 1911. On the dinosaurs of the Stormberg, South Africa. *Annals of the South African Museum,* 7, 291–312.

Carr-Crabaugh, M., and Kocurek, G. 1998. Continental sequence stratigraphy of a wet eolian system: A key to relative sea-level change. In *Relative Role of Eustasy, Climate, and Tectonics in Continental Rocks.* Stanley, K.W., and McCabe, P.J. (Eds.). SEPM Special Publication, 59: 213–228.

Chapelle, K.E., Barrett, P.M., Botha, J. and Choiniere, J.N. 2019. Ngwevu intloko: a new early sauropodomorph dinosaur from the Lower Jurassic Elliot Formation of South Africa and comments on cranial ontogeny in Massospondylus carinatus. *PeerJ,* 7: e7240. DOI: 10.7717/peerj.7240

Chen, T., Lai, Z., Liu, S., Wang, Y., Wang, Z.T., Miao, X., An, F., Yu, L. and Han, F. 2019. Luminescence chronology and palaeoenvironmental significance of limnic relics from the Badain Jaran Desert, northern China. *Journal of Asian Earth Sciences*, 177: 240–249. DOI: 10.1016/j.jseaes.2019.03.024

Clarke, M.L. and Rendell, H.M. 1998. Climate change impacts on sand supply and the formation of desert sand dunes in the south-west USA. *Journal of Arid Environments*, 39: 517–531. DOI: 10.1006/jare.1997.0372

Cohen, A.S. 2003. Paleolimnology: the history and evolution of lake systems. Oxford University Press. 500 pp.

Crompton, A. W. 1958. The Cranial morphology of a new genus and species of ictidosaurain. *Proceeding of the Zoological society of London*, 130: 183–216.

Davies, N.S., Lui, A.G., Gibling, M.R. and Miller, R.F. 2016. Resolving MISS conceptions and misconceptions: a geological approach to sedimentary surface textures generated by microbial and abiotic processes. *Earth Science Reviews*, 154: 210–246. DOI: 10.1016/j.earscirev.2016.01.005

Davies, N.S., Shillito, A.P. and McMahon, W.J. 2017. Short-term evolution of primary sedimentary surface textures (microbial, abiotic, ichnological) on a dry stream bed: modern observations and ancient implications. PALIOS, 32: 125–134. DOI: 10.2110/palo.2016.064

Dasgupta, P. 2002. Determination of paleocurrent direction from oblique sections of trough cross-stratification—A precise approach. *Journal of Sedimentary Research*, 72: 217–219.

Deynoux, M., Kocurek, G. and Proust, J.N. 1989. Late Proterozoic periglacial aeolian deposits on the west African platform, Taoudeni Basin, western Mali. *Sedimentology*, 36: 531–549. DOI: 10.1306/050401720217

do Amarante, F.B., Scherer, C.M., Aguilar, C.A.G., dos Reis, A.D., Mesa, V. and Soto, M. 2019. Fluvial-eolian deposits of the Tacuarembó formation (Norte Basin–Uruguay): Depositional models

and stratigraphic succession. *Journal of South American Earth Sciences*, 90: 355–376. DOI: 10.1016/j.jsames.2018.12.024

du Toit, A.L. 1904. Geological survey of the divisions of Elliot and Xalanga, Tembuland. *Annual report Geological Commission Cape Good Hope*, (1903), 169–205.

Du Toit, A.L. 1905. Geological survey of the division of Aliwal North, Herschel, Barkly East and part of Wodehouse: *Annual Report of the Geological Commission of the Cape of Good Hope*: 71–181.

Du Toit, A.L. 1910. Geological survey of Maclear and portions of Engcobo, Mount Fletcher, Qumbu and Mount Frere. *Annual Report of the Geological Commission of the Cape of Good Hope*, 69–108.

Du Toit, A.L. 1918. The zones of the Karroo System and their distribution. *Proceedings of the Geological Society of South Africa*, 21: 17–36.

Ellenberger, P. 1970. Les niveaux paléontologiques de premiere apparition des mammiféres primordiaux en Afrique du Sud et leur ichnologie: Establissement de zones stratigraphiques detaillées dans le Stormberg de Leshoto (Afrique du Sud)(Trias Superieur a Jurassique). In *IUGS, 2nd symposium on Gondwana stratigraphy and palaeontology*: 343–370.

El-Albani, A., Vachard, D., Kuhnt, W. and Thurow, J., 2001. The role of diagenetic carbonate concretions in the preservation of the original sedimentary record. *Sedimentology*, 48: 875–886. DOI: 10.1046/j.1365-3091.2001.00398.x

Eriksson, P.G. 1979. Mesozoic sheetflow and playa sediments of the Clarens Formation in the Kamberg area of the Natal Drakensberg. *South African Journal of Geology*, 82(2): 257–258.

Eriksson, P.G. 1981. A palaeoenvironmental analysis of the Clarens Formation in the Natal Drakensberg. *Transactions of the Geological Society of South Africa*, 84: 7–17.

Eriksson, P.G. 1986. Aeolian dune and alluvial fan deposits in the Clarens Formation of the Natal Drakensberg. *Transactions of the Geological Society of South Africa,* 89: 389–393.

Eyles, N. and Clark, B.M. 1986. Significance of hummocky and swaley cross-stratification in late Pleistocene lacustrine sediments of the Ontario basin, Canada. *Geology*, 14: 679–682. DOI: 10.1130/0091-7613(1986)14<679:SOHASC>2.0.CO;2

Fisher, Q.J., Raiswell, R. and Marshall, J.D. 1998. Siderite concretions from nonmarine shales (Westphalian A) of the Pennines, England; controls on their growth and composition. *Journal of Sedimentary Research*, 68: 1034–1045. DOI: 10.2110/jsr.68.1034

Forey, P. and Gardiner, B.G. 1973. A new dictyopygid from the Cave Sandstone of Lesotho, southern Africa. *Palaeontologia africana*, 15: 29–31.

Fourie, S. 1962. Further notes on a new tritylodontid from the Cave Sand-stone of South Africa. *Navorsinge Nasionale Museum Bloemfontein*, 2: 7–19.

Fourie, S. 1963. A new tritylodontid from the Cave Sandstone of South Africa. *Nature*, 198: 201. DOI: 10.1038/198201a0

Gibling, M.R. 2006. Width and thickness of fluvial channel bodies and valley fills in the geological record: a literature compilation and classification. *Journal of Sedimentary Research*, 76: 731–770. DOI: 10.2110/jsr.2006.060

Glennie, K.W. 1972. Permian Rotliegendes of northwest Europe interpreted in light of modern desert sedimentation studies. *AAPG Bulletin*, 56(6): 1048-1071. DOI: 10.1306/819A40AE-16C5-11D7-8645000102C1865D

Greenwood, B. and Sherman, D.J. 1986. Hummocky cross-stratification in the surf zone: flow parameters and bedding genesis. *Sedimentology*, 33: 3–45. DOI: 10.1111/j.1365-3091.1986.tb00743.x

Guerrero, M.C. and Wit, R.D. 1992. Microbial mats in the inland saline lakes of Spain. *Limnetica*, 8: 197–204.

Guerrero, M.C., Tadeo, A.B. and de Wit, R. 1994. Environmental factors controlling the development of microbial mats in inland saline lakes; the granulometric composition of the sediment. In *Microbial Mats*. Springer, Berlin, Heidelberg. 85–90. DOI: 10.1007/978-3-642-78991-5_9

Haughton, S.H. 1924. The fauna and stratigraphy of the Stormberg Series. *Annals of the South African Museum*, 12(8): 323–497.

Harms, J.C. 1979. Primary sedimentary structures. *Annual Review of Earth and Planetary Sciences*, 7(1): 227–248. DOI: 10.1146/annurev.ea.07.050179.001303

Hasiotis, S. T. 2006. Continental Trace Fossils. SEPM, Short Course Notes Number 51, Tulsa, Oklahoma, 132 pp.

Hasiotis, S. T., Platt, B. F., Reilly, M., Amos, K., Lang, S., Kennedy, D., Todd, J. and Michel, E. 2012, Actualistic studies of the spatial and temporal distribution of terrestrial and aquatic organism traces in continental environments to differentiate lacustrine from fluvial, eolian, and marine deposits in the geologic record, in O. W. Baganz, Y. Bartov, K. Bohacs, and D. Nummedal, eds., Lacustrine sandstone reservoirs and hydrocarbon systems: *AAPG Memoir* 95: 433 – 489.

Hasiotis, S.T., Chan, M.A. and Parrish, J.T. 2021. Defining bounding surfaces within and between eolian and non-eolian deposits, Lower Jurassic Navajo Sandstone, Moab Area, Utah, USA: Implications for subdividing erg system strata. *Journal of Sedimentary Research*, 91(12): 1275-1304. DOI: 10.2110/jsr.2021.027

High, L.R. and Picard, M.D. 1974. Reliability of cross-stratification types as paleocurrent indicators in fluvial rocks. *Journal of Sedimentary Research*, 44: 158–168. DOI: 10.1306/74D729AF-2B21-11D7-8648000102C1865D

Hofmann, J. 1996. The Lakes in the SE part of Badain Jaran Shamo, their limnology and geochemistry. *Geowissenschaften-Weinheim*, 14: 275–278.

Holzförster, F. 2007. Lithology and depositional environments of the Lower Jurassic Clarens Formation in the eastern Cape, South Africa. *South African Journal of Geology*, 110(4): 543–560. DOI: 10.2113/gssajg.110.4.543

Howell, J. and Mountney, N.P. 1997. Climatic cyclicity and accommodation space in arid to semi-arid depositional systems: an example from the Rotliegend Group of the UK southern North Sea. In Petroleum Geology of the Southern North Sea: Future Potential. Ziegler, K. Turner, P. and Daines, S. R (eds). *Geological Society Special Publication*. 123: 63–86. DOI: 10.1144/GSL.SP.1997.123.01.05

Hummel, G. and Kocurek, G. 1984. Interdune areas of the back-island dune field, northern Padre Island, Texas. *Sedimentary Geology*, 39: 1–26. DOI: 10.1016/0037-0738(84)90022-8

Hunter, R.E. 1977. Basic types of stratification in small eolian dunes. *Sedimentology*, 24: 361–387. DOI: 10.1111/j.1365-3091.1977.tb00128.x

Johnson, S.Y. 1989. Significance of loessite in the Maroon Formation (middle Pennsylvanian to lower Permian), Eagle basin, Northwest Colorado. *Journal of Sedimentary Research*, 59: 782–791. DOI: 10.1306/212F9070-2B24-11D7-8648000102C1865D

Johnson, M.R. 1976. Stratigraphy and sedimentology of the Cape and Karoo Sequences in the eastern Cape Province. Unpublished doctoral thesis, Rhodes University, Grahamstown, South Africa, 336pp. Available: http://hdl.handle.net/10962/d1005617

Jones, F.H., Scherer, C.M.S., Kuchle, J., 2016. Facies architecture and stratigraphic evolution of aeolian dune and interdune deposits, Permian Caldeirão Member (Santa Brígida Formation), *Brazilian Sedimentary Geology*, 337: 133–150.

Jubb, R.A. 1973. Brief synthesis of present information on the geographical and stratigraphical distribution of fossil fish within the Stormberg Series, South Africa. *Palaeontologia 47frican47*, 16: 17–23.

Kitching, J.W. and Raath, M.A. 1984. Fossils from the Elliot and Clarens Formation (Karoo sequence) of the northeastern Cape, Orange Free State and Lesotho, and a suggested biozonation based on tetrapods. *Palaeontologia africana47frican47*, 25: 111–125.

Kocurek, G. 1981. The significance of interdune deposits and bounding surfaces in aeolian dune sands. *Sedimentology*, 28: 753-780. DOI: 10.1111/j.1365-3091.1981.tb01941.x

Kocurek, G. and Dott, R.H. 1981. Distinction and uses of stratification types in the interpretation of eolian sand. *Journal of Sedimentary Petrology*, 51: 579–595. DOI: 10.1306/212F7CE3-2B24-11D7-8648000102C1865D

Kocurek, G. and Fielder, G. 1984. Adhesion Structures. *Journal of Sedimentary petrology*. 52: 1229–1241. DOI: 10.1306/212F8102-2B24-11D7-8648000102C1865D

Kocurek, G. and Havholm. K.G. 1993. Eolian Sequence Stratigraphy – conceptual framework. In *Recent Developments in Siliciclastic Sequence Stratigraphy*. Weimer, P. and Posamentier, H. W. (eds). American Association of Petroleum Geologists, Memoir, 58: 393–409.

Kocurek, G. and Lancaster, N. 1999. Aeolian system sediment state: theory and Mojave Desert Kelso dune field example. *Sedimentology*, 46: 505–515. DOI: 10.1046/j.1365-3091.1999.00227.x

Kocurek, G. and Nielson, J. 1986. Conditions favourable for the formation of warm-climate aeolian sand sheets. *Sedimentology*, 33: 795–816. DOI: 10.1111/j.1365-3091.1986.tb00983.x

Langford, R.P. and Chan, M.A. 1988. Flood surfaces and deflation surfaces within the Cutler Formation and Cedar Mesa Sandstone (Permian), southeastern Utah. *Geological Society of America Bulletin,* 100: 1541–1549. DOI: 10.1130/0016-7606(1988)100<1541:FSADSW>2.3.CO;2

Langford, R.P. 1989. Fluvial-aeolian interactions: Part I, modern systems. *Sedimentology*, 36: 1023–1035. DOI: 10.1111/j.1365-3091.1989.tb01540.x

Langford, R.P. and Chan, M.A. 1989. Fluvial-aeolian interactions: Part II, ancient systems. *Sedimentology*, 36: 1037–1051. DOI: 10.1111/j.1365-3091.1989.tb01541.x

Larrasoaña, J.C., Roberts, A.P. and Rohling, E.J. 2013. Dynamics of green Sahara periods and their role in hominin evolution. *PloS One*, 8: e76514. DOI: 10.1371/journal.pone.0076514

Loope, D.B. 1985. Episodic deposition and preservation of aeolian sands: a late Paleozoic example from southeastern Utah. *Geology*, 13: 73–76.

Loope, D.B. and Rowe, C.M. 2002. Long-lived pluvial episodes during deposition of the Navajo Sandstone. *The Journal of Geology*, 111: 223–232. DOI: 10.1086/345843

Loope, D.B., Dingus, L., Swisher III, C.C. and Minjin, C, 1998. Life and death in a Late Cretaceous dune field, Nemegt basin, Mongolia. *Geology*, 26: 27–30. DOI: 10.1130/0091-7613(1998)026<0027:LADIAL>2.3.CO;2

Loope, D.B., Swinehart, J.B. and Mason, J.P. 1995. Dune-dammed paleovalleys of the Nebraska Sand Hills: intrinsic versus climatic controls on the accumulation of lake and marsh sediments. *Geological Society of America Bulletin*, 107: 396–406. DOI: 10.1130/0016-7606(1995)107<0396:DDPOTN>2.3.CO;2

Majewski, W. 2000. Middle Jurassic concretions from Częstochowa (Poland) as indicators of sedimentation rates. *Acta Geologica Polonica*, 50: 431–439.

Major, J.J. 1997. Depositional processes in large-scale debris-flow experiments. *The Journal of Geology*, 105: 345–366. DOI: 10.1086/515930

Marshall, J.D. and Pirrie, D. 2013. Carbonate concretions – explained. *Geology Today,* 29: 53–62. DOI: 10.1111/gto.12002

McKee, E.D. 1966. Structures of dunes at White Sands National Monument, New Mexico (and a comparison with structures of dunes from other selected areas). *Sedimentology*, 7: 1–69. DOI: 10.1111/j.1365-3091.1966.tb01579.x

McKie, T. 2011. A comparison of modern dryland depositional systems with the Rotliegend Group of the Netherlands. *SEPM Special publication*, 98: 89–103.

Meijs, L., 1960. Notes on the occurrence of petrified wood in Basutoland. *Basutoland Notes and Records*, 2: 20–26.

Melchor, R.N. 2015. Application of vertebrate trace fossils to palaeoenvironmental analysis. *Palaeogeography, Palaeoclimatology, Palaeoecology*, 439: 79–96. DOI: 10.1016/j.palaeo.2015.03.028

Miall, A.D. 1974. Paleocurrent analysis of alluvial sediments; a discussion of directional variance and vector magnitude. *Journal of Sedimentary Research*, 44: 1174–1185. DOI: 10.1306/212F6C6C-2B24-11D7-8648000102C1865D

Miall, A.D. 1996 Geology of Fluvial Deposits. Berlin, Springer-Verlag, 582 pp.

Miall, A.D. 2016. Stratigraphy: A Modern Synthesis. Berlin: Springer-Verlag, 454 pp.

Mohrig, D., Ellis, C., Parker, G., Whipple, K.X. and Hondzo, M. 1998. Hydroplaning of subaqueous debris flows. *Geological Society of America Bulletin*, 110: 387–394. DOI: 10.1130/0016-7606(1998)110<0387:HOSDF>2.3.CO;2

Morsilli, M. and Pomar, L. 2012. Internal waves vs. surface storm waves: a review on the origin of hummocky cross-stratification. *Terra Nova*, 24: 273–282. DOI: 10.1111/j.1365-3121.2012.01070.x

Moulin, M., Fluteau, F., Courtillot, V., Marsh, J., Delpech, G., Quidelleur, X. and Gérard, M. 2017. Eruptive history of the Karoo lava flows and their impact on early Jurassic environmental change. *Journal of Geophysical Research: Solid Earth*, 122(2): 738–772. DOI: 10.1002/2016JB013354

Mountney, N.P. 2006. Eolian Facies Models. In Facies Models Revisited, H. Posamentier and R. G. Walker, Eds. *SEPM Special Publications*. 84. 19–83. DOI: 10.2110/pec.06.84.0019

Mountney, N.P. 2012. A stratigraphic model to account for complexity in aeolian dune and interdune successions. *Sedimentology*, 59: 964–989. DOI: 10.1111/j.1365-3091.2011.01287.x

Mountney, N.P. and Jagger, A. 2004. Stratigraphic evolution of an aeolian erg margin system: the Permian Cedar Mesa Sandstone, SE Utah, USA. *Sedimentology*, 52: 713–743. DOI: 10.1111/j.1365-3091.2004.00646.x

Mountney, N.P. and Russell, A.J. 2009. Aeolian dune-field development in a water table-controlled system: Skeiðarársandur, Southern Iceland. *Sedimentology*, 56: 2107–2131. DOI: 10.1111/j.1365-3091.2009.01072.x

Mountney, N.P. and Thompson, D.B. 2002. Stratigraphic evolution and preservation of aeolian dine and damp/wet interdune strata: an example from the Triassic Helsby Sandstone Formation, Cheshire Baisn, UK. *Sedimentology*, 49: 805–833. DOI: 10.1046/j.1365-3091.2002.00472.x

Moussa, A., Novello, A., Lebatard, A.E., Decarreau, A., Fontaine, C., Barboni, D., Sylvestre, F., Bourles, D.L., Paillès, C., Buchet, G. and Duringer, P. 2016. Lake Chad sedimentation and environments during the late Miocene and Pliocene: New evidence from mineralogy and chemistry of the Bol core sediments. *Journal of African Earth Sciences*, 118: 192–204. DOI: 10.1016/j.jafrearsci.2016.02.023

Muir, R.A., Bordy, E.M. and Prevec, R. 2015. Lower Cretaceous deposit reveals first evidence of a post-wildfire debris flow in the Kirkwood Formation, Algoa Basin, Eastern Cape, South Africa. *Cretaceous Research*, 56: 161–179. DOI: 10.1016/j.cretres.2015.04.005

Muir, R.A., Bordy, E.M., Mundil, R. and Frei, D. 2020. Recalibrating the breakup history of SW Gondwana: U–Pb radioisotopic age constraints from the southern Cape of South Africa. *Gondwana Research*, 84: 177–193. DOI: 10.1016/j.gr.2020.02.011

Mukaddam, R., Bordy, E.M., Lockley, M.G. and Chapelle, K.E. 2021. Reviving Kalosauropus, an Early Jurassic sauropodomorph track from southern Africa (Lesotho). *Historical Biology*, 33(11(: 2908-2930. DOI: 10.1080/08912963.2020.1834542

Mulder, T. and Alexander, J. 2001. The physical character of subaqueous sedimentary density flows and their deposits. *Sedimentology*, 48: 269–299. DOI: 10.1046/j.1365-3091.2001.00360.x

Norman, D.B., Crompton, A.W., Butler, R.J., Porro, L.B. and Charig, A.J. 2011. The Lower Jurassic ornithischian dinosaur Heterodontosaurus tucki Crompton & Charig, 1962: cranial anatomy, functional morphology, taxonomy, and relationships. *Zoological Journal of the Linnean Society*, 163(1): 182-276. DOI: 10.1111/j.1096-3642.2011.00697.x

Noffke, N. 2010. Geobiology: Microbial mats in sandy deposits from the Archean Era to today. Springer. 194 pp.

Noffke, N., Gerdes, G., Klenke, T. and Krumbein, W.E. 2001. Microbially induced sedimentary structures: a new category within the classification of primary sedimentary structures. *Journal of Sedimentary Research*, 71: 649–656. DOI: 10.1306/2DC4095D-0E47-11D7-8643000102C1865D

Olsen, P.E. and Galton, P.M. 1984. A review of the reptile and amphibian assemblages from the Stormberg of southern Africa, with special emphasis on the footprints and the age of the Stormberg. *Palaeontologia 49frican49*, 25: 87–110.

Paim, P.S.G., Scherer, C.M.S. 2007. High-resolution stratigraphy and depositional model of wind- and water-laid deposits in the ordovician Guaritas rift (Southernmost Brazil). *Sedimentary Geology*, 202(4): 776–795.

Picard, M.D. and High, L.R. 1970. Interference ripple marks formed by ephemeral streams. *Journal of Sedimentary Petrology*, 40: 708–711. DOI: 10.1306/74D7201D-2B21-11D7-8648000102C1865D

Picard, M.D. and High, L.R. 1973. Sedimentary structures of ephemeral streams. Elsevier, Amsterdam. 223 pp.

Pulvertaft, T.C.R. 1985. Aeolian dune and wet interdune sedimentation in the Middle Proterozoic Dala Sandstone, Sweden. *Sedimentary geology*, 44: 93–111. DOI: 10.1016/0037-0738(85)90034-X

Pye, K. 1995. The nature, origin and accumulation of loess. *Quaternary Science Reviews*, 14: 653–667. DOI: 10.1016/0277-3791(95)00047-X

Pye, K. and Tsoar, H. 1987. The mechanics and geological implications of dust transport and deposition in deserts with particular reference to loess formation and dune sand diagenesis in the northern Negev, Israel. *Geological Society, London, Special Publications*, 35: 139–156. DOI: 10.1144/GSL.SP.1987.035.01.10

Raath, M.A. and Yates, A.M. 2005. Preliminary report of a large theropod dinosaur trackway in Clarens Formation sandstone (Early Jurassic) in the Paul Roux district, northeastern Free State, South Africa. *Palaeontologia africana*, 41: 101-104.

Raiswell, R. 1971. The growth of Cambrian Liassic concretions. *Sedimentology*, 17: 147–171. DOI: 10.1111/j.1365-3091.1971.tb01773.x

Rosen, M.R., 1994. The importance of groundwater in playas: A review of playa classifications and the sedimentology and hydrology of playas. In Paleoclimate and basin evolution of playa systems. Rosen, M. R.(ed). Boulder, Colorado. *Geological Society of America Special paper* 289: 1–18. DOI: 10.1130/SPE289-p1

Scherer, C.M. and Lavina, E.L. 2005. Sedimentary cycles and facies architecture of aeolian–fluvial strata of the Upper Jurassic Guará Formation, southern Brazil. *Sedimentology*, 52: 1323–1341. DOI: 10.1111/j.1365-3091.2005.00746.x

Schieber, J., Bose, P.K., Eriksson, P.G., Banerjee, S., Sarkar, S., Altermann, W. and Catuneanu, O. 2007. Atlas of microbial mat features preserved within the siliciclastic rock record. Elsevier. Amsterdam. 311 pp.

Scott, A.C. 2010. Charcoal recognition, taphonomy and uses in palaeoenvironmental analysis. *Palaeogeography, Palaeoclimatology, Palaeoecology*, 291: 11–39. DOI: 10.1016/j.palaeo.2009.12.012

Scott, A.C., Cripps, J.A., Collinson, M.E. and Nichols, G.J. 2000. The taphonomy of charcoal following a recent heathland fire and some implications for the interpretation of fossil charcoal deposits. *Palaeogeography, Palaeoclimatology, Palaeoecology*, 164: 1–31. DOI: 10.1016/S0031-0182(00)00168-1

Seeley, H.G., 1894. On Hortalotarsus skirtopodus, a new Saurischian fossil from Barkly East, Cape Colony. *Journal of Natural History*, 14(84): 411–419. DOI: 10.1080/00222939408677828

Sellez-Martinez, J. 1996. Concretion morphology, classification, and genesis. *Earth Science Reviews*, 41: 177–210. DOI: 10.1016/S0012-8252(96)00022-0

Shaw, P.A. and Bryant, R.G. 2011. Pans, playas and salt lakes. In *Arid zone geomorphology: process, form and change in drylands*. Thomas, D. S. G. (ed). 373–401. DOI: 10.1002/9780470710777.ch15

Sidor, C.A. and Hancox, P.J. 2006. Elliotherium kersteni, a new tritheledontid from the lower Elliot Formation (Upper Triassic) of South Africa. *Journal of Paleontology*, 80(2): 333-342. DOI: 10.1666/0022-3360(2006)080[0333:EKANTF]2.0.CO;2

Smalley, I.J. and Smalley, V. 1983. Loess material and loess deposits: formation, distribution and consequences. In *Developments in Sedimentology*, 38: 51–68. DOI: 10.1016/S0070-4571(08)70788-X

Stanistreet, I.G. and Stollhofen, H. 2002. Hoanib River flood deposits of Namib Desert interdunes asanalogues for thin permeability barrier mudstone layers in aeolianite reservoirs. *Sedimentology*, 49: 719–736. DOI: 10.1046/j.1365-3091.2002.00458.x

Svendsen, J., Stollhofen, H., Krapf, C.B. and Stanistreet, I.G. 2003. Mass and hyperconcentrated flow deposits record dune damming and catastrophic breakthrough of ephemeral rivers, Skeleton Coast Erg, Namibia. *Sedimentary Geology*, 160: 7–31. DOI: 10.1016/S0037-0738(02)00334-2

Sweeney, M.R. and Loope, D.B. 2001. Holocene dune-sourced alluvial fans in the Nebraska Sand Hills. *Geomorphology*, 38: 31–46. DOI: 10.1016/S0169-555X(00)00067-2

Sylvestre, F., Schuster, M., Vogel, H., Abdheramane, M., Ariztegui, D., Salzmann, U., Schwalb, A., Waldmann, N. and Icdp Chadrill Consortium. 2018. The Lake CHAd Deep DRILLing project (CHADRILL)–targeting~ 10 million years of environmental and climate change in Africa. *Scientific drilling*, 24: 71–78. DOI: 10.5194/sd-24-71-2018

Tasch, P. 1984. Biostratigraphy and palaeontology of some conchostracan-bearing beds in southern Africa. *Palaeontologia africana*, 25: 61–85.

Teller, J.T. and Lancaster, N. 1990. Sedimentology and paleohydrology of Late Quaternary Lake deposits in the northern Namib sand sea, Namibia. *Quaternary Science Reviews*, 9: 343–364. DOI: 10.1016/0277-3791(90)90027-8

Tooth, S., 2009. Arid geomorphology: emerging research themes and new frontiers. *Progress in Physical Geography*, 33: 251–287. DOI: 10.1177/0309133309338135

Tsoar, H. and Pye, K. 1987. Dust transport and the question of desert loess formation. *Sedimentology*, 34: 139–153.

Tyler, S.W., Munoz, J.F. and Wood, W.W. 2006. The response of playa and sabkha hydraulics and mineralogy to climate forcing. *Groundwater*, 44: 329–338. DOI: 10.1111/j.1365-3091.1987.tb00566.x

Van Dijk, D.E. 1978. Trackways in the Stormberg. *Palaeontologia africana*, 21: 113–120.

Van Dijk, D.E. and Eriksson, P.G. 2021. Bipedal leaping Jurassic vertebrates in Southern Africa: proposed new ichnotaxon and inferred palaeoenvironment. *Transactions of the Royal Society of South Africa*, 76(3): 235–245. DOI: 10.1080/0035919X.2021.1964104

Van Eeden, O.R. and Keyser, A.W. 1971. Fossielspore in die Holkranssandsteen op Pont Drift, Distrik Soutpansberg, Transvaal. *Annals of the Geological Survey of South Africa*, 9: 135–137.

Van Hoepen, E.C.N. 1920. Contributions to the knowledge of the reptiles of the Karoo Formation. 5. A new dinosaur from the Stormberg Beds. *Annals of the Transvaal Museum*, 7: 77–9.

Viglietti, P.A., McPhee, B.W., Bordy, E.M., Sciscio, L., Barrett, P.M., Benson, R.B.J., Wills, S., Chapelle, K.E.J., Dollman, K.N., Mdekazi, C. and Choiniere, J.N. 2020. Biostratigraphy of the massospondylus assemblage zone (Stormberg group, karoo supergroup), South Africa. *South African Journal of Geology*, 123(2): 249-262. DOI: 10.25131/sajg.123.0018

Wang, Z., Chen, T., Lui, S. and Lai, Z. 2016. Aeolian origin of interdunal lakes in the Badain Jaran Desert, China. *Arabian Journal of Geosciences*, 9: 190. DOI: 10.1007/s12517-015-2062-6

Ward, J.D. 1988. Eolian, fluvial and pan (playa) facies of the Tertiary Tsondab Sandstone Formation in the central Namib Desert, Namibia. *Sedimentary Geology*, 55: 143–162. DOI: 10.1016/0037-0738(88)90094-2

Wehrmann, A., Gerdes, G. and Hofling, R. 2011. Microbial mats in a lower Triassic siliciclastic playa environment (Middle Buntsandstein, North Sea). In Microbial mats in siliciclastic depositional systems through time. Noffke, N. and Chafetz, H.S. (eds). *SEPM Special Publications,* 101: 177–190. DOI: 10.2110/sepmsp.101.177

Wilson, I.G. 1972. Aeolian bedforms – their development and origins. *Sedimentology,* 19: 173-210. DOI: 10.1111/j.1365-3091.1972.tb00020.x

Wu, X., Wang, X., Wang, Y. and Hu, B. X. 2017. Origin of water in the Badain Jaran Desert, China: new insights from isotopes. *Hydrology and Earth System Science*, 21: 4419–4431. DOI: 10.5194/hess-21-4419-2017

Yang, X., Lui, T. and Xiao, H. 2003. Evolution of megadunes and lakes in the Badain Jaran Desert, Inner Mongolia, China during the las 31,000 years. *Quaternary International*, 104: 99–112. DOI: 10.1016/S1040-6182(02)00138-6

Yang, X., Ma, N., Dong, J., Zhu, B., Xu, B., Ma, Z., and Liu, J. 2010. Recharge of the inter-dune lakes and Holocene climatic changes in the Badain Jaran Desert, western China. *Quaternary Research*, 73: 10–19. DOI: 10.1016/j.yqres.2009.10.009

Yue, D.P., Zhao, J.B., Ma, Y.D., Huang, X.G., Shao, T.J., Luo, X.Q. and Ma, A.H. 2019. Relationship between Landform Development and Lake Water Recharge in the Badain Jaran Desert, China. *Water*, 11: 1999. DOI: doi.org/10.3390/w11101999

Zhao, J., Ma, Y., Luo, X., Yue, D., Shao, T. and Dong, Z. 2017. The discovery of surface runoff in the megadunes of Badain Jaran Desert, China, and its significance. *Science China: Earth Sciences*, 60: 707–719. DOI: 10.1007/s11430-016-9019-2

Chapter 3.

The origin of the massive beds in the Clarens Formation: sediment grain characteristics in the Early Jurassic erg system of southern Africa

Abstract

The Lower Jurassic Clarens Formation is the youngest sedimentary unit of the Karoo Supergroup in the main Karoo Basin of southern Africa. It is generally considered to be of an aeolian origin due to its common classical aeolian features, such as very large- to large-scale, cross-bedded sandstones. In addition to the aeolian features, the Clarens Formation is also dominated by very thick- to thick, massive sandstones, whose origin is debated. Utilising grain features from known aeolian processes (i.e., from large-scale cross-beds), assessment of these grain properties of these ubiquitous massive sandstones were conducted. The grain features of the massive samples can be grouped into six different facies types (Facies 1–6) that are defined by their grain size, shape, sorting and fabric. The samples were compared to a baseline that was created from sandstones of known origin sampled from large-scale, dune cross-beds. Facies 1 has very similar grain features to the cross-bedded baseline and thus it is interpreted as deposits from migrating, wind-blown dunes. Facies 2 resulted from sandy dust fall, whereas Facies 3 is interpreted as an aeolian dust deposit that has grain features that are consistent with loess. Facies 4 shows features that are undiagnostic and could reflect a range of aeolian process responsible for its origin. Facies 5 and 6 show primary aeolian signatures with evidence of reworking in the grain fabric in a lacustrine and a fluvial setting, respectively. These six facies types represent a spectrum of processes that occurred in response to erg migration and atmospheric circulation patterns along the Clarens erg margin. The processes generated sand dunes, sand sheets, as well as sandy loess and typical loess deposits. The diversity of these aeolian deposits is evidence that: 1) conditions in southwestern Gondwana during the Sinemurian to Pliensbachian were pervasively dry and windy; and 2) various degrees of fluvial and lacustrine reworking of these aeolian deposits took place during the development of candidate composite surfaces along the erg margin.

3.1. Introduction

The Sinemurian to Pliensbachian Clarens Formation of southern Africa (Figure 3.1) has long been regarded as an aeolian deposit (e.g., du Toit, 1918), although a large proportion of the formation is dominated by structureless deposits with unclear origin. The presence of classical aeolian features, such as very large to large-scale cross-bedded sandstones, reinforces its narrative as a dominantly aeolian deposit having a strong west to east wind regime, as this was shown consistently and regionally from the forsest dip direction data in the cross-bedded sandstones (Beukes, 1969, 1970; Eriksson, 1981 1986; Bordy and Head, 2018). The massive beds within the Clarens Formation, however, have a debated origin and have been attributed to: 1) dust fall processes (and thus termed loess deposits or loessite; Ellenberger *et al*., 1964; Beukes, 1969, 1970; Johnson, 1976; Eriksson, 1981, 1986); 2) mass movement processes (Eriksson, 1981, 1986); and 3) destruction of primary internal structures by means of syn-sedimentary water infiltration (Beukes, 1969, 1970). However, robust evidence with which to substantiate these interpretations of the massive beds are lacking and this limits not only the understanding of their genesis but also the sedimentary dynamics of the

various subenvironments during the deposition of the Clarens Formation. These challenges are further exacerbated by the lack of diagnostic characteristics needed for the unambiguous classification of loessites (Meijer *et al*., 2020). For example, Johnson (1989) has described the following diagnostic features for the identification of loessite in the geological record: 1) homogeneity and dominance of silt as a result of selective transport; 2) lack of primary sedimentary structures (i.e., massiveness); 3) the nature of bedding contacts that suggest the blanketing of underlying topography; 4) inferred palaeogeography that indicates an upwind dust source; and 5) the absence of features (sedimentary structures, grain size trends, fossil content) that allow definitive environmental interpretations, such as very large-scale, cross-bedded sandstones with high foreset inclinations as aeolian deposition. Moreover, evaluation of subtle changes in grain size, grain shape, and grain fabric have also been used to distinguish the various aeolian processes evoked in the formation of massive beds (e.g., Smalley and Cabrera, 1970; Rogers and Smalley, 1983; Vandenberghe, 2013; Vandenberghe *et al.,* 2018). This study aims to analyse these subtle variations in grain properties to identify the origin of these long-debated massive deposits in the Clarens Formation.

3.2. Geological background

The Clarens Formation represents the uppermost sedimentary succession of the Karoo Supergroup, and combined with the Molteno and Elliot formations, forms the Stormberg Group (Johnson *et al*., 2006). Characteristically, the Clarens Formation has an exceptional lithological homogeneity throughout southern Africa, and within the main Karoo basin (MKB), it is dominated by thickly bedded, massive sandstone with very large to large-scale cross-bedded sandstones in lesser abundance. These sandstones are mostly fine- to very fine-grained, often silty and have a cream, pink, light green to buff colour (du Toit, 1905, 1918; Stockley, 1947; Robinson *et al*., 1969; Beukes, 1969, 1970; Johnson, 1976; Eriksson, 1981, 1986; Holzförster, 2007; Bordy and Head, 2018). The Clarens Formation has been interpreted as an aeolian depositional environment having a strong west to east wind regime as indicated by the regional measurements from foresets of large-scale cross-bedded sandstones (du Toit, 1905; 1918; Haughton, 1924; Stockley, 1947; Robinson *et al*., 1969; Beukes, 1969, 1970; Johnson, 1976; Eriksson, 1981, 1986; Holzförster, 2007; Bordy and Catuneanu, 2002; Bory *et al*., 2008; Bordy, 2009; Bordy and Head, 2018). In addition, the massive sandstones have been interpreted as originating from dust deposition (loess), mass movement processes related to high magnitude precipitation or the destruction of primary internal structures by water percolation (Beukes, 1969, 1970; Johnson, 1976; Eriksson, 1986). The appearance of lenticular sandstones and mudstones associated with sedimentary structures indicative of shallow-water features in the lower and upper parts of the succession, combined with the stratigraphic distribution of the massive sandstones versus large-scale sandstones prompted the classification of a threefold zonation in the Clarens Formation that may reflect climatic megacycles (Beukes, 1969, 1970; Bordy and Head, 2018).

The lower boundary with the Elliot formation is conformable, and is shown to be transitional, where red beds are interbedded with cream to pale green sandstones of the Clarens Formation (Johnson, 1976; Bordy and Head, 2018), making the placement of this lower boundary problematic. Bordy and Head (2018) suggested that where a thick transitional zone is developed, a combination of criteria be used for placement of the lower contact so that either the occurrence of a thick massive pale to cream sandstone or a change to dominantly large-scale, cross-bedded sandstones (i.e. aeolian

conditions) would be indicative of the contact and imply a shift in depositional environment. The upper contact with the Drakensberg Group basalts is also conformable and sharp, occurring at the stratigraphic arrival of extrusive volcanics above the sandstones of the Clarens Formation. Field evidence further demonstrates that this contact is transitional and diachronous across the basin, suggesting that both the aeolian and volcanic systems were active simultaneously during the onset of flood basalts associated with the Karoo-Ferrar large Igneous Province (Moulin *et al*., 2017; Bordy *et al*., 2020, 2021, in press).

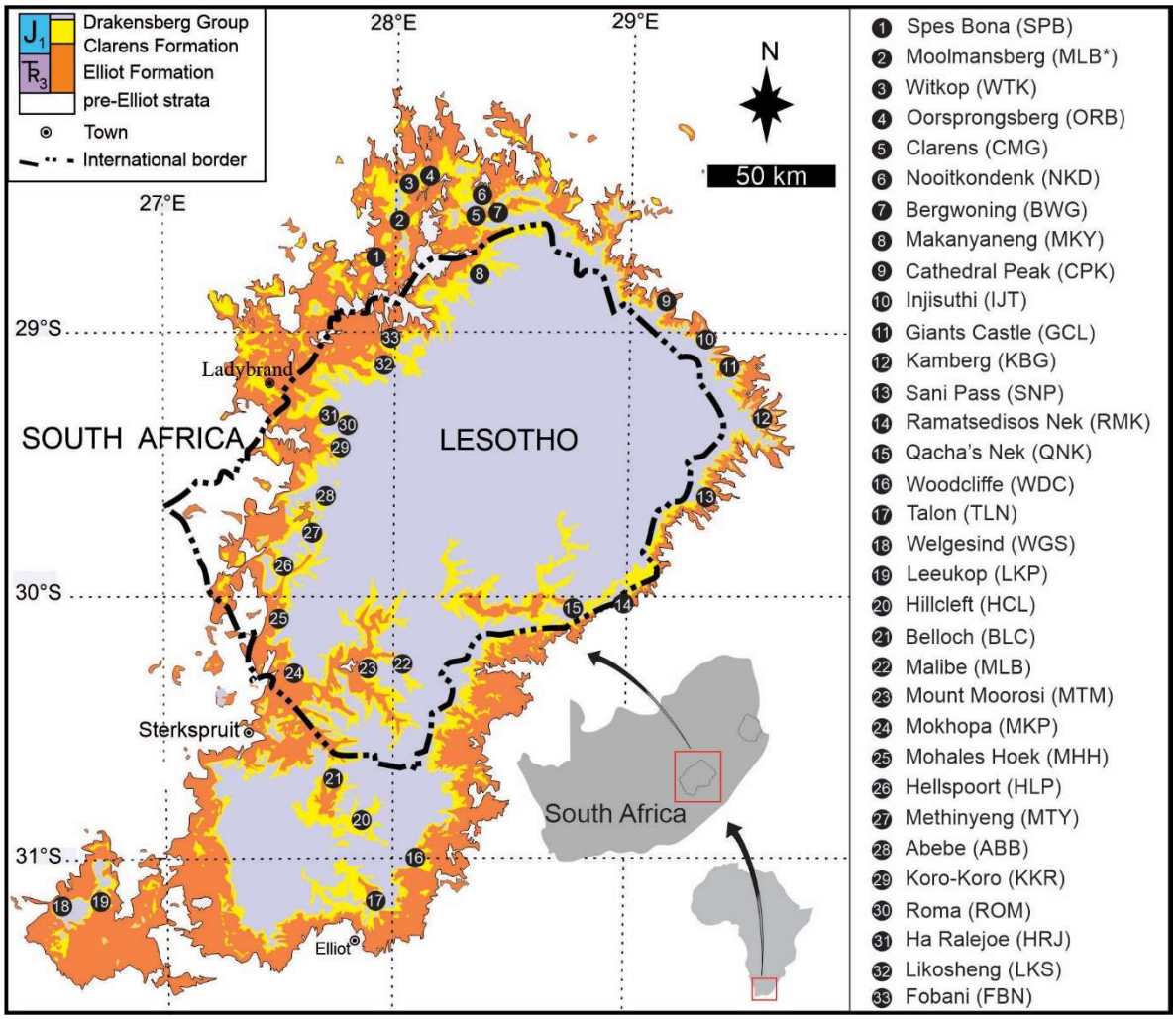

Figure 3.1. Simplified geological map of the upper Karoo Supergroup in the main Karoo Basin showing the locations of sedimentary logs measured in the Clarens Formation in South Africa and Lesotho. Names of study locations are listed on the right with abbreviated sample names in brackets (see Figure 3.2 for logs).

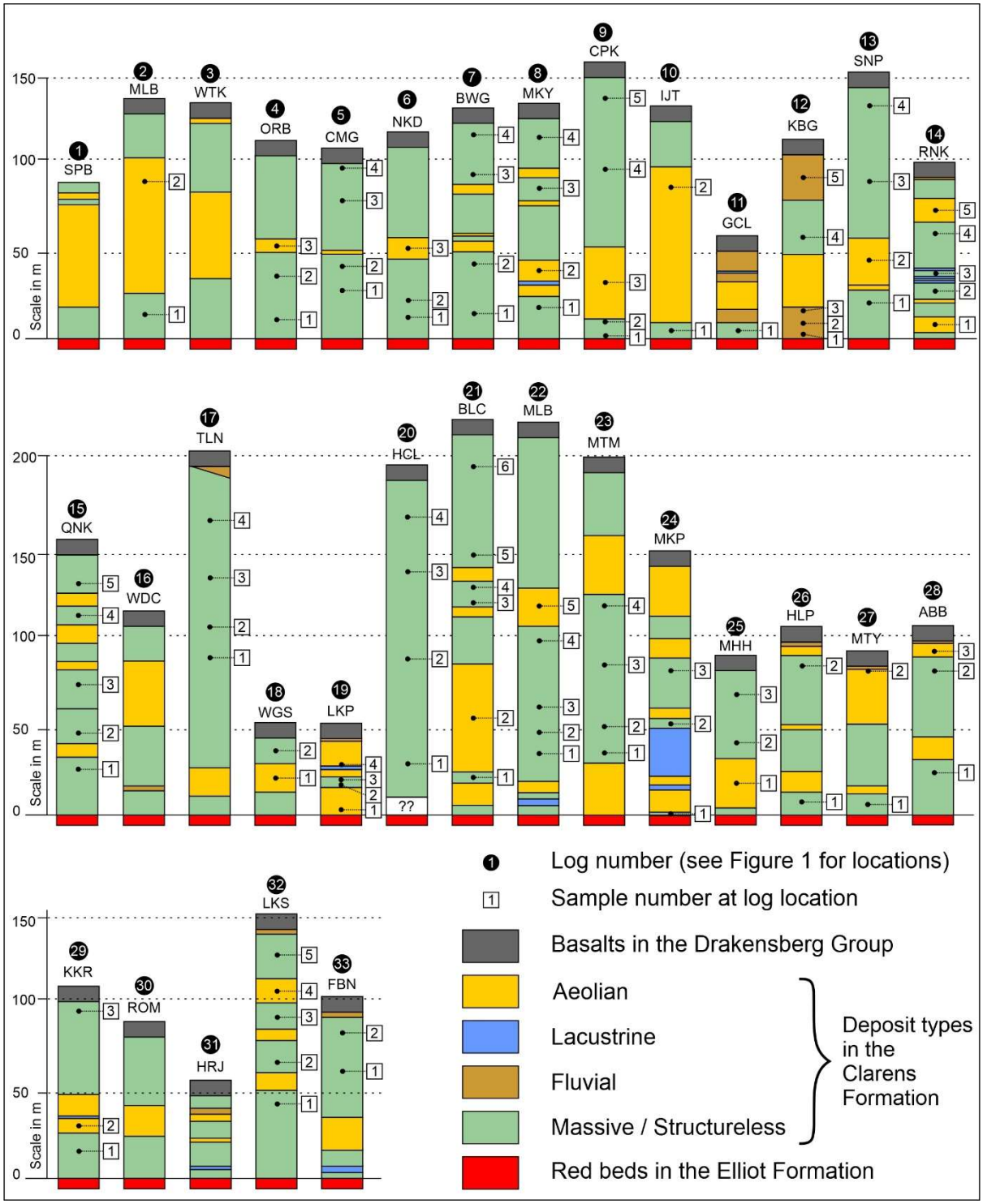

Figure 3.2. Simplified sedimentary logs of the Clarens Formation showing the sample location in each log and the interpreted main depositional processes derived from the outcrop-based observations. For the location of the sedimentary logs within the main Karoo Basin, see Figure 3.1.

3.3. Materials and methods

A total of 76 massive sandstone samples were collected from 33 sites throughout the MKB (Figure 3.1) and within the various stratigraphic zones of the Clarens Formation (Figure 3.2) with the aim to evaluate those grain parameters to determine the origin of the massive beds. Moreover, because large-scale cross-beds in the Clarens Formation were generated via demonstratable aeolian process (i.e., saltation, grain fall, and grain flow of sand particles in down-wind moving dunes), the grain parameters of the 17 cross-bedded samples (Table 3.1) were measured to serve as a baseline against which the grain properties of the massive beds of unknown origin were compared and classified.

Grain size and fabric analyses were conducted by means of thin-section point-counting under a standard petrographic microscope (Zeiss Axioscope). A total grain count of 100 is deemed sufficient for a moderately sorted sandstone by Johnson (1994) and provides a value within 10 to 13% of the true value at a confidence level of 90%. Using scaled photomicrographs, the long and short axes of grains were measured with the aid of ImageJ freeware software. Long and short axes were measured at perpendicular angles (Johnson, 1994). The grain size, being a function of the depositional process, reflects the variability of the process (e.g., flow strength). For this reason, the measure of central tendency is best represented by the mean that captures outlier effects related to depositional process dynamics. In addition, standard deviation, which shows the tendency of dispersion of a data set (Guan *et al*., 2013), is also a useful parameter, because it may reflect the nature of the aeolian process at work (e.g., extent of sorting). Axis relationships were also measured as these could relate to axes/aspect ratio and assist in determining the grain shape (Shang *et al*., 2018). The latter grain property is important, because loess particles are dominated by blade-shaped (elongated) grains (Smalley and Cabrera, 1970; Rogers and Smalley, 1983, Smalley and Marković, 2017).

Given the difficulty in distinguishing primary versus secondary depositional effects on aeolian grain properties (Vandenberghe *et al*., 2018), their classification in this study was attempted based on grain fabric analysis (Derbyshire *et al*., 1988; Wilkins *et al*., 2018). In particular, the classification of loessite was grounded in current methods developed by Wilkins *et al.* (2018), who promote a quantitative fabric analysis technique. This method entails the use of photomicrographs to establish the ordered fabric of grain orientations. Grains with a width to length ratio of 1:3 were targeted, and its angle measured relative to a horizontal reference line. A total of 50 measurements were taken for each sample and the results plotted on an equal area rose diagram with 10° bins (Rose.net freeware) to visually show the orientational scatter (Wilkins *et al*., 2018). In addition to the visual orientational scatter, the orientational variability was also calculated using the statistical R-value (i.e., consistency ratio). Using Rayleigh's test for directional randomness (Davis, 2002). The R-value of each sample was tested against the critical value derived from the data tables for a sample size (n) of 50 at a 0.01 level of significance (α) giving a value of 0.32. Where this critical value is exceeded, a preferred orientation is suggested, whereas an R-value below the critical value would be deemed to reflect a random grain fabric. The fabric from a stratified, fine-grained deposit shows a planar trend, whereas that of a typically unstratified deposit, like a loessite, shows a random fabric (Wilkins *et al.,* 2018).

Furthermore, grain parameters (e.g., shape, size) are also dependent on the mineralogy of the source rock along with post-depositional processes (Pye, 1987). Consequently, the clay fraction in the samples is ignored, because the proportion of authigenic clay is difficult to ascertain (Crouvi *et al*., 2008). Additional limitations are related to the quantification of grain diameters by means of a 2D measurements, because these do not accurately reflect the size and shape of a 3D object (Wilkins *et al*., 2018).

3.3.1 Parameters of the large-scale cross-bedded sandstones

Seventeen samples were selected from sites where the depositional processes could be interpreted with certainty — large-scale cross-bedded sandstones that represent migrating dunes. The grain properties of these large-scale, cross-bedded sandstones were derived from thin sections to provide the benchmark parameters for the classification of the massive beds of unknown origin (Table 3.1). Grain parameters in these samples of demonstratable origin suggest that a mean grain size of > 63 µm (sand class range), a standard deviation > 0.015 (Figure 3.3) and an elongation > 0.5 (Figure 3.4) are typical of sandstones that represent aeolian dune deposits within the Clarens Formation. The high standard deviation is suggestive of a wide grain size spread (sorting), whereas the high elongation reflects a scenario where the short and long axes are closer in size and resemble a square shape.

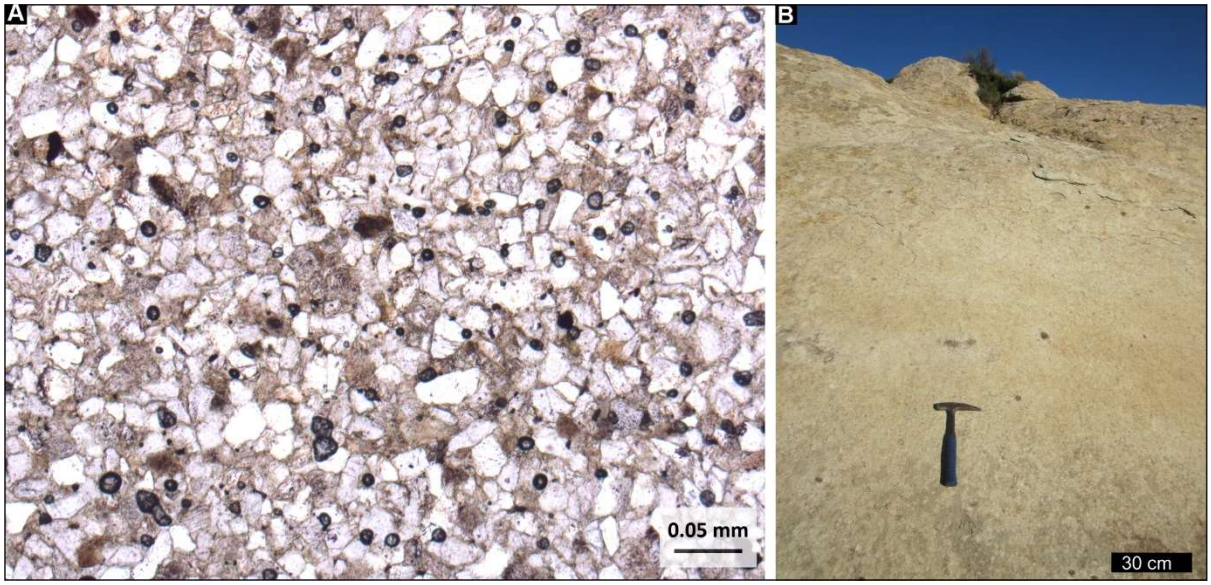

Figure 3.3: Massive deposits of the Clarens Formation**. A**. Thin section of the massive deposits from Nooitkondenk in the eastern Freestate. **B**. massive sandstone from the upper Clarens Formation at Welgesind in the Eastern Cape.

Table 3.1: Short and long axes of grains measured in thin sections of large-scale, cross-bedded sandstones in the Clarens Formation. For sample locations and their stratigraphic positions, see Figures 3.1 and 3.2.

Sample	Mean long axis (mm)	Standard deviation	Mean short axis (mm)	Elongation (short/long)	R value
BLC_02	0.079	0.021	0.048	0.601	0.253
CPK_03	0.063	0.02	0.032	0.508	0.105
HLP_03	0.058	0.015	0.039	0.677	0.129
IJT_02	0.068	0.013	0.038	0.561	0.498
KKR_02	0.095	0.023	0.053	0.555	0.189
L3_03	0.071	0.019	0.038	0.529	0.479
LKP_01	0.055	0.011	0.029	0.52	0.132
LKS_04	0.094	0.026	0.056	0.591	0.093
MHH_01	0.069	0.018	0.037	0.529	0.179
MKY_02	0.086	0.026	0.047	0.544	0.302
MLB_02*	0.073	0.02	0.038	0.525	0.235
MLB_05	0.063	0.013	0.037	0.578	0.124
NKD_03	0.063	0.017	0.03	0.48	0.381
ORB_03	0.093	0.027	0.056	0.603	0.161
RNK_05	0.058	0.014	0.031	0.526	0.097
SNP_02	0.057	0.014	0.03	0.522	0.135
WGS_01	0.059	0.011	0.032	0.543	0.362

3.4. Results

Origin of massive sandstone facies

Comparing the grain parameters in the massive beds of unknown origin to those samples of a demonstratable origin (i.e., aeolian cross-beds; Table 3.1) proved to be diagnostic in identifying the sedimentary processes responsible for the massive beds (Table 3.2). The 76 samples from the massive beds of unknown origin have been divided into six types of sedimentary facies that relate to six different depositional processes, which are comparable to modern processes in aeolian settings.

3.4.1 Facies 1: Migrating dune origin

Description: This massive sandstone type is characterised by a sandy mean grain-size range of 500-63 µm, a standard deviation of > 0.015 (Figure 3.4; 3.5; 3.6), and displays an elongation of > 0.5 (Figure 3.4; 3.6; Table 3.2). For this facies type, the R-value is undiagnostic.

Interpretation: The grain size, standard deviation and elongation in this facies is very similar to the grain properties of the large-scale, cross-bedded samples. This similarity suggests that Facies 1 resulted from saltation and may represent migrating dunes. Primary structures are not preserved, and Beukes (1969, 1970) suggested that this may be the effect of percolating rainwater that destroyed the primary structures soon after deposition. In addition, high rates of precipitation could have resulted in sand flows and large-scale slumping of dune faces that would have destroyed

primary structures, a process that is common in ancient and modern aeolian systems (Loope *et al*., 1998; Sweeney and Loope, 2001; Simpson *et al.*, 2002; Heness *et al*., 2014, Chan *et al*., 2020). Even though dunes are reworked in such cases, the aeolian characteristics of the sediment grains are maintained (Vandenberghe, 2013). Alternatively, this type may also be interpreted as aeolian sand sheets, where the internal structures are not preserved, but overall, such an origin would be associated with tabular, laterally extensive beds. Moreover, the dimensions of the massive deposits also does not support this interpretation.

3.4.2 Facies 2: Sandy dust origin

Description: This massive sandstone type is defined by a fine sandy mean grain-size range of 250-63 µm, a standard deviation of > 0.015 (Figure 3.3; 3.6), and an elongation of < 0.5 (Figure 3.4; 3.6; Table 3.2). The R-value for this type is below the 0.32 critical value threshold.

Interpretation: Despite the grain size within the fine-grained sand class fraction, the fact that the standard deviation and elongation are below the threshold of the large-scale, cross-bedded baseline suggest that this facies type has an aeolian dust origin. The standard deviation, which reflects the range of the grain size classes in the sample, indicates low dispersion (Guan *et al*., 2013) and reflects the energy consistency of the transporting agent in moving the sediment grains. The standard deviation for Facies 2 is small and distinctive of a loess deposit (Kovács, 2010; Vandenberghe, 2013). The R-value below the critical value indicates that a random grain orientation is evident in the fabric, another feature typical of a loess deposit (Wilkens *et al.,* 2018). A fine-grained sand component may also be dominant in marginal loess settings that represent a shift to cover sand or dune belts (Novotny, 2011; Vandenberghe, 2013). Where loess has a sand component > 20%, it can be classified as a sandy loess (Pye, 1987). This facies type is also recognized in the Clarens Formation of Lesotho by Ellenberger *et al*. (1964). Using the sand component of loess for the Chinese Loess Plateau, Ding *et al*. (1999) indicated that sandy loess may reveal dynamics of, and proximity to desert margins. This would, therefore, imply that Facies 2 may be the result of a combined process involving both saltation and short-term suspension and is most likely derived from a sand source with a location ranging between hundreds of meters to a few kilometers away from the site of deposition (Tsoar and Pye, 1987; Vandenberghe, 2013). These sand source areas may be nearby river terraces, sandy barforms in exposed riverbeds, and sand dunes (Enzel *et al*., 2010), and in the case of the Clarens Formation, represent a close dune source.

3.4.3 Facies 3: Aeolian dust origin

Description: This facies is defined by a mean grain size within the silt size class of 20-63 µm, a standard deviation of < 0.015 (Figure 3.4; 3.6), and an elongation of < 0.5 (Figure 3.4; Table 3.2). These characteristics are in contrast with those in the large-scale, cross-bedded samples. Although the mean grain size is silt, a sand component of up to 10 % can be present (Figure 3.5). In this facies type, the R-value is below the critical value for Rayleigh's test.

Interpretation: The dominant silt grain-size, low standard deviation, and elongation below that of the cross-bedded origin sample thresholds suggest that this facies type is of aeolian dust origin. Similar to facies 2, the typical low standard deviation is indictive of effective grain sorting processes, whereas the low elongation is typical of blade-shape particles (Rogers and Smalley, 1993; Pye, 1995; Kovács, 2010; Vandenberghe, 2013, Smalley and Markovic, 2017). In addition, an R-value below the critical value suggests a random grain fabric that is characteristic of a loessite (Wilkens *et al*., 2018)

rather than reworked loess or non-aeolian silt. The bulk of the grains size of this facies type is above 50 µm, which results from short-term suspension that occurs at low atmospheric levels (Tsoar and Pye, 1987; Sun *et al*., 2002; Vandenberghe, 2013), and has also been linked to proximal dust sources in the Negev desert in Israel and the Chinese Loess Plateau (Sun *et al*., 2002; Crouvi *et al*., 2008; Amit *et al*., 2011; Vandenberghe, 2013). In China, this grain size was also interpreted to transport proximal dust sources by dust storms during the summer season (Sun *et al*., 2002).

3.4.4 Facies 4: Transitional origin

Description: This type of massive sandstone displays a grain size within the silt size class range of <63 µm, however, neither the standard deviation nor elongation is above the estimated 0.015 and 0.5 threshold (Table 3.2), respectively. In addition, the ineffective diagnostic capability of the R-value to distinguish between loess deposition and other aeolian processes (migrating dunes) makes it an undiagnostic feature for this type.

Interpretation: The variables in Facies 4 appear to be undiagnostic with regards to a specific depositional process when compared to the samples of cross-bedded origin. The occurrence of either the standard deviation above the 0.015 threshold or the elongation above the 0.5 threshold could be indicative of a mixing of processes. For this reason, the classification of this facies type has been given the designation of *transitional,* reflecting potentially transitional depositional processes between typical desert dunes (i.e., saltation) and loess accumulation (via short-term suspension; Pye, 1987, 1995), which is common in erg-margin settings due to the proximity of loess depositional environments to erg settings. This facies may become better interpreted when evaluated in terms of the palaeo-geographic and stratigraphic position (i.e., in combination with facies relationships to lateral, over- and underlying sedimentary rocks; Lehmkuhl *et al*., 2016; Vandenberghe, 2013; Vandenberghe *et al*., 2018). Regardless of the grain parameters being undiagnostic for a specific origin, the grain size within the typical loess range (silt) combined with a random grain fabric would, however, suggest that this facies type contains a large aeolian dust (loess) component.

3.4.5 Facies 5: Reworked origin

Important to note is that reworked sediments in aeolian settings retain the characteristics of the primary source material (Vandenberghe, 2013, Vandenberghe *et al*., 2018). For this reason, the classification of this massive sediment type is hinged on the retention of aeolian signatures within the grain characteristics where the R-value does not conform to the aforementioned facies types. Facies 5 is defined by the R-value that shows a preferred orientation in the grain fabric (planar). Whether the sediment was aqueously reworked or in gravity-driven processes is not definitive, however, Wilkens *et al.* (2018) shows that planar fabrics are consistent with aqueous reworking. The following two reworked facies types are defined.

3.4.5.1 Facies 5a: Lacustrine reworked origin

Description: This massive sample type displays a silt-dominated grain size, a standard deviation of < 0.015 (Figure 3.3), and an elongation of < 0.5 (Figure 3.4 and Table 3.2). The sample shows horizontal to subhorizontal grain orientation and has an R-value that is above the 0.32 critical value for Rayleigh's test.

Interpretation: This type has identical properties as that of Facies 3 (aeolian dust), with the exception of the R-value that shows a preferred orientation of the grain fabric. The aeolian grain-size signature is retained and given the loessite criteria of Wilkens *et al.* (2018) as having a random grain fabric, could be secondary loess that was aqueously reworked. More specifically, this facies is classified as having a lacustrine origin where sediments settled into the lake out of aeolian suspension (Vandenberghe, 2013; Vandenberghe *et al.,* 2018). Keeping in mind that bioturbation may also influence the grain fabric of lacustrine reworked sediments (Wilkens *et al*., 2018), the interpretation of a massive deposit with a preferred grain fabric orientation needs to be evaluated cautiously, with all associated sedimentary evidence. The occurrence of lacustrine deposits within the Clarens Formation (Figure 3.2; Beukes, 1969, 1970; Bordy and Head, 2018) is, thus, consistent with such an interpretation.

3.4.5.2 Facies 5b: Fluvially reworked origin

Description: This type is characterised by a grain size within the sand class range of >63 μ, a standard deviation of > 0.015 (Figure 3.4; 3.6) and an R-value of > 0.32 (Figure 3.5; 3.6; Table 3.2). The elongation appears to be undiagnostic.

Interpretation: The grain size in the sand range and the high standard deviation suggest that this facies type may, in part, represent a migrating dune origin, although not all Facies 1 criteria are met. The R-value above the critical value indicates a preferred grain orientation and imply a reworking of aeolian sediments. Vandenberghe *et al*. (2018) suggested that coarser material can be incorporated when fluvial action reworks aeolian sediments. In addition, a fluvially reworked aeolian deposit displays a poorer sorting compared to aeolian sediments reworked in a lacustrine setting (Vandenberghe *et al.,* 2018). The higher standard deviation in facies 5.2 relative to facies 5.1 suggest less efficient sorting in the fluvially reworked facies type.

Table 3.2: Re-interpretation of the massive (structureless) sandstone samples based on grain parameters after a comparison to grain features in large-scale, cross-bedded sandstones. For sample locations and their stratigraphic positions, see Figures 3.1 and 3.2. For the re-interpreted logs, see Figure 3.8.

Sample	Mean long axis (mm)	Standard deviation	Mean short axis (mm)	Eongation (Short/long)	R value	Facies type	Interpretation
BLC_01	0.153	0.045	0.095	0.618	0.154	1	Aeolian dune migration
BLC_03	0.064	0.022	0.034	0.530	0.162	1	Aeolian dune migration
BLC_04	0.100	0.036	0.060	0.602	0.129	1	Aeolian dune migration
BLC_05	0.063	0.018	0.031	0.494	0.516	5b	Reworked fluvial
BLC_06	0.064	0.015	0.034	0.523	0.464	5b	Reworked fluvial
BWG_01	0.057	0.016	0.027	0.473	0.172	4	Transitional
BWG_02	0.099	0.027	0.048	0.484	0.262	1	Aeolian dune migration
BWG_03	0.062	0.016	0.028	0.453	0.187	3	Loess

BWG_04	0.066	0.018	0.032	0.486	0.113	2	Sandy loess
CMG_01	0.063	0.016	0.028	0.450	0.352	5a	Reworked lacustrine
CMG_02	0.079	0.025	0.041	0.522	0.539	1	Aeolian origin
CMG_03	0.065	0.039	0.029	0.445	0.269	2	Sandy loess
CMG_04	0.062	0.017	0.030	0.488	0.376	5a	Reworked lacustrine
CPK_01	0.058	0.015	0.027	0.460	0.306	3	Loess
CPK_02	0.053	0.012	0.024	0.454	0.066	3	loess
CPK_04	0.046	0.011	0.022	0.476	0.148	3	Loess
CPK_05	0.059	0.042	0.027	0.450	0.271	4	Transitional
FBN_01	0.046	0.013	0.023	0.514	0.230	4	Transitional
FBN_02	0.054	0.010	0.027	0.502	0.290	4	Transitional
GCL_01	0.032	0.006	0.016	0.495	0.060	3	Loess
HCL_01	0.059	0.016	0.027	0.466	0.131	4	Transitional
HCL_02	0.057	0.015	0.027	0.481	0.258	3	loess
HCL_03	0.059	0.015	0.029	0.489	0.056	3	loess
HCL_04	0.056	0.013	0.027	0.484	0.176	3	Loess
HLP_01	0.060	0.011	0.029	0.484	0.683	5a	Reworked lacustrine
HLP_02	0.058	0.014	0.029	0.510	0.311	3	Loess
IJT_01	0.047	0.008	0.021	0.455	0.111	3	loess
KKR_01	0.049	0.010	0.023	0.466	0.111	3	Loess
KKR_03	0.056	0.014	0.027	0.481	0.160	3	Loess
L3_01	0.067	0.024	0.034	0.498	0.087	2	Sandy loess
L3_02	0.059	0.011	0.032	0.535	0.251	4	Transitional
LKP_02	0.054	0.012	0.027	0.493	0.142	3	Loess
LKP_03	0.059	0.015	0.029	0.485	0.479	5a	Reworked lacustrine
LKP_04	0.060	0.014	0.028	0.461	0.648	5a	Reworked lacustrine
LKS_01	0.052	0.010	0.026	0.493	0.316	3	Loess
LKS_02	0.055	0.013	0.027	0.486	0.020	3	loess
LKS_03	0.053	0.014	0.029	0.544	0.265	4	Transitional
LKS_05	0.059	0.016	0.032	0.547	0.215	1	Aeolian dune migration
MHH_02	0.046	0.010	0.023	0.495	0.087	3	Loess
MHH_03	0.055	0.014	0.029	0.524	0.123	4	Transitional
MKP_01	0.040	0.009	0.016	0.413	0.102	3	Loess
MKP_02	0.062	0.013	0.028	0.450	0.222	3	loess
MKP_03	0.054	**0.017**	0.027	0.499	0.273	4	Transitional
MKY_01	0.052	0.011	0.025	0.474	0.304	3	Loess
MKY_03	0.058	**0.024**	0.030	**0.521**	0.236	1	Aeolian dune migration
MKY_04	0.061	**0.015**	0.032	**0.532**	0.151	1	Aeolian dune migration
MLB_01	0.056	**0.016**	0.028	0.497	0.253	4	Transitional

MLB_01*	0.061	**0.018**	0.029	0.479	0.147	4	Transitional
MLB_02	0.049	0.011	0.029	**0.601**	0.248	1	Aeolian dune migration
MLB_03	0.057	0.014	0.029	**0.513**	0.082	4	Transitional
MLB_04	**0.067**	**0.044**	0.031	0.471	0.262	2	Sandy loess
MTM_01	0.048	0.012	0.025	0.525	0.232	3	Loess
MTM_02	0.047	0.014	0.024	0.509	0.120	3	Loess
MTM_03	0.060	**0.016**	0.031	**0.525**	0.122	1	Aeolian dune migration
MTM_04	0.045	0.009	0.024	**0.531**	0.295	4	Transitional
MTY_01	0.054	0.012	0.027	0.491	0.037	3	Loess
NKD_01	0.051	**0.016**	0.025	0.492	0.044	4	Transitional
NKD_02	0.057	**0.019**	0.026	0.458	0.142	4	Transitional
ORB_01	0.053	0.014	0.027	**0.505**	0.243	4	Transitional
ORB_02	0.057	0.014	0.029	**0.508**	0.155	4	Transitional
QNK_01	0.051	0.014	0.032	**0.635**	0.088	1	Aeolian dune migration
QNK_02	0.058	0.011	0.030	**0.511**	0.211	4	Transitional
QNK_03	0.051	0.011	0.029	**0.574**	**0.427**	5a	Reworked lacustrine
QNK_04	0.060	**0.015**	0.030	**0.503**	**0.366**	5a	Reworked lacustrine
QNK_05	0.058	0.013	0.030	**0.518**	0.315	4	Transitional
RMK_02	0.057	0.012	0.028	0.482	**0.500**	5a	Reworked lacustrine
RMK_03	0.053	0.010	0.028	**0.534**	**0.434**	5.1	Reworked lacustrine
RMK_04	0.055	0.013	0.028	**0.510**	**0.357**	5.1	Reworked lacustrine
SNP_01	0.052	0.012	0.025	0.494	0.180	3	Loess
SNP_03	0.048	0.010	0.023	0.479	0.125	3	Loess
SNP_04	0.055	0.011	0.029	**0.522**	0.132	4	Transitional
TLN_01	0.050	**0.017**	0.021	0.424	0.083	2	Sandy loess
TLN_02	0.052	0.010	0.025	0.492	0.210	3	Loess
TLN_03	0.053	0.011	0.024	0.455	0.112	3	Loess
TLN_04	0.052	0.012	0.023	0.436	0.185	3	Loess
WGS_02	**0.065**	**0.015**	0.031	0.474	0.073	2	Sandy loess

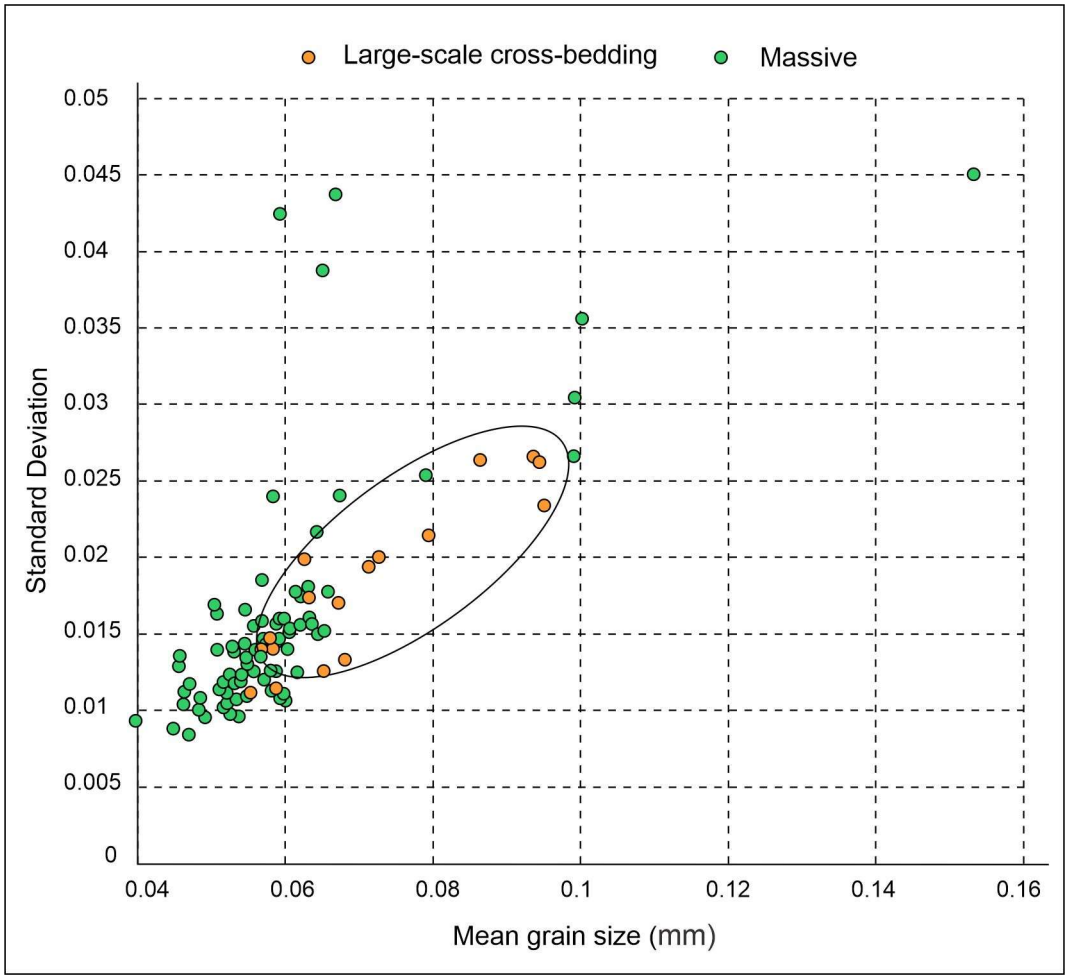

Figure 3.4. Mean grain size of the 99 Clarens Formation samples plotted against the standard deviation. Note that most cross-bedded sandstones have a standard deviation of > 0.015.

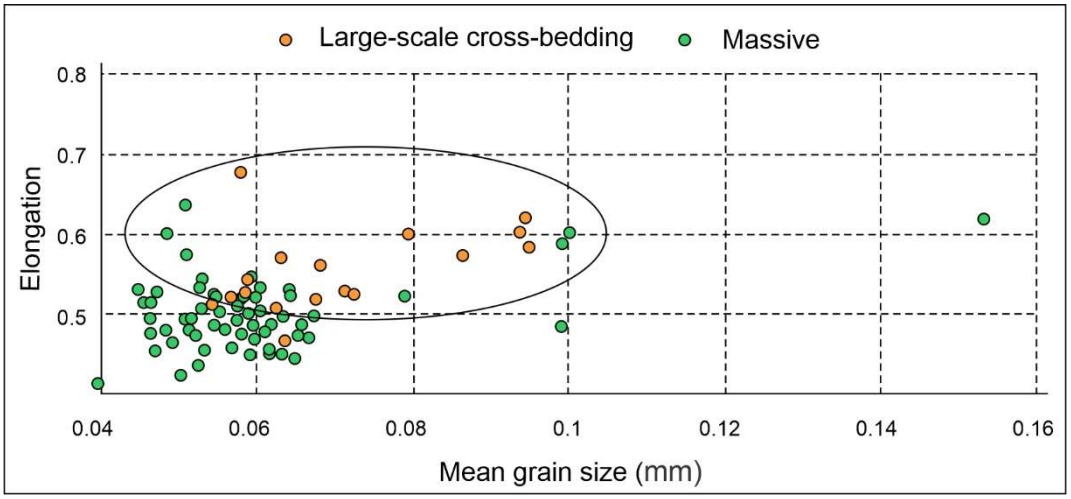

Figure 3.5. Mean grain size (long axis) of the 99 Clarens Formation samples plotted against the elongation (short/long). Note that most cross-bedded sandstones have an elongation of > 0.5.

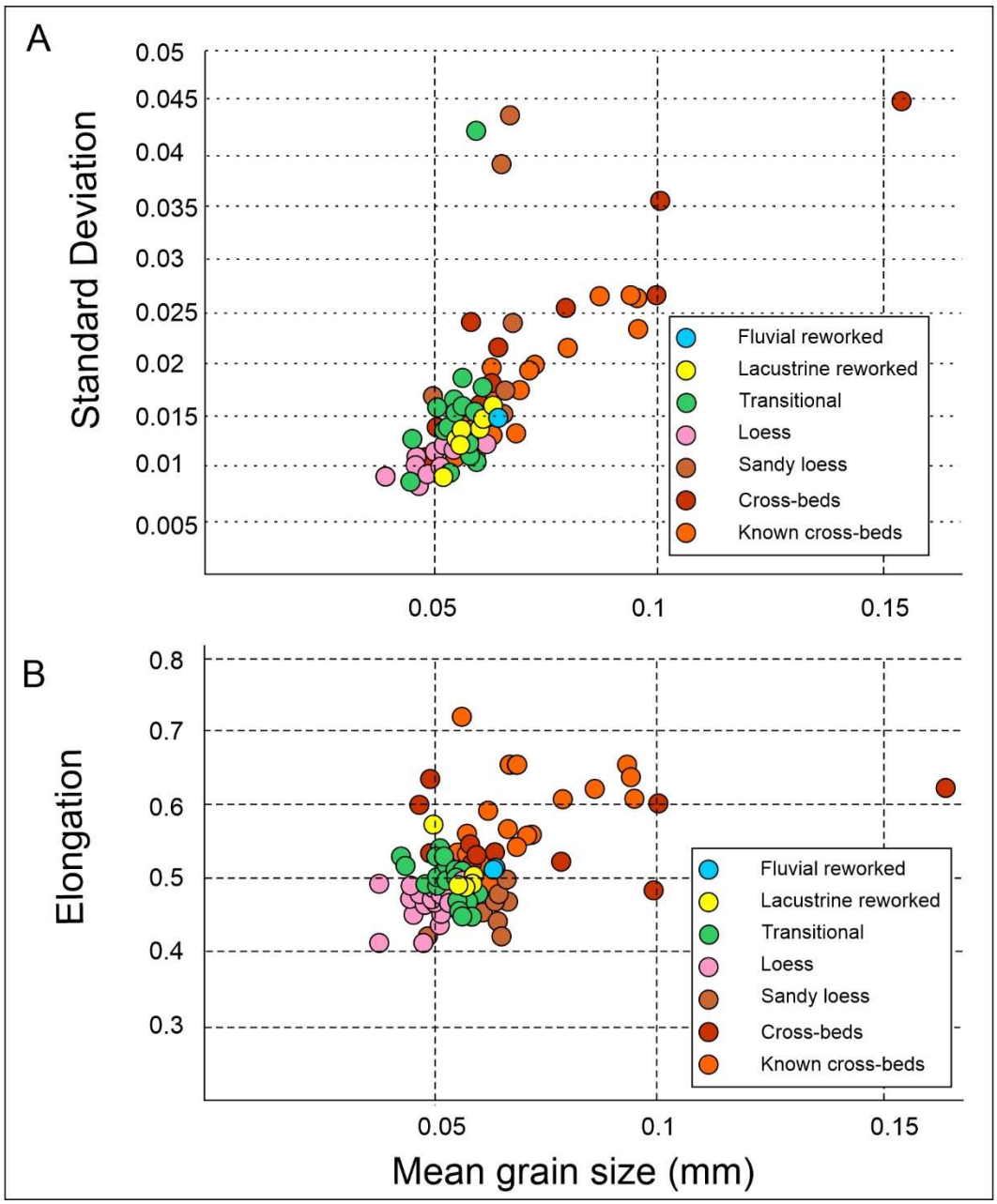

Figure 3.6: Massive deposit classification clusters based on standard deviation (A) and elongation (B).

3.4.6 Comparison of the facies types

The cumulative grain size percentage graph (Figure 3.7) shows the interpreted populations of processes that range from migrating dunes (large-scale, cross-bedded sandstones) to settling of aeolian dust (loess) from suspension. Facies 2 (sandy loess) and Facies 5b (fluvially reworked) appear to incorporate a sandy fraction, as the curves tend towards the coarser, sandier side of the graph, whereas Facies 2 still maintains a relatively narrow range of grain size classes, which is typical of loess (Kovács, 2010; Vandenberghe, 2013). In addition, Facies 5b (fluvially reworked) shows a trend similar to Facies 1 (windblown sand) in the finer fraction (coarse silt) and switches to a more loess-like trend towards the sand fraction, suggesting a mixed sediment source. According to Vandenberghe *et al*. (2018), this inclusion of a sand component is the result of incorporation of

sediment along the surface during the reworking process, whereas the sand component in the sandy loess may represent changes in the available source material or relative position to the erg margin (Tsoar and Pye, 1987; Pye, 1995; Ding *et al*., 1999; Vandenberghe *et al*., 2013). The curves of Facies 4 (transitional) and that of Facies 5a (lacustrine reworked) show a tendency towards that of Facies 3 (aeolian dust), although the finer fraction of Facies 5a appears to trend towards that of Facies 1 (windblown sand), suggesting a mixed sediment source skewed towards a loess component. Given that Facies 5a reflects a reworked loess, which maintains the original aeolian signatures, airfall processes would have been dominant, with minor input from a sandier source (e.g., lake margin; Vandenberghe, 2013; Vandenberghe *et al*., 2018). Despite the lack of definitive signatures within the grain parameters, Facies 4 (transitional) tends towards that of Facies 3 (loess–Figure 3.7), which points to a loess origin. The stratigraphic association of these deposits, as established from the field relationships, would suggest that overall, these varying types of sediments a–e due to a continuum of processes that generate sand dunes and loess blankets as described by Pye (1995). In this scenario, lateral transition exists between sand dunes, sand sheets, sandy loess, and loess and thus these deposits can occur in vertical stratigraphic order in rock successions, as seen for the Qacha's Nek locality (see Section 3.4).

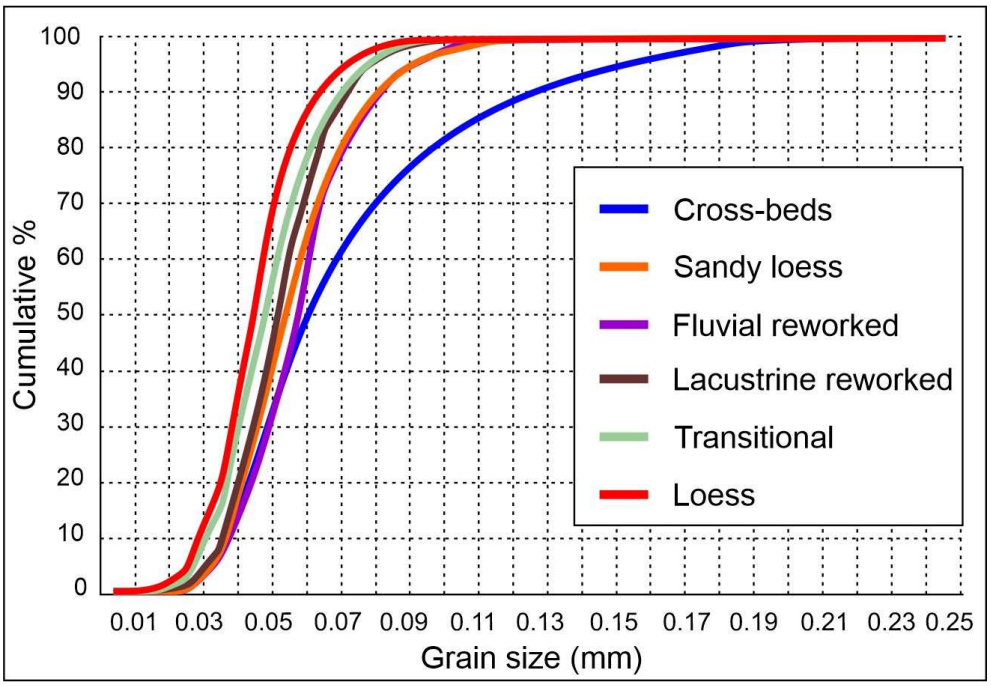

Figure 3.7. Cumulative grain size percentage graph of the 99 Clarens Formation samples showing the six main sedimentary process identified in them.

3.4.7. Qacha's Nek massive beds: a case study

Description: This site is located close to the town of Qacha's Nek in south-eastern Lesotho (Figure 3.1). Here, the ~ 150-m-thick Clarens Formation is dominated by massive layers that are interbedded with large-scale, cross-bedded sandstones (Figure 3.6). Five rock samples, taken from different stratigraphic elevations (Figures 3.1; 3.8), revealed that despite four of the samples being silt-dominated, two (QNK-3 and 4) have a grain fabric and can be classified as Facies 5a (lacustrine reworked). Of the remaining samples, two (QNK-2 and 5) have undiagnostic grain features, with silt-

size grains and an R-values that do not exceed the critical value. Sample QNK-01 shows an elongation similar to that of Facies 1 (windblown sand). The grain size of QNK-01 is coarse silt, the elongation is high (0.63), and the standard deviation is just below the selected cut-off threshold of 0.015.

Interpretation: The measurements of the Qacha's Nek samples are a pertinent illustration of how grain features can assist in distinguishing various depositional processes. Sample QNK-01 is interpreted as Facies 1 (large-scale cross-bedded) on the basis of the strong elongation and the standard deviation, although the grain size is coarse silt. This fits well with the overlying facies as a large-scale cross-bedded sandstone. Sample QNK-02 exhibits characteristics of Facies 4 (transitional) given that the mean grain size is silt, the standard deviation is undiagnostic and the grain fabric is random (Figure 3.6), indicating a primary loess deposit. It should be noted that bioturbation can also result in random grain fabric (Wilkins *et al.,* 2018). Both samples QNK-03 and QNK-04 have similar grain features to Facies 3 (loess), however, the diagnostic R-values show a preferred orientation that would suggest a lacustrine-reworked origin (i.e., Facies 5.1). Lastly, sample QNK-05 shows grain features similar to Facies 4 (transitional), where a silt grain size and a random grain fabric orientation could imply a primary loess component and thus an aeolian dust origin deposited as a transitional environment (i.e., Facies 3).

Overall, the Qacha's Nek site reflects the development of an initial erg setting with migrating dunes (Figure 3.9A) that transitioned into a landscape where dust deposition resulted in thick and extensive loess deposits (Figure 3.9B) downwind of an active erg system. Expansion of the erg and the appearance of large dunes may have dammed water courses, so that dune-dammed shallow lakes developed along the erg margin during wetter phases in this erg system (Figure 3.9C). Alternatively, the flooding may be related to a raised water-table, which could be corroborated, albeit cautiously, by the lack of fluvially reworked sediments. Dunes would have intermittently migrated over these lake deposits during more arid phases (Figure 3.7C). Eventually, erg retreat resulted in the renewed deposition of loess, and aeolian dust blanketing the lacustrine sediments (Figure 3.7D).

Dynamics and evolution of erg margins are controlled by complex spatial and temporal variations of parameters, such as sediment supply and availability, carrying capacity of the wind and water table fluctuations (Mountney and Jagger, 2004). These would have controlled the migration of the erg and deposition of loess down-wind of the erg along with the complex and close spatial relationships of the various facies at the Qacha's Nek site. The interpreted lacustrine deposits, suggested to have been generated during wet phases, promoted the formation of candidate composite surfaces (flood surfaces of Langford and Chan, 1988; Mountney and Jagger, 2004; Mountney, 2006; Hasiotis *et al.,* 2021). Such large interdunal lakes usually develop along erg margins during expansion of the interdunes, when non-climbing dune migration takes place, such as the case of the Cedar Mesa Sandstone in Utah, USA (Langford and Chan, 1988; Mountney and Jagger 2004).

3.5. Discussion

Grain characteristics have been used to classify aeolian deposits, because these grain parameters are related to the process of formation and ultimately depositional environment. Aeolian sediments are transported in various ways depending on the frequency, magnitude, and direction of the transporting wind. The distance travelled by dust in suspension is dependent on the wind regime. For example, local winds that are limited to the lower atmosphere only transport dust up to

hundreds of meters to a few kilometers (Pye, 1984; 1987; Tsoar and Pye, 1987). Large-scale systems, such as cyclones, create a high degree of turbulence in the atmosphere that result in strong vertical mixing of air columns and allow for dust to be lifted into higher atmospheric layers that are then distributed across the globe (Pye, 1984; 1987; Tsoar and Pye, 1987). These ultimately influence the grain size, which is dependent on factors such as: 1), the size distribution of the source area; 2) the distance of the depositional site from the source; and 3) timing and frequency of precipitation (Pye and Tsoar, 1987). However, Vandenberghe *et al*. (2018) suggest that, in addition to the transport distance, the occurrence of these grain-size variations in aeolian sediments also result from fluctuating local and regional wind strength and circulation patterns, the topography within the basin and changing climatic conditions.

Generally, loess occurs as extensive, uniform sheets that blanket the landscape (Smalley and Vita-Finzi, 1968; Muhs, 2013). According to Pye (1995), the key criteria for a sediment to be considered loess is that: 1) the grain size is predominantly in the silt size fraction; and 2) the accumulation is of a subaerial nature. Three fractions are common in primary loess: 51 – 60 µm, 35–40 µm and 25–31 µm, of which the 35–40 µm fraction appears to be the most dominant in primary loess successions (Vandenberghe, 2013; Vandenberghe *et al*., 2018). The grain size for the investigated massive beds in the Clarens Formation is coarser than that of typical loess and mostly falls in the 50 to 60 µm fraction. This coarse fraction of aeolian dust would have been transported by surface winds during short suspension episodes and accumulated in adjacent downwind areas to form massive deposits of loess (Tsoar and Pye, 1987; Pye 1987; Sun *et al*., 2002). Suspended dust particles are generally finer than 50 µm (Tsoar and Pye, 1987) and particles between 25 to 65 µm are transported in short-term suspension clouds that occur near the surface (Tsoar and Pye, 1987; Vandenberghe *et al*., 2018). Given this threshold, grains larger than 20 µm should reflect a proximal source (Tsoar and Pye, 1987; Sun *et al*., 2004; Crouvi *et al*., 2008).

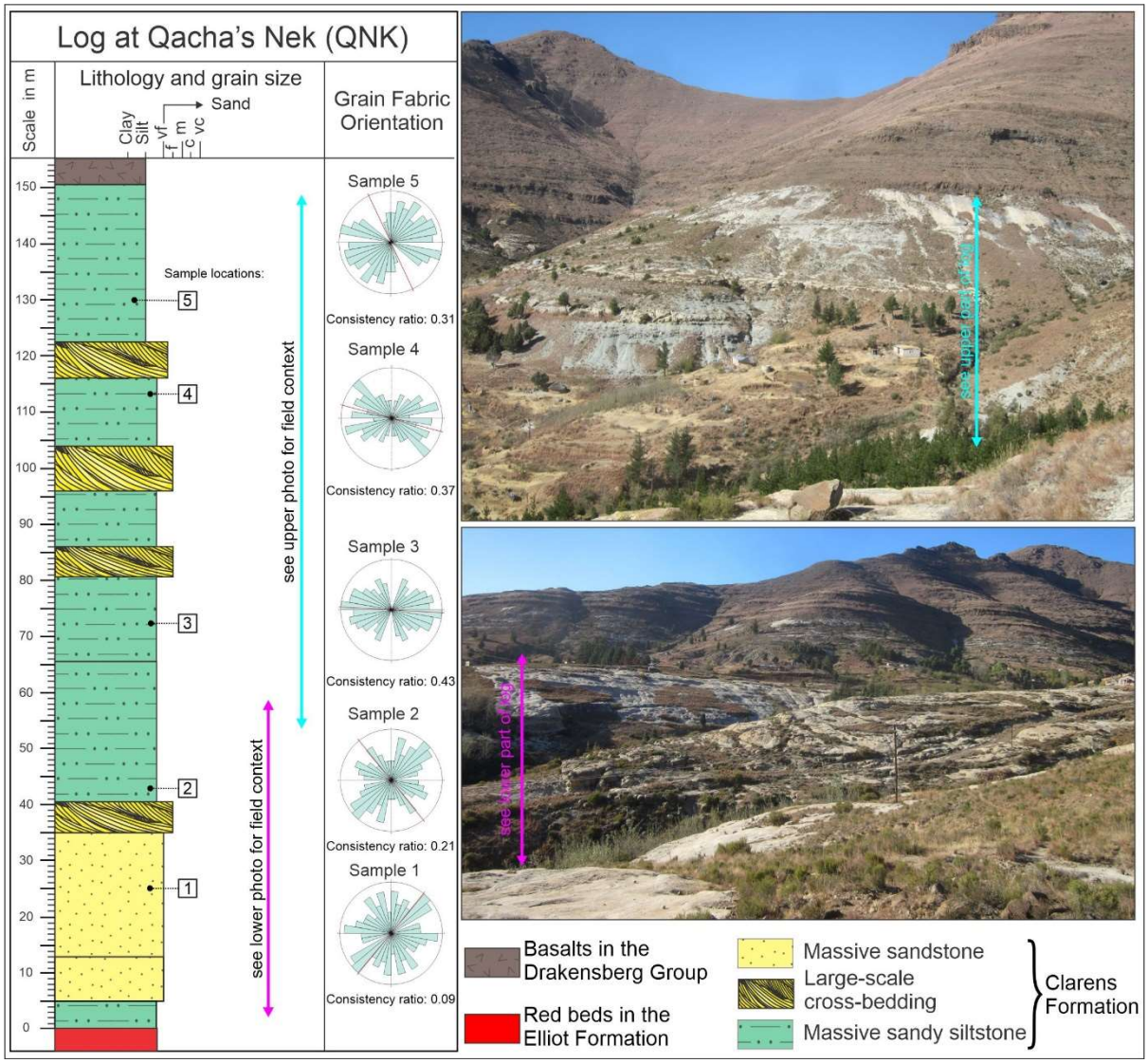

Figure 3.8: Sedimentary log at the Qacha's Nek site with grain fabric represented by rose diagrams and consistency ratios (see Table 3.2). The pink and blue arrows in the log correspond to those in the photographs on the right where they mark the logged stratigraphic intervals.

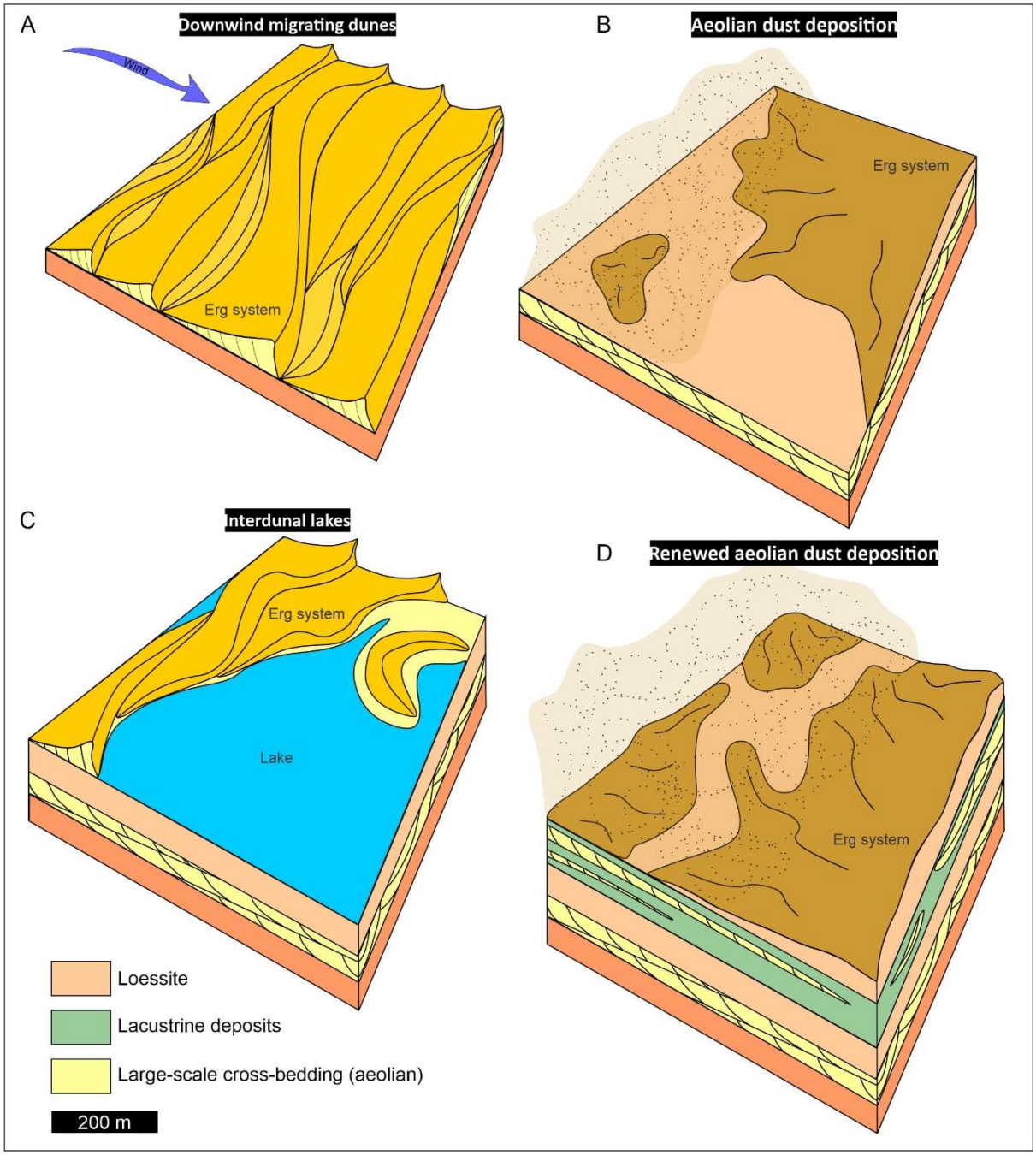

Figure 3.9. Evolution of the depositional environment near the Qacha's Nek site. **A.** Migrating dunes interpreted from Facies 1. **B**. Aeolian dust deposition (loess) down-wind from an erg system interpreted from Facies 3. **C**. Development of large interdunal lakes dammed by large dunes along an erg margin interpreted from Facies 5a. **D**. Renewed loess deposition interpreted from Facies 4. Note the stacking of the facies within the stratigraphic framework (also see sedimentary log #15 in Figures 3.2, 3.6 and 3.8).

The existence of a suitable sediment trap is important for long-term accumulation and thick loess deposits are more likely to form when a semi-arid basin is close to the source of the dust (Tsoar and Pye, 1987). In areas where wind speeds reduceand weaken or an increase in surface roughness is observed, dry deposition will occur (Pye, 1995). Dust can, therefore, be trapped by topographic irregularities, vegetated and/or moist surfaces that allow for the long-term accumulation of dust (Pye, 1995; Dubois *et al.*, 2012; Meijer *et al*., 2020). Although vegetation is believed to be one of the foremost trapping mechanisms, it is not essential for the accumulation of loess and other efficient dust-trapping mechanisms may appear locally in desert and erg margin settings (Pye and Tsoar, 1987). However, the lack of peri-desert loess along the Sahara Desert has been attributed to a lack of vegetational traps in these areas (Tsoar and Pye, 1987; Goudie and Middleton, 2001; 2006). Despite the presence of locally developed palaeosols reported in the Clarens Formation (Ellenberger *et al*., 1964) as well as various plant fossils (e.g., Meijs 1960; Ellenberger 1970; Haupt 2018), a general absence of vertical root structures or other palaeosol indicators in the massive units of the Clarens Formation could suggest that vegetation played a subordinate role in the accumulation of these loess deposits and dust-trapping was more likely related to topography. This may advocate for high dust sedimentation rates (Muhs and Bettis, 2003, Hasiotis *et al*., 2021) in an environment that was dry and windy (Chan, 1999).

In parts of the study area, a sandy loessite dominates the grain-size population (e.g., samples BWG-04, CMG-03, ABB-01; Figure 3.8). This is not typical for primary loess and has been reported from the Peoria loess deposits of Nebraska in the USA, where loess contains up to 40% sand with a modal size of 50–65 µm (Winspear and Pye, 1995). Here, dust accumulation is attributed to persistent and prevailing north-westerly winds that transported fine sand by a combination of saltation, modified saltation and short-term suspension processes (Pye, 1987; Tsoar and Pye, 1987; Winspear and Pye, 1995; Pye, 1995). The interpreted sandy loess of the Clarens Formation appears to be mostly associated with large-scale, cross-bedded sandstones (Figure 3.8). This stratigraphic relationship lends validity to a transitional state between aeolian dunes, sand sheets, and loess, as mentioned by Pye (1987; 1995). This is also observed in the Peoria loess of Nebraska (Mason *et al*., 2011), and similarly, in the loess deposits of the northern Negev in Israel that exemplify an interfingering relationship of various aeolian deposits. In the Negev desert, loess is mainly of coarse-grained silt size (20–60 µm) (Ginzbourg and Yaalon, 1963), and the coarse fraction (50 to 60 µm) has been suggested to represent a quartz-rich dune-sand source located in the northern Sinai and western Negev (Yaalon and Ginzbourg, 1964; Crouvi *et al*., 2008; Crouvi *et al*., 2010; Enzel *et al*., 2010). For this reason, the sandy loess (Facies 2) in the Clarens Formation may reflect a locally derived sand component (proximal source).

The loess deposits of the Clarens Formation were frequently reworked by lacustrine and fluvial processes, where the aeolian signature is still retained within the reworked grain characteristics. These two reworking processes are described as lacustro-aeolian and fluvio-aeolian (Vandenberghe, 2013). Lacustrine reworking (Facies 5a) usually occurs due to: 1) direct airfall of silt from suspension into the lake; and 2) traction current via channel flow or surface runoff into the lake from the lake margin (Vandenberghe *et al*., 2018). The latter generally has a coarser component as a result of lake margin processes. Well-sorted lake deposits can be taken as evidence for an extensive, lake setting where sedimentation occurs below the wave-base or strong dust fall component (Vandenberghe *et al.,* 2018). In the former case and in absence of bioturbating organisms, laminated lacustrine facies are expected (Tiercelin *et al.,* 1992; Frostick, 1997). In the case of the Clarens Formation, lacustrine reworked deposits (Facies 5a) show evidence for a prominent dust fall component, although a sand component is also observed and suggest the influence of lake margin processes. In the fluvially reworked deposits (Facies 5b) of the Clarens Formation, a coarser and sandier component is

observed, and occurs due to the incorporation of coarser material from the sediment during fluvial activity (Vandenberghe, 2013; Vandenberghe *et al.,* 2018). These lacustrine- and fluvial-reworking processes may have resulted from the development of candidate composite surfaces along erg margins during more humid phases (Mountney and Jagger, 2004; Mountney, 2006), as seen for the Qachas Nek area.

The relative position of an erg upwind of a dust deposit (loess) has been regarded as a palaeogeographic criteria by Johnson (1989) as part of the classification of loessite. Given the prevalent west to east wind regime during the deposition of the Clarens Formation (Beukes, 1969, 1970; Eriksson, 1981, 1986; Bordy and Head, 2018), the interpreted loessite deposits were located down-wind of a vast, mobile erg system that was active in southwestern Gondwana in the Early Jurassic. Similar observations of loess located down-wind of erg systems are that of the Negev loess that is located downwind from the Sinai-Negev erg system, and the Chinese Loess Plateau where loess deposits are also interbedded with aeolian sand along the erg margin (Muhs and Bettis, 2003; Crouvi *et al*., 2010).

Overall, the origin of the massive beds in the Clarens Formation point to a wide array of aeolian processes that reflect accumulation in sand dunes, sand sheets, and dust blankets (i.e., sandy loess and loess). The sediments also appear to be reworked in parts and could represent conditions associated with a shifting erg margin. The coarse nature of the massive beds further suggests that a large, locally derived, sandy sediment component was incorporated into the deposit. These massive beds could be linked to short term suspension episodes such as dust storms or more consistent westerly winds associated with regional atmospheric circulation patterns. The current data is insufficient to establish the Early Jurassic monsoonal circulation patterns in the study area. The presence of extensive loessite and associated deposits show that this part of southwestern Gondwana was subjected to dry and windy conditions with phases of more humid conditions as evidenced by the interbedded lacustrine and fluvial strata documented in previous studies (Beukes, 1969, 1970; Eriksson, 1981, 1986; Bordy and Head, 2018) as well as the massive beds with fluvio-lacustrine origin reported in this study.

3.6. Conclusion

The origin of massive deposits in the Clarens Formation have long been a subject of debate, and despite various interpretations, resolving the origin of these massive deposits has been hindered by a lack of robust petrographic, field sedimentological, and stratigraphic evidence. Herein, the application of grain size and other grain features have been used to successfully identify the origin of similar massive deposits in modern aeolian environments. Utilising these grain features (e.g. size, shape), massive samples of unknown origin were compared to a baseline that was created from sandstones of a demonstrated origin sampled from large-scale, dune cross-beds. The results not only corroborate but also refine the various interpretations of the origin of these massive deposits made earlier by Beukes (1969, 1970), Ellenberger *et al.* (1964), Johnson (1976) and Eriksson (1981, 1986). Six facies types were identified and can be associated with modern aeolian settings from both primary (aeolian sand dunes to dust) and reworked (lacustrine and fluvial) origin. The strong west to east wind regime that was active during deposition of the Clarens Formation suggests that these extensive, massive deposits were located downwind of a vast, dynamic erg system. Ultimately, these six facies reflect a spectrum of aeolian products that range from migrating dunes to sand sheets, sandy loess, and ultimately to loess deposits along the erg margin. This spectrum of products is the result of short-term suspension events (dust storms) and more consistent long-term westerly winds.

Localized lacustrine and fluvial processes also mixed locally derived, relatively coarser sediments into the dust deposits. The various aeolian deposits indicate that these primary aeolian sediments were intermittently reworked by fluvial and lacustrine processes that operated along the erg margin setting in southwestern Gondwana during the pervasively dry and windy Early Jurassic.

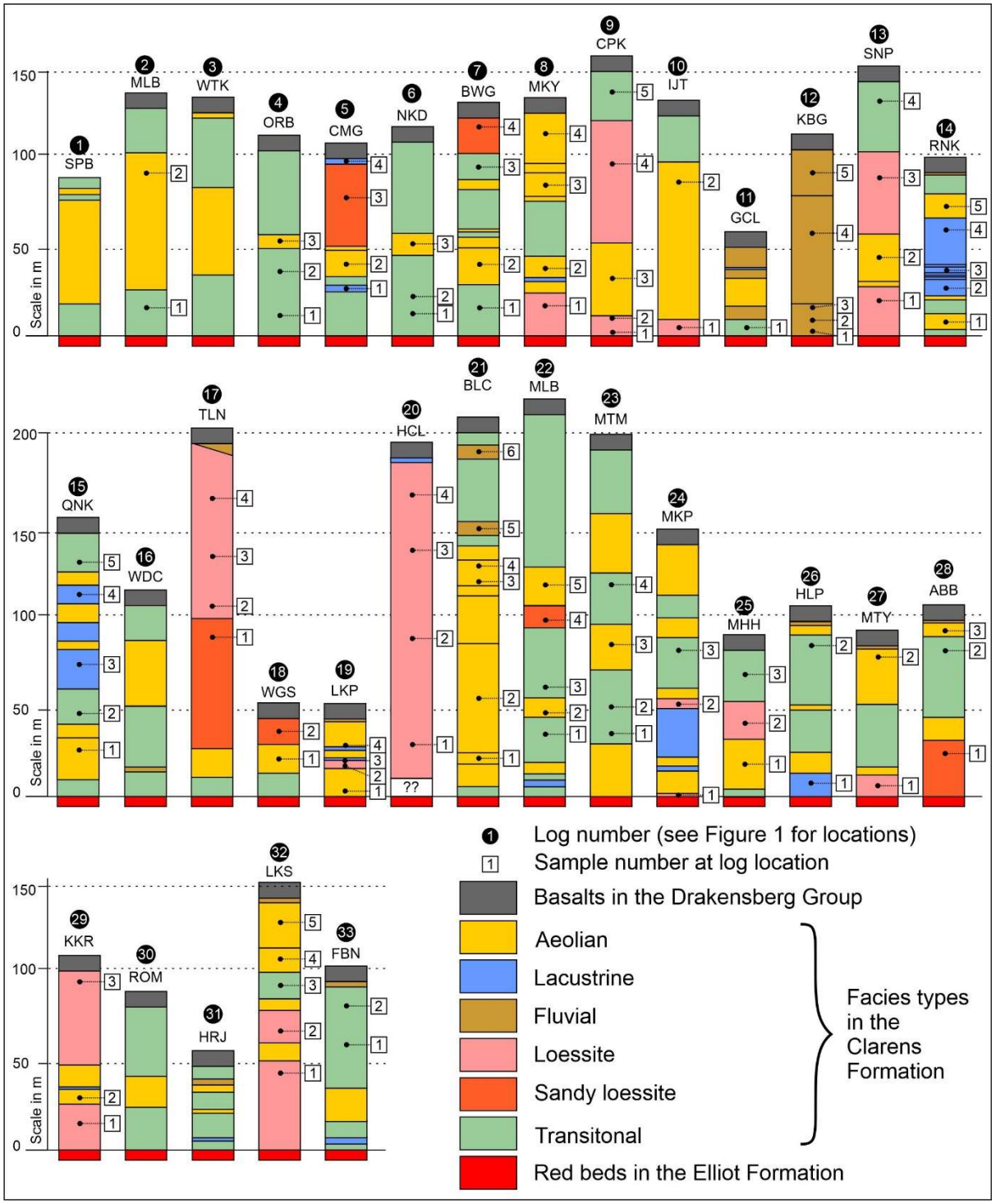

Figure 3.10. Simplified sedimentary logs showing the interpretation of the massive,structureless strata in the Clarens Formation. Compare to Figure 3.2 and Table 3.2. For the location of the sedimentary logs within the main Karoo Basin, see Figure 3.1.

3.7. References

Amit, R., Enzel, Y., Crouvi, O., Simhai, O., Matmon, A., Porat, N., McDonald, E. and Gillespie, A.R. 2011. The role of the Nile in initiating a massive dust influx to the Negev late in the middle Pleistocene. *GSA Bulletin*, 123: 873–889. DOI: 10.1130/B30241.1

Beukes, N.J. 1969. Die sedimentologie van die Etage Holkranssandsteen, sisteem Karoo. Unpublished MSc dissertation, University of the Orange Free State, Bloemfontein, 138pp. Available: http://hdl.handle.net/11660/7671

Beukes, N.J. 1970. Stratigraphy and sedimentology of the Cave Sandstone stage, Karoo System. In: S.H. Haughton (Ed), Proceedings and papers of the 2nd Gondwana symposium. Council for Scientific and Industrial Research, Pretoria: 321–341.

Bordy, E.M. 2008. Enigmatic trace fossils from the aeolian Lower Jurassic Clarens Formation, southern Africa. *Palaeontologia Electronica*, 11: 16A.

Bordy, E.M. and Catuneanu, O. 2002. Sedimentology and palaeontology of upper Karoo aeolian strata (Early Jurassic) in the Tuli Basin, South Africa. *Journal of African Earth Sciences*, 35(2): 301–314. DOI: 10.1016/S0899-5362(02)00103-3

Bordy, E.M., Bumby, A.J., Catuneanu, O. and Eriksson, P.G. 2009. Possible trace fossils of putative termite origin in the Lower Jurassic (Karoo Supergroup) of South Africa and Lesotho. *South African Journal of Scienc*e, 105(9-10): 356–362.

Bordy, E.M. and Head. H.V. 2018. Lithostratigraphy of the Clarens Formation (Stormberg Group, Karoo Supergroup), South Africa. *South African Journal of Geology*, 121: 119–130. DOI: 10.25131/sajg.121.0009

Bordy, E.M., Rampersadh, Abrahams, M., Lockley, M.G. and Head, H.V. 2020. Tracking the Pliensbachian–Toarcian Karoo firewalkers: Trackways of quadruped and biped dinosaurs and mammaliaforms. *PloS ONE,* 15(1): e0226847. DOI: 10.1371/journal.pone.0226847

Bordy, E.M., Haupt, T.N. and Head, H.V. 2021. Karoo lava-fed deltas and a petrified forest from the Lower Jurassic of southern Gondwana. Palaeogeography, *Palaeoclimatology, Palaeoecology*, 575: 110484. DOI: 10.1016/j.palaeo.2021.110484

Chan, M.A. 1999. Triassic loessite of north-central Utah; stratigraphy, petrophysical character, and paleoclimate implications. *Journal of Sedimentary Research*, 69: 477–485. DOI: 10.2110/jsr.69.477

Chan, M.A., Hasiotis, S.T. and Parrish, J.T. 2020. Hierarchical scales of soft-sediment deformation in erg deposits, Lower Jurassic Navajo Sandstone, Moab area, Utah, USA. *Journal of Sedimentary Research*, 90(9): 1068-1093. DOI: 10.2110/jsr.2020.57

Crouvi, O., Amit, R., Enzel, Y. and Gillespie, A.R. 2010. Active sand seas and the formation of desert loess. *Quaternary Science Reviews*, 29: 2087–2098. DOI: 10.1016/j.quascirev.2010.04.026

Crouvi, O., Amit, R., Enzel, Y., Porat, N. and Sandler, A. 2008. Sand dunes as a major proximal dust source for late Pleistocene loess in the Negev Desert, Israel. *Quaternary Research*, 70: 275–282. DOI: 10.1016/j.yqres.2008.04.011

Davis, J.C. and Sampson, R.J. 2002. Statistics and data analysis in geology. New York: Wiley, 646 pp.

Derbyshire, E., Billard, A., Van Vliet-Lanoë, B., Lautridou, J.P. and Cnr, M.C. 1988. Loess and palaeoenvironment: some results of a European joint programme of research. Journal of *Quaternary Science*, 3: 147–169. DOI: 10.1002/jqs.3390030206

Ding, Z., Sun, J., Rutter, N.W., Rokosh, D. and Liu, T. 1999. Changes in sand content of loess deposits along a north–south transect of the Chinese Loess Plateau and the implications for desert variations. *Quaternary Research*, 52: 56–62. DOI: 10.1006/qres.1999.2045

Dubois, M., Goldstein, R. H., and Hasiotis, S. T., 2012. Climate controls on siliciclastic sedimentation in an aggradational landscape in marine-continental (carbonate-siliciclastic) Wolfcampian cyclothems. Sedimentology, (59): 1782–1816.

Du Toit, A.L., 1904. Geological survey of the divisions of Elliot and Xalanga, Tembuland. Annual Report Geological Commission Cape Good Hope, (1903): 169–205.

Du Toit, A.L. 1918. The zones of the Karroo System and their distribution. *Proceedings of the Geological Society of South Africa*, 21: 17–36.

Ellenberger, P. 1970. Les niveaux paléontologiques de premiere apparition des mammiféres primordiaux en Afrique du Sud et leur ichnologie: Establissement de zones stratigraphiques detaillées dans le Stormberg de Leshoto (Afrique du Sud) (Trias Superieur a Jurassique). In IUGS, 2nd symposium on gondwana stratigraphy and palaeontology, 343–370.

Ellenberger, F., Ellenberger, P., Fabre, J., Ginsburg, L. and Mendrez, C. 1964. The Stormberg Series of Basutoland (South Africa). In *Reports of the 22nd International Geological Congress*, 9: 320–330.

Enzel, Y., Amit, R., Crouvi, O. and Porat, N. 2010. Abrasion-derived sediments under intensified winds at the latest Pleistocene leading edge of the advancing Sinai–Negev erg. *Quaternary Research*, 74: 121–131. DOI: 10.1016/j.yqres.2010.04.002

Eriksson, P.G., 1981. A palaeoenvironmental analysis of the Clarens Formation in the Natal Drakensberg. *Transactions of the Geological Society of South Africa*, 84: 7–17.

Eriksson, P.G. 1986. Aeolian dune and alluvial fan deposits in the Clarens Formation of the Natal Drakensberg. *Transactions of the Geological Society of South Africa,* 89: 389–393.

Frostick, L.E. 1997. The east african rift basins. In *Sedimentary basins of the World.* Elsevier, 3: 187-209.

Ginzburg, D. and Yaalon, D.H. 1963. Petrography and origin of the loess in the Be'er Sheva Basin. *Israel Journal of Earth Sciences*, 12: 68–70.

Goudie, A.S. and Middleton, N.J. 2001. Saharan dust storms: nature and consequences. *Earth-Science Reviews*, 56: 179–204. DOI: 10.1016/S0012-8252(01)00067-8

Goudie, A.S. and Middleton, N.J. 2006. Desert dust in the global system. Springer Science & Business Media: Heidelberg. 287 pp.

Guan, Q., Zhang, J., Wang, L., Pan, B., Gui, H. and Zhang, C. 2013. Discussion of the relationship between dustfall grain size and the desert border, taking the southern border of the Tengger Desert and the southern dust deposit area as an example. *Palaeogeography, Palaeoclimatology, Palaeoecology*, 386: 1–7. DOI: 10.1016/j.palaeo.2013.01.017

Hasiotis, S.T., Chan, M.A. and Parrish, J.T. 2021. Defining bounding surfaces within and between eolian and non-eolian deposits, Lower Jurassic Navajo Sandstone, Moab Area, Utah, USA: Implications for subdividing erg system strata. *Journal of Sedimentary Research*, 91(12): 1275–1304. DOI: https://doi.org/10.2110/jsr.2021.027

Haughton, S.H. 1924. The fauna and stratigraphy of the Stormberg Series. *Annals of the South African Museum*, 12(8): 323–497.

Haupt, T. 2018. Palaeoenvironmental change from the Hettangian to the Toarcian in Moyeni (Quthing District), southwestern Lesotho. Unpublished MSc dissertation, University of Cape Town, Cape Town, South Africa, 112 pp. Available: http://hdl.handle.net/11427/30021

Heness, E.A., Simpson, E.L., Bumby, A.J., Eriksson, P.G., Eriksson, K.A., Hilbert-Wolf, H.L., Okafor, O.J., Linnevelt, S., Malenda, H.F. and Modungwa, T. 2014. Evidence for climate shifts in the ~ 2.0 Ga upper Makgabeng Formation erg, South Africa. *Palaeogeography, Palaeoclimatology, Palaeoecology*, 409: 265–279. DOI: 10.1016/j.palaeo.2014.05.016

Holzförster, F. 2007. Lithology and depositional environments of the Lower Jurassic Clarens Formation in the eastern Cape, South Africa. *South African Journal of Geology*, 110(4): 543–560. DOI: 10.2113/gssajg.110.4.543

Johnson, M.R. 1994. Thin section grain size analysis revisited. *Sedimentology*, 41: 985–999. DOI: 10.1111/j.1365-3091.1994.tb01436.x

Johnson, M.R., Anhauesser, C.R. and Thomas, R.J. 2006. The Geology of South Africa. Geological Society of South Africa. Council for Geoscience, 691 pp.

Johnson, S.Y. 1989. Significance of loessite in the Maroon Formation (middle Pennsylvanian to lower Permian), Eagle basin, Northwest Colorado. *Journal of Sedimentary Research*, 59: 782–791. DOI: 10.1306/212F9070-2B24-11D7-8648000102C1865D

Johnson. M.R. 1976. Stratigraphy and sedimentology of the Cape and Karoo sequences in the Eastern Cape Province. Unpublished MSc dissertation, Rhodes University, Grahamstown, South Arica, 351 pp. Available: http://hdl.handle.net/10962/d1005617

Kovács, J. 2008. Grain-size analysis of the Neogene red clay formation in the Pannonian Basin. *International Journal of Earth Sciences*, 97: 171–178. DOI: 10.1007/s00531-006-0150-2

Langford, R.P. and Chan, M.A. 1988. Flood surfaces and deflation surfaces within the Cutler Formation and Cedar Mesa Sandstone (Permian), southeastern Utah. *Geological Society of America Bulletin*, 100: 1541–1549. DOI: 10.1130/0016-7606(1988)100<1541:FSADSW>2.3.CO;2

Lehmkuhl, F., Zens, J., Krauß, L., Schulte, P. and Kels, H. 2016. Loess-paleosol sequences at the northern European loess belt in Germany: distribution, geomorphology and stratigraphy. *Quaternary Science Reviews*, 153: 11–30. DOI: 10.1016/j.quascirev.2016.10.008

Loope, D.B., Dingus, L., Swisher III, C.C. and Minjin, C. 1998. Life and death in a Late Cretaceous dune field, Nemegt basin, Mongolia. *Geology*, 26: 27–30. DOI: 10.1130/0091-7613(1998)026<0027:LADIAL>2.3.CO;2

Mason, J.A., Swinehart, J.B., Hanson, P.R., Loope, D.B., Goble, R.J., Miao, X. and Schmeisser, R.L. 2011. Late Pleistocene dune activity in the central Great Plains, USA. *Quaternary Science Reviews*, 30: 3858–3870. DOI: 10.1016/j.quascirev.2011.10.005

Meijer, N., Dupont-Nivet, G., Licht, A., Trabucho-Alexandre, J., Bourquin, S. and Abels, H.A. 2020. Identifying eolian dust in the geological record. *Earth-Science Reviews*, 211: 103410.

Meijs, L. 1960. Notes on the occurrence of petrified wood in Basutoland. *Basutoland Notes and Records*, 2: 20–26. DOI: 10.1016/j.earscirev.2020.103410

Moulin, M., Fluteau, F., Courtillot, V., Marsh, J., Delpech, G., Quidelleur, X. and Gérard, M. 2017. Eruptive history of the Karoo lava flows and their impact on early Jurassic environmental change. *Journal of Geophysical Research: Solid Earth*, 122(2): 738–772. DOI: 10.1002/2016JB013354

Mountney, N.P. 2006. Eolian Facies Models. In Facies Models Revisited, H. Posamentier and R. G. Walker, Eds. *SEPM Special Publications,* 84: 19–83. DOI: 10.2110/pec.06.84.0019

Mountney, N.P. and Jagger, A. 2004. Stratigraphic evolution of an aeolian erg margin system: the Permian Cedar Mesa Sandstone, SE Utah, USA. *Sedimentology*, 52: 713–743. 10.1111/j.1365-3091.2004.00646.x

Muhs, D.R. 2013. The geologic records of dust in the Quaternary. *Aeolian Research*, 9: 3–48. DOI: 10.1016/j.aeolia.2012.08.001

Muhs, D.R., Bettis, E.A., Chan, M.A. and Archer, A.W. 2003. Quaternary loess-paleosol sequences as examples of climate-driven sedimentary extremes. *Special Papers-Geological Society of America,* 53–74.

Novothny, Á., Frechen, M., Horváth, E., Wacha, L. and Rolf, C. 2011. Investigating the penultimate and last glacial cycles of the Süttő loess section (Hungary) using luminescence dating, high-resolution grain size, and magnetic susceptibility data. *Quaternary International*, 234: 75–85. DOI: 10.1016/j.quaint.2010.08.002

Pye, K. 1987. Aeolian dust and dust deposits. Elsevier, 334 pp.

Pye, K. 1995. The nature, origin and accumulation of loess. *Quaternary Science Reviews*, 14: 653–667. DOI: 10.1016/0277-3791(95)00047-X

Pye, K. and Tsoar, H. 1987. The mechanics and geological implications of dust transport and deposition in deserts with particular reference to loess formation and dune sand diagenesis in the northern Negev, Israel. *Geological Society, London, Special Publications*, 35: 139–156. DOI: 10.1144/GSL.SP.1987.035.01.10

Pye, K., 1984. Loess. *Progress in Physical Geography*, 8: 176–217. DOI: 10.1177/030913338400800202

Robinson, D.N., Beer, H.M., Nutsch, F.M., and Trumpelman, F. 1969.The geology and oil potential of the Stormberg Group. Unpublished report. Southern Oil Exploration Corporation, Johannesburg.

Rogers, C.D.F. and Smalley, I. J. 1993. The shape of loess particles. *Naturwissenschaften*, 80: 461–462. DOI: 10.2478/v10085-009-0039-y

Shang, Y., Kaakinen, A., Beets, C.J. and Prins, M.A. 2018. Aeolian silt transport processes as fingerprinted by dynamic image analysis of the grain size and shape characteristics of Chinese loess and Red Clay deposits. *Sedimentary Geology*, 375: 36–48. DOI: 10.1016/j.sedgeo.2017.12.001

Simpson, E.L., Eriksson, K.A., Eriksson, P.A. and Bumby, A.J. 2002. Eolian dune degradation and generation of massive sandstone bodies in the Paleoproterozoic Makgabeng Formation, Waterberg Group, South Africa. *Journal of Sedimentary Research*, 72: 40–45. DOI: 10.1306/050701720040

Smalley, I.J. and Cabrera, J.G. 1970. The shape and surface texture of loess particles. *Geological Society of America Bulletin*, 81(5): 1591–1596. DOI: 10.1130/0016-7606(1970)81[1591:TSASTO]2.0.CO;2

Smalley, I.J. and Marković, S.B. 2017. Controls on the nature of loess particles and the formation of loess deposits. *Quaternary International*, 30: p.1e5. DOI: 10.1016/j.quaint.2017.08.021

Smalley, I.J. and Smalley, V. 1983. Loess material and loess deposits: formation, distribution and consequences. *Developments in Sedimentology*, 38: 51–68. DOI: 10.1016/S0070-4571(08)70788-X

Smalley, I.J. and Vita-Finzi, C. 1968. The formation of fine particles in sandy deserts and the nature of desert loess. *Journal of Sedimentary Research*, 38: 766–774. DOI: 10.1306/74D71A69-2B21-11D7-8648000102C1865D

Stockley, G.M. 1947. The Geology of Basutoland. *Geological Magazine*, 77(6): 444–460.

Sun, D., Bloemendal, J., Rea, D.K., Vandenberghe, J., Jiang, F., An, Z. and Su, R. 2002. Grain-size distribution function of polymodal sediments in hydraulic and aeolian environments, and numerical partitioning of the sedimentary components. *Sedimentary Geology*, 152: 263–277. DOI: 10.1016/S0037-0738(02)00082-9

Sweeney, M.R. and Loope, D.B. 2001. Holocene dune-sourced alluvial fans in the Nebraska Sand Hills. *Geomorphology*, 38: 31–46. DOI: 10.1016/S0169-555X(00)00067-2

Tiercelin, J.J., Soreghan, M., Cohen, A.S., Lezzar, K.E. and Bouroullec, J.L. 1992. Sedimentation in large rift lakes: example from the Middle Pleistocene—Modern deposits of the Tanganyika

Trough, East African Rift System. *Bulletin des Centres de Recherches, Exploration-Production Elf-Aquitaine;(France),* 16: 83–111.

Tsoar, H. and Pye, K. 1987. Dust transport and the question of desert loess formation. *Sedimentology*, 34: 139–153. DOI: 10.1111/j.1365-3091.1987.tb00566.x

Vandenberghe, J. 2013. Grain size of fine-grained windblown sediment: A powerful proxy for process identification. *Earth-Science Reviews*, 121: 18–30. DOI: 10.1016/j.earscirev.2013.03.001

Vandenberghe, J., Sun, Y., Wang, X., Abels, H.A. and Liu, X. 2018. Grain-size characterization of reworked fine-grained aeolian deposits. *Earth-Science Reviews*, 177: 43–52. DOI: 10.1016/j.earscirev.2017.11.005

Wilkins, A.D., Hurst, A., Wilson, M.J. and Archer, S. 2018. Palaeo-environment in an ancient low-latitude, arid lacustrine basin with loessite: The Smith Bank Formation (Early Triassic) in the Central North Sea, UK Continental Shelf. *Sedimentology*, 65: 335–359. DOI: 10.1111/sed.12382

Winspear, N.R. and Pye, K., 1995. Textural, geochemical and mineralogical evidence for the origin of Peoria Loess in central and southern Nebraska, USA. *Earth Surface Processes and Landforms*, 20: 735–745. DOI: 10.1002/esp.3290200805

Yaalon, D.H. and Ginzbourg, D. 1966. Sedimentary characteristics and climatic analysis of easterly dust storms in the Negev (Israel). *Sedimentology*, 6: 315–332. 10.1111/j.1365-3091.1966.tb01898.x

Chapter 4.

Sedimentary evolution of an Early Jurassic erg, as recorded in the Clarens Formation (Karoo Supergroup) of southern Africa

Abstract

The Lower Jurassic Clarens Formation represents the youngest sedimentary succession of the Stormberg Group in the Karoo Supergroup of southern Africa. This Sinemurian to Pliensbachian sedimentary unit is dominated by thick to very thick beds of massive and very large- to large-scale, cross-bedded sandstone, which were interpreted as deposits of an aeolian system with intermittent wet conditions throughout. The informal zonation of the Clarens Formation contains an upper and lower massive zone, which are separated by the middle zone that typically contains the large-scale, cross-bedded sandstones. Field evidence from this study confirms the dominance of Massive (68 %) and Aeolian Dune (20 %) deposits with minor Ephemeral Channel, Sand Sheet and Pluvial deposits, while Ephemeral Unconfined Fluvial and Debris Flow deposits represent the smallest proportion (1% and less). The spatiotemporal distribution of the deposits can be explained by a typical erg margin deposit controlled by short- and long-term drivers where short-term, water table fluctuations controlled the spatial expression of the lateral facies distribution, whereas vertical facies changes are attributed to erg expansion as a result of climate change. During humid climatic phases, small, isolated dune fields with dominant downwind loess plains developed with fluvial incursions from the southern and eastern basin margins. During aridification, increased sediment input allowed for the expansion of the erg and migration of the margin, which also shifted non-aeolian facies towards the east. The reported facies distributions, therefore, confirm the validity of the zonation of the Clarens Formation that is consistent with the wet-dry-wet climate megacycle seen in the Tethyan margin of Gondwana during the Sinemurian and Pliensbachian, and thus suggesting that it may have been a global feature. Thickness trends across the basin show a subtle decrease from south to north along with extreme thickness fluctuations in the south. These thickness patterns are comparable to the trends reported for the underlying Elliot Formation, specifically the upper Elliot Formation, indicating that deposition continued in the foresag setting in the terminal evolutionary phase of the main Karoo Basin.

4.1. Introduction

Long-term climatic and tectonic drivers exert an important control on the development of aeolian sedimentary systems and their preservation in the rock record, and thus, ancient sedimentary deposits can reflect the spatiotemporal variations in these geological drivers. Climatic cyclicity has been described in the Lower Jurassic Clarens Formation of southern Africa (Figure 4.1), which has been interpreted as an aeolian deposit with complex interactions of aeolian, fluvial, and lacustrine processes in a vast desert setting (du Toit, 1905; Van Eeden, 1937; Stockley, 1947; Beukes, 1969, 1970; Eriksson, 1981,1986; Bordy and Catuneanu, 2001; Holzförster, 2007; Bordy and Head, 2018). The most extensive work on this mainly aeolian succession has been that of Beukes (1969, 1970), who interpreted a wet-dry-wet climate megacycle during the deposition of the Clarens Formation. Despite the documented record of fluvial and lacustrine deposits in the Clarens Formation, the detailing of the extent of fluvio-lacustrine and aeolian interactions in this desert setting is still

lacking. This chapter focuses on evaluating the facies and their association within the Clarens Formation to refine its spatiotemporal relationships, distribution, and geological controls within this ancient erg system and to place the climate of southwestern Gondwana into the Early Jurassic global context.

4.2 Geological background

The Lower Jurassic Clarens Formation, along with the underlying Elliot and Molteno formations comprise the Stromberg Group of the Karoo Supergroup. It has a conformable relationship with both the underlying Elliot Formation and the overlying flood basalts of the Drakensberg Group, more specifically that of the lower Barkly East Formation (Lock *et al*., 1974; Marsh and Eales, 1984; Moulin *et al*., 2011, 2017; Bordy *et al*., 2021). The gradational lower contact with the Elliot Formation is represented by a transitional interval where red beds and fine-grained sandstones of pale colour are interbedded, making classification of the contact challenging — see explanation in Bordy and Head (2018). The upper contact is sharp, undulates and is identified by the first appearance of extrusive volcanics associated with the Drakensberg Group (Beukes, 1970; Eriksson, 1981; Bordy and Head, 2018). Sandstone interbeds having a similar lithological characteristic to that of the Clarens Formation appear amongst the Barkly East Formation, suggesting continued sedimentation in between phases of early lava extrusion.

The Clarens Formation has an average thickness of 90 to 150 m across most of the outcrop area. Dramatic thickness fluctuations are particularly abundant in the south, where the largest thickness of over 300 m occurs (between Barkly East and Elliot) and where the succession is completely missing locally (du Toit, 1904, 1905, 1910; Beukes, 1969, 1970; Robinson, 1969; Johnson, 1976; Holzförster, 2007). In the northern outcrop area, a more subdued thickness variation is typical (Beukes, 1969, 1970; Eriksson, 1981, 1986; Bordy and Head, 2018). These south to north thickness changes are in good agreement with the tectonic setting of the main Karoo Basin (MKB; Figure 4.1B) during the final phases of its evolution. Accommodation in the basin has been widely accepted to have been created by flexural tectonics in a foreland system in response to subduction of the palaeo-Pacific plate along the Panthalassan margin of Gondwana (Catuneanu *et al*., 1998, 2005). The MKB is, therefore, considered a retro-arc foreland basin (Cole, 1992, Catuneanu *et al*., 1998, 2005). In this context, the smaller extent of the MKB during the deposition of the Stromberg Group (Figure 4.1B) is attributed to foresag subsidence during the orogenic unloading in the Cape Fold Belt (Bordy *et al*., 2004b, 2005; Hanson et al., 2009). This unloading also resulted in the upliftment and erosion of the pre-Stormberg units on a regional scale (Bordy *et al*., 2004b). Foresag sedimentation was subsequently terminated by volcanism associated with the Karoo-Ferrar Large Igneous Province that was followed by the break-up of Gondwana (Beukes, 1970; Eriksson, 1981; Duncan, 1997; Bordy and Head, 2018; Muir *et al*., 2020). Beukes (1969, 1970), based on a regional study, classified three stratigraphic zones within the Clarens Formation, a lower and an upper zone where massive sandstones dominate the succession, and a middle zone where very large- to large-scale, cross-bedded sandstones become dominant over massive sandstones (Zone 1 to 3, respectively). In addition to the massive nature of zones 1 and 3, sedimentary features indicative of shallow water processes are also diagnostic for these zones and for this reason the zonation was ascribed to a wet-dry-wet climatic megacycle (Beukes, 1969, 1970; Bordy and Head, 2018). For the eastern outcrop area along the KwaZulu-Natal Drakensberg, Eriksson (1979, 1981, 1986) documented the occurrence of facies related to wadi channel and alluvial fan processes amongst the aeolian processes. These

features were ascribed to a spatial component in the palaeoenvironment of the Clarens Formation, where the erg centre was dominated by large-scale, cross-bedded sandstones, with a wet aeolian system along the erg margin preserved in the eastern outcrop area. The documentation of freshwater fish (*Semionotus capensis),* crocodylomorphs (*Notochampsa istedana*), plant fragments, and petrified tree trunks (Broom, 1904; du Toit, 1904; Haughton, 1924; Stockley, 1947; Meijs, 1960; Jubb, 1973; Forey and Gardiner, 1974; Bordy and Catuneanu, 2002; Bamford, 2004; Bordy *et al*., 2021; Dollman *et al*., 2021) supports the interpretation of episodic wet phases suggesting that the palaeoenvironment may not have been as harsh as initially thought (Bordy and Head, 2018). Moreover, field evidence presented by Bordy *et al*. (2020; in press) suggest that localised ecosystems continued to thrive on the Clarens landscape during the initiation of volcanism at the turn of the Pliensbachian-Toarcian eruptive episode (Karoo-Ferrar Large Igneous Province).

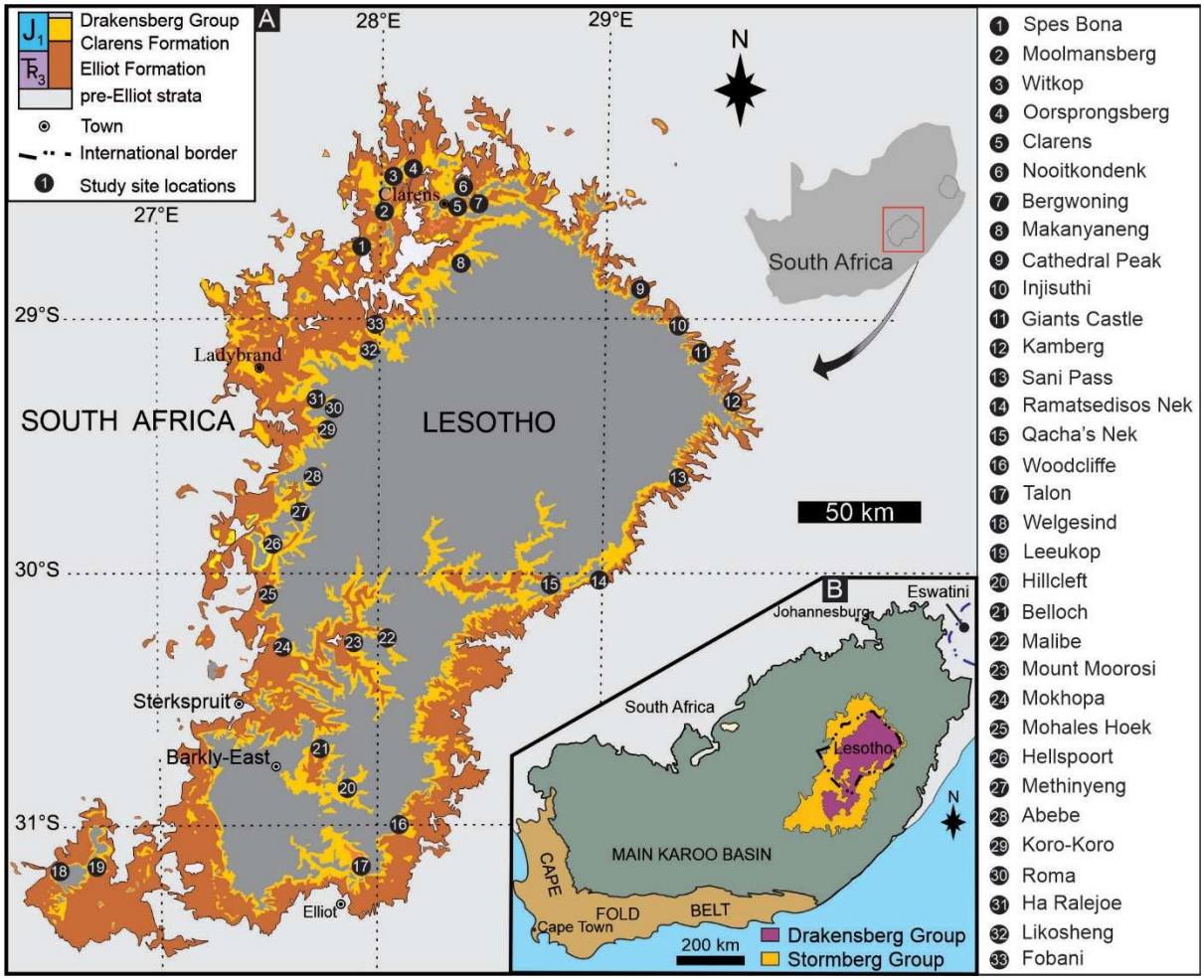

Figure 4.1: Geological context of the Clarens Formation study sites in the main Karoo Basin (MKB) of southern Africa. **A**. Geological map of the upper Stormberg Group showing the study site locations (site names listed on the right). **B**. The position of the main Karoo Basin in southern Africa, note the smaller scale of the Stormberg Group outcrop area.

4.3 Methods

Extensive regional sedimentological field work was conducted across the MKB of southern Africa, where outcrops of the Clarens Formation (Figure 4.1A) were analysed for grain size, sedimentary structures, composition, lithology, and under- and overlying facies-contact types in combination with the measurement of detailed centimetre-scale sedimentary logs. This is based on the well-established sedimentary facies analysis method delineated by Miall (1974, 1985, 1996) and commonly applied in aeolian rock successions (e.g., Mountney and Howell, 2000; Mountney and Thompson, 2002; Mountney and Jagger, 2004; Mountney, 2006; Hassan *et al*., 2018). Photo panels of large-scale outcrops were also constructed to document and understand the three-dimensional nature of the facies (Table 4.1), facies associations (Table 4.2) and their spatial relationships (Miall, 1996; Mountney, 2006). Palaeocurrents were measured from the foreset dip direction of well-developed large-scale cross-bedded sandstones (Figure 4.14B) to understand the Early Jurassic source areas and sediment distribution patterns across this part of southwestern Gondwana (High and Picard, 1974; Miall, 1974; Dasgupta, 2002; Miall, 2016).

A total of 33 sedimentary logs were recorded to assess the facies distribution over the outcrop area (Figure 4.1A). Using ©2021 Google Earth Pro software, facies maps showing the distribution and proportions of facies associations (see section 3.3) were generated by extracting facies association data from each sedimentary log both from this study and the re-interpreted logs from Beukes (1969) and Eriksson (1983)—see Appendix 5 and 6. This process was repeated for each of the different stratigraphic zones of the Clarens Formation. Since the facies proportions were extracted from 2D sedimentary logs, they reflect semiquantitative estimations for small areas, which may not be fully representative of the facies associations throughout the basin.

The thickness map of the Clarens Formation (see section 3.4) was generated from thickness data derived from this study and previous work (e.g., du Toit, 1904, 1905; Stockley, 1947; Beukes, 1969; Robinson, 1969; Eriksson, 1983). The latter dataset was tested for quality using digital elevation (terrain) tool in ©2021 Google Earth Pro software. The cleaned-up (quality assured) thickness values were imported into QGIS and a 0.5 by 0.5 degree overlay block grid created as part of the estimation input, comma separated value (CSV) files. The thickness estimation was conducted with an ordinary kriging method using the *gstat* and *sp* packages in Rstudio (Pebesma, 2004; Pebesma and Bivand, 2005; Bivand *et al*., 2013; R Development Core Team, 2013). The final thickness estimate was done using a 0.5 by 0.5-degree grid through the outcrop area, a 0.5-degree search neighbourhood and a spherical variogram model having the following parameters: a) a range of 0.5, b) a sill of 3300 and, c) a nugget of 500 (Appendix 8). The R script for the thickness estimate is presented in Appendix 7.

4.4. Results

4.4.1 Facies

The facies types in the Clarens Formation have been discussed by Eriksson (1981, 1983, 1986) based on studies conducted in the KwaZulu-Natal Drakensberg region (Figure 4.1). Eriksson (1981, 1986) defined four facies types: 1) a laminated, fine-grained, convoluted sandstone unit that is

interbedded with mudstones and very fine-grained sandstones having a lacustrine origin associated with sheetflood deposits; 2) a medium- to coarse-grained cross-stratified sandstone unit that reflects the deposits of desert flood-related braided-wadi channels and sheet flooding; 3) a massive sandstone unit formed in mass-movement processes linked to flooding events, and 4) a very large- to large-scale cross-bedded sandstone that formed by dune migration. In this regional study of the Clarens Formation, 15 lithofacies and seven distinctive facies associations are defined (Tables 4.1 and 4.2), and are, in part, consistent with the four facies types of Eriksson (1981, 1986).

Table 4.1: Aeolian, fluvial, and lacustrine lithofacies in the Clarens Formation.

Code	Lithofacies	Description	Interpretation
Sse	Massive sandstone	Very fine- to fine-grained sandstones; thick to very thick beds; fine sand to coarse silt grain size; same as facies three of Eriksson (1981, 1986).	Dust deposits (loess) or aeolian dune deposits without preserved internal structure
Ste	Large-scale, cross-bedded sandstone	Fine- to medium-grained sandstones; thick to very thick beds; same as facies four of Eriksson (1981, 1986)	Deposits of migrating aeolian dunes
Sle	Low-angle cross-bedded sandstone	Fine- to medium-grained sandstones; thick to very thick beds	Aeolian sand sheets or dune plinth deposits (translatent ripple stratification)
Sm	Massive sandstone	Fine- to medium grained sandstones; medium to thick beds, thin beds	Dune slumping or hyperconcentrated flow deposits
Sh	Horizontally laminated sandstone	Fine- to medium-grained sandstones; medium to thick beds	Upper flow regime flood deposits
Sl	Low-angle, cross-bedded sandstone	Fine- to medium-grained sandstones; often associated with Sh; thin beds	Upper flow regime flood deposits
Sp	Planar cross-bedded sandstone	Fine- to medium-grained sandstones; thick beds; Same as facies two of Eriksson (1981, 1986).	Lower flow regime, migration of channel bars
Sr	Ripple cross-laminated sandstone or ripple marked surfaces	Asymmetrical, symmetrical and interference ripples	Wave (bidirectional) and current (unidirectional) flow in a low-energy environment; changing hydrodynamic conditions indicated by interference ripples
Sw	Convolutely-laminated sandstone	Soft-sediment deformation of laminated sandstones; similar to facies one of Eriksson (1981, 1986)	Rapid deposition and high sediment load in ephemeral channels and sheetfloods
Sae	Wavy-laminated sandstone	Fine-grained sandstones; medium thick beds	Adhesion deposit that forms when dry sand clings to a damp surface

Fl	Laminated mudstone	Thin to thick beds; similar to facies one of Eriksson (1981, 1986)	Subaqueous settling of wind-blown sediment
Fm	Massive mudstone	Thin to thick beds; similar to facies one of Eriksson (1981, 1986)	Suspension settling from water column and wind derived material into lake, bioturbated
Gmc	Mudstone-clast conglomerate	Rip-up mudstone clasts in massive sandstone	Deposits from erosive, high-energy flow
B	Basalt	Basalt lenses in large-scale, cross-bedded sandstone	Basalt flow dammed in dune field
Ds	Desiccation cracks	Polygonal pattern of shallow fissures often filled with sandstones; associated with Sr	Drying of the wet sediment layer

Table 4.2: Aeolian, fluvial, and lacustrine lithofacies associations in the Clarens Formation.

Facies association	**Lithofacies**	**Diagnostic features**	**Depositional process**
FA 1	Ste, Sle	Very large to large-scale cross-bedded sandstones; medium to fine-grained sand	Migrating dunes; dune plinth deposits
FA 2	Sse	Structureless sandstones; very fine sand to coarse silt grain size, laterally extensive	Aeolian dust, suspension fallout
FA 3	Sle, ste	horizontally stratified and low-angle cross-bedded sandstones; Fine – to very fine-grained sand	Migrating wind ripples
FA 4	Sh, Sp, Sw, Gmc	Lenticular, laterally extensive, planar cross-bedded sandstones; basal mud clast conglomerate; coarse to medium grained	Channel fill
FA 5	Sm, Sh, Sl, Sr	Massive to horizontally stratified sandstones; transitioning to low-angle and ripple cross-laminated sandstones, tabular	Unconfined flow
FA 6	Fm, Fl, Sm	Laminated/massive mudstones, lenticular to laterally extensive	Settling of mud from water column.
FA 7	Gm, Sm	Massive sandstone to conglomerate; basalt clasts	Hyperconcentrated flows/debris flow

4.4.1.1 Facies Association 1 (FA 1)

Description: This facies association comprises very fine- to medium-grained, pale orange to off-white sandstones that are well-sorted and arranged in trough cross-bedded sets (Ste – Figure 4.2) with a sharp lower and upper bounding surface (Figure 4.2A–C). Laterally extensive, tabular packages appear throughout the basin. Within these, individual sets range in thickness from 0.5 to 2 m, whereas multiple stacked sets have thicknesses of roughly 2 to 10 m with extreme thicknesses of up to 40 m also recorded in places. Two internal arrangement patterns can be identified: 1) abundant occurrences of massive sandstone wedges that thin downslope and varies in thickness from 2 to 8 cm; (Figure 4.4A, B) and 2) millimetre-scale sandstone laminae packages that appear to thin upslope (Figure 4.4A, B) with a thickness range of 5 to 30 cm. Cross-beds are tangential towards the bed bottom (Figure 4.2C) and may in places truncate onto basal sandstones to form bedset deviation surfaces (Figures 4.2B, C). In parts, low-angle, cross-bedded sandstones (Sle) also appear interbedded with large-scale, cross-bedded sandstones (Ste – Figure 4.2D). Although Facies Association 1 is identified throughout the basin, key sites where it is well preserved are at Balloch, Sani Pass, Koro-Koro and Likosheng (Figures 4.1–4.3). The most comprehensive exposure of very large- to large-scale, cross-bedded sandstones are preserved at Balloch, where bedset deviation surfaces are particularly abundant (Figure 4.3). At Methinyeng, large-scale, cross-bedded sandstones are interbedded with lenses of basalt (Figure 4.1, 4.5A–D), and can be shown to form a continuous lava body where the lenses (Figures 15B and D) represent extensions of the main lava flow. A ropey texture is preserved on the baked lower contact with the massive sandstone (Figure 4.5C) that contains charcoalified plant and wood fragments. These isolated basalt bodies are overlain by horizontal to low-angle, cross-bedded sandstones.

Interpretation: Very large- to large-scale, cross-bedded sandstones (Ste), along with the associated low-angle, cross-bedded sandstones (Sle), suggest that the facies association resulted from migrating dunes (Kocurek and Dott, 1981; Mountney, 2006). The internal stacking arrangement of the sandstones as laminated wedges and massive sandstone wedges represent translatent ripple stratification and grainflow strata that are typical of dune slip-face processes (Hunter, 1977; Rubin and Hunter, 1981; Kocurek and Dott, 1981; Kocurek, 1991; Mountney, 2006). This type of aeolian stratification indicates the dominance of grainflow processes with interbedded tongues of translatent ripple stratification as described by Kocurek (1991). This is shown to represent alternating winds, where a transverse direction results in grainflow slipface advancement and an oblique or inverse wind direction that results in along slope lee-face transport (Rubin and Hunter, 1983; Kocurek, 1991; Crabaugh and Kocurek, 1993). The laminated wedges could represent grainfall laminae (Hunter, 1977; Rubin and Hunter, 1981), however, its appearance as wedges that thicken towards the lower part of the cross-beds (Figure 4.5A) is more consistent with a translatent ripple stratification interpretation. In addition, the dominant preservation of grainflow strata within large-scale, cross-bedded sandstones suggests that dunes were relatively large (Rubin and Hunter, 1981; Kocurek and Dott, 1981). A positive correlation between dune height and grainflow thickness has also been described (e.g., Hunter, 1977; Kocurek and Dott, 1981), which also supports a large dune height for dunes of the Clarens Formation. The low-angle, cross-bedded sandstones found amongst the cross-bedded sandstones can be related to dune plinth deposits as dunes migrate over one another and fill dune hollows (Hunter, 1977; Rubin and Hunter, 1981; Kocurek and Havholm, 1993; Mountney, 2006). These dune plinth deposits result from wind ripple lamination that form on dunes with low to moderate inclinations (Mountney, 2006). The abundance of reactivation surfaces along with the observed foreset stacking arrangement indicates that the wind regime may not have been

unimodal (Hunter, 1981; Kocurek, 1991; Kocurek and Day, 2018). The abundance of bedset deviation surfaces at Balloch further suggests the development of compound draa in this area and represents the superimposition of smaller dunes along draa flanks (Mountney, 2006, Hasiotis *et al.,* 2021).

The geometry of the basalt bodies within the large-scale, cross-bedded sandstones (Ste) in the uppermost Clarens Formation show that the lava flowed into an active dune field, where aeolian bedforms controlled the lava flow direction (cf. Jerram *et al.,* 2000). The charred plant and wood fragments further suggest that the interdunes may have contained small ponds with trees and plants. Moreover, the presence of these bodies implies that the aeolian system was still active during the initial stages of lava extrusion as part of a coeval interfingering relationship. Therefore, these basalt lenses are not lenses, but rather extensions of basalt flows where the outcrop orientation does not allow for the observation of the entire flow. Moreover, the low-angle, cross-bedded sandstone (Sl) overlying the basalt lenses (B) could suggest that sediment availability was influenced by the lava flows, as sand sheets (Sle) are associated with limited sediment availability (Kocurek and Nielson, 1986). Jerram *et al*. (2000) show evidence that a change in bedform size during continuous lava flow deposition may corroborate such an interpretation, although here associated with the appearance of sand sheets rather than a change in bedform size. This facies association has been commonly described in the literature (e.g., du Toit, 1904; Stockley, 1947; Beukes, 1969, 1970; Johnson, 1976; Eriksson, 1981, 1986; Bordy and Head, 2018), and has been linked with the informal zonation of the Clarens Formation by Beukes (1969, 1970) based on its abundant appearance sandwiched between the upper and a lower zone that are dominated by massive sandstones.

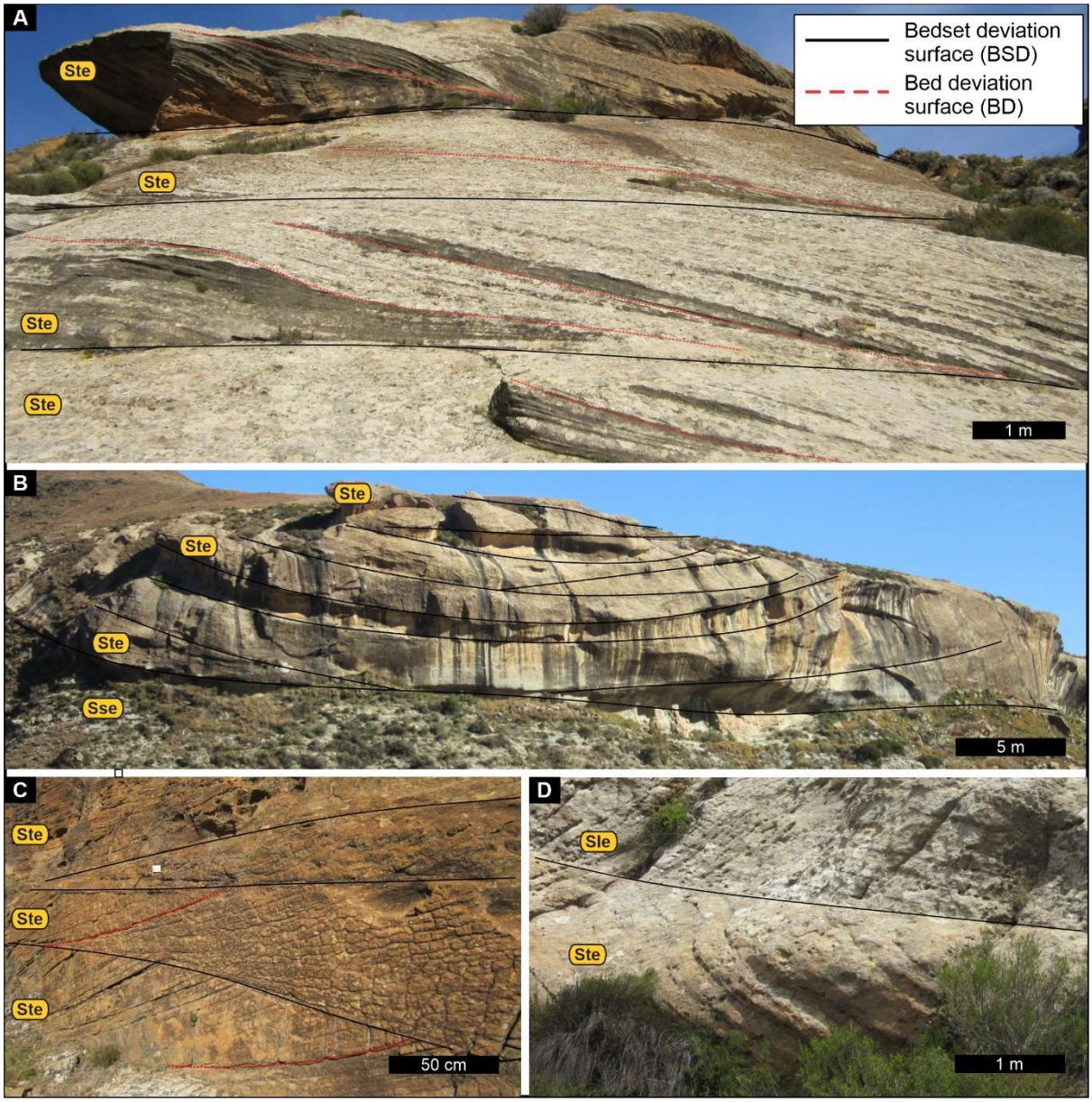

Figure 4.2: Facies Association 1. **A**. Large-scale cross bedded sandstone co-sets at Balloch with reactivation surfaces marked in red dotted line. **B**. Large-scale, cross-bedded sandstone cosets in cross sectional view (W-E) close to Hillcleft. **C**. Large-scale, cross-bedded sandstone with erosional contacts at Koro-Koro. Note the tangential nature of the foresets towards the bottom contact. **D**. Large-scale, cross-bedded sandstone associated with low-angle, cross-bedded sandstone at Witkop. See Table 4.1 for facies description and Figure 4.1 for site locations. Bounding surface hierarchy from Hasiotis *et al*., 2021.

doe

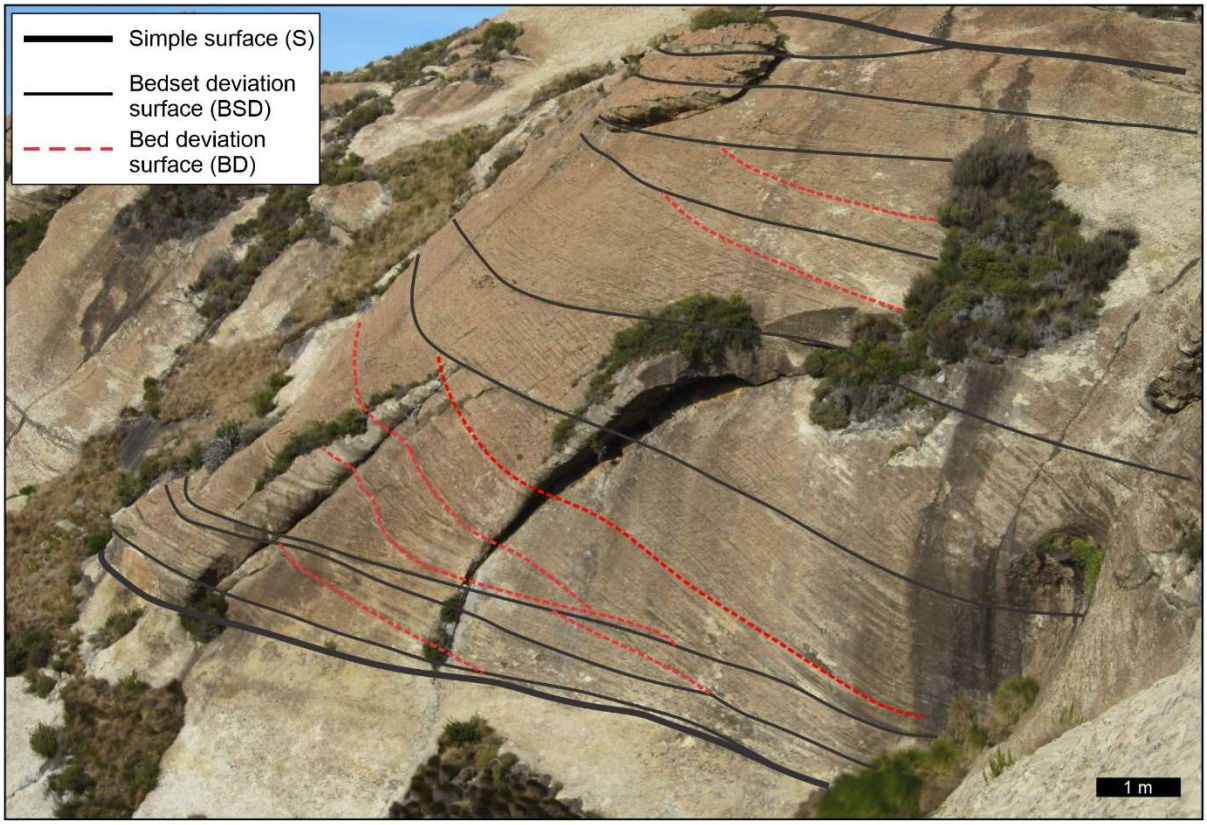

Figure 4.3: Bounding surface arrangements in Facies Association 1 at Balloch. For site location, see Figure 4.1. Bounding surface hierarchy based on Hasiotis *et al*., 2021.

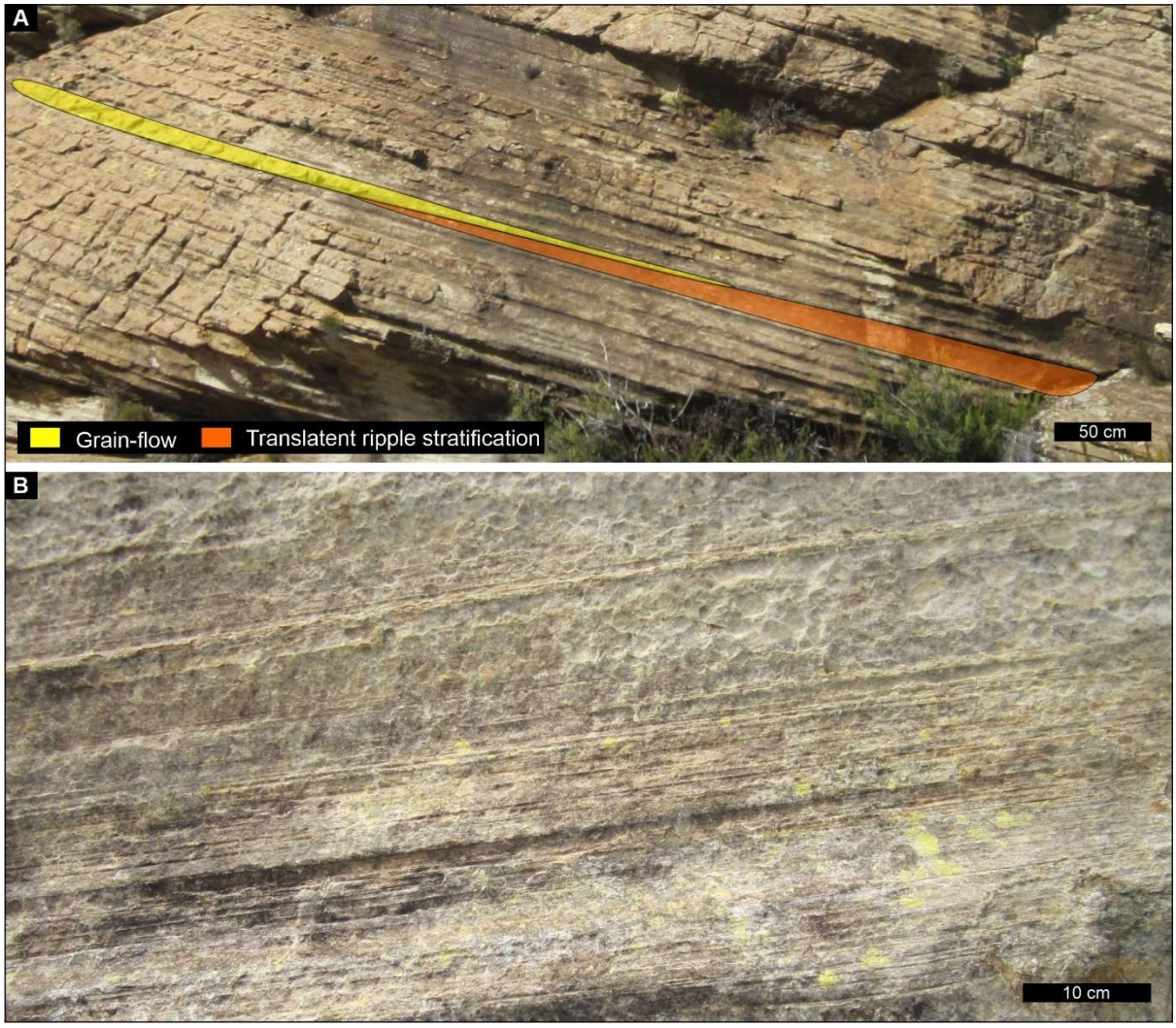

Figure 4.4: Aeolian dune stacking arrangement within large-scale cross-bedded sandstones in the in Facies Association 1. **A**. Overview of grainflow and translatent ripple stratification that forms the foresets of large-scale cross-beds at Balloch. **B**. Close-up view of translatent ripple stratification interbedded with wedges of massive grainflow strata at Roma. For site locations, see Figure 4.1.

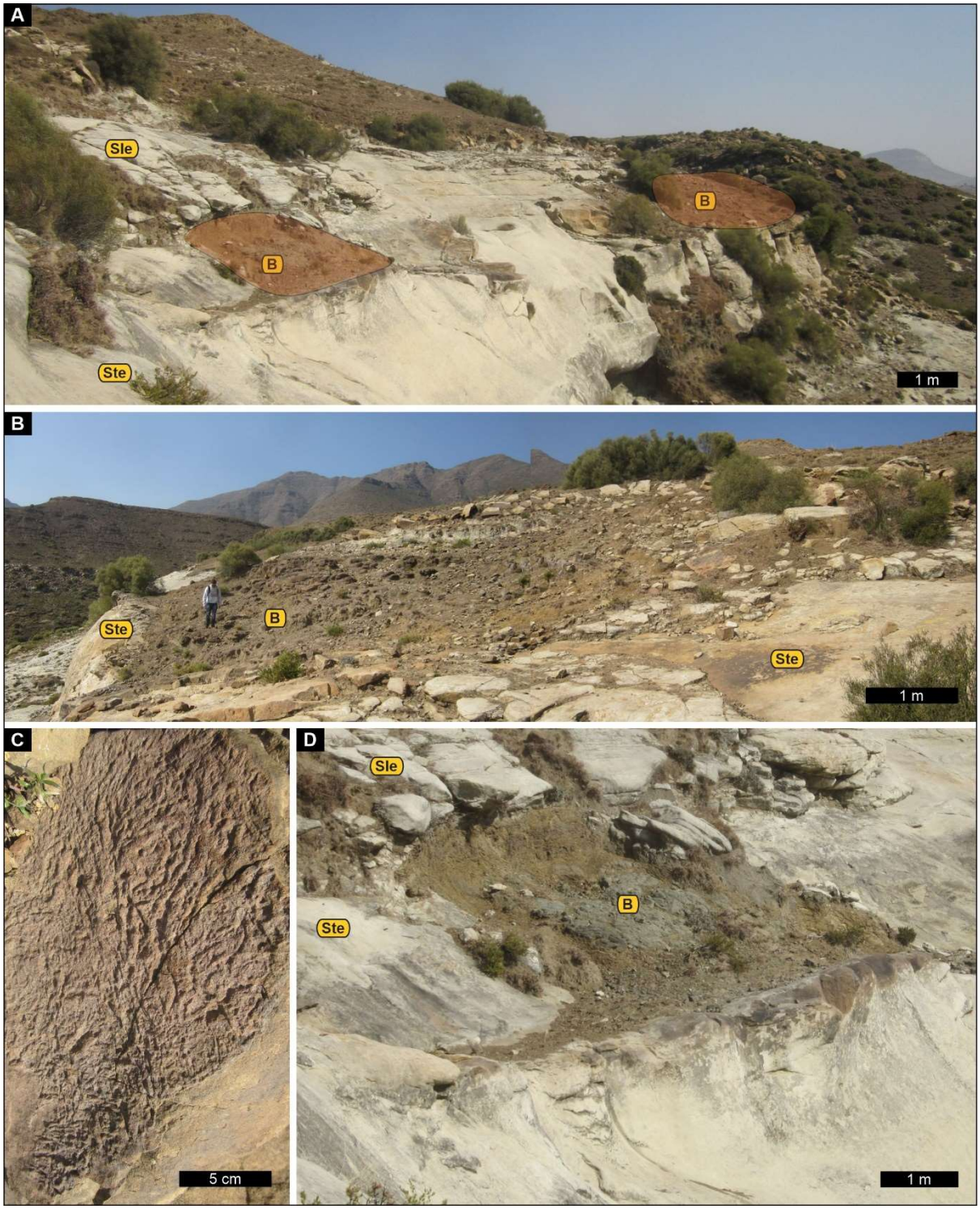

Figure 4.5: Basalt interbedded with Facies Association 1 at Methinyeng. **A**. Large-scale, cross-bedded sandstones with interbedded lenses of basalt. **B**. Close-up view of the larger basalt lens. **C**. Baked basal surface of the basalt lens with ropey surface texture. **D**. Close-up view of the smaller basalt lens within large-scale, cross-bedded sandstone. See Table 4.1 for facies descriptions and Figure 4.1 for site location.

4.4.1.2 Facies Association 2 (FA 2)

Description: The Clarens Formation is dominated by massive sandstones that are laterally extensive (Figure 4.6), thick to very thickly bedded and composed of very fine silty sand to sandy silt. Sandstones are moderately to well sorted and are light pink, green, cream to buff in colour. These structureless sandstones (Sse — Table 4.1) are found throughout the basin, mostly associated with the basal and upper parts of the Clarens Formation (Figure 4.6A), although they are also locally interbedded with large-scale, cross-bedded sandstones and smaller scale siltstones (Figure 4.6B). Characteristically, the massive sandstones appear very homogenous in outcrops (Figure 4.6C) and as such, they were specifically investigated using sedimentary grain-size, grain shape and grain fabric trends to determine possible processes of deposition (see Chapter 3). Therefore, this facies association is not described in more detail herein.

Interpretation: Typically, Facies Association 2 in the Clarens Formation and elsewhere have been interpreted as dune slumping during intense rainstorms in modern and ancient aeolian systems (eg., Eriksson, 1983, 1986; Loope *et al*., 1998; Sweeney and Loope, 2001; Simpson *et al.*, 2002; Heness *et al*., 2014). Based on grain characteristics investigated in Chapter 3, the massive sandstones can be subdivided into six different facies types with the following origin categories: 1) migrating dunes in which the internal structures have not been preserved, 2) sandy dust (sandy loess), 3) sediments associated with aeolian dust (loess), 4) a transitional sediment that does not show unique grain characteristics and represents a mixed sedimentary origin as a continuum between aeolian dunes and dust, 5) reworked aeolian dust into a lacustrine environment and, 6) fluvially reworked aeolian sediments. Overall, these six Massive deposit types represent deposition related to dust storms in the dynamic, regional erg system in southwestern Gondwana due to local and regional Early Jurassic atmospheric circulation patterns (see Chapter 3; Vanderberghe, 2013).

Figure 4.6: Facies Association 2. **A**. Massive deposits in the upper part of the Clarens Formation at Qachas Nek. **B**. Massive deposits with interbedded siltstone. **C**. Massive deposits from Cathedral Peak with stream-cut potholes.

4.4.1.3 Facies Association 3 (FA 3)

Description: Facies Association 3 occurs as horizontally laminated (Sh) to low-angle cross-bedded (Sl) facies in laterally continuous tabular sandstone bodies (Figure 4.7). These sheet-like sandstones are very fine- to medium-grained and well sorted with a thickness that ranges between 0.5 to 5 m, although extreme thicknesses of up to 10 m are recorded in parts. Individual laminae are 2 to 4 mm, and in parts appear to be interbedded with massive wedges (Figure 4.7B). Upper and lower contacts appear as mostly sharp horizontal to less abundant undulating surfaces. Cross-bedded sandstones (Ste) are also locally present (Figure 4.7C-D). Facies Association 3 has been identified at Leeuwkop, Sani Pass, Kamberg, Hellspoort, Ramatsediso's Nek and Balloch (Figure 4.1), and Beukes (1969) also recorded them in his sedimentary logs.

Interpretation: Sets of horizontally stratified (Sh) and low-angle, cross-bedded sandstones (Sl) are the expression of aeolian sand sheets that come about when wind ripples migrate and climb in a dry aeolian setting (Hunter, 1977; Kocurek and Nielson, 1986; Mountney, 2006; Do Amarerante *et al*.,

2019). The internal structure of the wind ripples is often not distinguishable due to the uniformity of the grainsize within the deposit (Mountney, 2006), and the preservation of sandstone laminae may indicate that Facies Association 3 is composed of sub critically climbing translatent ripple strata (Hunter, 1977; Kocurek, 1991), whereas the interbedded massive sandstone wedges may reflect laminated sandstones in which the structures are obscured by weathering. The formation of aeolian sand sheets require very specific conditions and usually form where dune formation is inhibited, typically during times of limited sediment availability related to increased moisture (Kocurek and Nielson, 1986). Sand sheets in modern desert settings are frequently associated with erg borders or underlie deserts (Mountney, 2006). Similarly, thick sand sheet deposits within the Clarens Formation mostly developed close to erg margins and may have been associated with the leading edge (fore erg) or trailing margin (back erg) of the aeolian system (Kocurek and Nielson, 1986; Porter, 1986, 1987; Langford and Chan, 1993; Cosgove *et al*., 2021). In addition, sand sheets showing planar surfaces have also been linked to a high water-table and may also be interbedded with cross-bedded sandstones (Kocurek and Nielson, 1986; Langford and Chan, 1993; Mountney, 2006). Such facies associations may develop in transitional zones such as areas where a change from fluvial to aeolian processes occur (Cain and Mountney; 2009). Evidence for this is seen at Balloch, where cross-bedded sandstones (Ste) are found interbedded with horizontally stratified (Sh) sandstones and represent the development of small-scale dunes amongst sand sheets (Kocurek and Dott, 1981; Kocurek and Nielson, 1986; Mountney, 2006; Trewin, 1993).

4.4.1.4 Facies Association 4 (FA 4)

Description: Facies Association 4 comprises stacked laterally extensive, lenticular to ribbon-like sandstone bodies consisting of very fine - to coarse-grained, gritty sandstone with thicknesses that vary between 0.5 and 1.5 m. Typically, horizontal stratification (Sh) and planar cross-bedded sandstones (Sp – Figures 4.7B and 4.8A–B) are present and preserves soft-sediment deformation (recumbent cross-bedding) structures (Sw) throughout (Figure 7C). Lenses of intraformational mudstone-clast conglomerates (Gmc) mark the bases of the sandstones (Figure 4.8A–B), while rip-up mudstone clasts are also incorporated into basal parts of the channel-shaped sandstones (Figure 4.9C). This facies association is best preserved at Kamberg and, to a lesser extent, at Ha Ralejoe and Woodcliffe. At Woodcliffe, *ex-situ* petrified wood fragment (Figure 4.9D) was recorded a few m away from a cross-bedded sandstone (Sp) outcrop.

Interpretation: The combination of planar cross-bedded (Sp), horizontally stratified sandstones (Sh) and intraformational mudstones clasts conglomerates (Gmc) suggest that Facies Association 4 represents channel fill deposits, possibly in a low-sinuosity braided fluvial system (Miall, 1985; Hasan *et al*., 2018; Priddy and Clarke*,* 2020). Cross-bedded sets of sandstones suggest the migration of subaqueous channel bars, whereas the intraformational mudstone-clast conglomerate suggest high-energy conditions that reworked and cannibalised finer grained in-channel and/or over bank deposits (Hassan *et al*., 2018; Priddy and Clark, 2020). The associated soft-sediment deformation (recumbent cross-bedding) reflects the strength of current drag that induced down slope gravitational slip during such high sediment load episodes (Allen and Banks, 1972; Hassan *et al*., 2018), and is characteristic of Facies Association 4. Furthermore, the sandy, highly mobile sediment surface was likely sparsely vegetated as suggested by the absence of palaeosols or in situ overbank fines (Cain and Mountney, 2009). This facies association was also described from the KwaZulu-Natal Drakensberg by Eriksson (1981, 1986) and was interpreted as the product of wadi processes and distal alluvial fan systems that were situated in the south and the east of the basin.

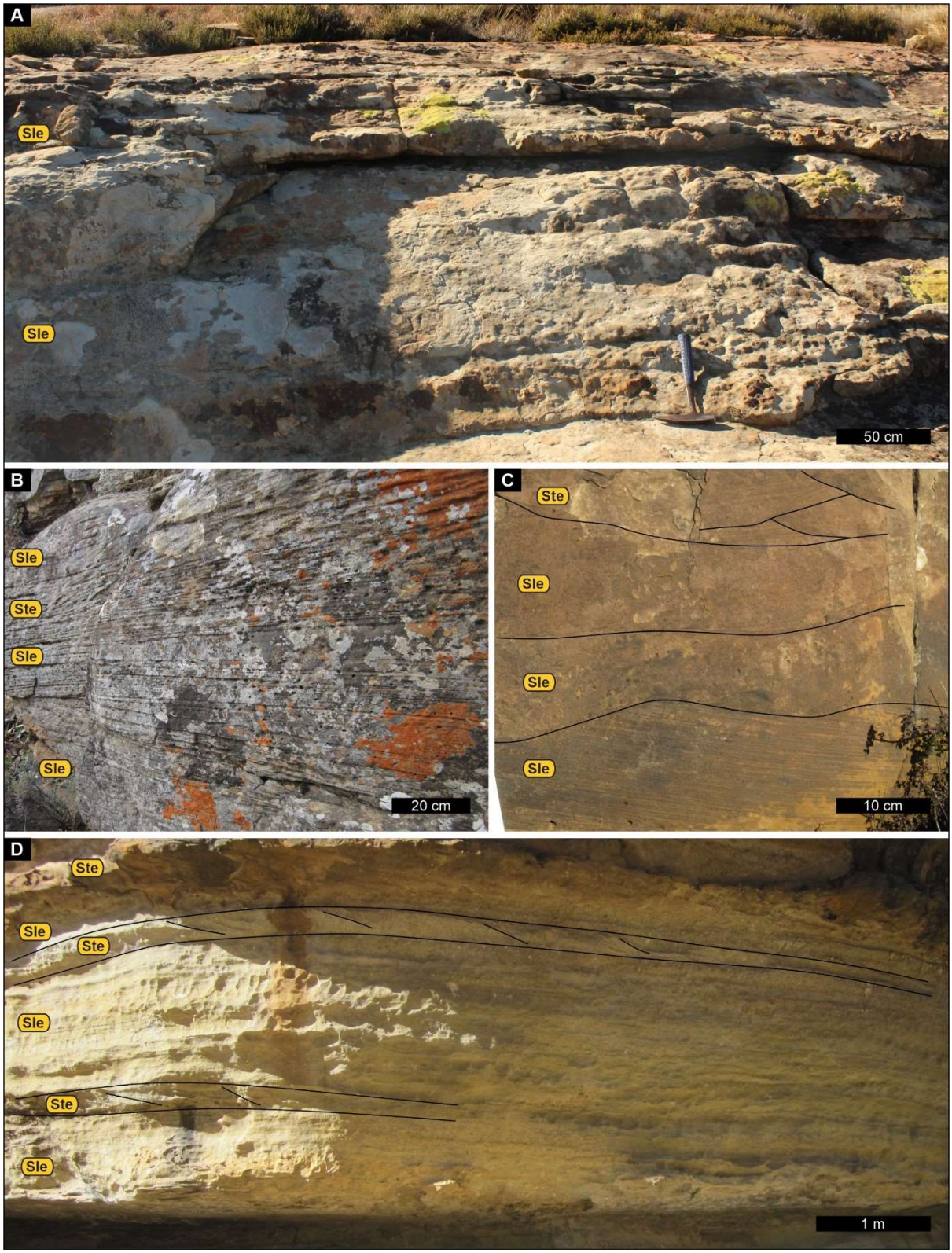

Figure 4.7: Facies Association 3. **A**. Low-angle, cross-bedding at Ramatsediso's Nek. **B**. Low-angle, cross-bedding interbedded sandstone wedges and laminae at Kamberg. **C**. Low-angle, cross-bedding interbedded with small-scale cross-bedding at Hellspoort. **D**. Low-angle, cross-bedding grading into horizontal stratification and interbedded with small-scale cross-bedding at Balloch. See Table 4.1 for facies descriptions and Figure 4.1 for site locations.

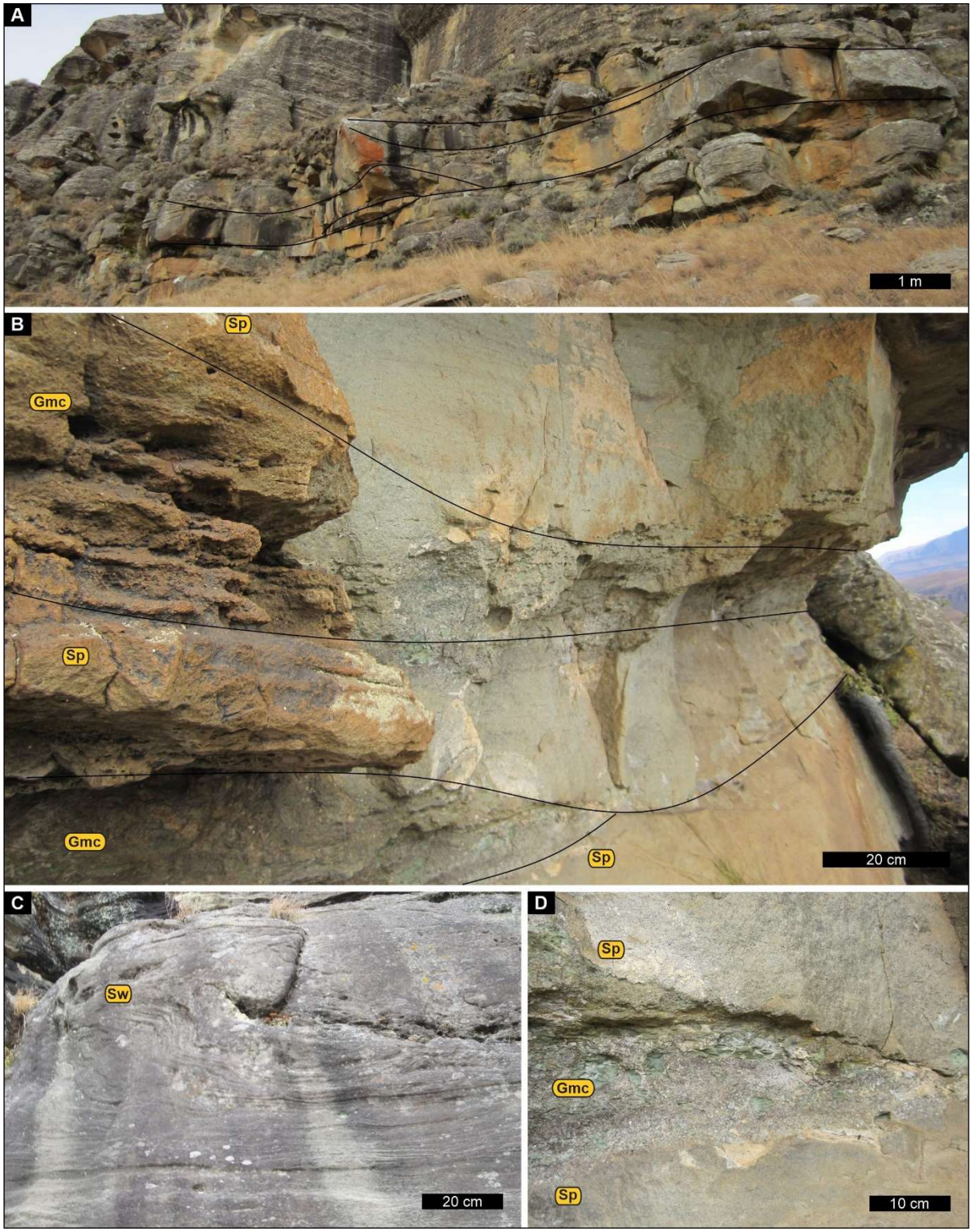

Figure 4.8: Facies Association 4 at Kamberg. **A**. Multi-storey channel feature in the lower succession. **B**. Close-up view of the basal cross-bedded sandstones with conglomerate lenses. **C**. Soft-sediment deformation structure. **D**. Conglomerate lens in planar cross-bedded sandstones; note the rip-up mudstone clasts that indicate reworking. See Table 4.1 for facies descriptions and Figure 4.1 for site location.

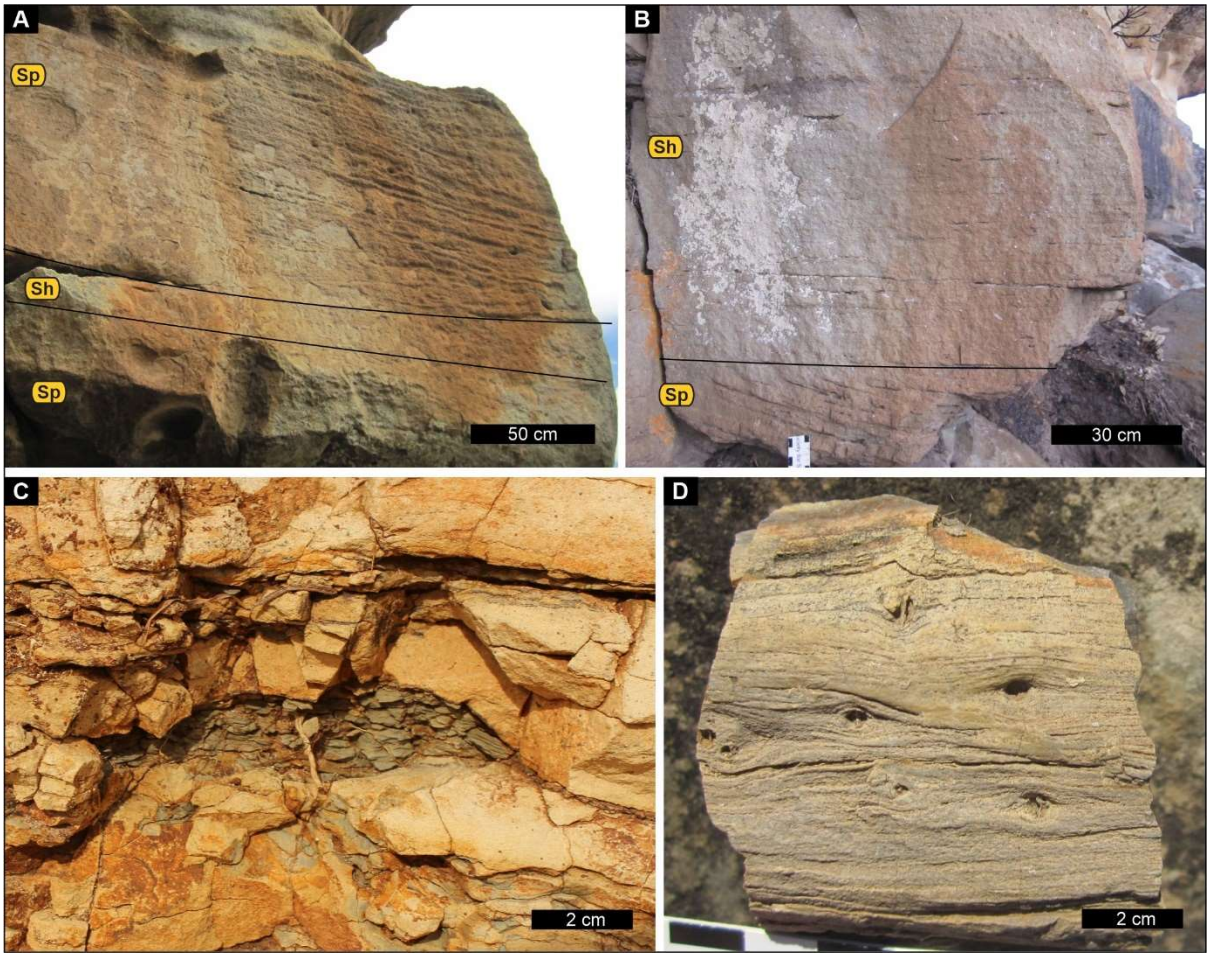

Figure 4.9: Facies Association 4. **A**. Horizontally stratified sandstones typically occur amongst planar cross-bedded sandstones at Kamberg. **B**. Planar cross-bedded sandstones transitioning into horizontally stratified sandstones indicating decreasing energy. **C**. Close-up view of the rip-up mudstone clasts common within the basal part of cross-bedded sandstones at Ha Ralejoe. **D**. Ex-situ petrified wood fragment located near planar cross-bedded sandstone outcrops at Woodcliffe. See Table 4.1 for facies descriptions and Figure 4.1 for site locations.

4.4.1.5 Facies Association 5 (FA 5)

Description: Facies Association 5 comprise laterally extensive, tabular, white to light pink, very fine - to medium-grained sandstones with thicknesses varying between 0.5 and 1 m. Repeated cycles of massive (Sm – Figure 4.10A), horizontal (Sh – Figure 4.10B) and low-angle cross-bedded sandstones (Sl – Figure 4.10C) are common. The Sm-Sh-Sl cycles transition into ripple cross-laminated (Sr – Figure 4.10A and inset) sandstones that show ripple marks, and in places, are associated with desiccation cracks (Figure 4.10D). This facies association is best preserved at Ramatsediso's Nek, Likosheng and Kamberg, occurring towards the upper contact with the Drakensberg Group, and has also been described in KwaZulu Natal (Eriksson, 1981, 1984, 1986; Van Dijk and Eriksson, 2021).

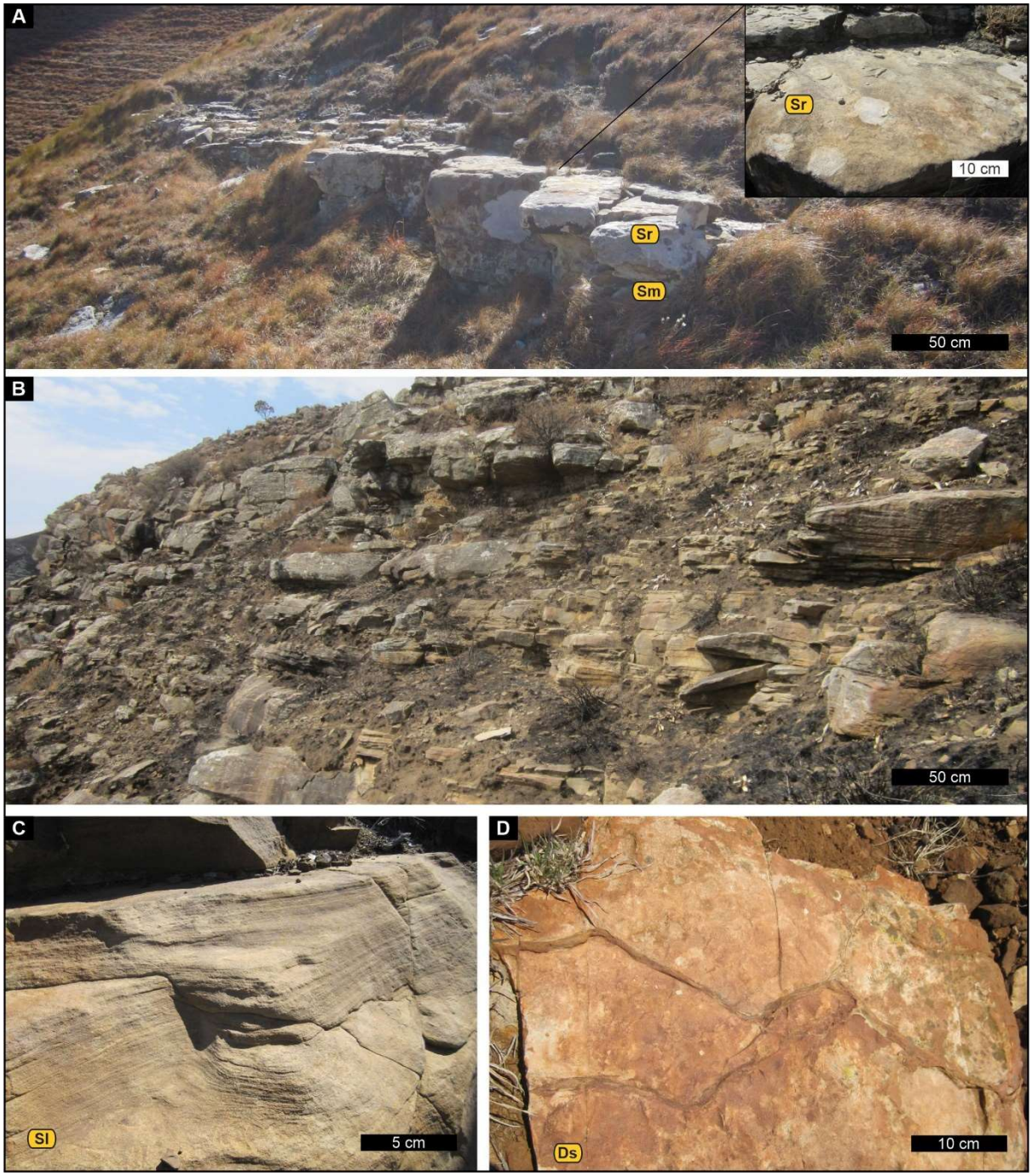

Figure 4.10: Facies Association 5. **A**. Laterally extensive tabular massive sandstone with ripple cross-lamination and ripple marks (inset) on the upper surface at Ramatsediso's Nek. **B**. Stacked, thinly bedded, laterally extensive, horizontally stratified sandstones at Kamberg. **C**. Low-angle cross-bedding at Likosheng close to the upper contact. **D**. Desiccation cracks on a bedding plane surface in the uppermost part of the succession at Likosheng. See Table 4.1 for facies descriptions and Figure 4.1 for site locations.

Interpretation: Association of massive (Sm), horizontally stratified (Sh), low-angle, cross-bedded (Sl) and ripple cross-laminated (Sr) sandstones are interpreted as poorly confined to unconfined subaqueous sand sheets of fluvial origin (Hampton and Horton, 2007, North and Davidson, 2012; Mayoral *et al*, 2021). Horizontal stratification suggests upper flow regime conditions that was short-

lived resulting in sheetlike geometries (McKee *et al*., 1966). The transition from horizontal to low-angle, cross-bedding indicates changes in flow energy, while ripple-cross lamination and the occurrence of ripple marks on upper bedding planes suggest waning flow conditions associated with termination of flow (Hampton and Horton, 2007). These sedimentary features are representative of deposition within wide, ephemeral streams with initial upper flow regime conditions (Mckee *et al*., 1966; Mountney, 2006). Massive sandstones may be related to deposition of hyperconcentrated flows during periods of high rainfall (Priddy and Clark, 2020).

4.4.1.6 Facies Association 6 (FA 6)

Description: The components of Facies Association 6 comprise lenticular to laterally extensive tabular green to dark grey laminated (Fl – Figure 4.11A, B) to massive mudstones (Fm – Figure 4.11C) that are ~ 0.5- to 40-m-thick. Wavy-laminated (Sae), horizontally stratified (Sh), low-angle, cross-bedded (Sl) to massive sandstones (Sm) are interbedded with the mudstones (see Chapter 2). The mudstones can be mapped over lateral distances of ~ 30 m to > 5 km. They may laterally wedge out, onlapping to large-scale, cross-bedded (Ste – Figure 4.11C) or massive sandstones (Sse). In parts, convoluted bedding is associated with the mudstones and load casts are common at the base of the overlying massive sandstones (Figure 4.11A, B). The sandstones interbedded with the mudstones preserve a range of sedimentary structures: ripple marks, interference ripples, microbially influenced sedimentary structures (MISS), plant and charcoal fragments, rill marks, desiccation cracks, snail trail or flying traces, and vertebrate footprints. Pluvial deposits in the Clarens Formation have been investigated in Chapter 2, and specifics relating to the spatial distribution, aeolian-lacustrine interaction and genesis are discussed in that chapter.

Interpretation: Lenticular to laterally extensive mudstones represent deposition within small-scale ponds, to large-scale lakes, whereas convoluted beds and load casts indicate rapid burial while the sediments were still wet (Selker, 1993). Silt likely entered the waterbodies in two ways, from direct dust fall processes and, secondly, from lake margin processes that occurred on the lake edge (Mountney, 2006; Vandenberghe, 2013, Vandenberghe *et al*., 2018). Wavy-laminated sandstones (Sae) suggest adhesion lamination processes, where dry sand adheres to a damp surface typical in interdune areas (Kocurek, 1981; Hummel and Kocurek, 1984; Mountney, 2006). The appearance of laterally extensive massive (Sm) sandstones with convoluted bedding represent flood-related hyperconcentrated flows into interdunes and lakes (Svendsen *et al*., 2003, Priddy and Clark, 2020). Moreover, rill marks, adhesion structures, possible snail trail or flying traces, and symmetrical ripple marks are all associated with lake margin processes during emergence of the sediments. Fossil fish (Figure 4.11D) have also been identified within this facies association of the Clarens Formation (Haughton, 1924, Jubb, 1973 – Figure 4.11D), although not documented in this study.

As shown in Chapter 2, pluvial deposits (FA6) in the Clarens Formation are interpreted as products of: 1) small ponds that form in interdune hollows, 2) large-scale lakes with abundant lake marginal process preservation and 3) large-scale lakes where interdunes were large enough to develop flood-related hyperconcentrated flows. The development of these different lake settings was a function of the physical distance from the erg margin (Chapter 2).

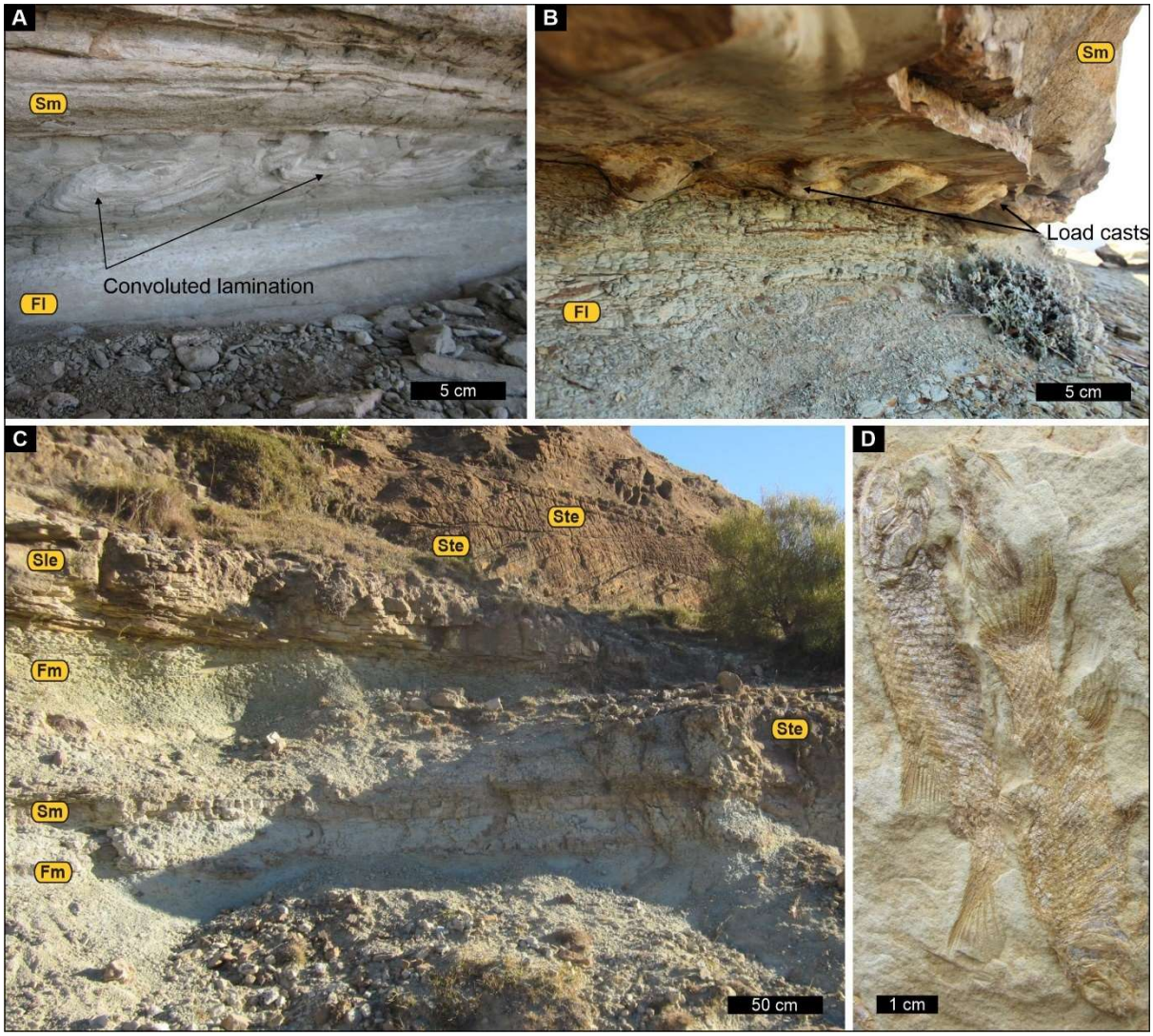

Figure 4.11: Facies Association 6. **A**. Laminated mudstone with convolute bedding at Leeuwkop. **B**. Laminated mudstones with overlying load casts at Ramastediso's Nek. **C**. Lenticular massive mudstone interbedded with low-angle and large-scale cross-bedded sandstone layers at Koro-Koro. **D**. *Semionotus capensis* associated with the Facies Association 6 here seen in a sandstone building block on the farm Rietfontein close to Clarens, Free State, South Africa. See Table 4.1 for facies descriptions and Figure 4.1 for site locations.

4.4.1.7 Facies Association 7 (FA 7)

Description: This facies association is characterised by lenticular, massive to crudely stratified, dark brown to grey sandstones (Sm) with basalt pebbles and massive, matrix-supported conglomerates (Gm). These facies are also associated with very fine-grained massive silty sandstones (Sse) and horizontally stratified (Sh), low-angle, cross-bedded (Sl) and ripple cross-laminated (Sr) sandstones. It is rarely observed across the basin. In places, plant impressions and charred plant fragments are present (Figure 4.12D).

Interpretation: Lenticular, massive sandstones (Sm) associated with massive conglomerates (Gmc) are interpreted as a debris-flow or hyperconcentrated-flow deposits generated by flash floods within the erg. Given the dark colour and the inclusion of basalt pebbles in Facies Association 7, a nearby

basalt source is highly likely. Debris-flow deposits and reworked basaltic material incorporated into the uppermost Clarens Formation have also been discussed by Bordy *et al*. (2021; see their Figures 4.3, 4.4, 4.5).

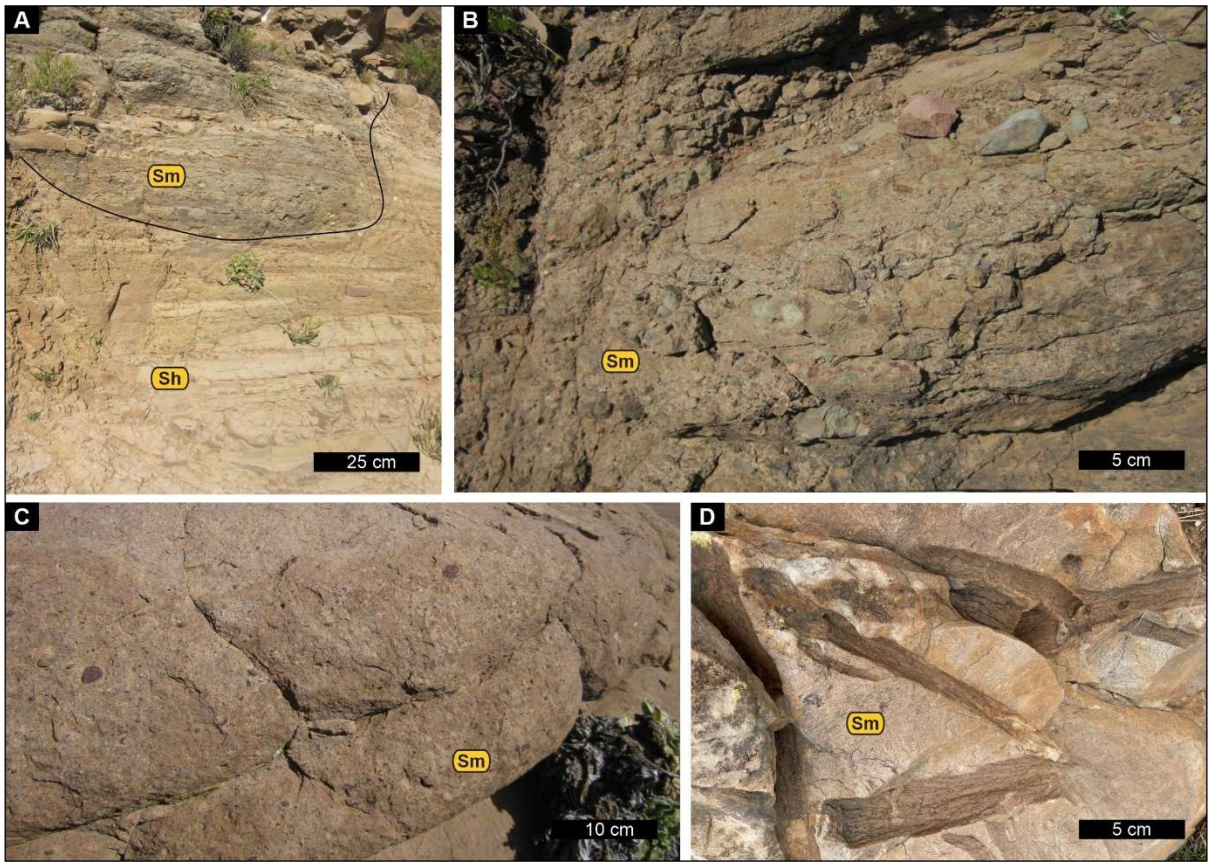

Figure 4.12: Facies Association 7. **A**. Lenticular Debris Flow deposits among Facies Association 5 at the Talon section. **B**. Close up of Facies Association 7 from A. **C**. Massive sandstone with isolated clasts from Talon section. **D**. Wood impressions in a massive sandstone associated with Facies Association 7 at the Methinyeng study site.

4.4.2 The upper contact of the Clarens Formation

Description: Typically, the contact undulates with an amplitude of 2.5 m (Figure 4.13D) and shows evidence of lava baking and preservation features (e.g., ropey texture - Figure 4.13A, C), wind ripple marks (Figure 4.13A), desiccation cracks (Figure 4.13A) and striations (Figure 4.13C). In parts, basalt lenses occur within sandstones, while at Mount Moorosi, a sandstone interbed within the basalts has an onlapping relationship with the youngest (and topographically highest) sandstone bed in the Clarens Formation (Figure 4.13D). In addition, sandstones associated with the upper contact frequently show ripple cross-lamination (Sr – Figure 4.14D), horizontal stratification (Sh – Figure 4.14D), low-angle cross-bedding (Sl) and less often, plant impressions (Figure 4.14E), charred plant fragments and *in situ* and *ex-situ* petrified wood fragments (Figure 4.14B).

Interpretation: The ropey surface texture preserved atop sandstones along the contact with the overlying basalts reflects the emplacement of low-viscosity pahoehoe lava flows over, soft, unlithified sandstones (also see Bordy *et al.*, 2020, their fig. 5A, B). In addition, striations atop the youngest Clarens Formation sandstones could indicate that locally the lava flowed in a W-E direction (Jerram *et al.*, 1999; Jerram and Stollhofen, 2002; Petry *et al.*, 2007). The undulating upper contact of the Clarens Formation suggests that the lava poured out onto a dune field where dunes appear to have temporarily dammed the lava flow, which was also discussed by Beukes (1969, 1970) as well as Bordy *et al*. (2021). The sandstone interbed that laps onto the youngest sandstone of the Clarens Formation, along with the appearance of wind ripples, indicates that the aeolian system was still active while the lava inundated the dune field. Moreover, the preservation of the wind ripple structures on the contact suggests that the lava flow passively blanketed the landscape (Jerram and Stollhofen, 2002). The combination of horizontally stratified (Sh) and ripple cross-laminated (Sr) sandstones are typical of unconfined fluvial flow (Hampton and Horton, 2007) and suggests that the facies association, in close proximity or in contact with the basalt, was deposited in relatively wet conditions, possibly in ephemeral unchannelised flow as described in section 3.1.5. This wetter phase in the terminal depositional period of the Clarens Formation is further strengthened by the presence of plant impressions, petrified wood fragments and in situ tree trunks (Bordy *et al*., 2021).

4.4.3 Facies association distribution and proportions

The facies association distribution and proportions of the Clarens Formation show that Facies Association 2 (Massive) dominates both zones 1 and 3 (Figure 4.15A, C) with Facies Association 1 (Aeolian dune) being subordinate. Facies Association 6 (Pluvial) is more prevalent in zone 1, whereas in zone 3 Facies Association 3 (Aeolian sand sheets) is in higher abundance. In zone 2 (Figure 4.15B), Facies Association 1 dominates, and thus this facies association is the defining feature for zone 2 (Figure 4.15B). Facies Association 3 and Facies Association 4 (ephemeral channel) are present in all zones, although the former is the least abundant in zone 3 (Figure 4.15 C), whereas the latter is most abundant in zone 1. Overall, Facies Association 2 is the most dominant within the Clarens Formation (Figure 4.15D), followed by Facies Association 1. The rarely observed Facies Association 7 (Debris flow) is the least abundant (< 1%) and confined to zones 1 and 3 only (Figure 4.15).

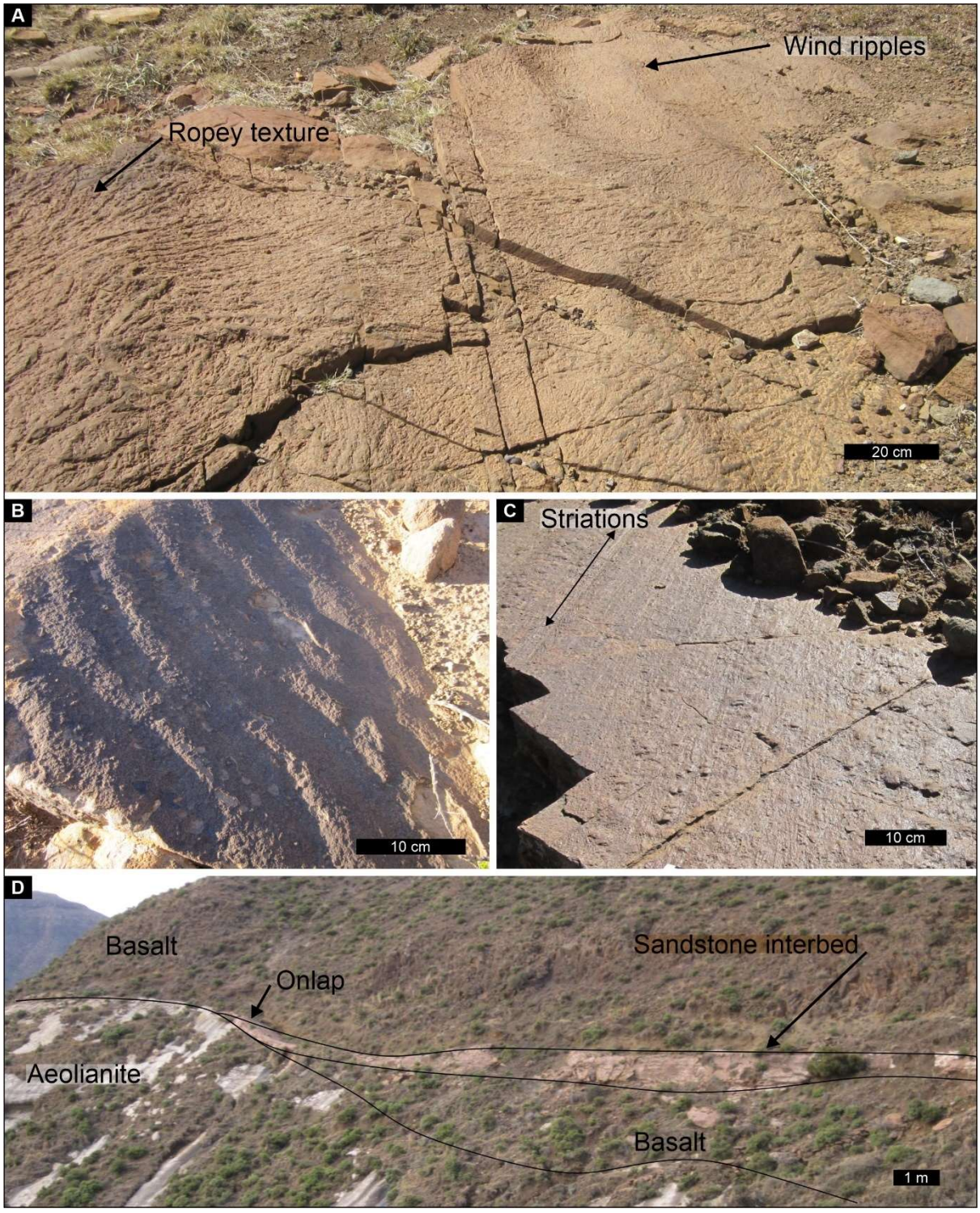

Figure 4.13: Field features along the upper contact of the Clarens Formation. **A**. Wind ripples and ropey texture on the upper bedding plane of sandstones at Methinyeng. **B**. Ripple marks at Hellspoort. **C**. W-E oriented striations on the upper bedding plane of sandstones directly overlain by basalts. **D**. Onlapping relationship between a massive, uppermost Clarens Formation sandstone and a sandstone interbed within the overlying basalts of the lower Drakensberg Group (Barkly-East Formation) at Mount Moorosi. For site locations, see Figure 4.1.

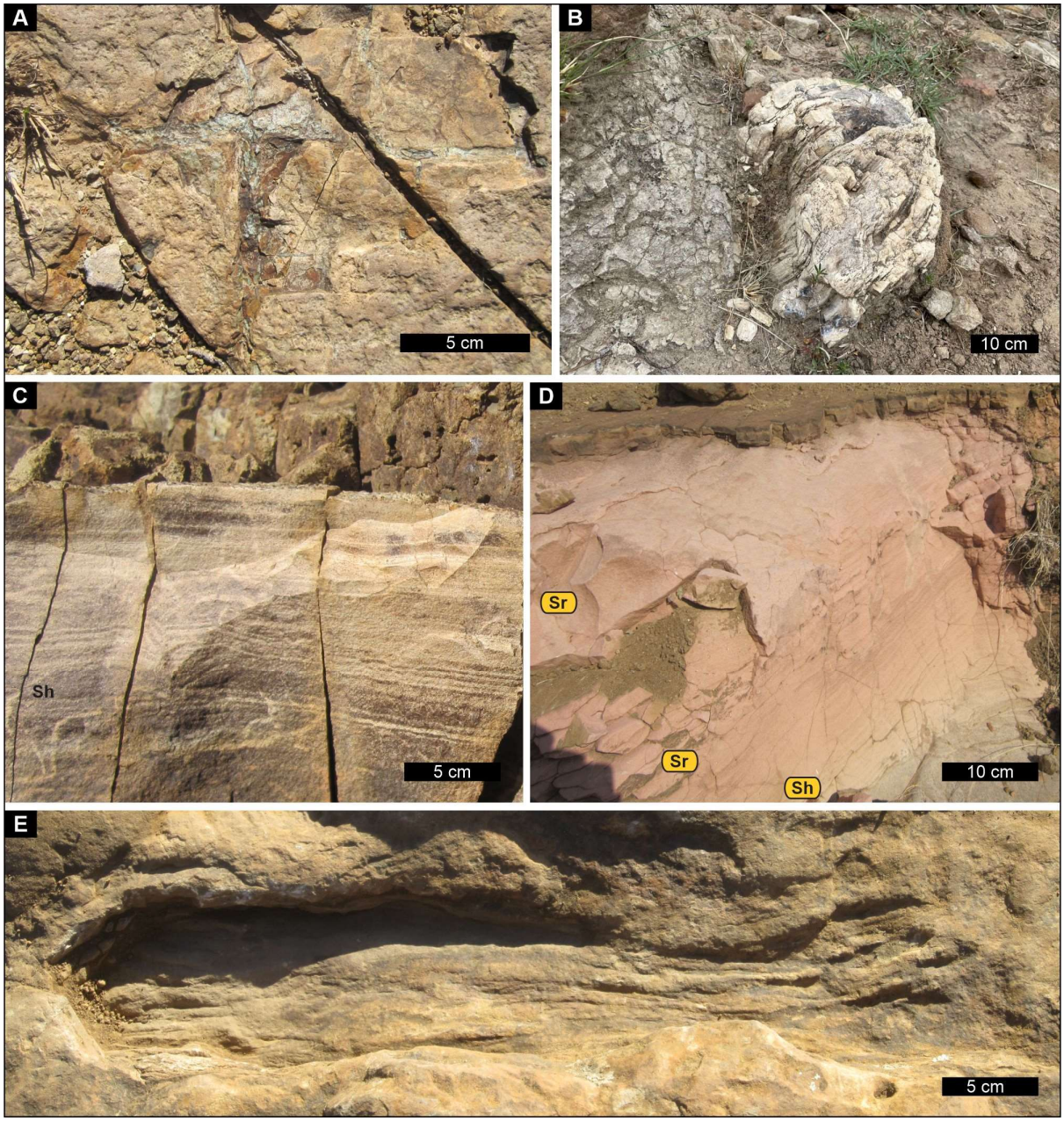

Figure 4.14: Field features along and near the upper contact of the Clarens Formation. **A**. Desiccation cracks on the upper contact at Leeuwkop. **B**. In-situ tree trunk found on the contact at Methinyeng. **C**. Horizontally stratified sandstone below the upper contact. **D**. Ripple cross-laminated sandstone below the upper contact at Methinyeng. **E**. Plant impression in massive sandstone ~ 1 m below the upper contact. See Table 4.1 for facies descriptions and Figure 4.1 for site locations.

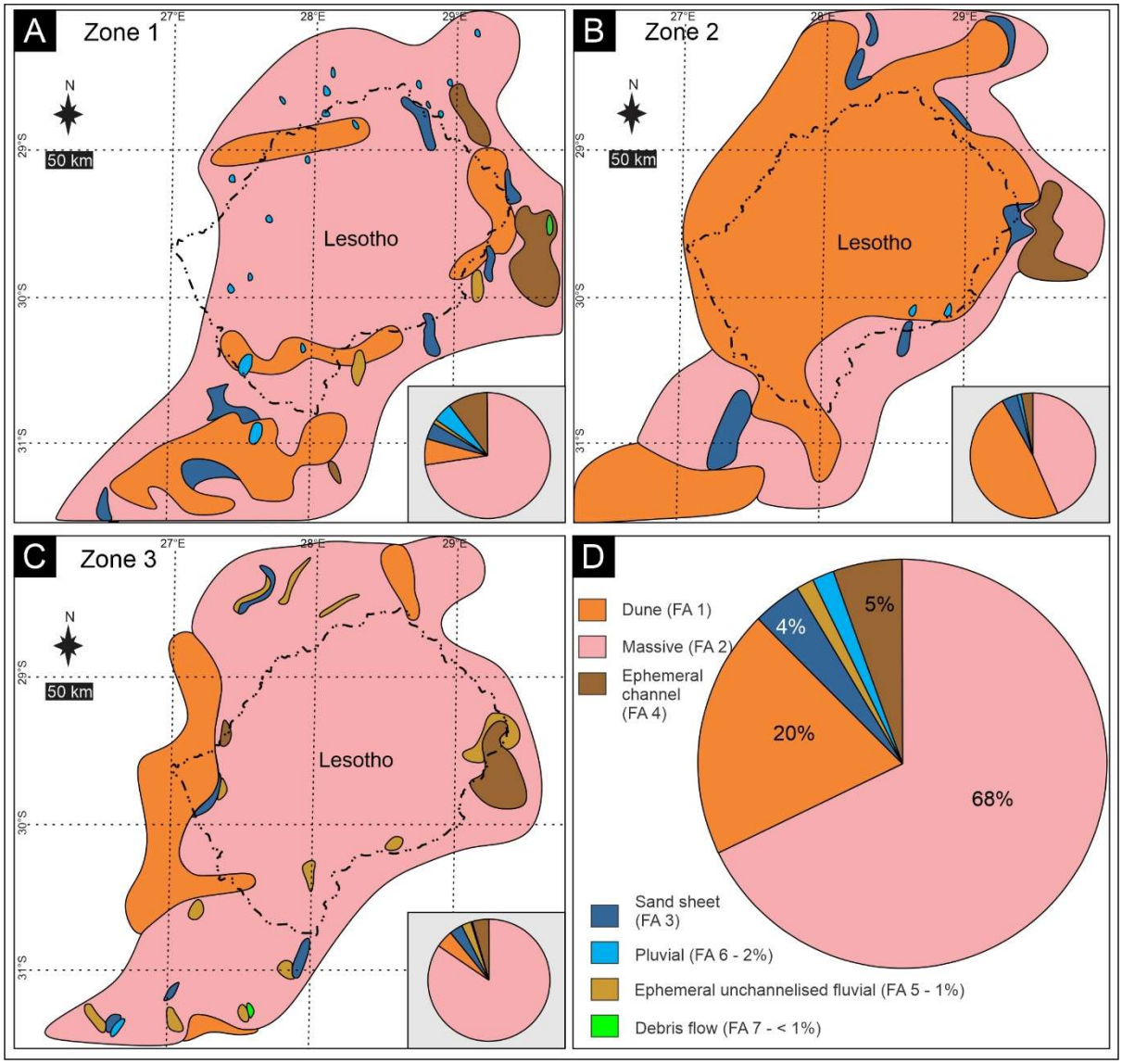

Figure 4.15: Facies association distribution and proportions of the Clarens Formation. **A**. Zone 1. **B**. Zone 2. **C**. Zone 3. **D**. Overall facies association proportions of the Clarens Formation.

4.4.4 Formation thickness and palaeocurrents

The input data for the thickness estimation of the Clarens Formation includes 33 data points observed during this study and 94 thickness data points extracted from du Toit (1904, 1905), Stockley (1947), Beukes (1969), Robinson (1969) and Eriksson (1984), which are all outcrop measurements from sedimentary logs and detailed, field-mapping exercises. The measurements of Stockley (1947) are based on the principles outlined by Van Eeden (1937), where the transitional succession with the underlying Elliot Formation is included into the Clarens Formation thickness data, and for this reason may reflect slightly different thicknesses than those reported in other studies. These combined results show that a range of 100 to 150 m represents a better average thickness for the Clarens Formation (Figure 4.15A), and that the maximum thickness value of the unit is 300 m (Figure 4.15C). As already pointed out by Beukes (1969), the Clarens Formation reaches its thickest part in the Eastern Cape and southern Lesotho along a trough axis running northeast to southwest (Figure 4.15A). Despite the localised thickness fluctuations (e.g., 0 m near Qachas Nek, Elliot and Maclear in the Eastern Cape of South Africa - Figure 4.15A, C), a subtle regional south to

north decrease in thickness is apparent given that the 200 m contours are only traceable in the southern outcrop area. In addition, the thickness distribution is more consistent in the northern outcrop area. Palaeowind directions measured from the foreset dip-directions of large-scale cross-bedded sandstones (mostly associated with the Facies Association 1 – see Section 4.3.1.1) record a flow direction from roughly west to east with a high consistency ratio (Figure 4.16B), although a localised deviation from the overall trend is observed in the basal large-scale cross-bedded sandstones at Balloch.

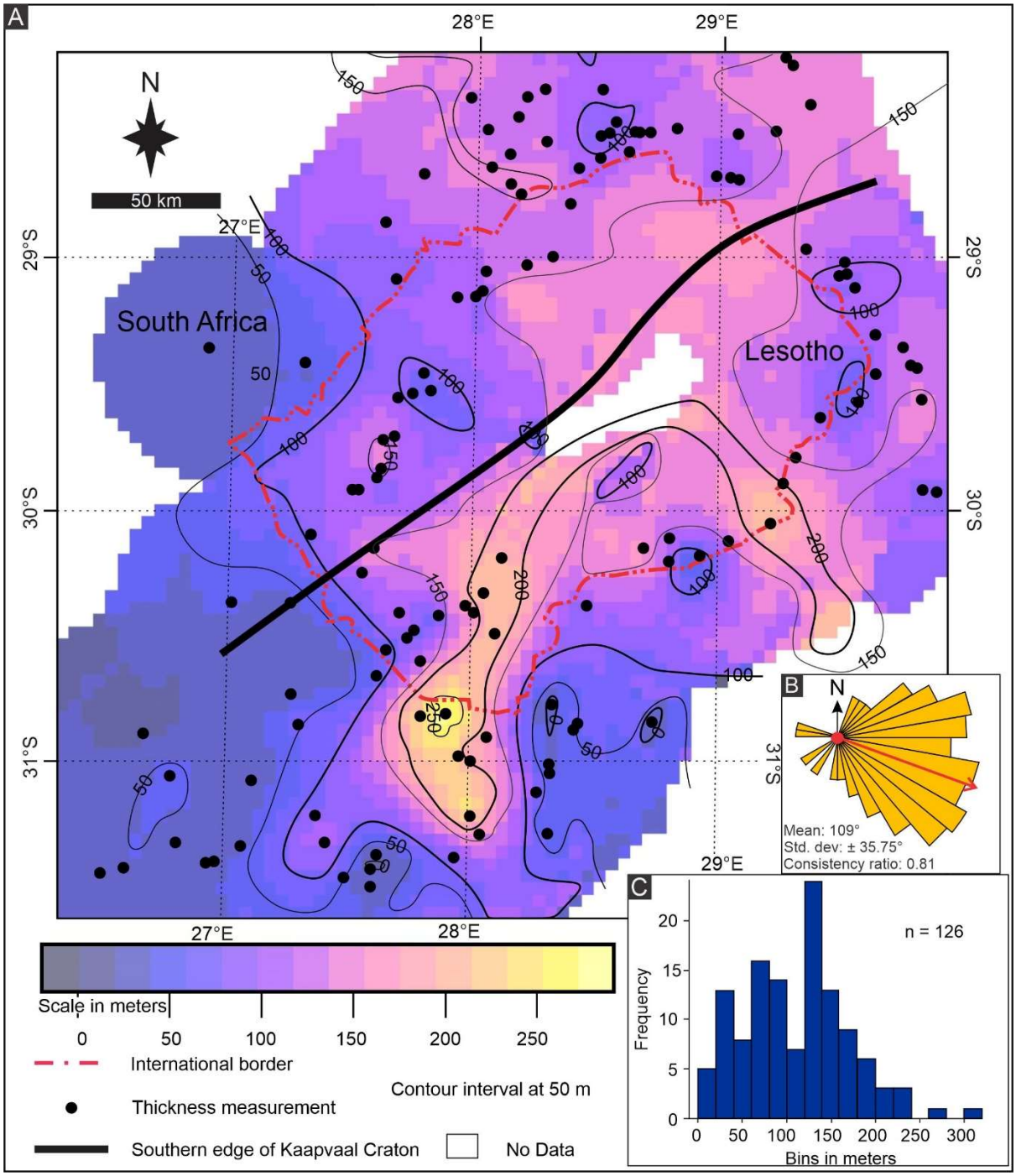

Figure 4.16: Isopach and palaeocurrent data of the Clarens Formation in the MKB. **A**. Thickness map with 50 m interval contour lines. Note the highest thickness zone in southern and central Lesotho. **B**. Palaeocurrent rose of measured flow directions in the Facies Association 1. **C**. Histogram of thickness data points showing a range from 0 to >300 m. 4.5. Discussion

4.5.1 Depositional model

The distribution of facies associations in the Clarens Formation suggests that various large-scale drivers were at work during the deposition of this largely aeolian system. As shown in Figure 4.14, the erg was relatively dynamic with expansions and contractions throughout the depositional period. These fluctuations were concomitant with dramatic lateral facies shifts that can be attributed to changes within a typical zoned erg system, where variations in facies are a result of spatial fluctuations in the erg (dry inner erg to wet erg margin/outer erg conditions - Langford and Chan, 1989; Kocurek and Havholm, 1993; Mountney and Jagger, 2002; Mountney, 2006; Mayoral *et al*., 2021). Moreover, the vertical facies changes (i.e., tripartite zonation of the formation) reflect erg margin shifts related to a temporal wet-dry-wet climate megacycle as first identified by Beukes (1969, 1970), and recently refined by Bordy *et al.* (2021) for the middle to upper Clarens Formation in southern-central Lesotho.

4.5.1.1 Zone 1: Establishment of aeolian conditions

The facies distribution for the oldest zone in the Clarens Formation indicates relatively small and isolated dune fields with associated aeolian sand sheets preserved along the erg margins. The development of sand sheets has been linked to conditions that limit the development of aeolian dunes such as diminishing sand supply and flooding and/or water-table rise (Kocurek and Nielson, 1986; Langford and Chan, 1993; Mountney, 2006). Sand sheets have also been shown to be prevalent along the fore erg and often appear associated with transitional environments where fluvial and aeolian processes interact (Porter, 1986; Mountney, 2006; Al-Masrahy and Mountney, 2015). Facies associations on the eastern margin suggests the presence of ephemeral channel deposits that were highly cannibalistic, reworking older in-channel and/or overbank deposits. Moreover, pluvial deposits appearing in close proximity to Facies Association 1 is indicative of wet interdune conditions.

Deposition of loess may be favoured during a transition to more humid conditions (Pye, 1995), and therefore massive sandstones downwind from the interpreted erg deposits also suggest the presence of sandy loess to loess deposits, which in turn indicate the prevalence of dust storms. Overall, the isolated nature of migrating aeolian dune deposits, which co-occurs with pluvial deposits (i.e., interdune deposits), reflects a wet-to-dry aeolian system, while the co-occurrence of massive and aeolian sand sheet depsits suggest that this part of the Clarens Formation was dominated by erg margin processes during a humid period. Massive deposits can also be linked to dune slumping related to high precipitation and water infiltration as documented in modern and ancient aeolian settings (Loope *et al*., 1998; Sweeney and Loope *et al*, 2001; Simpson *et al.*, 2002; Heness *et al*., 2014), which also supports a more humid climate interpretation for Zone 1.

4.5.1.2 Zone 2: Expansion of the erg

The facies association distribution in Zone 2 of the Clarens Formation shows a notable increase in aeolian dune deposits (Figure 4.14B) along with massive and aeolian sand sheet deposits. This increase in Facies Association1 suggests that an expansion of the erg took place, possibly concomitant with increased sand availability. Similar erg expansion in the Permian Organ Rock Formation in the USA was linked to climatic aridification (Cain and Mountney, 2009). In addition, the general lack of dry interdunal facies suggests that this part of the Clarens Formation was deposited

under dry aeolian conditions (Kocurek and Havholm, 1993; Langford and Chan, 1993), while localized lacustrine and fluvial deposits (Facies Association 4,5 and 6)can be ascribed to the incursion of fluvio-lacustrine systems along the southern and eastern outcrop areas.

4.5.1.3 Zone 3: Shrinkage of the erg

Facies associations within Zone 3 (Figure 4.14C) indicate the dominance of massive depositswith subordinate aeolian dune and aeoian sand sheet deposits. The prevalence of massive deposits suggests that dust storms were again active. Similar to Zone 1, the presence of aeolian dust deposits can imply humid conditions that enhances dust deposition (Pye, 1995). Spatially, aeolian sand sheet deposits appear in close proximity to the migrating aeolian dune deposits which is limited to the western outcrop area, while Facies Association 5 appear sporadically to the east of these. Overall, this may be indicative of an increase in surface moisture that limited wind-blown sediment availability resulting in erg margin retreat and shrinking of the erg. This allowed for the incursion of fluvio-lacustrine processes into the dune field, resulting in episodic wet aeolian conditions. Limited occurrence of debris flow processes (with basaltic material incorporated into it) and basalts amongst migrating aeolian dunes in the uppermost Clarens Formation suggests that the aeolian system was still active during a wet period in the late Pliensbachian during the outpouring of the earliest Karoo lava flows (March *et al.,* 1997; Moulin *et al*., 2011, 2017; Svenson *et al.,*2012). Moreover, the occurrence of terminal shallow lakes associated with lava deltas in the Clarens Formation during a Late Pliensbachian humid phase and before large-scale extrusion of the Karoo lava flows was discussed in Bordy *et al*. (2021).

4.5.2 Synthesis of the erg development

Interpretation of the Clarens Formation as a vast sand sea succession date back to some 100 years ago to du Toit (1918, p.36). The formation of these desert conditions in the MKB during the Early Jurassic was suggested to be the cause of the latitudinal position of the MKB along with the orographic effect of the Cape Fold Belt that would have created a rain-shadow effect. This further exacerbated the continental interior position of the MKB (Loope *et al.*, 2004; Bordy, 2008; Bordy and Head, 2018). As reviewed in Bordy and Head (2018), Beukes (1969, 1970) recorded the three stratigraphic zones in the Clarens Formation that reflect a temporal wet-dry-wet megacycle across the basin, whereas Eriksson (1981, 1986) identified spatial domains in the Clarens Formation in the KwaZulu-Natal Drakensberg region. This synthesis shows that both spatial and temporal controls were active during the deposition of the Clarens Formation. The lateral facies changes illustrate a transition from dry erg interior to wet erg margin typical of spatial variation in wetness conditions in a large erg system (Mountney and Thompson, 2002; Mountney and Jagger, 2004), whereas the vertical facies changes illustrate dramatic erg margin shifts related to temporal climate megacycles (Figures 4.14, 4.16). This implies that during humid conditions, the erg was smaller and allowed for the incursion of more fluvial and lacustrine systems into the dune field while aeolian dust deposition (loess) dominated downwind. During arid conditions, sediment availability increased and resulted in erg growth at the expense of the dust plains, while also pushing fluvial and lacustrine processes further east. During the initial stages of Karoo lava extrusion, the aeolian system and related marginal lacustro-fluvial processes were still active. Given this field-based evidence associated with the upper contact, a conformable relationship is confirmed for the contact between the Clarens Formation and the overlying Drakensberg Group (also see Bordy *et al*., 2021).

4.5.3 Comparison with ancient fluvial-aeolian deposits

The distribution of the facies associations combined with the facies proportions per zone (Figure 4.14), indicates that large-scale, spatiotemporal changes occurred in the depositional environment. These may be related to spatial and temporal fluctuations in sediment supply and availability, combined with atmospheric circulation patterns and climate fluctuations (Kocurek and Havholm, 1993; Mountney and Thompson, 2002; Mountney and Jagger, 2004; Mountney, 2006). These facies can broadly be attributed to deposition along an erg margin and identified based on various features and criteria. These criteria are: 1) differences in grain size and sorting that would represent downwind changes; 2) changes in the complexity of dune-size and stratification; 3) changes in dune spacing; 4) an increase in sand sheet abundance; 5) the prevalence of bioturbation and; 6) an increase in facies associated with non-aeolian deposition (Langford and Chan, 1993). When considering these, an increase in non-aeolian deposits, a downwind grain size decrease as well as increased aeolian sand sheet- and massive deposist suggests that deposition of the Clarens Formation occurred along an erg margin to outer erg.

Such erg dynamics are well documented from various ancient aeolianites (e.g., Candeleros Formation of Argentina – Mayoral *et al*., 2021; the Cedar Mesa Sandstone in the USA – Langford and Chan, 1993; Mountey and Jagger, 2004; Gahlo du Miguel Formation in Brazil – Basilici *et al*., 2020), where damp and wet interdunes progressively increased towards the erg-margin, a classical feature of the zoned erg deposition model (Mountney and Jagger, 2004; Mountney, 2006). In addition, the level of the water table, along with its temporal fluxes, also play an important role in the complexity of the aeolian facies (Mountney and Thompson, 2002; Mountney and Jagger, 2004, Mountney, 2006), and therefore interdunes expand and contract in response to relative water-table fluctuations which results in several stacking pattern expressions based on how these parameters interacted.

A typical erg margin deposit has been described by Mountney and Jagger (2004) for the Cedar Mesa sandstone, and similarly, in the Galho do Miguel Formation of SE Brazil. For the Cedar Mesa Sandstone, Mountney and Jagger (2004) observed temporal fluctuations in bedform size and angle of climb combined with episodic changes in the relative water table. In the case of the Candeleros Formation, facies have been interpreted by Mayoral *et al*. (2021) as a typical erg margin deposit where stratigraphical changes in the facies associations can be attributed to the expansion and contraction of the erg. In essence, episodes of erg contractions were related to a rise in water-table, whereas erg expansions reflected a fall in water table (Mayoral *et al*., 2021). Similarly, the Clarens Formation reflects expansions and contractions of the erg when a water table fall allowed for the increased availability of sediments for entrainment. During phases of humid climate, moisture restricted the availability of sediment, and in turn, affected sediment availability for the construction of dune bedforms (Crabaugh and Kocurek, 1993; Neuman and Scott, 1998; Mountney and Russell, 2009, Al-Masrahy and Mountney, 2015). This type of fluvial interaction is described by Al-Masrahy and Mountney (2015) as one influenced by a raised water table and can be classified based on the appearance of characteristic wet and damp aeolian features such as adhesion structures, wavy lamination, aqueous ripple marks, brecciated laminae, and contorted structures. Such features have been identified for the lower Clarens Formation (Chapter 2), supporting the occurrence of a raised water table for Zone 1. These phases of raised water tables are well known to stimulate accumulation and preservation in aeolian systems, particularly where it is linked to a subsiding basin (Mountney and Thompson, 2002; Al-Masrahy and Mountney, 2015), such as that of the tectonic

setting of the Clarens Formation in the subsiding foresag of the Karoo Foreland system (Bordy *et al*., 2004b, 2005). Loess deposits with close dune sources often preserve interbedded sandstones from both dust and dune facies (Pye, 1995; Al-Masrahy and Mountney, 2015) and this type of interfingering relationship has been documented on the Chinese Loess Plateau, where large-scale, cross-bedded sand has been observed within loess deposits. Based on optically stimulated luminescence dating, the dunes were interpreted to have formed in a period of amplified aridity (Long *et al.*, 2012). These results can be used to infer a strong climatic control on the abundance of migrating dunes and suggests a similar case for the abundance of migrating aeolian dune deposits identified in zone 2 of the Clarens Formation.

Episodic fluvial incursions may be prevalent along fluvially dominated erg margins, and several types of fluvial interactions can be identified in modern erg margin settings (Mountney and Jagger, 2004; Mountney, 2006; Al-Masrahy-and Mounty, 2015). The preservation ephemeral channel deposits and ephemeral unconfined fluvial deposits on the eastern erg margin of the Clarens Formation reflects differing degrees of fluvial erg infiltration throughout the succession. This type of fluvial-aeolian interaction is described by Al-Masrahy and Mountney (2015) as fluvial infiltrations linked to multiple sheetflood sources. Fluvial systems of this type are expressed as unconfined deposition along a relatively low-gradient plain being particularly active after rainstorm events (Al-Masrahy and Mountney, 2015; Priddy and Clarke, 2020). Such unconfined flow can also be explained by the effect of rainstorms on the desert landscape, where limited infiltration of water into the subsurface is offset by high precipitation volumes resulting in overland flow (Goudie, 2013). This feature may explain the wide geographic distribution of ephemeral unconfined fluvial deposits in the Clarens Formation, especially for the upper Clarens Formation (Zone 3).

Overall, the current reassessment of the distribution of facies associations confirms both the validity of the tripartite zonation of the Clarens Formation as defined by Beukes (1969, 1970) and his interpretation of a wet-dry-wet climate megacycle during deposition. Similar climatic megacycles have been observed in other ancient aeolian systems associated with fluvio-lacustrine processes and attest to the common interaction of wet-to-dry aeolian processes in the Clarens Formation.

4.5.4 Early Jurassic climate in southwestern Gondwana

Globally, the Early Jurassic is characterized by extreme environmental variations, when the dominant warm conditions were interrupted by episodic cool phases (Price, 1999; Bagli *et al*., 2020). The arid climate during the Early Jurassic of southwestern Gondwana has been attributed to the continentality of the MKB combined with the orographic effect of the Cape Fold Belt during the Late Triassic to Early Jurassic (Veevers, 2004; Bordy, 2008; Bordy and Head, 2018), a trend that has been associated with many Jurassic deposits of southwestern Gondwana (Holzförster *et al*, 1999; Jerram *et al*., 1999, 2000; Loope *et al*, 2001: Figure 1;Bordy and Catuneanu, 2002; Scherer and Lavina, 2005; Scherer and Goldberg, 2010; do Amarante *et al*., 2019). The Clarens Formation also shows prominent vertical facies changes that suggests a more complex wet-dry-wet climatic megacycle during deposition (Figure 4.16). In addition to the classical work of Beukes (1960, 1970) and Eriksson (1979, 1981, 1986), Rampersadh *et al*. (2018) and Bordy *et al*. (2021) have also described field evidence for the wet periods associated with the lower and uppermost Clarens Formation, respectively. Despite the evidence that northern Gondwana (south Tethys Sea) was a more arid

relative to the north-western Tethys (Aberhan, 2001; van de Schootbrugge *et al*., 2005), Baghli *et al.* (2020) has shown that the climatic trend for northern Gondwana is very similar to that of Boreal and Tethyan sections (Hesselbo *et al*., 2000; McArthur *et al*., 2000; Jenkyns *et al*., 2002; Bailey *et al*., 2003; Rosales *et al*., 2004; Van de Schootbrugge *et al*., 2005; Gomez *et al*., 2008; Suan *et al*., 2010; Dera *et al*., 2011; Armendariz *et al*., 2012; Korte and Hesselbo, 2012; Li *et al*., 2012; Harazim *et al*., 2013) with the exception of negative oxygen and carbon isotope excursions close to the lower and upper boundaries of the Pliensbachian.

The field-based evidence from this study combined with absolute age dates (Chapter 5) and the suggested global climatic trend recorded in the Tethyan region indicates a late Sinemurian cooling, an early Pliensbachian warming followed by an early late Pliensbachian cooling phase (Dera *et al*., 2011; Gomez *et al*., 2016; Arabas *et al*., 2017; Baghli, 2021; Bordy *et al*., 2020, 2021). Given the facies associations within the Clarens Formation, the general climate in southwestern Gondwana can be envisioned as semi-arid to arid having a dry aeolian system with episodic phases of wet aeolian activity, while windy and dusty conditions prevailed along the outer erg to erg margin. Ephemeral lakes and rivers were active along the erg margin, and during humid phases, precipitation may have resulted in a relative rise of the water table.

Global atmospheric circulation patterns of Chandler *et al.* (1992) as discussed by Loope *et al.* (2004 – see their Figure 4.4) suggests that seasonal wind reversal occurred in both the southern and northern hemispheres during the Early Jurassic of Pangaea and appears to be consistent with the measured SE directed wind regime that was interpreted for the Clarens Formation, given the palaeolatitue of the basin (Sciscio *et al*., 2017). This has also been identified in Jurassic aeolianites in the USA and Brazil that show a strong seasonality associated with a monsoonal palaeo-climate (Parrish and Peterson, 1988; Chandler *et al*., 1992; Loope *et al*., 2004; Scherer and Goldberg, 2010). These reversals were reported to cause strong dune migrating north-westerlies and weaker southerly winds for the Navajo Sandstone, resulting in a consistent north-westerly trend in the palaeo-flow directions. Although monsoonal seasonality has not been observed in the Clarens Formation, foresets in large-scale, cross-bedded sandstones being composed of grainflow and translatent ripple cross-lamination can indicate a strong seasonality in wind patterns (Kocurek, 1991). In a similar way, the consistent south-east directed foresets within the Facies Association 1 of the Clarens Formation may be related to such mid-latitude westerlies associated with atmospheric circulation linked to large-scale Hadley flow, which is believed to have been active since the Palaeozoic (Scotese *et al.,* 1999*;* Cosgrove *et al*., 2021a). During the summer months, seasonal reversals came about as a result of the movement of the intertropical convergence zone (ITCZ) and caused weaker south-westerly winds that may have led to the deposition of the translatent ripple stratification. Despite various Pangaea atmospheric circulation models (Kutzbach and Gallimore, 1989; Kutzbach, 1994), the consistent south-easterly oriented cross-bed foreset measurements reported from the Clarens Formation (Figure 4.17) supports the Early Jurassic circulation model of Chandler *et al.* (1992).

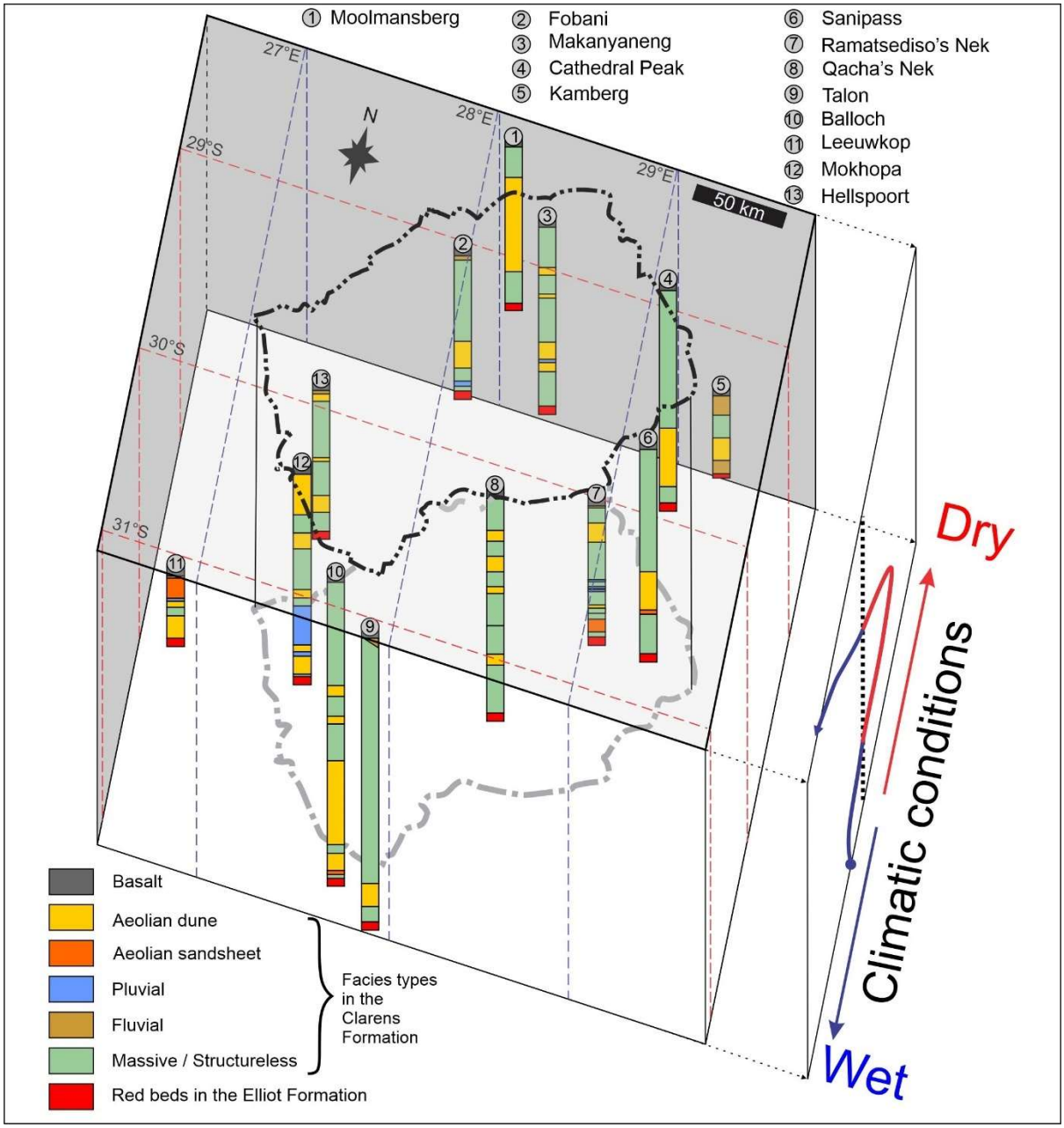

Figure 4.17: Climatic cyclicity in the Lower Jurassic Clarens Formation shown with the aid of a few representative simplified logs.

4.5.5 Thickness trends of the Clarens Formation in the Karoo foreland basin context

The current thickness estimation map (Figure 4.14A) confirms the previously identified northeast-southwest directed trough (Beukes, 1969, 1970; Robinson *et al.*, 1969; Johnson, 1976; Eriksson, 1981, 1986) as well as the extreme but localised thickness fluctuations in the southern outcrop area. Sites where the Clarens Formation is absent have been ascribed to early onset lava extrusion, or alternatively, localised erosion due to authigenic processes (e.g., scouring by rivers) or non-deposition of the sediments due to varied dune distribution across paleo-topographic heights (e.g., du Toit, 1905, 1910, 1917; Beukes, 1969, 1970; Robinson *et al.*, 1969).

The northeast–southwest oriented thickness trough in the Clarens Formation isopach map aligns well with the orientation of the southern edge of the Kaapvaal Craton (Figure 4.14; Schmitz and Rooyani, 1987, Skinner *et al*., 1992; Bordy *et al*., 2004b, Bordy *et al*., 2005). Therefore, the subtle regional decrease in thickness in the Clarens Formation could be related to rheological (e.g., viscoelastic) variations in the Karoo basement, where the depositional area that is underlain by the Namaqua Natal Mobile Belt was more prone to subsidence compared to the regions underlain by the more rigid Kaapvaal Craton (Schmitz and Rooyani, 1987; Bordy *et al*., 2005). Similar thickness trends related to the basement rheology as well as to the position of the southern edge of the Kaapvaal Craton have been observed in the pre-Clarens Formation depositional history of the MKB (e.g., Molteno Formation – Hancox, 1998; Elliot Formation – Bordy *et al*., 2004b, 2005). Noted that there is no significant facies changes seen for the Clarens Formation in terms of this boundary, thickness differences in the pluvial deposits of the Clarens Formation (see Chapter 2) that are attributed to both climatic factors and differential subsidence, may be related to the aforementioned variation in basement rheology. Moreover, the thickness trend in the Clarens Formation, being consistent with thickness trends for the Elliot Formation, supports the terminal foresag basin model for the upper Stromberg Group (e.g., Bordy *et al*. 2004b, 2005). However, syn-sedimentary normal faulting in the Clarens Formation at Moyeni (Haupt, 2018) and Siberia (Bordy *et al*., 2004b) also suggests that, at least locally, extensional tectonics in the MKB may have started to be active from the Sinemurian onwards.

4.6. Conclusion

The facies of the Clarens Formation reflect a depositional environment where eastward migrating dunes and down-wind aeolian dust were deposited along the erg margin of an extensive aeolian system. Aeolian sand sheets formed transitional features along erg margin, while fluvial-lacustrine systems penetrated the inner erg from the east. Contemporaneous climatic trends reported from the Tethyan margin of Gondwana are closely mimicked by the wet-dry-wet megacycle identified in the Clarens Formation suggesting that this may have been of global significance in the Early Jurassic. This climatic megacycle is based on the vertical facies changes that initially reflect an episode of wet aeolian deposition, when limited sediment availability enhanced the deposition of aeolian dust on an extensive downwind loess plain. Following the wet phase, aridification of the environment resulted in increased aeolian sediment supply causing an expansion of the erg. The subsequent wet phase in the aeolian system ensued across most of the basin and was still active during the onset of early extrusion of the continental flood basalts associated with the Karoo-Ferrar Igneous Province. The thickness trends indicate a subtle north to south increase with extreme localised thickness fluctuations in the southern outcrop area, whereas the northern outcrop area shows a more constant thickness. This thickness trend may reflect the variation in the basement rheology and supports the foresag basin model during the terminal phase of the MKB evolution.

4.7. References

Aberhan, M., 2001. Bivalve palaeobiogeography and the Hispanic Corridor: time of opening and effectiveness of a proto-Atlantic seaway. *Palaeogeography, Palaeoclimatology, Palaeoecology*, 165(3-4): 375–394. DOI: 10.1016/S0031-0182(00)00172-3

Allen, J.R.L. and Banks, N.L. 1972. An interpretation and analysis of recumbent-folded deformed cross-bedding. *Sedimentology*, 19(3-4): 257–283. DOI: 10.1111/j.1365-3091.1972.tb00024.x

Al-Masrahy, M. A. and Mountney, N. P. 2015. A classification scheme for fluvial–aeolian system interaction in desert-margin settings. *Aeolian Research*, 17: 67–88. DOI: 10.1016/j.aeolia.2015.01.010

Armendáriz, M., Rosales, I., Bádenas, B., Aurell, M., García-Ramos, J.C. and Piñuela, L. 2012. High-resolution chemostratigraphic records from Lower Pliensbachian belemnites: Palaeoclimatic perturbations, organic facies and water mass exchange (Asturian basin, northern Spain). *Palaeogeography, Palaeoclimatology, Palaeoecology*, 333: 178–191. DOI: 10.1016/j.palaeo.2012.03.029

Bailey, T.R., Rosenthal, Y., McArthur, J.M., Van de Schootbrugge, B. and Thirlwall, M.F. 2003. Paleoceanographic changes of the Late Pliensbachian–Early Toarcian interval: a possible link to the genesis of an Oceanic Anoxic Event. *Earth and Planetary Science Letters*, 212(3-4): 307–320. DOI: 10.1016/S0012-821X(03)00278-4

Basilici, G., Mesquita, Á.F., Soares, M.V.T., Janočko, J., Mountney, N.P. and Colombera, L. 2021. A Mesoproterozoic hybrid dry-wet aeolian system: Galho do Miguel Formation, SE Brazil. *Precambrian Research*, 359: 106216. DOI: 10.1016/j.precamres.2021.106216

Beukes, N.J. 1969. Die sedimentologie van die Etage Holkranssandsteen, sisteem Karoo. Unpublished MSc dissertation, University of the Orange Free State, Bloemfontein, 138 pp. Available: http://hdl.handle.net/11660/7671

Beukes, N.J. 1970. Stratigraphy and sedimentology of the Cave Sandstone stage, Karoo System. In: S.H. Haughton (Ed), Proceedings and papers of the 2nd Gondwana symposium. Council for Scientific and Industrial Research, Pretoria: 321–341.

Bordy, E.M. 2008. Enigmatic trace fossils from the aeolian Lower Jurassic Clarens Formation, southern Africa. *Palaeontologia Electronica*, 11: 16A.

Bordy, E.M. and Catuneanu, O. 2001. Sedimentology of the upper Karoo fluvial strata in the Tuli Basin, South Africa. *Journal of African Earth Sciences*, 33(3-4):605–629. DOI: 10.1016/S0899-5362(01)00090-2

Bordy, E.M., Hancox, P.J. and Rubidge, B.S. 2004a. Basin development during the deposition of the Elliot Formation (Late Triassic-Early Jurassic), Karoo Supergroup, South Africa. *South African Journal of Geology*, 107(3): 397-412. DOI: 10.2113/107.3.397

Bordy, E.M., Hancox, P.J. and Rubidge, B.S. 2004b. Fluvial style variations in the Late Triassic–Early Jurassic Elliot Formation, main Karoo Basin, South Africa. *Journal of African Earth Sciences*, 38(4): 383-400. DOI: 10.1016/j.jafrearsci.2004.02.004

Bordy, E.M., Hancox, P.J. and Rubidge, B.S. 2005. The contact of the Molteno and Elliot formations through the main Karoo Basin, South Africa: a second-order sequence boundary. *South African Journal of Geology*, 108(3): 351-364. DOI: 10.2113/108.3.351

Bordy, E.M. 2008. Enigmatic trace fossils from the aeolian Lower Jurassic Clarens Formation, southern Africa. *Plaeontologia Electronica*, 11: 16A.

Bordy, E.M. and Head. H.V. 2018. Lithostratigraphy of the Clarens Formation (Stormberg Group, Karoo Supergroup), South Africa. *South African Journal of Geology*, 121: 119–130. DOI: 10.25131/sajg.121.0009

Bordy, E.M., Rampersadh, A., Abrahams, M., Lockley, M.G. and Head, H.V. 2020. Tracking the Pliensbachian–Toarcian Karoo firewalkers: Trackways of quadruped and biped dinosaurs and mammaliaforms. *Plos one*, 15(1): e0226847. DOI: 10.1371/journal.pone.0226847

Bordy, E.M., Haupt, T.N. and Head, H.V. 2021. Karoo lava-fed deltas and a petrified forest from the Lower Jurassic of southern Gondwana. *Palaeogeography, Palaeoclimatology, Palaeoecology*, 575: 110484. DOI: 10.1016/j.palaeo.2021.110484

Broom, R. 1904. On a new crocodilian genus (Notochampsa) from the Upper Stormberg beds of South Africa. *Geological Magazine*, 1: 582–584.

Cain, S.A. and Mountney, N.P. 2009. Spatial and temporal evolution of a terminal fluvial fan system: the Permian Organ Rock Formation, South-east Utah, USA. *Sedimentology*, 56(6): 1774–1800. DOI: 10.1111/j.1365-3091.2009.01057.x

Catuneanu, O., Hancox, P.J. and Rubidge, B.S. 1998. Reciprocal flexural behaviour and contrasting stratigraphies: a new basin development model for the Karoo retroarc foreland system, South Africa. *Basin research*, 10(4): 417–440. DOI: 10.1046/j.1365-2117.1998.00078.x

Catuneanu, O., Wopfner, H., Eriksson, P.G., Cairncross, B., Rubidge, B.S., Smith, R.M.H. and Hancox, P.J. 2005. The Karoo basins of south-central Africa. *Journal of African Earth Sciences*, 43(1-3): 211–253. DOI: 10.1016/j.jafrearsci.2005.07.007

Chandler, M.A., Rind, D. and Ruedy, R. 1992. Pangaean climate during the Early Jurassic: GCM simulations and the sedimentary record of paleoclimate. *Geological Society of America Bulletin*, 104(5): 543–559. DOI: 10.1130/0016-7606(1992)104<0543:PCDTEJ>2.3.CO;2

Crabaugh, M. and Kocurek, G. 1993. Entrada Sandstone: an example of a wet aeolian system. *Geological Society, London, Special Publications*, 72(1): 103–126. DOI: 10.1144/GSL.SP.1993.072.01.11

Cole, D.I. 1992. Evolution and development of the Karoo Basin. In: De Wit, M.J., and Ransome, I.G.D. (eds), Inversion Tectonics of the Cape Fold Belt, Karoo and Cretaceous Basins of Southern Africa, Balkema: Rotterdam, The Netherlands, 87–99 pp.

Cosgrove, G.I.E., Colombera, L. and Mountney, N. P. 2021. Quantitative analysis of the sedimentary architecture of eolian successions developed under icehouse and greenhouse climatic conditions. *GSA Bulletin*. DOI: https://doi.org/10.1130/B35918.1

Cosgrove, G.I.E., Colombera, L. and Mountney, N. P. 2021. A database of Aeolian Sedimentary Architecture for the characterization of modern and ancient sedimentary systems. *Marine and Petroleum Geology*, 127: 104983. DOI: 10.1016/j.marpetgeo.2021.104983

Dasgupta, P. 2002. Determination of paleocurrent direction from oblique sections of trough cross-stratification—A precise approach. *Journal of Sedimentary Research,* 72: 217–219. DOI: 10.1306/050401720217

Dera, G., Brigaud, B., Monna, F., Laffont, R., Pucéat, E., Deconinck, J.F., Pellenard, P., Joachimski, M.M. and Durlet, C. 2011. Climatic ups and downs in a disturbed Jurassic world. *Geology*, 39(3): 215–218. DOI: 10.1130/G31579.1

do Amarante, F.B., Scherer, C.M., Aguilar, C.A.G., dos Reis, A.D., Mesa, V. and Soto, M. 2019. Fluvial-eolian deposits of the Tacuarembó formation (Norte Basin–Uruguay): Depositional models and stratigraphic succession. *Journal of South American Earth Sciences*, 90: 355–376. DOI: 10.1016/j.jsames.2018.12.024

Dollman, K.N., Clark, J.M., Viglietti, P.A., Browning, C. and Choiniere, J.N. 2021. Revised anatomy, taxonomy and biostratigraphy of Notochampsa istedana Broom, 1904, a Lower Jurassic crocodyliform from the Clarens Formation (Stormberg Group), and its implications for early crocodyliform phylogeny. *Journal of Systematic Palaeontology,*1–25. DO: 10.1080/14772019.2021.1948926

Duncan, R.A., Hooper, P.R., Rehacek, J., Marsh, J.S. and Duncan, A.R. 1997. The timing and duration of the Karoo igneous event, southern Gondwana. *Journal of Geophysical Research,* 102: 18127–18138. DOI: 10.1029/97JB00972

du Toit, A.L. 1904. Geological survey of the divisions of Elliot and Xalanga, Tembuland. Annual report Geological Commission Cape Good Hope (1903), 169–205.

Du Toit, A.L. 1905. Geological survey of the division of Aliwal North, Herschel, Barkly East and part of Wodehouse: Annual Report of the Geological Commission of the Cape of Good Hope. 71–181.

Du Toit, A.L. 1910. Geological survey of Maclear and portions of Engcobo, Mount Fletcher, Qumbu and Mount Frere. Annual Report of the Geological Commission of the Cape of Good Hope. 69–108.

Du Toit, A.L. 1918. The zones of the Karroo System and their distribution. *Proceedings of the Geological Society of South Africa*, 21, 17–36.

Eriksson, P.G. 1979. Mesozoic sheetflow and playa sediments of the Clarens Formation in the Kamberg area of the Natal Drakensberg. *South African Journal of Geology*, 82(2): 257–258.

Eriksson, P.G. 1981. A palaeoenvironmental analysis of the Clarens Formation in the Natal Drakensberg. *Transactions of the Geological Society of South Africa*, 84: 7–17.

Eriksson, P.G. 1983. A palaeoenvironmental study of the Molteno, Elliot and Clarens Formations in the Natal Drakensberg and northeastern Orange Free State. Unpublished doctoral dissertation, University of Natal, Pietermaritzburg.

Eriksson, P.G. 1986. Aeolian dune and alluvial fan deposits in the Clarens Formation of the Natal Drakensberg. *Transactions of the Geological Society of South Africa*, 89: 389–393.

Forey, P. and Gardiner, B.G. 1973. A new dictyopygid from the Cave Sandstone of Lesotho, Southern Africa. *Palaeontologia africana*, 15: 29–31.

Gómez, J.J., Goy, A., and Canales, M.L. 2008. Seawater temperature and carbon isotope variations in belemnites linked to mass extinction during the Toarcian (Early Jurassic) in Central and Northern Spain. Comparison with other European sections. *Palaeogeography, Palaeoclimatology, Palaeoecology*, 258(1-2): 28–58. DOI: 10.1016/j.palaeo.2007.11.005

Goudie, A.S., 2013. Arid and semi-arid geomorphology. Cambridge university press. 454 pp.

Hampton, B.A. and Horton, B.K. 2007. Sheetflow fluvial processes in a rapidly subsiding basin, Altiplano plateau, Bolivia. *Sedimentology*, 54(5): 1121–1148. DOI: 10.1111/j.1365-3091.2007.00875.x

Hancox, P.J. 1998. A stratigraphic, sedimentological and palaeonviron-mental synthesis of the Beaufort-Molteno contact in the Karoo Basin. Unpublished doctoral dissertation, University of the Witwatersrand, Johannesburg, South Africa.

Hanson, E.K., Moore, J.M., Bordy, E.M., Marsh, J.S., Howarth, G. and Robey, J.V.A. 2009. Cretaceous erosion in central South Africa: Evidence from upper-crustal xenoliths in kimberlite diatremes. *South African Journal of Geology*, 112(2): 125-140. DOI: 10.2113/gssajg.112.2.125

Harazim, D., Van De Schootbrugge, B.A.S., Sorichter, K., Fiebig, J., Weug, A., Suan, G. and Oschmann, W. 2013. Spatial variability of watermass conditions within the European Epicontinental Seaway during the Early Jurassic (Pliensbachian–Toarcian). *Sedimentology*, 60(2): 359–390. DOI: 10.1111/j.1365-3091.2012.01344.x

Hassan, M.S., Venetikidis, A., Bryant, G. and Miall, A.D. 2018. The sedimentology of an ERG margin: the Kayenta–Navajo transition (Lower Jurassic), Kanab, Utah, USA. *Journal of Sedimentary Research*, 88(5): 613–640. DOI: https://doi.org/10.2110/jsr.2018.31

Haughton, S.H. 1924. The Fauna and stratigraphy of the Stormberg Series. *Annals of the South African Museum*, 8: 1–517.

Haupt, T. 2018. Palaeoenvironmental change from the Hettangian to Toarcian in Moyeni (Quthing District), Southwestern Lesotho. Unpublished MSc dissertation, University of Cape Town, 112pp. Available: http://hdl.handle.net/11427/30021

Heness, E.A., Simpson, E.L., Bumby, A.J., Eriksson, P.G., Eriksson, K.A., Hilbert-Wolf, H.L., Okafor, O.J., Linnevelt, S., Malenda, H.F. and Modungwa, T. 2014. Evidence for climate shifts in the ~ 2.0 Ga upper Makgabeng Formation erg, South Africa. *Palaeogeography, Palaeoclimatology, Palaeoecology*, 409: 265–279. DOI: 10.1016/j.palaeo.2014.05.016

Hesselbo, S.P., Gröcke, D.R., Jenkyns, H.C., Bjerrum, C.J., Farrimond, P., Bell, H.S.M. and Green, O.R. 2000. Massive dissociation of gas hydrate during a Jurassic oceanic anoxic event. *Nature*, 406(6794): 392–395. DOI: 10.1038/35019044

High, L.R. and M.D. Picard. 1974. Reliability of cross-stratification types as paleocurrent indicators in fluvial rocks. *Journal of Sedimentary Research,* 44: 158–168. DOI: 10.1306/74D729AF-2B21-11D7-8648000102C1865D

Holzförster, F., Stollhofen, H. and Stanistreet, I.G. 1999. Lithostratigraphy and depositional environments in the Waterberg-Erongo area, central Namibia, and correlation with the main Karoo Basin, South Africa. *Journal of African Earth Sciences*, 29(1): 105-123. 10.1016/S0899-5362(99)00083-4

Holzförster, F. 2007. Lithology and depositional environments of the Lower Jurassic Clarens Formation in the eastern Cape, South Africa. *South African Journal of Geology*, 110(4): 543–560. DOI: 10.2113/gssajg.110.4.543

Hummel, G. and Kocurek, G. 1984. Interdune areas of the back-island dune field, North Padre Island, Texas. *Sedimentary Geology*, 39(1-2): 1–26. DOI: https://doi.org/10.1016/0037-0738(84)90022-8

Hunter, R.E. 1977. Basic types of stratification in small eolian dunes. *Sedimentology*, 24: 361–387. DOI: 10.1111/j.1365-3091.1977.tb00128.x

Hunter, R.E, 1981. Stratification styles in eolian sandstones: some Pennsylvanian to Jurassic examples from the western interior USA. SEPM special Publications, 31: 315–329.

Hunter, R. E. and Rubin, D. M. 1983. Interpreting cyclic cross-bedding, with an example from the Navajo Sandstone. In *Developments in Sedimentology*, Elsevier, 38: 429–454. DOI: 10.1016/S0070-4571(08)70808-2

Jenkyns, H.C., Jones, C.E., Gröcke, D.R., Hesselbo, S.P. and Parkinson, D.N. 2002. Chemostratigraphy of the Jurassic System: applications, limitations and implications for palaeoceanography. *Journal of the Geological Society*, 159(4): 351–378. DOI: ttps://doi.org/10.1144/0016-764901-130

Jerram, D.A., Mountney, N. and Stollhofen, H. 1999. Facies architecture of the Etjo Sandstone Formation and its interaction with the basal Etendeka Flood Basalts of northwest Namibia: implications for offshore prospectivity. *Geological Society, London, Special Publications*, 153(1): 367–380. DOI: 10.1144/GSL.SP.1999.153.01.22

Jerram, D.A. and Stollhofen, H. 2002. Lava–sediment interaction in desert settings; are all peperite-like textures the result of magma–water interaction?. *Journal of Volcanology and Geothermal Research*, 114(1-2): .231–249. DOI: 10.1016/S0377-0273(01)00279-7

Jerram, D.A., Mountney, N.P., Howell, J.A., Long, D. and Stollhofen, H. 2000. Death of a sand sea: an active aeolian erg systematically buried by the Etendeka flood basalts of NW Namibia. *Journal of the Geological Society,* 157(3): 513–516. DOI: 10.1144/jgs.157.3.513

Johnson, M.R. 1976. Stratigraphy and sedimentology of the Cape and Karoo Sequences in the eastern Cape Province. Unpublished doctoral dissertation, Rhodes University, Grahamstown, South Africa, 336pp. Available at http://hdl.handle.net/10962/d1005617

Jubb, R.A. 1973. Brief synthesis of present information on the geographical and stratigraphical distribution of fossil fish within the Stormberg Series, South Africa. *Palaeontologia africana*, 16: 17–23.

Kocurek, G. 1991. Interpretation of ancient eolian sand dunes. *Annual Reviews: Earth and Planetary Science*, 19: 43–75. DOI: 10.1146/annurev.ea.19.050191.000355

Kocurek, G. and Dott, R.H. 1981. Distinction and uses of stratification types in the interpretation of eolian sand. *Journal of Sedimentary Petrology*, 51: 579–595. DOI: 10.1306/212F7CE3-2B24-11D7-8648000102C1865D

Kocurek, G. and Nielson, J. 1986. Conditions favourable for the formation of warm-climate aeolian sand sheets. *Sedimentology*, 33(6): 795–816. DOI: 10.1111/j.1365-3091.1986.tb00983.x

Kocurek, G. and Havholm. K.G. 1993. Eolian Sequence Stratigraphy – conceptual framework. In *Recent Developments in Siliciclastic Sequence Stratigraphy*. Weimer, P. and Posamentier, H. W. (eds). American Association of Petroleum Geologists, Memoir 58: 393–409.

Kocurek, G. and Day, M. 2018. What is preserved in the aeolian rock record? A Jurassic Entrada Sandstone case study at the Utah–Arizona border. *Sedimentology*, 65(4): 1301–1321. DOI: 10.1111/sed.12422

Korte, C. and Hesselbo, S.P. 2011. Shallow marine carbon and oxygen isotope and elemental records indicate icehouse-greenhouse cycles during the Early Jurassic. *Paleoceanography*, 26(4): PA4219. DOI: 10.1029/2011PA002160

Kutzbach, J.E. 1994. Idealized Pangean climates: sensitivity to orbital change. *Geological Society of America: Special Papers*, 288: 41–56.

Kutzbach, J.E. and Gallimore, R.G. 1989. Pangaean climates: megamonsoons of the megacontinent. *Journal of Geophysical Research: Atmospheres*, 94(D3): 3341–3357. DOI: 10.1029/JD094iD03p03341

Langford, R.P. and Chan, M.A. 1989. Fluvial-aeolian interactions: Part II, ancient systems. *Sedimentology*, 36(6): 1037–1051. DOI: 10.1111/j.1365-3091.1989.tb01541.x

Langford, R.P. and Chan, M.A. 1993. Downwind changes within an ancient dune sea, Permian Cedar Mesa Sandstone, southeast Utah. In *Aeolian Sediments: Ancient and Modern*. Pye, K and Lancaster, N (eds). International Association of Sedimentologists, 109–126pp. DOI: 10.1002/9781444303971.ch8

Li, Q., McArthur, J.M. and Atkinson, T.C. 2012. Lower Jurassic belemnites as indicators of palaeo-temperature. *Palaeogeography, Palaeoclimatology, Palaeoecology*, 315: 38–45. DOI: 10.1016/j.palaeo.2011.11.006

Lock, B.E., Paverd, A.L. and Broderick, T.J. 1974. Stratigraphy of the Karoo volcanic rocks of the Barkly East district. *Transactions of the Geological Society of South Africa*. 77:177–129.

Loope, D.B., Dingus, L., Swisher III, C.C. and Minjin, C. 1998. Life and death in a Late Cretaceous dune field, Nemegt basin, Mongolia. *Geology*, 26: 27–30. DOI: 10.1130/0091-7613(1998)026<0027:LADIAL>2.3.CO;2

Loope, D.B., Rowe, C.M. and Joeckel, R.M. 2001. Annual monsoon rains recorded by Jurassic dunes. *Nature*, 412(6842): 64–66. DOI: 10.1038/35083554

Loope, D.B., Steiner, M.B., Rowe, C.M. and Lancaster, N. 2004. Tropical westerlies over Pangaean sand seas. *Sedimentology*, 51(2): 315-322. DOI: 10.1046/j.1365-3091.2003.00623.x

Marsh, J.S., Eales, H.V. 1984. The chemistry and petrogenesis of igneous rocks of the Karoo central area, Southern Africa. In: Erlank, A.J. (Ed.), Petrogenesis of the Volcanic Rocks of the Karoo Province. *Geological Society of South Africa, Special Publication*, 13: 27–67.

McArthur, J.M., Donovan, D.T., Thirlwall, M.F., Fouke, B.W. and Mattey, D. 2000. Strontium isotope profile of the early Toarcian (Jurassic) oceanic anoxic event, the duration of ammonite

biozones, and belemnite palaeotemperatures. *Earth and Planetary Science Letters*, 179(2): 269–285. DOI: 10.1016/S0012-821X(00)00111-4

McClintock, M., Marsh, J.S. and White, J.D. 2008. Compositionally diverse magmas erupted close together in space and time within a Karoo flood basalt crater complex. *Bulletin of Volcanology*, 70(8): 923–946. DOI: 10.1007/s00445-007-0178-6

McKee, E.D. 1966. Structures of dunes at White Sands National Monument, New Mexico (and a comparison with structures of dunes from other selected areas). *Sedimentology*, 7: 1–69. DOI: 10.1111/j.1365-3091.1966.tb01579.x

Meijs, L. 1960. Notes on the occurrence of petrified wood in Basutoland. Roma, Basutoland: Pius XII University Collage, Papers No. 2: 8 pp.

Miall, A.D. 1974. Paleocurrent analysis of alluvial sediments; a discussion of directional variance and vector magnitude. *Journal of Sedimentary Research,* 44: 1174–1185. DOI: 10.1306/212F6C6C-2B24-11D7-8648000102C1865D

Miall, A.D. 1974. Paleocurrent analysis of alluvial sediments; a discussion of directional variance and vector magnitude. *Journal of Sedimentary Research,* 44: 1174–1185. DOI: 10.1306/212F6C6C-2B24-11D7-8648000102C1865D

Miall, A. D. 1985. Architectural-element analysis: a new method of facies analysis applied to fluvial deposits. *Earth Science Reviews*. 22(4): 261–308. DOI: 10.1016/0012-8252(85)90001-7

Miall, A.D. 1996. Geology of Fluvial Deposits. Springer-Verlag: Berlin, 582 pp.

Miall, A.D. 2016. Stratigraphy: A Modern Synthesis. Springer-Verlag: Berlin, 454 pp.

Moulin, M., Fluteau, F., Courtillot, V., Marsh, J., Delpech, G., Quidelleur, X., Gérard, M. and Jay, A.E. 2011. An attempt to constrain the age, duration, and eruptive history of the Karoo flood basalt: Naude's Nek section (South Africa). *Journal of Geophysical Research: Solid Earth*, 116(B07403). DOI: 10.1029/2011JB008210

Moulin, M., Fluteau, F., Courtillot, V., Marsh, J., Delpech, G., Quidelleur, X. and Gérard, M. 2017. Eruptive history of the Karoo lava flows and their impact on early Jurassic environmental change. *Journal of Geophysical Research: Solid Earth*, 122(2): 738–772. DOI: 10.1002/2016JB013354

Mountney, N.P. 2006. Eolian facies models. In *Facies Models Revisited*. Mountney, N. P. Posamentier, H. W. and Walker, R. G. (eds). SEPM Special Publication, 84: 19–83. DOI: 10.2110/pec.06.84.0019

Mountney, N.P. and Jagger, A. 2004. Stratigraphic evolution of an aeolian erg margin system: the Permian Cedar Mesa Sandstone, SE Utah, USA. *Sedimentology*, 52: 713–743. DOI: 10.1111/j.1365-3091.2004.00646.x

Mountney, N.P. and Thompson, D.B. 2002. Stratigraphic evolution and preservation of aeolian dine and damp/wet interdune strata: an example from the Triassic Helsby Sandstone Formation, Cheshire Basin, UK. *Sedimentology*, 49: 805–833. DOI: 10.1046/j.1365-3091.2002.00472.x

Muir, R.A., Bordy, E.M., Mundil, R. and Frei, D. 2020. Recalibrating the breakup history of SW Gondwana: U–Pb radioisotopic age constraints from the southern Cape of South Africa. *Gondwana Research*, 84: 177-193. DOI: 10.1016/j.gr.2020.02.011

Neuman, C.M. and Scott, M.M. 1998. A wind tunnel study of the influence of pore water on aeolian sediment transport. *Journal of Arid Environments*, 39(3): 403–419. DOI: 10.1006/jare.1997.0371

North, C.P. and Davidson, S.K. 2012. Unconfined alluvial flow processes: recognition and interpretation of their deposits, and the significance for palaeogeographic reconstruction. *Earth-Science Reviews*, 111(1-2): 199–223. DOI: 10.1016/j.earscirev.2011.11.008

Parrish, J.T. and Peterson, F. 1988. Wind directions predicted from global circulation models and wind directions determined from eolian sandstones of the western United States—A comparison. *Sedimentary Geology*, 56(1-4): 261–282. DOI: 10.1016/0037-0738(88)90056-5

Pebesma, E.J., 2004. Multivariable geostatistics in S: the gstat package. *Computers and Geosciences*, 30: 683-691. DOI: 10.1016/j.cageo.2004.03.012

Pebesma, E.J., R.S. Bivand, 2005. Classes and methods for spatial data in R. *R News,* 5 (2), https://cran.r-project.org/doc/Rnews/.

Pérez Mayoral, J., Argüello Scotti, A., Apesteguía, S. and Veiga, G.D. 2021. High-resolution analysis of an erg-margin system from the cretaceous Candeleros Formation (La Buitrera paleontological area, Río Negro province, Argentina): An approach to different scales of fluvial-aeolian interactions. *Latin American Journal of Sedimentology and Basin Analysis*, 28(1): 37–59.

Petry, K., Jerram, D.A., Delia del Pilar, M. and Zerfass, H. 2007. Volcanic-sedimentary features in the Serra Geral Fm., Paraná Basin, southern Brazil: examples of dynamic lava-sediment interactions in an arid setting. *Journal of Volcanology and Geothermal Research*, 159(4): 313–325. DOI: 10.1016/j.jvolgeores.2006.06.017

Priddy, C.L. and Clarke, S.M. 2020. The sedimentology of an ephemeral fluvial–aeolian succession. *Sedimentology*, 67(5): 2392–2425. DOI: 10.1111/sed.12706

Price, G.D. 1999. The evidence and implications of polar ice during the Mesozoic. *Earth-Science Reviews*, 48(3): 183–210. DOI: 10.1016/S0012-8252(99)00048-3

Porter, M.L. 1986. Sedimentary record of erg migration. *Geology*, 14(6): 497–500. DOI: 10.1130/0091-7613(1986)14<497:SROEM>2.0.CO;2

Porter, M.L. 1987. Sedimentology of an ancient erg margin: the Lower Jurassic Aztec Sandstone, southern Nevada and southern California. *Sedimentology*, 34(4): 661–680. DOI: 10.1111/j.1365-3091.1987.tb00793.x

Pye, K. 1987. Aeolian dust and dust deposits. Elsevier, 334 pp.

Pye, K. 1995. The nature, origin and accumulation of loess. *Quaternary Science Reviews,* 14: 653–667. DOI: 10.1016/0277-3791(95)00047-X

R Core Team. 2014. R: A language and environment for statistical computing. R Foundation for Statistical Computing, Vienna, Austria. Available: http://www.R-project.org/

Rampersadh, A., Bordy, E.M., Sciscio, L. and Abrahams, M. 2018. Dinosaur behaviour in an Early Jurassic palaeoecosystem–uppermost Elliot Formation, Ha Nohana, Lesotho. *Annales Societatis Geologorum Poloniae*, 88: 163–179. 10.14241/asgp.2018.010

Robinson, D.N., Beer, H.M., Nutsch, F.M., andTrumpelman, F. 1969.The geology and oil potential of the Stormberg Group. Unpublished report. Southern Oil Exploration Corporation, Johannesburg.

Rosales, I., Quesada, S. and Robles, S. 2004. Paleotemperature variations of Early Jurassic seawater recorded in geochemical trends of belemnites from the Basque–Cantabrian basin, northern Spain. *Palaeogeography, Palaeoclimatology, Palaeoecology*, 203(3-4): 253–275. DOI: 10.1016/S0031-0182(03)00686-2

Rubin, D.M. and Hunter, R.E. 1981. Bedform climbing in theory and nature. *Sedimentology*, 29: 121–138. DOI: 10.1111/j.1365-3091.1982.tb01714.x

Scherer, C.M. and Lavina, E.L. 2005. Sedimentary cycles and facies architecture of aeolian–fluvial strata of the Upper Jurassic Guará Formation, Southern Brazil. *Sedimentology*, 52(6): 1323–1341. DOI: 10.1111/j.1365-3091.2005.00746.x

Scherer, C.M. and Goldberg, K. 2010. Cyclic cross-bedding in the eolian dunes of the Sergi Formation (Upper Jurassic), Recôncavo Basin: Inferences about the wind regime. *Palaeogeography, Palaeoclimatology, Palaeoecology*, 296(1-2): 103–110. DOI: 10.1016/j.palaeo.2010.06.018

Schmitz, G. and Rooyani, F. 1987. Lesotho: Geology, geomorphology, soils. National University of Lesotho, 204 pp.

Sciscio, L., de Kock, M., Bordy, E.M. and Knoll, F. 2017. Magnetostratigraphy across the Triassic-Jurassic boundary in the main Karoo Basin. *Gondwana Research*, 51: 177-192. DOI: 10.1016/j.gr.2017.07.009

Scotese, C.R., Boucot, A.J. and McKerrow, W.S. 1999. Gondwanan palaeogeography and palaeoclimatology. *Journal of African Earth Sciences*, 28(1): 99-114. DOI: 10.1016/S0899-5362(98)00084-0

Selker, J.S. 1993. Expressions for the formation of load casts in soft sediment. *Journal of Sedimentary Research*, 63(6): 1149–1151. DOI: 10.1306/D4267CCB-2B26-11D7-8648000102C1865D

Simpson, E.L., Eriksson, K.A., Eriksson, P.A. and Bumby, A.J. 2002. Eolian dune degradation and generation of massive sandstone bodies in the Paleoproterozoic Makgabeng Formation, Waterberg Group, South Africa. *Journal of Sedimentary Research*, 72: 40–45. DOI: 10.1306/050701720040

Skinner, E.M.W., Clement, C.R., Gurney, D.B., Apter, D.B. and Hatton, C.J. 1992. The distribution and tectonic setting of South-African Kimberlites. *Russian Geology and Geophysics*, 33 (10): 26–31.

Stockley, G. M. 1947. The Geology of Basutoland. *Geological Magazine*, 77(6): 444–460. DOI: 10.1017/S0016756800071600

Sweeney, M.R. and Loope, D.B. 2001. Holocene dune-sourced alluvial fans in the Nebraska Sand Hills. *Geomorphology*, 38: 31–46. DOI: 10.1016/S0169-555X(00)00067-2

Suan, G., Mattioli, E., Pittet, B., Mailliot, S. and Lécuyer, C. 2008. Evidence for major environmental perturbation prior to and during the Toarcian (Early Jurassic) oceanic anoxic event from the Lusitanian Basin, Portugal. *Paleoceanography*, 23(1): PA1202. DOI: 10.1029/2007PA001459

Svendsen, J., Stollhofen, H., Krapf, C.B. and Stanistreet, I.G. 2003. Mass and hyperconcentrated flow deposits record dune damming and catastrophic breakthrough of ephemeral rivers, Skeleton Coast Erg, Namibia. *Sedimentary Geology*, 160: 7–31. DOI: 10.1016/S0037-0738(02)00334-2

Trewin, N.H. 1993. Mixed aeolian sand sheet and fluvial deposits in the Tumblagooda Sandstone, Western Australia. *Geological Society, London, Special Publications*, 73(1): 219–230. DOI: 10.1144/GSL.SP.1993.073.01.13

Vandenberghe, J. 2013. Grain size of fine-grained windblown sediment: A powerful proxy for process identification. *Earth-Science Reviews*, 121: 18–30. DOI: 10.1016/j.earscirev.2013.03.001

Vandenberghe, J., Sun, Y., Wang, X., Abels, H.A. and Liu, X. 2018. Grain-size characterization of reworked fine-grained aeolian deposits. *Earth-Science Reviews*, 177: 43–52. DOI: 10.1016/j.earscirev.2017.11.005

Van de Schootbrugge, B., Bailey, T.R., Rosenthal, Y., Katz, M.E., Wright, J.D., Miller, K.G., Feist-Burkhardt, S. and Falkowski, P.G. 2005. Early Jurassic climate change and the radiation of organic-walled phytoplankton in the Tethys Ocean. *Paleobiology*, 31(1): 73–97. DOI: 10.1666/0094-8373(2005)031<0073:EJCCAT>2.0.CO;2

Van Eeden, O. R. 1937. The geology of the country around Bethlehem and Kestell, with special reference to oil indications. *Memoirs of the Geological Survey of South Africa*. 33: 68pp.

van Dijk, D.E. and Eriksson, P.G. 2021. Bipedal leaping Jurassic vertebrates in Southern Africa: proposed new ichnotaxon and inferred palaeoenvironment. *Transactions of the Royal Society of South Africa*: 76(3), 235–245. DOI: 10.1080/0035919X.2021.1964104

Veevers, J.J. 2004. Gondwanaland from 650–500 Ma assembly through 320 Ma merger in Pangea to 185–100 Ma breakup: supercontinental tectonics via stratigraphy and radiometric dating. *Earth-Science Reviews*, 68(1-2): 1–132. DOI: 10.1016/j.earscirev.2004.05.002

Chapter 5.

Sedimentation tempo in an Ealy Jurassic erg system: refined chronostratigraphy and provenance for the Clarens Formation of southern Africa

Abstract

The Clarens Formation, representing the final depositional phase in the main Karoo Basin, is an aeolianite that formed as part of a vast desert system across southwestern Gondwana in the Early Jurassic. Its source areas are commonly attributed to the recycling of pre-existing sedimentary successions, an inference extrapolated from a few localized studies in the east of the basin. The Early Jurassic age of the formation is largely deduced from the biostratigraphy and geochronology of the underlying Elliot Formation, and absolute age dates of the overlying Drakensberg Group. The current study offers the first ever regional perspective of the source areas, basin-wide sediment supply mechanisms and a chronostratigraphic framework of the Clarens Formation. To these ends, petrographic analysis of 100 sandstone samples and U-Pb dating of 21 detrital zircon samples were utilized. A high zircon-tourmaline-rutile heavy mineral content, combined with evidence of zircons with distinct microtextural inner and outer growth events and the lack of a diverse heavy mineral suite, confirm that the detritus was largely derived from recycled sedimentary sources, whereas its uniform sandstone composition suggests that the sediment was homogenised over southern Africa. Given the dominance of a Pan-African detrital zircon population, the sediment was likely recycled from the Saldania and Damara Belts. The Early Jurassic zircons are interpreted to reflect volcanism in Patagonia and Antarctica, which were situated to the south and southwest of the study area. Furthermore, support for a close primary granitic source, likely to the west of the basin, is indicated by the presence of unstable minerals such as hornblende, garnet and titanite, as well as feldspar. Subordinate sediment volumes, characterised by polycrystalline quartz and a dominant Grenvillian zircon population, are attributed to fluvial processes that transported detritus from the east, possibly from the western Antarctic Haag Nunataks terrain. Overall, a broad chronostratigraphic framework that is consistent with existing age constraints can be established for the Clarens Formation based on Early Jurassic detrital zircon signals. These maximum depositional ages suggest that the lower zone is of late Sinemurian age, the middle zone is of early Pliensbachian age, whereas the upper zone is of late Pliensbachian age. This trend is particularly prevalent in the south of the basin, where these signals are incorporated into each zone, respectively, and towards the north and northeast, they appear in the subsequent younger zone, which may demonstrate that sediment was primarily supplied from the south and southwest towards the north and northeast.

5.1. Introduction

Generally, aeolian sediments are characterized by a high degree of monocrystalline quartz with a very uniform heavy mineral assemblage dominated by zircons that are extremely robust and can survive multiple cycles of erosion and weathering (Fedo *et al*., 2003; Muhs, 2004; Gehrels, 2012; Garzanti *et al*., 2013; Anderson *et al*., 2015; 2016). The use of detrital geochronology from detrital zircons may, therefore, be a useful tool in provenance studies related to aeolian deposits and may allude to sedimentary features such as sediment supply mechanisms. Along with existing age constraints, these can be valuable in determining spatiotemporal controls on erg development (Muhs, 2004; Bertolini *et al*., 2021). The Clarens Formation has long been associated with aeolian deposition that took place during the Ealy Jurassic (du Toit, 1905; Stockley, 1949; Beukes, 1969,1970; Johnson, 1976; Eriksson, 1981, 1986; Bordy and Head, 2018), and formed part of an extensive erg system that stretched throughout southwestern Gondwana. Remnants of this vast ancient desert system can be found across southern Africa in many Karoo-aged basins, most of which lack provenance studies (Bowden, 2013; Andersen *et al*., 2016, Viglietti *et al*., 2017; Zieger *et al*., 2020). Currently, the depositional age of the Clarens Formation has been interpreted to be Early Jurassic (Sinemurian to Pliensbachian) based on biostratigraphy of the underlying Elliot Formation (du Toit, 1905; Haughton, 1929; Knoll, 2005; McPhee *et al*., 2017; Bordy and Head, 2018; Bordy *et al*., 2020) in combination with chronostratigraphic constraints from a limited detrital zircon dataset and the geochronology of the overlying Drakensberg Basalts (Duncan *et al*., 1997; Moulin *et al*., 2011; Svensen *et al*., 2012; Moulin *et al*., 2017; Rademan, 2018; Abrahams, 2020; Bordy *et al*., 2020, 2021). A detailed regional chronostratigraphic framework has not yet been developed for the Clarens Formation. Furthermore, source areas for the Clarens Formation have been shown to reflect pre-Clarens Karoo units, which was reworked into the Clarens Basin as inferred from petrographic work by Beukes (1969, 1970), Eriksson (1981, 1986), and Eriksson *et al*. (1996). Given the poorly constrained provenance and the relatively poorly defined age of the Clarens Formation, this study utilises detrital zircon geochronology and petrographic techniques to refine: 1) the chronostratigraphic framework of the formation and 2) the regional erg dynamics and its palaeo-domains.

5.2. Geological background

The aeolian Clarens Formation, within the upper Stormberg Group of the Karoo Supergroup, crops out in several Karoo-aged basins within southern Africa, such as the main Karoo Basin (MKB) in South Africa and Lesotho and the Springbok Flats, Lebombo, Tshipise, Tuli and Lephalale-Ellisras basins in and around South Africa (Smith *et al*., 1993; Bordy and Had, 2018). Co-eval aeolianites are found in Namibia (Etjo Formation), Zimbabwe (Forest Sandstone) and Botswana (Ntane, Tsheung and Bodibeng Sandstone Formations; Thompson, 1975; Stagman, 1978; Visser, 1984; Smith *et al*., 1993; Holzfortser *et al*., 1999; Bordy and Head, 2018), highlighting the extensive geographic distribution of this erg system within southwestern Gondwana in the Early Jurassic. The conformable lower contact with the Elliot Formation is considered transitional and is marked by interbedded red beds and cream to pale coloured aeolian sandstones in the basal zone. The conformable upper contact with the Drakensberg Group is sharp due to the lithological contrast between the sedimentary and igneous rocks, nonetheless this complex interbedded relationship is also transitional and indicates that aeolian and volcanic processes coexisted in the Early Jurassic (Moulin, 2017; Bordy *et al*., 2020b, 2021, in press; Chapter 4).

The Clarens Formation in the MKB is dominated by massive to large-scale, cross-bedded, fine- to very fine-grained silty sandstone, with a cream, pink to pale green colour. Lenticular sandstones with ripple marks, ripple cross-lamination, desiccation cracks and horizontal lamination are mostly confined to the lower and upper parts of the formation (Beukes, 1969, 1970; Johnson, 1976; Eriksson, 1981, 1986; Bordy and Head, 2018; Van Dijk and Eriksson, 2021). Mudstones are comparatively rare, and generally appear as thin (< 30 cm) lenticular beds that are interbedded with sandstones. Throughout the basin, the thickness of the formation fluctuates from 10 to over 300 m, however, on average a thickness of 100 to 150 m is a fair representation of the unit's regional thickness (du Toit, 1905; 1918; Beukes, 1969; Johnson, 1976; Eriksson, 1981, 1986).

Sandstone petrography of the Clarens Formation shows that the unit is dominated by quartz-rich felspathic wackes, and minor arkosic arenites or subarkosic to quartz wackes (Beukes, 1970, Eriksson, 1986; Eriksson *et al*., 1994; Bordy and Head, 2018). The medium- to very fine-grained silty sand grains are typically poorly sorted, with the sand grains being better rounded than the silt grains. The heavy mineral suite consists of zircon, rutile, tourmaline, epidote, titanite, garnet, riebeckite and hornblende (Koen, 1955; Beukes, 1970; Eriksson *et al*., 1994). To date, a limited dataset of maximum depositional ages based on detrital zircons is available for the Clarens Formation, with work done by Rademan (2018), Abrahams (2020), Nxumalo (2020) and Bordy *et al*. (2020).

The Clarens Formation also hosts a diverse fossil assemblage that includes vertebrates (tetrapod bone fossils; fossil fish – Haughton, 1924; Crompton, 1958; Gow; 1981; Kitching and Raath, 1984; Stockley, 1947; Jubb, 1973; Forey and Gardiner, 1973; Bordy and Head, 2018), invertebrates (crustaceans, insects – Haughton, 1924; Tasch, 1984), various ichno-fossils of both vertebrates and invertebrates (Haughton, 1924; Ellenberger, 1970; Van Eeden and Keyser, 1971; Van Dijk, 1978; Eriksson, 1981; Olsen and Galton, 1984; Raath and Yates, 2005; Van Dijk and Eriksson, 2021; Abrahams *et al*., 2021), plant impressions, petrified wood and tree trunks (Haughton, 1924; Stockley, 1947; Meijs, 1960; Bordy and Catuneanu, 2002; Bamford, 2004; Bordy *et al*., 2021). It is therefore envisaged that the Clarens Formation hosted locally diverse paleo-ecosystems throughout the deposition of the unit, which continued well beyond the initiation of the large-scale continental flood basalts at the Pliensbachian–Toarcian boundary (Duncan et l., 1997; Moulin, 2011; Svensen *et al*., 2012; Muir *et al*., 2020; Bordy *et al*., 2021).

Palaeoflow measurement from the large-scale, cross-bedded sandstones indicate that a prominent west to east wind regime existed over southwestern Gondwana during the Early Jurassic (du Toit, 1905; Beukes, 1969, 1970; Eriksson, 1981, 1986, Bordy, 2008; Bordy *et al*., 2009; Bordy and Head, 2018). Overall, the dominance of both large-scale, cross-bedded and massive sandstones, especially in the middle part of the formation, point to the development of aeolian conditions with migrating dunes and possibly windblown dust. The lenticular sandstones and mudstones, confined to the lower and upper part of the formation, are suggestive of wet conditions within the erg system (Beukes, 1969, 1970; Bordy, 2008; Bordy and Head, 2018). These features, concentrated in three stratigraphic zones, prompted Beukes (1969, 1970) to explain them with wet-dry-wet climatic megacycles during the deposition of the formation. In contrast to Beukes' temporal climatic changes, Eriksson (1981, 1986) defined spatial domains in the Clarens Formation and suggested the

co-existence of a dry inner erg to the west of the basin and a wet desert setting in the south, southeast, and east of the basin.

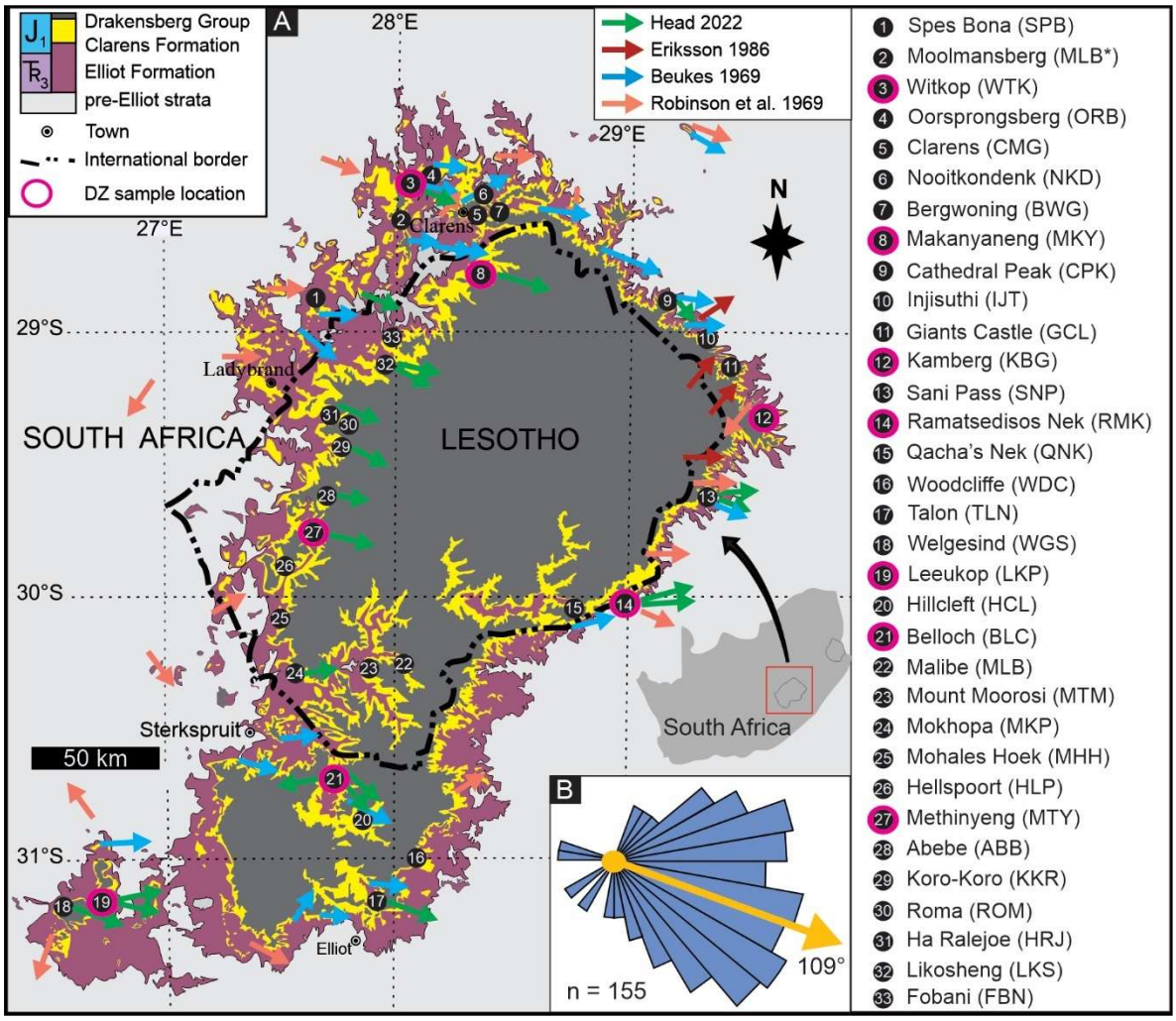

Figure 5.1: Geological context of the Clarens Formation rock samples within the Main Karoo Basin (MKB). **A**. Geological map with study and sample locations and the palaeo-flow directions marked for each study site in this study and data from Eriksson (1986), Beukes (1969) and Robinson *et al.* (1969). **B**. Rose diagram of the measured palaeo-flow directions in the Clarens Formation from this study; n – sample number.

5.3. Methods

To investigate the provenance and chronostratigraphy of the Clarens Formation (Figure 5.1), a total of 110 rock samples were collected for petrographic analysis, and 21 samples were collected for U-Pb dating using laser ablation inductively coupled plasma ionization mass spectrometry (LA ICP-MS). Petrographic analysis was carried out using a transmitted light microscope (Leica DM 750P) and employing the Gazzi-Dickinson point counting technique, where a total of 300 points were counted per sample for a representative estimate (Gazzi, 1966; Ingersoll *et al.*, 1984). Where large rock fragments are encountered (polycrystalline), crystals directly under the cross-hairs was taken to represent the clast (Ingersoll, 1984). The ternary diagram for classification is compiled using Q by

summing all quartz grains, L by allocating chert to the lithic fragments along, and F by grouping all feldspar grains (Garzanti, 2019). The point-counting results are illustrated following the sandstone classification scheme of Garzanti *et al*. (2018a) and Garzanti (2019). Sample point count breakdowns are listed in Appendix 9.

Detrital zircon samples were collected from each of the stratigraphic zones as defined by Beukes (1969, 1970) to ensure a complete spatiotemporal representation of the zircon diversity from the Clarens Formation (Figure 5.1A). The samples were prepared at the Central Analytical Facilities (CAF) at Stellenbosch University following a similar technique as outlined by Tucker *et al*. (2013). Magnetic and heavy liquid mineral separations were preceded by crushing, milling, and panning of the samples. Samples were also imaged on the Scanning Electron Microscope (SEM) to detect zircon zoning. LA-ICP-MS U-Pb analysis was completed at the EATH LAB at the University of the Witwatersrand (Johannesburg, South Africa). A detailed description of analysis parameters and metadata tables can be seen in Appendix 10 and 11. Data reduction was conducted in Iolite v 3.5 (Paton *et al*., 2011) utilising VizualAge (Petrus and Kamberg, 2012), while absolute ages and uncertainties (2σ) were calculated using IsoplotR of Vermeesch (2018) where a 95-105% concordance threshold was applied to the analysis results. In addition, concordia (Wetherill plots – Appendix 12), cumulative percentage plots and kernel density estimates (KDE) were also plotted in IsoplotR of Vermeesch (2018). To evaluate trends in zircon morphology, the long axis, short axis and roundness of zircons were measured using Image-J software to calculate the elongation factor as described by Gartner *et al*. (2013). During zircon ablation spot selection, where a zircon showed distinct microtextural growth zones, these were targeted to constrain the growth events. Clarens Formation zircon datasets and supplementary materials are available on the following link: https://figshare.com/s/6788ee86634ce85c9009

5.4. Results

5.4.1. Petrography

Petrographic analysis indicates that the Clarens Formation sandstones are comprised of quartzose sandstones with a mean composition of 74% quartz, 22% feldspar and 4% rock fragments (i.e., mean $Q_{74}F_{22}L_4$ in the Garzanti 2019 classification). Five out of the 100 samples (Figure 5.3) are either pure quartzose (CMG-02; KKR-02; MTM-01) or quartz-rich feldspatho-quartzose (CPK-04; BWG-04) sandstones. The detailed sandstone classification of each sample is shown in Appendix 9. Monocrystalline quartz dominates (96%) over polycrystalline quartz, where monocrystalline quartz shows both non-undulatory (60%) and undulatory extinction under cross-polars. Polycrystalline quartz grains showed mostly less than four crystals with non-sutured boundaries. The feldspar component is mostly plagioclase (95%) with minor K-feldspar. Both twinned and untwinned feldspar were identified (Figure 5.4). Lithic fragments are mostly chert and shales and are underrepresented in most samples. Sandstone classifications (Figure 5.3) show that a slightly higher lithic content is observed in the southern, northern, and eastern outcrop areas, as compared to that of the central outcrop area.

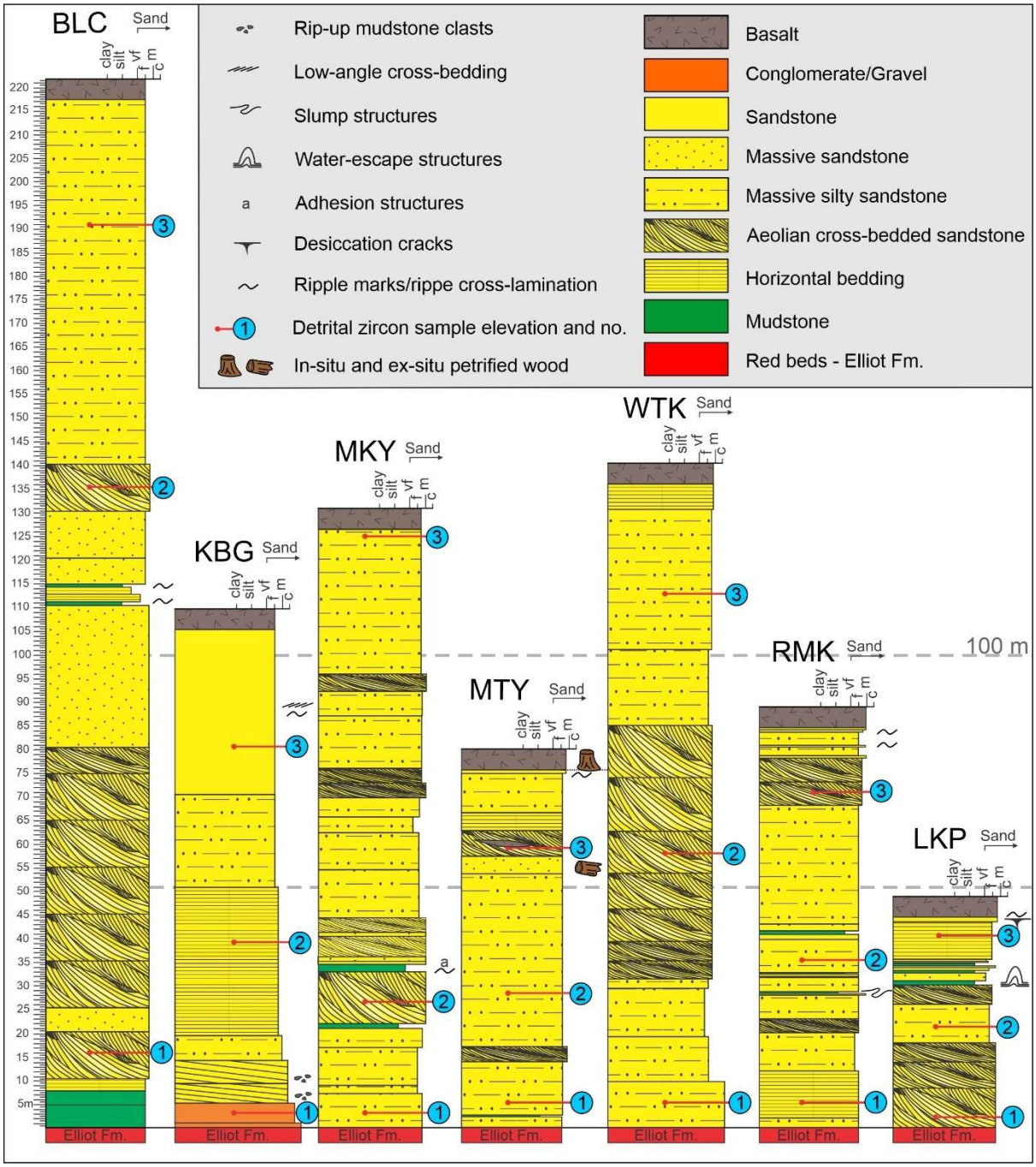

Figure 5.2: Sedimentary logs and stratigraphic locations of detrital zircon samples in the Clarens Formation. Note that samples labelled '1', '2' and '3' are from the three different zones of the Clarens Formation. See Figure 5.1 for log abbreviations and locations.

Overall, the sandstones are moderately to well sorted with some samples showing poor sorting. Compared to samples from the massive sandstone deposits, a slightly better sorting characterizes the large-scale, cross-bedded sandstones. The sandstones are composed of medium- to very fine-grained sand to silty sand with low sphericity. Most grains are sub-angular to sub-sounded, and the larger grains are generally better rounded (Figure 5.4). The grains are well packed with long and point contacts. In most samples, the matrix (here defined as grains < 30 µm in diameter – Gazzi, 1966; Garzanti, 2016) represents between 5–10% of the rock (i.e. framework grains represent 90 to 95%). Regional trends in grain shape and size in the Clarens Formation are detailed in Chapter 3, however, it should be noted that except for a slight west to east fining (Beukes, 1969), no spatiotemporal grain morphology and size trends were detected in the current study.

Heavy minerals identified in the samples are zircon, tourmaline, rutile, green to brown hornblende, garnet, epidote, titanite and opaque minerals (Figure 5.4). The most abundant are the combination of zircon, tourmaline and rutile (ZTR) which are the most stable minerals, capable of surviving several cycles of sedimentary reworking. No spatiotemporal distribution trends were identified within the heavy mineral component throughout the outcrop area. Samples from the lowermost Clarens Formation at Kamberg were collected from ephemeral channel deposits as discussed in Chapter 4. These samples (KMB-01, KMB-02) display a larger grain size (grit to very coarse-grained sand) that contain abundant polycrystalline quartz having sutured crystals (Figure 5.5A, B, D). Lithic fragments of volcanic origin (Lv) were identified in samples from the debris flow deposits in the uppermost Clarens Formation at Talon (Figure 5.5C; see Chapter 4).

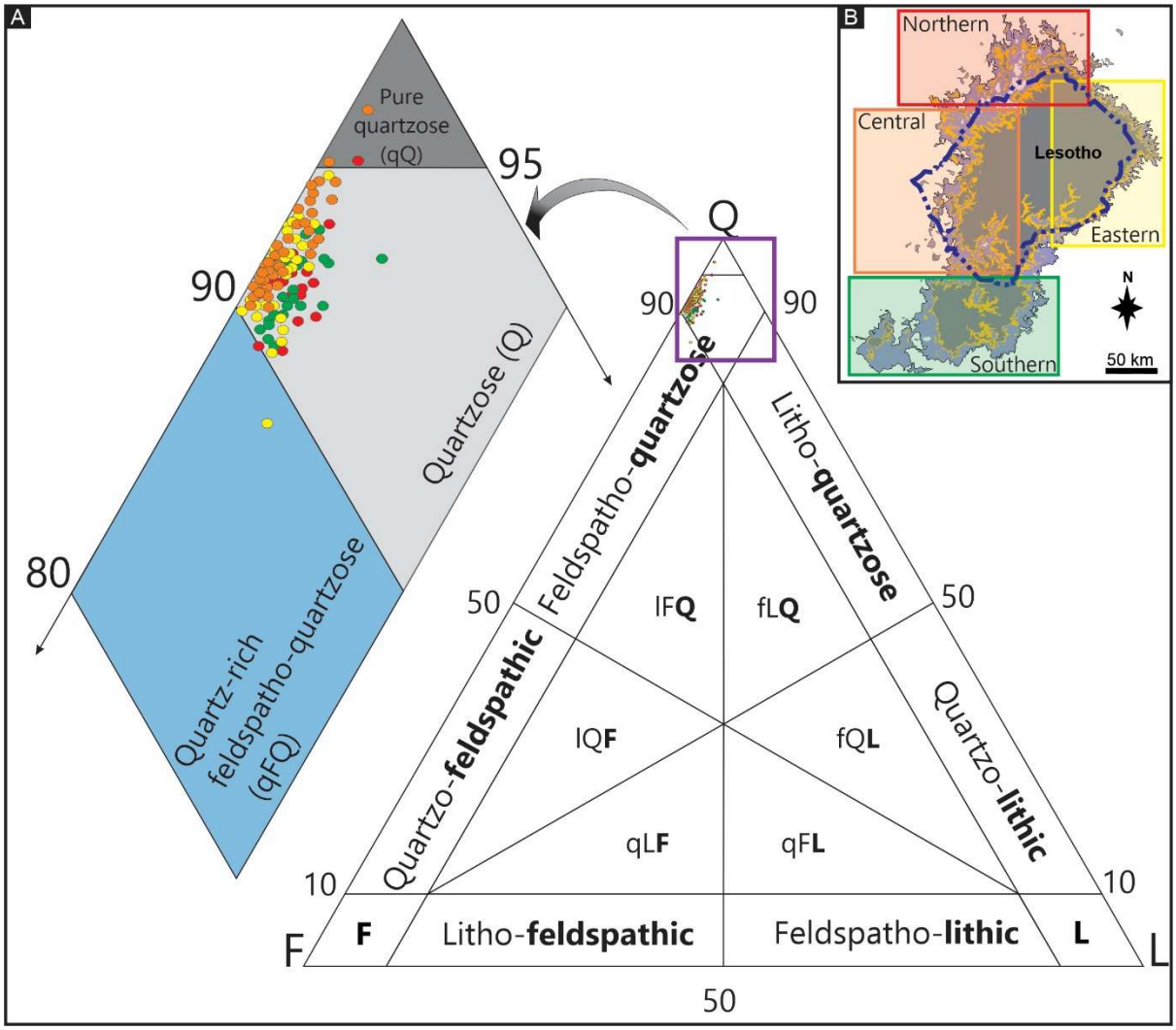

Figure 5.3: Sandstone composition of the 100 Clarens Formation samples based on the Garzanti (2019) classification scheme (**A**). For regional sample locations, see colour coded map inset (**B**). Abbreviations: Q – Total quartz, F – K-feldspar and plagioclase, L –Total Lithics including chert. Note that the samples taken from the northern (red), eastern (yellow) and southern (green) sampling areas contain relatively more lithics than the central (orange) samples.

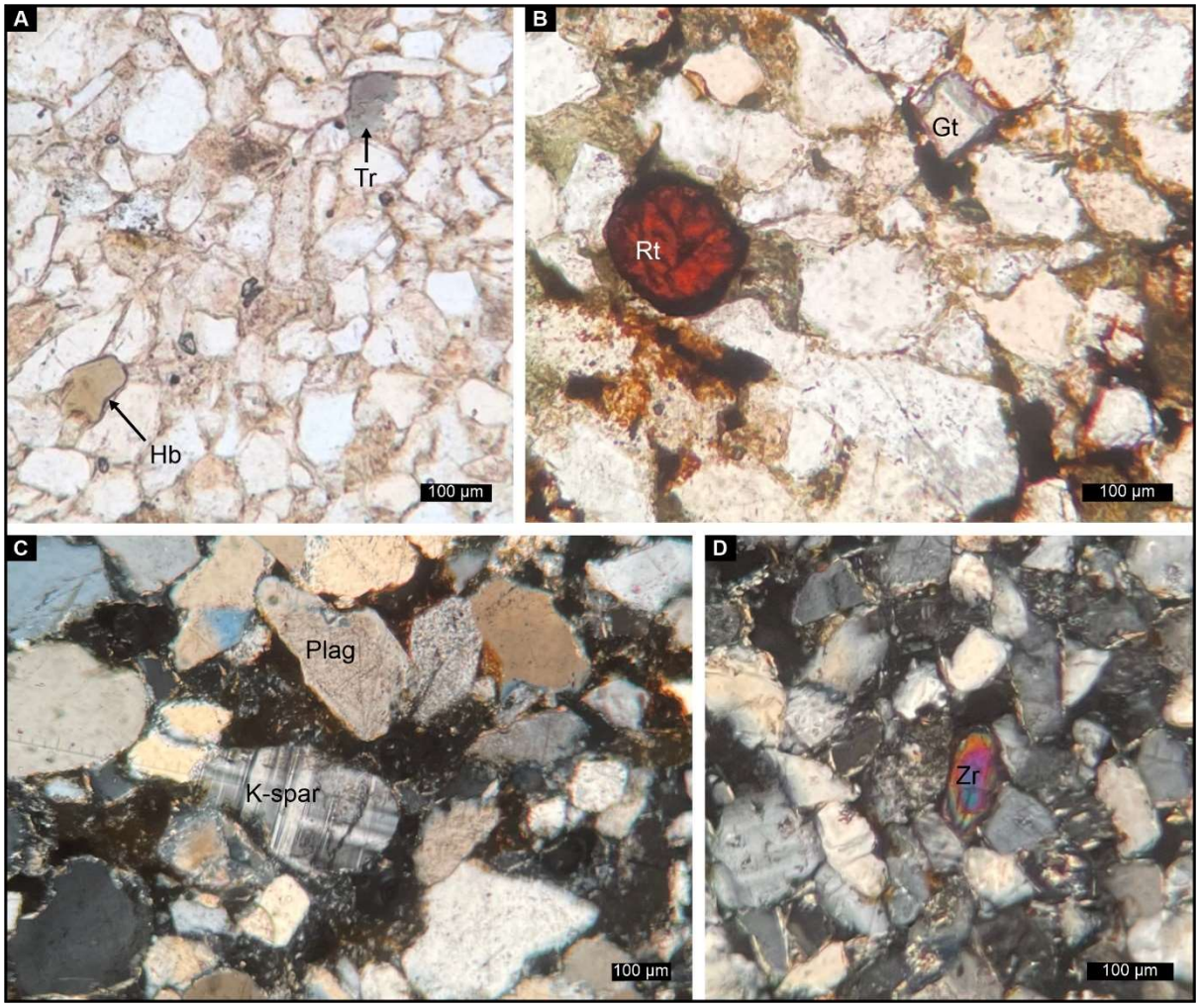

Figure 5.4: Photomicrographs of common and accessory minerals in the Clarens Formation. **A**. Yellow-brown hornblende (Hb) and tourmaline (Tr) in a quartz-dominated sandstone – PPL. **B**. Rutile (Rt) and garnet (Gt) in PPL. **C**. K-feldspar (K-Spar) and plagioclase (Plag) amongst quartz in XPL. **D**. Zircon (Zr) amongst quartz in XPL. Note that the sandstones are subrounded to subangular and are moderately to well sorted.

5.4.2 Palaeocurrents

During this study, the palaeoflow directions measured from 155 large-scale, cross-bedded sandstones, mostly from the middle zone of the formation, indicate a strong west- to east wind regime with a mean of 109°, a standard deviation of 35.75° and a consistency ratio of 0.81. Despite this strong west to east trend, localised variations in paleocurrents are observed to such an extreme that, for example at Balloch, foresets dip towards the west (Figure 5.1).

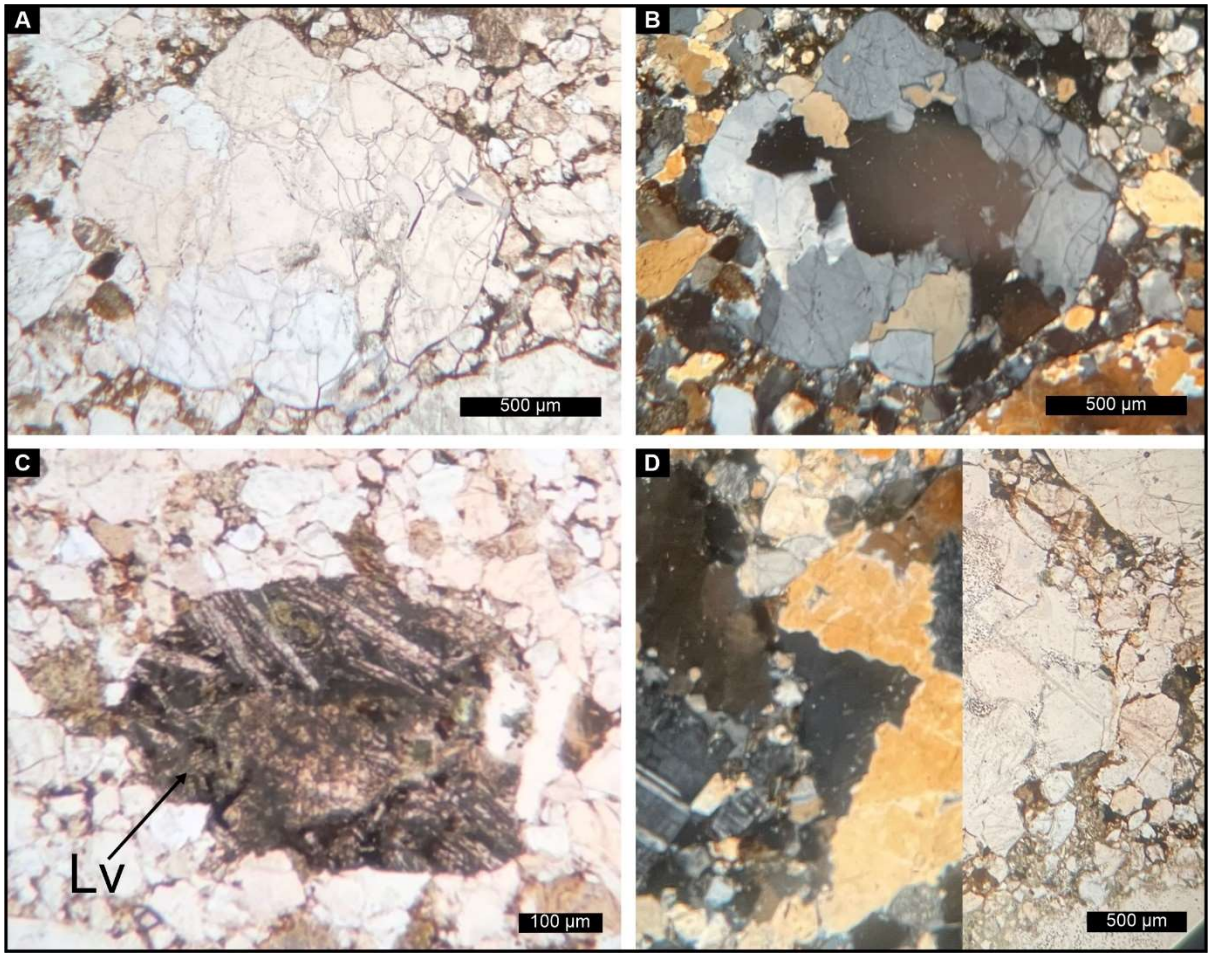

Figure 5.5: Photomicrographs of rare lithic fragments in the Clarens Formation. **A** and **B**. Polycrystalline quartz in PPL (A) and XPL (B). **C**. Rare volcanic lithic fragment (Lv) in the uppermost part of the Clarens Formation at Talon – PPL. **D**. Polycrystalline quartz with crystals showing sutured contacts in the lowermost Clarens Formation at Kamberg – XPL left, PPL right. See Figure 5.1 for locations.

5.4.3 Detrital zircon geochronology

5.4.3.1 Provenance

A total of 21 samples were analysed, where 2341 ablated zircons resulted in 1833 concordant dates (Figures 5.9; 5.10). The zircon data shows a spread of dates from roughly 3300 to 183 Ma. The dates are dominated by the Cambrian to early Neoproterozoic component (Pan-African – 40%), followed by Tonian-Stenian (Grenvillian – 12%), Permian (12%) and Ordovician (7%) components, while mid Palaeoproterozoic and Archean signatures are small to rare (Figures 5.9 and 5.10).

The distribution of these signatures appears to be rather homogeneous throughout the sampled area, with the exception of the samples from the ephemeral channel deposits at Kamberg (KMB-01), in which a Tonian-Stenian signature dominates, and the Permian signal is significantly reduced (Figures 5.9 and 5.10). In sample BLC-01, the largest signal is represented by the Pan-African

component, which is also the highest Pan-African component from all samples, while its Tonian-Stenian signal is significantly smaller compared to other samples (Figure 5.10). Elongation and roundness measurements for the zircons did not reveal any trends with regards to date correlations, however, zircons with Early Jurassic dates show euhedral to slightly rounded shapes and are all igneous in nature (Figure 5.6). Zircon types were identified as mostly igneous having oscillatory and magmatic sector zoning as identified from zircon microtexture analysis (Corfu *et al*., 2003), whereas some have metamorphic overgrowths. A total of 91 distinct inner versus outer microtextural growth zones, identified on the various sample CL images, were ablated, with 55 growth zone pairs (distinct inner and outer microtextures) giving results that are within a 95 to 105 % concordance threshold (Figure 5.6 F-I). Overall, these zircons with distinct inner and outer growth zones suggest mostly the development of Permian to Pan-African growth events. However, five of these distinct microtextural zones show results that reflect a Tonian-Stenian (Grenvillian) inner growth event while the outer growth texture reflects a Pan-African growth event (Figure 5.6 F-I). In terms of provenance signals, the Kamberg grouped sample shows the most deviation as compared to the combined Clarens Formation samples (Figure 5.11).

5.4.3.2 Maximum depositional age determinations

Maximum depositional ages (MDA; Table 5.1, Figures 5.7, 5.9, 5.10 and 5.11) were calculated using metrics discussed by Dickinson and Gehrels (2009) and Coutts *et al*. (2019). These include: 1) youngest single grain – YSG, 2) a cluster of 3 or more youngest grains that overlaps at 2σ – YC2σ(3+) and 3) an additional method where a youngest cluster of 2 or more zircons overlap at 2σ – YC2σ(2+) (Bordy *et al*., 2020). These metrics were chosen because youngest clustered metrics are conservative and produce a result that is less susceptible to Pb loss, while YSG has been shown to be among the most accurate methods for age calculations (Coutts *et al*., 2019). Despite YSG metric's predisposition to produce data that may not reflect the true depositional age, for this study, single grains appear to produce results that fall within the existing chronostratigraphic and biostratigraphic constraints (Duncan *et al*., 1997; Knoll, 2005; Moulin *et al*., 2011; Svensen *et al*., 2012; Moulin *et al*., 2017; Rademan, 2018; Bordy *et al*., 2020). Furthermore, a similar approach as Bordy *et al*. (2020) in selecting the appropriate MDA metric was followed, where a preferred MDA may reflect any of the metrics that can be justified as most reliable in terms of the broader geological evidence. The Early Jurassic zircon results only represent a small fraction of the population and its appearance throughout the various samples is considered here as strong evidence that these signals are indeed valid.

Overall, 14 of the 21 samples produced dates that are in-line with current age estimates, the results of which can be found in Table 5.1. From the total 14 MDA's, 7 represent a YSG metric and 7 are from the YC2σ(2+) metric. The remaining 7 samples have calculated MDAs where none of the metrics produced a result within the age estimate for the Clarens Formation, as they are significantly older than the true depositional age (TDA). This may be attributed to a very low percentage of near-depositional age zircons, or a lack thereof, incorporated into the sediments (Andersen *et al*., 2016; Bordy *et al*., 2020). Within the concordant results, only two dates were excluded as it was not consistent with the existing age constraints of the Clarens Formation.

The results of samples from zone 1 (lower Clarens Formation) show that the consistent MDAs are of late Sinemurian age (RMK-01: *192.9 ± 1.3*; BLC-01: *195.6 ± 0.91* – Table 5.1; Figure 5.7). Samples used for inferences of the depositional age for zone 1 were entirely from the south and southeast of the basin, whereas samples from zone 1 in the north, central and eastern outcrop areas yielded no chronostratigraphically consistent MDAs (Table 5.1; Figure 5.7). Samples from Zone 2 (Middle Clarens Formation) have MDAs of early Pliensbachian age (RMK-02: *188.1 ±3.6*; LKP-02: *188.2 ± 0.9, MYY-02: 189.5 ± 3.8* – Table 5.1; Figure 5.7) and samples with this signal are located towards the southeast and southwest of the basin (Figures 5.1 and 5.8), whereas the northern, central and eastern parts do not show this signal. One of the zone 2 samples (MKY-02 – Table 5.1; Figure 5.7) have a late Sinemurian MDA. Zone 3 sample results (upper Clarens Formation) indicate mostly MDAs of late Pliensbachian age (MKY-03: *183.5 ± 5.6*; BLC-03: *183.45 ± 2.15*; RMK-03: *181.3 ± 3.7* – Figure 5.7) with three samples (MTY-03; WTK-03; KBG-03) having an MDA of early Pliensbachian age. Samples from zone 3 with this signal are situated in the north, south and southeast of the basin (Figure 5.8). The combination of the sample results points to three significant ages for the Clarens Formation, the late Sinemurian, the early Pliensbachian, and the late Pliensbachian. These zircon signals appear to have been incorporated into the various zones of Clarens Formation (Figures 5.7 and 5.8).

Table 5.1: Various metrics for the maximum depositional ages (MDA) of the Clarens Formation. For location and stratigraphic position, see Figures 5.1 and 5.2. Bold dates are the preferred MDAs for a given sample. Green indicates zone 1 samples, yellow indicates zone 2 samples and orange indicates zone 3 samples. See text for details.

Sample	Preferred MDA		YSG		YC2σ(2+)		YC2σ(3+)	
	Date	2σ	Date	2σ	Date	2σ	Date	2σ
BLC-GC-03	183.45	2.15	183.1	6.8	**183.45**	**2.15**	250	2.3
BLC-GC-02	183.99	1.84	183.4	5.1	**183.99**	**1.84**	245.66	1.74
BLC-GC-01	195.6	0.91	191.4	5.4	**195.6**	**0.91**	195.63	0.95
KBG-GC-03	187.6	2.6	**187.6**	**2.6**	204.5	1.0	257.6	0.8
KBG-GC-02	215.3	3.2	**215.3**	**3.2**	247.3	1.2	254.5	0.9
KBG-GC-01	200.1	2.4	**200.1**	**2.4**	524.0	1.7	524.0	1.7
LKP-GC-03	224.5	1.6	202.1	4.3	**224.5**	**1.6**	241.3	1.3
LKP-GC-02	188.2	0.9	185.5	4.7	**188.2**	**0.9**	188.2	0.9
LKP-GC-01	183.1	1.2	180.8	3.5	**183.1**	**1.2**	183.1	1.2
MKY-GC-03	183.5	5.6	**183.5**	**5.6**	243.8	1.3	243.8	1.3
MKY-GC-02	191.7	4.3	**191.7**	**4.3**	242.1	1.1	242.1	1.1
MKY-GC-01	241.3	1.3	208.7	3.4	**241.3**	**1.3**	241.3	1.3
MTY-GC-03	187	3.3	**187**	**3.3**	248.4	1.2	248.4	1.2
MTY-GC-02	189.5	3.8	**189.5**	**3.8**	191.1	1.0	191.1	1.0
MTY-GC-01	247.4	1.5	209.6	4.1	**247.4**	**1.5**	273.3	1.0
RMK_GC-03	181.3	3.7	**181.3**	**3.7**	201.3	1.5	242.3	1.4
RMK_GC-02	188.1	3.6	**188.1**	**3.6**	257.1	1.8	267.6	1.7
RMK_GC-01	192.9	1.3	191.1	3.6	**192.9**	**1.3**	264.4	0.9
WTK-GC-03	188.9	0.6	187.1	1.9	**188.9**	**0.6**	188.9	0.6
WTK-GC-02	254.3	1.1	238.8	2.7	**254.3**	**1.1**	267.7	1.8
WTK-GC-01	246.8	0.7	228.7	2.7	**246.8**	**0.7**	246.8	0.7

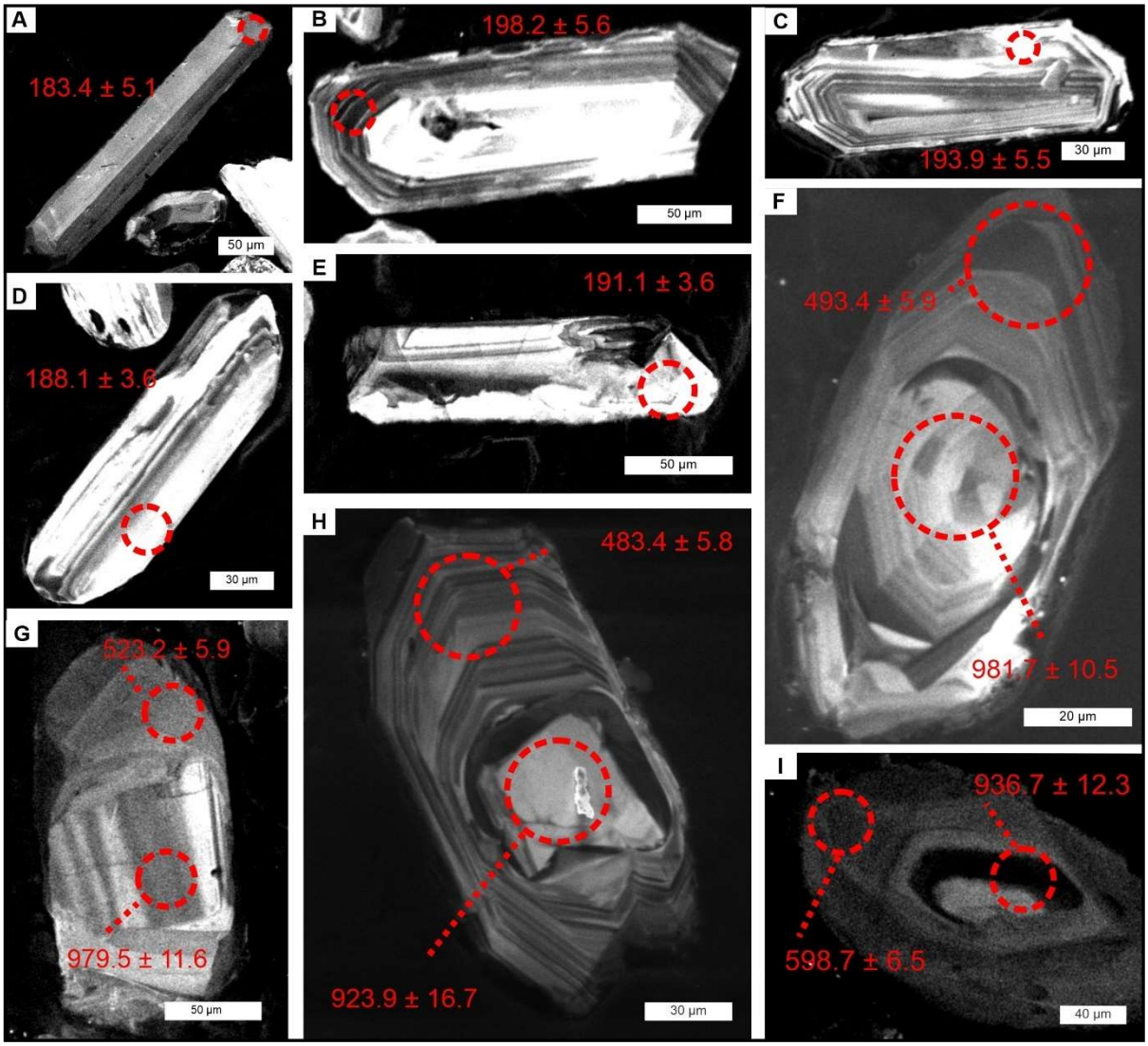

Figure 5.6: Zircons with young dates and concordant core rim pairs. **A – E**. Igneous zircons with euhedral to slightly rounded shape. **F – I**. Distinct microtextural growth zones on zircons that are consistent with a Tonian-Stenian inner texture and a Pan-African outer texture. Red circles represent the ablation area (to scale), and the red numbers are dates in Ma with 2σ uncertainty.

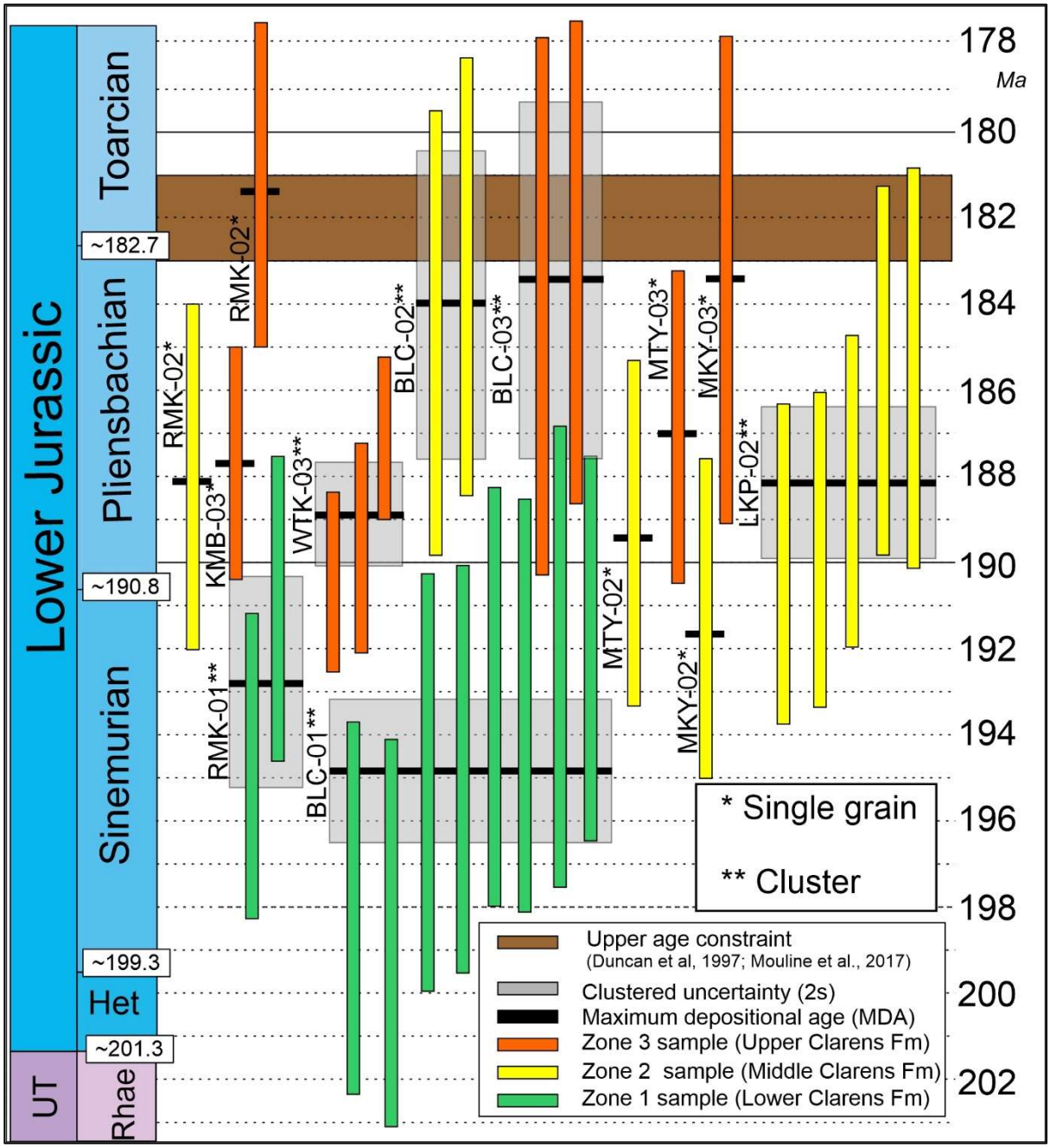

Figure 5.7: Distribution of the preferred maximum depositional ages from each zoned zircon sample that is consistent with existing chronostratigraphic constraints of the Clarens Formation. Bar heights (yellow, green, orange, and grey) depict 2σ uncertainty.

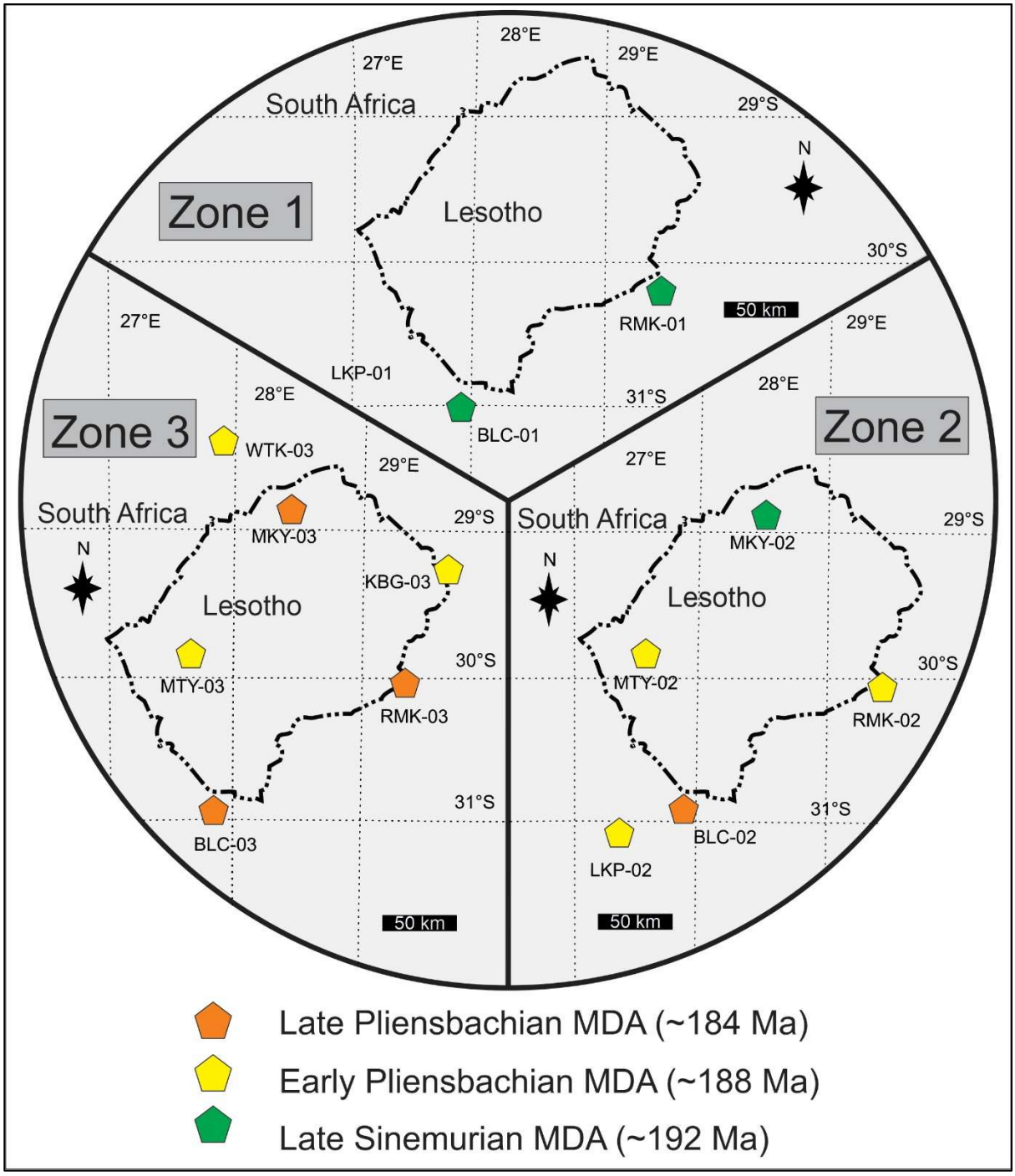

Figure 5.8: Zonal distribution of the maximum depositional ages (MDA) throughout the outcrop area of the Clarens Formation. See Table 5.1 for MDA results.

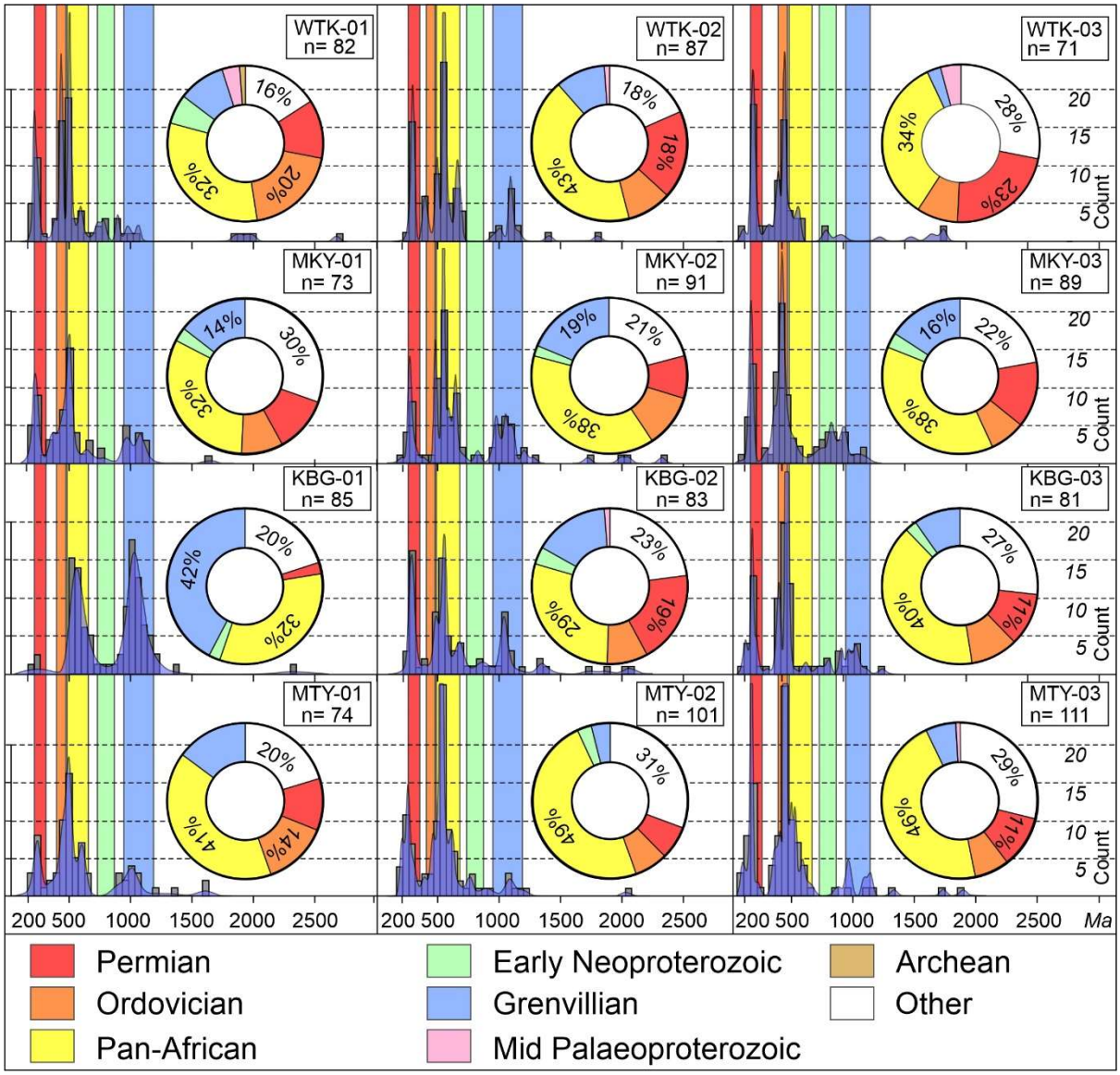

Figure 5.9: Kernel density estimates (KDE) of 12 samples from the northern outcrop area combined with donut plots depicting the percentage of each sample that can be attributed to the large-scale tectonic events listed in the legend. Note that the white box in the upper right corner shows the name of each sample along with the total number of concordant results included in the KDE plot.

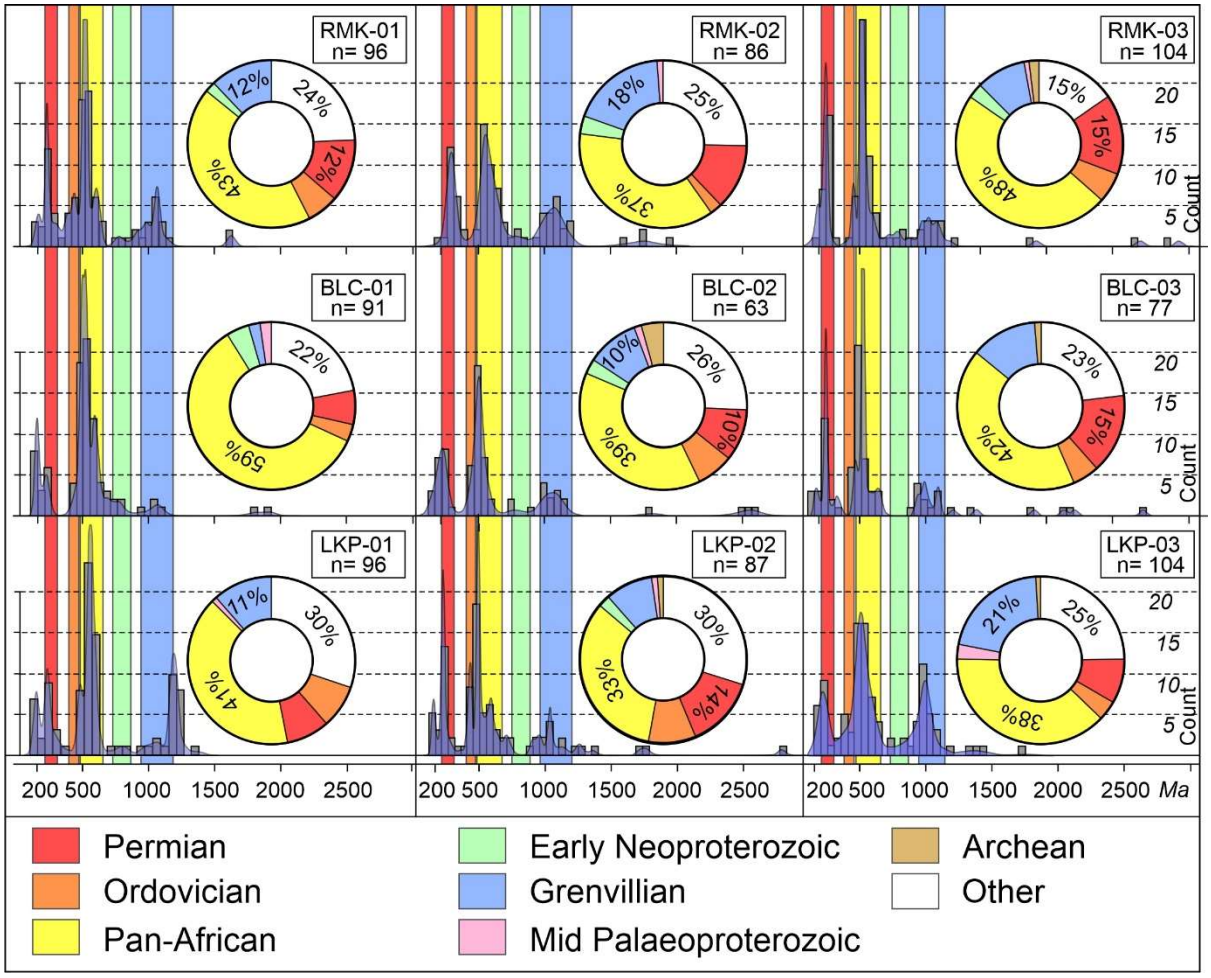

Figure 5.10: Kernel density estimates (KDE) of 9 samples from the southern outcrop area combined with donut plots depicting the percentage of each sample that can be attributed to the large-scale tectonic events listed in the legend. Note that the white box in the upper right corner shows the name of each sample along with the total number of concordant results included in the KDE plot.

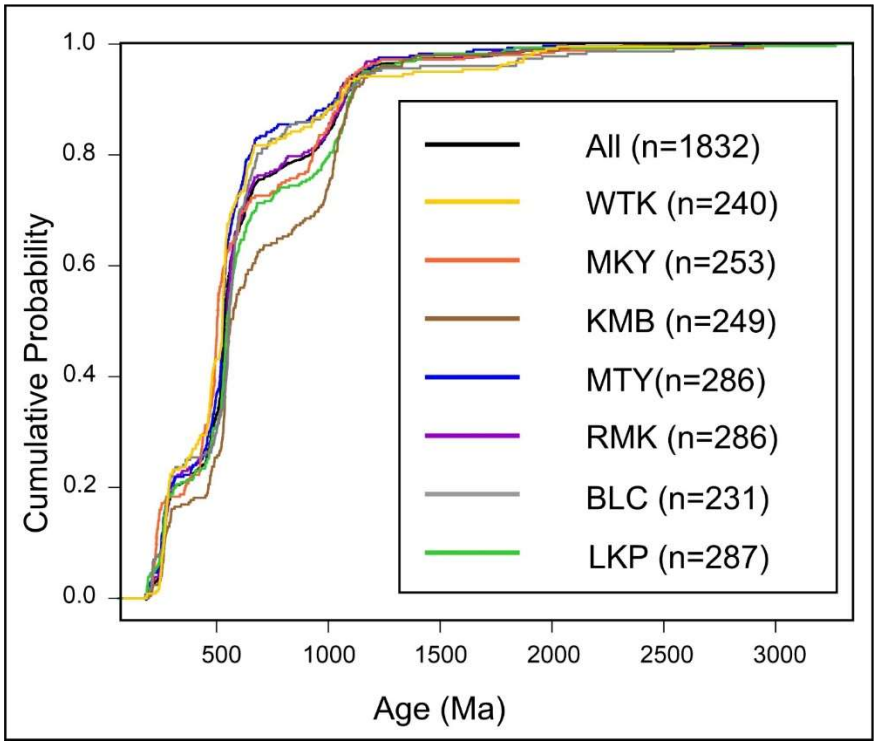

Figure 5.11: Cumulative probability plots for all samples combined and grouped per sample location.

5. Discussion

5.5.1 Petrography

The interpretation of detrital modes in provenance studies should be approached cautiously as the effect of diagenetic dissolution in favour of stable to ultra-stable heavy minerals may bias and distort the narrative (Garzanti *et al*., 2018b). Diagenetic dissolution can cause a very uniform heavy mineral suite by diagenetic modification of detritus because burial promotes the selective survival of ultra-stable minerals such as zircon, tourmaline, and rutile (ZTR). Sediments sourced from mostly recycled sedimentary sources will, therefore, result in a lack of diversity in heavy mineral suites and this bias will be retained for detritus reworked into a new sedimentary basin (Johnson *et al*., 1993; Garzanti *et al*., 2013, 2018b; Garzanti, 2017). The dominance of ultra-stable ZTR heavy minerals in the Clarens Formation, along with the uniform heavy mineral suite, indicates a strong recycled component incorporated into the sediments, while the uniform nature of the sandstone compositions may point towards sediment homogenization (Weltje and von Eynatten, 2004; Morton and Hallsworth, 2007; Garzanti, 2016; Garzanti *et al*., 2006; 2014; 2018b; Bertolini *et al*., 2020). The presence of unstable minerals such as epidote, hornblende, titanite and garnet may reflect incorporation of sediment supplied from primary sources into the basin. The presence of these unstable minerals, specifically amphiboles (hornblende), may also be indicative of shallow burial depths for the Clarens Formation, as amphibole is considered to be unstable at relatively shallow burial depths (Morton and Hallsworth, 2007; Garzanti *et al*., 2018b). It should be noted that the heavy mineral suite represents a small proportion of the detritus in the Clarens Formation and was also reported as such by Eriksson *et al*. (1994).

The abundance of non-undulatory monocrystalline quartz is shown by Blatt and Christie (1963) to reflect a recycled assemblage, whereas the presence of polycrystalline quartz may point towards primary sources (Basu *et al*., 1975; Basu, 1985). Results as reported by Basu *et al*. (1975) were based on medium grained sandstones, while the sandstones in the Clarens Formation mostly represent fine to very fine silty sand and thus the dominance of monocrystalline quartz is not a reliable indicator of the source terrain. However, monocrystalline quartz has also been associated with aeolian deposits because of its recycled nature (Muhs, 2004; Garzanti *et al*., 2013). Given the number of crystals in the polycrystalline grains are mostly less than four, it is suggested that this primary source was likely of plutonic igneous or high-grade metamorphic nature (Basu *et al*., 1975; Basu, 1985). The inclusion of epidote and amphibole along with garnet within the mineral assemblage could strengthen the argument for a metamorphic basement source, as these minerals are associated with regional metamorphic terrains (Garzanti *et al*., 2007; Schneider *et al*., 2016).

The medium- to very fine-grained sandstones are typical of aeolian transported sand, where silty and sandy silt represent dust fall processes as described in Chapter 3. The rounding trend is related to abrasion during aeolian transport, which results in breakage and chipping of large grains into smaller grains that tend to be more angular. Typically, quartz dominates desert sediments because of its mechanical and chemical stability and the availability of recycled quartz sources (Muhs, 2004; Garzanti, 2019). This results in a pure quartzose (qQ) sandstones being very common in areas dominated by ancient aeolian processes. However, the slightly higher feldspar content in addition to the dominance of quartzose (Q) samples in the Clarens Formation may reflect an exposed granitic basement in close proximity, such as the case for dunes in western Egypt and the Sinai Desert (Grarzanti, 2019). Bordy *et al*. (2004) reported the same trend in feldspar content for the underlying upper Elliot Formation, attributing this feldspar increase to crustal scale faults that exposed basement rocks along the west of the Elliot basin. This proximal basement source may have persisted into the Lower Jurassic Clarens Formation. Alternatively, increased feldspar has also been linked to changes in aridity, as is the case for the aridification trend in the Stormberg Group (Bordy *et al*., 2020, 2021). However, this climatic feature is shown to be of lesser significance when compared to basement sources of feldspar (Bordy *et al*., 2004).

The relatively higher abundance of lithic fragments in the southern, northern and eastern outcrop areas indicate that the sources of these rock fragments were located proximal to these margins of the basin and fed sediment via fluvial and alluvial processes. The lack of lithics in the central outcrop area suggests that, here, sediments were mostly sourced from the west as part of the dominant, compositionally more mature aeolian detritus that represent distal sources. Furthermore, localised occurrences of polycrystalline quartz with sutured contacts and more than four crystals per grain may be representative of a low rank metamorphic source (Basu *et al*., 1975; Basu, 1985). The occurrence of this sample in fluvial deposits with palaeocurrent flow towards the west and northwest (Eriksson, 1979, 1981, 1986) supports the argument for a distinct source terrain in the east, most likely of metamorphic affinity. In addition, the occurrence of rare volcanic lithic fragments in the uppermost Clarens Formation at Talon (Figure 5.5c) may indicate the incorporation of primary volcanic material, further supporting the idea of an earlier onset of basaltic volcanism in the southern part of the Clarens basin relative to the north (see below and Moulin *et al*., 2017; Bordy *et al*., 2021).

5.5.2 Detrital zircon provenance

The main contribution of detrital zircons reflects a Pan-African signal that can be linked to the Damara and Saldania Belts during the formation of Gondwana (Rino, *et al*., 2008; Foster *et al*., 2015; Frimmel *et al*., 2013). Similar prominent Pan-African signals have been identified in other successions of Karoo-age along southwestern Gondwana (Pinto *et al*., 2015; Linol *et al*., 2016; Viglietti *et al*., 2018; Zieger *et al*., 2020). The Grenvillian signal is the second most abundant, and sedimentary source terranes with this signal can be attributed to the genesis of the Namaqua-Natal Mobile Belt (Bial *et al*., 2015) and the western Sierras Pampeanas that formed part of the Grenvillian orogeny of western Gondwana (Casquet *et al*., 2008; Rino *et al*., 2008; Rapela *et al*., 2010).

A Permian signal also represents a significant population proportion that was observed in the Clarens Formation. Euhedral zircons described by Viglietti *et al*. (2018) from the Permo-Triassic in the MKB have been interpreted as Permian primary ashfall zircons, whereas zircons from the Clarens Formation with this Permian signal shows moderate rounding. This feature may indicate that incorporation of Permian signals in the population can be ascribed to recycling from older Karoo sedimentary rocks, particularly the Permo-Triassic Beaufort Group (Viglietti *et al*., 2018). This feature has also been identified in zircons of the Lower Jurassic Etjo Formation in Namibia (Zieger *et al*., 2020). The Ordovician signal present in the Clarens Formation population is thought to be linked to the Daseado Massif (Pankhurst *et al*., 2006; Bowden, 2013) or the Famatinian Belt of the eastern Sierras (Pankhurst *et al*., 2006; Rapela *et al*., 2010; Viglietti *et al*., 2018), whereas rare mid-Palaeoproterozoic and Archean signals may reflect a source terrain of either the Orange River Group or the Richtersveld Magmatic arc within the Namaqua Sector (Minaar, 2011; Hofmann *et al*., 2014; Macey *et al*., 2017; Zieger *et al*., 2020) or the Transvaal Supergroup and Kheis Subprovince (Van Niekerk, 2006; Viglietti *et al*., 2018; Zieger *et al*., 2020). The presence of zircons with distinct inner and outer growth zones associated with a Grenvillian and Pan-African growth event respectively, could further suggest that these zircons may have been repeatedly reworked.

Given the dates that are consistent with the known age constraints of the Clarens Formation, the Early Jurassic signals identified in the zircon samples may represent a reworked primary source, albeit a faint one. Furthermore, the appearance of these signals in the basal Clarens Formation in the south and the progressive migration and incorporation into the middle and upper parts of the succession northward, is strong evidence that the source was situated in the south to southwest, and that the basin was filled from the south to southwest. It is not clear what the source was, however, zircons from ash beds in the Suurberg Group, which is of similar age, has been shown to reflect volcanism that was active in Patagonia and the Antarctic Peninsula (Muir *et al.*, 2020). This volcanism was associated with the Chon Aike LIP that was situated in the southwest of Gondwana (Feraud *et al*., 1999; Pankhurst *et al*., 2000; Muir *et al*., 2020- their Figure 5.8; Pol *et al*., 2020) where pyroclastic ash plumes originated and were subsequently windswept towards the various Early Jurassic basins. This source is, therefore, consistent, both in position and age, to be the contributor of the Early Jurassic zircon signals incorporated into the detritus of the Clarens Formation. Throughout the samples of the Clarens Formation, the provenance reflects a major contribution from a Pan-African signal, however, a unique sample is identified at the Kamberg area (KBG-01) where the basal sample has an overwhelming contribution that reflects a Grenvillian signal. This is further evidenced by the cumulative probability plots that indicate a significant difference in the spread of the Kamberg zircon dates (Figure 5.11), coarser sandstones that are often gritty in places and the abundant appearance of polycrystalline quartz for thin section samples in this part of the

succession. Sedimentary strata from the basal Clarens Formation of the Kamberg area consists of fluvial channel deposits (Eriksson, 1981, 1986; Chapter 4) with palaeoflow directions towards the southwest, indicating a source terrain in the northeast to east. Given the palaeogeography of Gondwana in the Early Jurassic, and that the source most likely reflects a high-grade metamorphic terrain (see section 5.4.1), the western Antarctic Haag Nunataks, could be regarded as a possible source for this localised part of the succession (Jacob *et al*., 2008; Rino *et al*., 2008, Jordan *et al*., 2020).

5.5.3 Chronostratigraphic framework

Overall, the Clarens Formation reflects at least an ~8-9 Myr depositional history in the main Karoo Basin (Figure 5.7). More specifically, the chronostratigraphically consistent MDAs in the 3 zones of the unit suggest that zone 1 (lower Clarens Formation) is late Sinemurian, zone 2 (middle Clarens Formation) is early Pliensbachian and zone 3 (upper Clarens Formation) is late Pliensbachian (Figures 5.8–5.10). The late Sinemurian age of the lower Clarens Formation is also observed in one sample (Q6) taken in the south of the basin at the boundary of the upper Elliot and Clarens formations (see Bordy *et al*. 2020). Two samples (MTY-02; MKY-02) in zone 2 and three samples (KBG-03; WTK-03; MTY-03) in Zone 3 have anomalous ages being Late Sinemurian and Early Pliensbachian (Figure 5.7). The fact that both the late Sinemurian (Zone 1) and early Pliensbachian (Zone 2) signals are not present in samples from the central, eastern and northern parts of the associated zones, respectively, but are present in the younger zones, may suggest that zircons with these age signals gradually spread towards the northeast from a primary source in the south and southwest (Figures 5.8, 5.9 and 5.10). This zircon-signal trend may be a reflection of preservation bias in the succession or large-scale source dynamics (see above), or both. The basinal distribution of these zircon signals may, therefore, reflect source dynamics rather than providing conclusive age constraints. Alternatively, the spatiotemporal trend in the zircon signals may indicate that aeolian conditions could have been established in the north first. This idea is in line with that of Beukes (1969, 1970), who proposed that the northward drifting Gondwana, given its palaeolatitude, would have resulted in the establishing of aeolian conditions in the north first, with gradual, subsequent onset of desert condition towards the south of the basin. This notion is supported by the proposed north-south diachronous eruption of the basaltic lava of the Karoo-Ferrar Large Igneous Province (Moulin *et al*., 2017; Bordy *et al*., 2021), which most likely had an early onset in the south of the basin. Early Pliensbachian zircons grains from the upper Clarens Formation in the Springbok Flats area north of the MKB (MDA = 187 ± 1.6 Ma; Nxulamo, 2020) and from the lower Clarens Formation in the southern MKB (MDA = 187.5 ± 1.6 Ma; Bordy *et al*., 2020), corroborate the proposed earlier onset of the Karoo basalt volcanism.

Despite the inherent flaws in age calculations based on maximum depositional ages (Spencer *et al*., 2016; Andersen *et al*., 2019; Gehrels *et al*, 2019; Herriot *et al*., 2019; Rossingol *et al*., 2019; Bordy *et al*., 2020), the result appears to provide a broad chronostratigraphic framework where three age signals can be associated with the respective zones, particularly in the south of the basin. These are: 1) a late Sinemurian age signal for the lower Clarens Formation, also identified in the transitional lower contact (Bordy *et al*., 2020); 2) an early Pliensbachian age signal for the middle Clarens Formation; and 3) a late Pliensbachian signal for the upper Clarens Formation. The signals could reflect sediment supply dynamics related to a zircon source that was largely contemporaneous with the deposition of the Clarens Formation, which might have been distal volcanic eruptions in

Patagonia (i.e., supplying primary ashfall zircons; Muir *et al*., 2020). These newly established MDAs for the Clarens formation that range from the late Sinemurian to late Pliensbachian provide a meaningful age framework for the terminal Karoo times, especially when assessed in relation to current biostratigraphic and chronostratigraphic evidence from the upper Stormberg and lower Drakensberg Groups (Duncan *et al*., 1997; Moulin *et al*., 2011; Svensen *et al*., 2012; Moulin *et al*., 2017; Rademan, 2018; Abrahams, 2020; Bordy *et al*., 2020, 2021Knoll, 2005; Muir *et al*., 2020). Although the results neatly fit the broad geological consensus of the upper Karoo, these new MDAs should not be regarded as conclusive age constraints of the Clarens Formation, because the dataset is based on detrital zircon ages and thus it does not lend itself to such definite age determinations. Rather, the results can be regarded as a starting point for a more systematic approach for future geochronological work, such as more complex sampling, to enhance our understanding of the erg dynamics and spatiotemporal relationship that existed between the north and the south of the main Karoo Basin during the deposition of the Clarens Formation.

5.5.4 Provenance synthesis

Detritus within the cover successions of southern Africa has been shown to consists largely of recycled sedimentary rocks (Vorster, 2014; Andersen *et al*., 2016) and this feature is strongly echoed in the Clarens Formation as evidenced by a high degree of ZTR heavy minerals, a lack of variation in the heavy mineral suite, a high degree of rounding in the zircons and the identification of zircon age trends that reflect the same signals as those in older Karoo and Pan-African aged successions (Andersen *et al*., 2016; Viglietti *et al*., 2017; Bordy *et al*, 2020).When comparing the zircon populations from the Clarens Formation to that of the known Beaufort Group, a strong similarity is evident, although the proportions of each zircon age population is different (Viglietti *et al*., 2017). The Clarens Formation succession is dominated by zirco142ns that have a Pan-African signal, whereas a Permian signal dominates in the Beaufort Group (Viglietti *et al*., 2017). This similarity suggests that the Beaufort Group may represent a source of the Clarens Formation, albeit only a partial component, as a shift to a dominant Pan-African signal is observed. This, in turn, could indicate a larger input from the Damaran and Saldanian Orogenic Belts and a change in source dynamics relative to the pre-existing Karoo successions during Clarens times. This recycling of pre-Clarens Karoo rocks was also envisaged by Beukes (1969, 1970), Eriksson (1986) and Eriksson *et al*. (1994).

When comparing existing published and unpublished zircon data (unpublished theses) for the Clarens Formation to the samples from this study, a similarity in the age patterns is evident, having a slightly different proportion. Additional zircon data includes one sample each from Bordy *et al*. (2020; UMC; MKB), Rademan (2018 – Map 6; MKB), Nxumalo (2020; BK-1-1; Springbok Flats Basin), and Zieger *et al*. (2020; NAM349; Etjo Formation in Namibia). A similar source terrain for the Elliot and Clarens Formations was suggested based on the heavy mineral component, which relates to the main Karoo Basin Realm A of Zieger *et al*. (2020). This trend is supported by the change in source dynamics for the upper Elliot Formation where a west to east source input is reported to have activated in the Early Jurassic (Bordy *et al*., 2004). Using statistical dissimilarity calculations, Zieger *et al*. (2020) determined that a common recycling history exists for the Upper Triassic and Lower Jurassic in southwestern Gondwana, and this may suggest a similar source terrain for the aeolianites across southern Africa in the Early Jurassic. Furthermore, the similarity of the sandstone compositions and the provenance signals in both the massive and large-scale cross-bedded facies (as discussed in Chapter 4) further suggests that these facies were derived from the same source, and that the downwind transitional deposits to sandy loess and loess may have been sourced from the

upwind dunes as discussed in Chapter 3, which in turn is suggestive of large-scale homogenisation of the sediments of the Clarens Formation and other regional Early Jurassic aeolianites.

The presence of a primary source is indicated by the appearance of unstable minerals in the heavy mineral suite and the appearance of a small percentage of polycrystalline quartz, the combination of which point to a primary metamorphic source. However, the extensive evidence for a high degree of recycled material incorporated into the detritus of the Clarens Formation show that primary source inputs were obscured by the overwhelming input of recycled material. Therefore, meaningful provenance conclusions are masked by homogenisation of the source sediments which only highlights the polycyclic nature of the Clarens Formation detritus. No spatial variation in the source areas can be identified, except for a localised source in the east with a dominant Grenvillian signal and associated input of polycrystalline quartz, most likely reflecting the western Antarctic Haag Nunataks terrain. The young source in the south may be attributed to source dynamics related to volcanism associated with the Chon Aike Large Igneous Province that was situated to the southwest of the Clarens Basin. This source is interpreted to have produced the Early Jurassic signals observed in the Clarens Formation and its incorporation into the respective zones is responsible for the broad chronostratigraphic framework.

5.6. Conclusion

Existing provenance studies of the Clarens Formation have been largely focused on petrographic work and given the modern use of single mineral analysis to aid such enquiry, zircon geochronology can offer new insights regarding source areas and supply mechanisms. In addition, this can also provide a better understanding of the age constraints related to the development and evolution of the Clarens Formation. The combination of current zircon geochronology and petrographic studies show that the Clarens Formation detritus can be attributed to mainly recycled pre-existing sedimentary successions. This is indicated by the presence of high ZTR minerals, the lack of a diverse heavy mineral suite, zircons that show distinct inner and outer growth events and the dominance of zircon populations that can be linked to large-scale tectonics event, particularly zircons associated with a Pan-African signal that dominates the samples. The major source areas are interpreted as that of the Damara and Saldania Orogenic Belts, whereas minor sources can be linked to the Namaqua-Natal Mobile Belt and the western Sierras Pampeanas, both providing Grenvillian zircon age signal. Although the strong recycled nature of the Clarens Formation detritus complicates many aspects of the provenance information, a primary source is inferred from the appearance of unstable heavy minerals and the higher feldspar content as compared to the sandstone composition of both modern and ancient desert systems. Localised provenance variations are only seen in the east of the basin, where a dominance of polycrystalline quarts and a prominent Grenvillian signal is associated with sedimentary facies that is interpreted to have been sourced from the east of the basin. Early Jurassic zircon signals appear throughout the stratigraphy of the Clarens Formation, associated with euhedral to slightly rounded zircons. The source for these zircons is interpreted to represent pyroclastic ash plumes derived from volcanism that was active in Patagonia and Antarctica during the Early Jurassic and has been identified in similar aged sedimentary successions of southern Africa. The Early Jurassic zircon signal identified in the Clarens Formation samples and used in the MDA calculations suggest that a broad chronostratigraphic framework can be interpreted for the Clarens Formation where the basal zone shows a late Sinemurian age, the middle zone reflects an early Pliensbachian age and the upper zone having a late Pliensbachian age, particularly in the south of the basin. Future work may include evaluating zircon datasets in relation to spatiotemporal basin dynamics to shed light on the evolution of the north and south of the basin.

5.7. References

Abrahams, M. 2020. Evaluation of tridactyl theropod tracks in southern Africa: quantitative morphometric analysis across the Triassic–Jurassic boundary. Unpublished doctoral thesis, University of Cape Town. Available: http://hdl.handle.net/11427/32436

Abrahams, M., Bordy, E.M. and Knoll, F. 2021. Hidden for one hundred years: a diverse theropod ichnoassemblage and cross-sectional tracks from the historic Early Jurassic Tsikoane ichnosite (Clarens Formation, northern Lesotho, southern Africa). *Historical Biology*, 33(10): 2504–519. DOI: 10.1080/08912963.2020.1810681

Andersen, T. 2014. The detrital zircon record: Supercontinents, parallel evolution—Or coincidence?. *Precambrian Research*, 244: 279-287. DOI: 10.1016/j.precamres.2013.10.013

Andersen, T., Elburg, M. and Cawthorn-Blazeby, A. 2016. U–Pb and Lu–Hf zircon data in young sediments reflect sedimentary recycling in eastern South Africa. *Journal of the Geological Society*, 173(2): 337–351. DOI: 10.1144/jgs2015-006

Andersen, T., Elburg, M.A. and Magwaza, B.N. 2019. Sources of bias in detrital zircon geochronology: Discordance, concealed lead loss and common lead correction. *Earth-Science Reviews*, 197: 102899. DOI: 10.1016/j.earscirev.2019.102899

Bamford, M.K. 2004. Diversity of the woody vegetation of Gondwanan Southern Africa. *Gondwana Research*, 7(1): 153–164. DOI: 10.1016/S1342-937X(05)70314-2

Basu, A., Young, S.W., Suttner, L.J., James, W.C. and Mack, G.H. 1975. Re-evaluation of the use of undulatory extinction and polycrystallinity in detrital quartz for provenance interpretation. *Journal of Sedimentary Research*, 45(4): 873–882. DOI: 10.1306/212F6E6F-2B24-11D7-8648000102C1865D

Basu, A. 1985. Reading provenance from detrital quartz. In *Provenance of arenites*. Springer: Dordrecht. 231–247pp.

Bertolini, G., Marques, J.C., Hartley, A.J., Da-Rosa, A.A., Scherer, C.M., Basei, M.A. and Frantz, J.C. 2020. Controls on Early Cretaceous desert sediment provenance in south-west Gondwana, Botucatu Formation (Brazil and Uruguay). *Sedimentology*, 67(5): 2672–2690. DOI: 10.1111/sed.12715

Beukes, N.J. 1969. Die sedimentologie van die Etage Holkranssandsteen, sisteem Karoo.Unpublished MSc dissertation, University of the Orange Free State, Bloemfontein, 138pp. Available: http://hdl.handle.net/11660/7671

Beukes, N.J. 1970. Stratigraphy and sedimentology of the Cave Sandstonen stage, Karoo System. In: S.H. Haughton (Editor), Proceedings and papers of the 2nd Gondwana symposium. Council for Scientific and Industrial Research, Pretoria, 321–341.

Bial, J., Büttner, S.H., Schenk, V. and Appel, P. 2015. The long-term high-temperature history of the central Namaqua Metamorphic Complex: Evidence for a Mesoproterozoic continental back-arc in southern Africa. *Precambrian Research*, 268: 243–278. DOI: 10.1016/j.precamres.2015.07.012

Blatt, H. and Christie, J.M. 1963. Undulatory extinction in quartz of igneous and metamorphic rocks and its significance in provenance studies of sedimentary rocks. *Journal of Sedimentary Research*, 33(3): 559–579. DOI: 10.1306/74D70EBB-2B21-11D7-8648000102C1865D

Bordy, E.M. 2008. Enigmatic trace fossils from the aeolian Lower Jurassic Clarens Formation, southern Africa. *Palaeontologia Electronica*, 11: 16A.

Bordy, E.M. and Catuneanu, O. 2002. Sedimentology and palaeontology of upper Karoo aeolian strata (Early Jurassic) in the Tuli Basin, South Africa. *Journal of African Earth Sciences*, 35(2): 301–314. DOI: 10.1016/S0899-5362(02)00103-3

Bordy, E.M., Hancox, P.J. and Rubidge, B.S. 2004. Provenance study of the Late Triassic-Early Jurassic Elliot Formation, main Karoo Basin, South Africa. *South African Journal of Geology*, 107(4): 587-602. DOI: 10.2113/gssajg.107.4.587

Bordy, E.M., Bumby, A.J., Catuneanu, O. and Eriksson, P.G. 2009. Possible trace fossils of putative termite origin in the Lower Jurassic (Karoo Supergroup) of South Africa and Lesotho. *South African Journal of Science*, 105(9-10): 356–362.

Bordy, E.M. and Head, H.V. 2018. Lithostratigraphy of the Clarens Formation (Stormberg Group, Karoo Supergroup), South Africa. *South African Journal of Geology*, 2018, 121(1): 119–130. DOI: 10.25131/sajg.121.0009

Bordy, E.M., Abrahams, M., Sharman, G.R., Viglietti, P.A., Benson, R.B., McPhee, B.W., Barrett, P.M., Sciscio, L., Condon, D., Mundil, R. and Rademan, Z. 2020a. A chronostratigraphic framework for the upper Stormberg Group: Implications for the Triassic-Jurassic boundary in southern Africa. *Earth-Science Reviews*, 203: 103120. DOI: 10.1016/j.earscirev.2020.103120

Bordy, E.M., Rampersadh, A., Abrahams, M., Lockley, M.G. and Head, H.V. 2020b. Tracking the Pliensbachian–Toarcian Karoo firewalkers: Trackways of quadruped and biped dinosaurs and mammaliaforms. *Plos one*, 15(1): e0226847. DOI: 10.1371/journal.pone.0226847

Bowden, L.L. 2014. A comparative study of detrital zircon ages from river sediment and rocks of the Karoo Supergroup (Late Carboniferous to Jurassic), Eastern Cape Province, South Africa: Implications for the tectono-sedimentary evolution of Gondwanaland's southern continental margin. Unpublished doctoral thesis, University of Johannesburg.

Casquet, C., Pankhurst, R.J., Rapela, C.W., Galindo, C., Fanning, C.M., Chiaradia, M., Baldo, E., González-Casado, J.M. and Dahlquist, J.A. 2008. The Mesoproterozoic Maz terrane in the Western Sierras Pampeanas, Argentina, equivalent to the Arequipa–Antofalla block of southern Peru? Implications for West Gondwana margin evolution. *Gondwana Research*, 13(2): 163–175. DOI: 10.1016/j.gr.2007.04.005

Corfu, F., Hanchar, J.M., Hoskin, P.W. and Kinny, P. 2003. Atlas of zircon textures. *Reviews in mineralogy and geochemistry*, 53(1): 469–500. DOI: 10.2113/0530469

Coutts, D.S., Matthews, W.A. and Hubbard, S.M. 2019. Assessment of widely used methods to derive depositional ages from detrital zircon populations. *Geoscience Frontiers*, 10(4): 1421–1435. DOI: 10.1016/j.gsf.2018.11.002

Crompton, A.W. 1958. The Cranial morphology of a new genus and species of ictidosaurain. *Proceeding of the Zoological society of London*, 130: 183–216.

Dickinson, W.R. and Gehrels, G.E. 2009. Use of U-Pb ages of detrital zircons to infer maximum depositional ages of strata: A test against a Colorado Plateau Mesozoic database. *Earth and Planetary Science* Letters, 288(1): 115–125. DOI: 10.1016/j.epsl.2009.09.013

Duncan, R.A, Hooper, P.R., Rehacek, J., Marsh, J. and Duncan, A.R. 1997. The timing and duration of the Karoo igneous event, southern Gondwana. *Journal of Geophysical Research: Solid Earth*. 102(B8): 18127-18138. DOI: 10.1029/97JB00972

du Toit, A.L. 1905. Geological survey of the division of Aliwal North, Herschel, Barkly East and part of Wodehouse: *Annual Report of the Geological Commission of the Cape of Good Hope,* 71–181.

Du Toit, A.L. 1918. The zones of the Karroo System and their distribution. *Proceedings of the Geological Society of South Africa*, 21: 17–36.

Ellenberger, P. 1970. Les niveaux paléontologiques de premiere apparition des mammiféres primordiaux en Afrique du Sud et leur ichnologie: Establissement de zones stratigraphiques detaillées dans le Stormberg de Leshoto (Afrique du Sud)(Trias Superieur a Jurassique). In *IUGS, 2nd symposium on Gondwana stratigraphy and palaeontology*: 343–370.

Eriksson, P.G. 1981. A palaeoenvironmental analysis of the Clarens Formation in the Natal Drakensberg. *Transactions of the Geological Society of South Africa*, 84: 7–17.

Eriksson, P.G. 1986. Aeolian dune and alluvial fan deposits in the Clarens Formation of the Natal Drakensberg. *Transactions of the Geological Society of South Africa*, 89: 389–393.

Eriksson, P.G., McCourt, S. and Snyman, C.P. 1994. A note on the petrography of upper Karoo sandstones in the Natal Drakensberg: implications for the Clarens Formation palaeoenvironment. *South African Journal of Geology*, 97(1): 101–106.

Féraud, G., Alric, V., Fornari, M., Bertrand, H. and Haller, M. 1999. 40Ar/39Ar dating of the Jurassic volcanic province of Patagonia: migrating magmatism related to Gondwana break-up and subduction. *Earth and Planetary Science Letters*, 172(1-2): 83-96. DOI: 10.1016/S0012-821X(99)00190-9

Frimmel, H.E., Basei, M.A., Correa, V.X. and Mbangula, N. 2013. A new lithostratigraphic subdivision and geodynamic model for the Pan-African western Saldania Belt, South Africa. *Precambrian Research*, 231: 218-235. DOI: 10.1016/j.precamres.2013.03.014

Forey, P. and Gardiner, B.G. 1973. A new dictyopygid from the Cave Sandstone of Lesotho, southern Africa. *Palaeontologia* , 15: 29–31.

Foster, D.A., Goscombe, B.D., Newstead, B., Mapani, B., Mueller, P.A., Gregory, L.C. and Muvangua, E. 2015. U–Pb age and Lu–Hf isotopic data of detrital zircons from the Neoproterozoic Damara Sequence: Implications for Congo and Kalahari before Gondwana. *Gondwana Research*, 28(1): 179–190. DOI: 10.1016/j.gr.2014.04.011

Gärtner, A., Linnemann, U. Sagawe, A., Hofmann, M. Ullrich and Kleber, A. 2013. Morphology of zircon crystal grains in sediments – characteristics, classifications, definitions. *Geologica Saxonica*, 59: 65–73.

Garzanti, E. 2017. The maturity myth in sedimentology and provenance analysis. *Journal of Sedimentary Research*, 87(4): 353–365. DOI: 10.2110/jsr.2017.17

Garzanti, E. 2019. Petrographic classification of sand and sandstone. *Earth-Science reviews*, 192: 545–563. DOI: 10.1016/j.earscirev.2018.12.014

Garzanti, E., Ando, S. and Vezzoli, G. 2006. The continental crust as a source of sand (southern Alps cross section, northern Italy). *The Journal of Geology*, 114(5): 533–554. DOI: 10.1086/506159

Garzanti, E., Doglioni, C., Vezzoli, G. and Ando, S. 2007. Orogenic belts and orogenic sediment provenance. *The Journal of Geology*, 115(3): 315–334. DOI: 10.1086/512755

Garzanti, E., Vermeesch, P., Andò, S., Vezzoli, G., Valagussa, M., Allen, K., Kadi, K.A. and Al-Juboury, A.I. 2013. Provenance and recycling of Arabian desert sand. *Earth-Science Reviews*, 120: 1–19. DOI: 10.1016/j.earscirev.2013.01.005

Garzanti, E., Vermeesch, P., Padoan, M., Resentini, A., Vezzoli, G. and Andò, S. 2014. Provenance of passive-margin sand (Southern Africa). *The Journal of Geology*, 122(1): 17–42. DOI: 10.1086/674803

Garzanti, E., Dinis, P., Vermeesch, P., Andò, S., Hahn, A., Huvi, J., Limonta, M., Padoan, M., Resentini, A., Rittner, M. and Vezzoli, G. 2018a. Dynamic uplift, recycling, and climate control on the petrology of passive-margin sand (Angola). *Sedimentary Geology*, 375: 86–104. DOI: 10.1016/j.sedgeo.2017.12.009

Garzanti, E., Andò, S., Limonta, M., Fielding, L. and Najman, Y. 2018b. Diagenetic control on mineralogical suites in sand, silt, and mud (Cenozoic Nile Delta): Implications for provenance reconstructions. *Earth-Science Reviews*, 185: 122–139. DOI: 10.1016/j.earscirev.2018.05.010

Gazzi, P. 1966. Le arenarie del flysch sopracretaceo dell'Appennino modenese; Correlazioni coni flysch di Monghidoro. *Minerelogica et Petrographica Acta*, 12: 69–97.

Gehrels, G. 2011. Detrital zircon U-Pb geochronology: Current methods and new opportunities. In *Tectonics of sedimentary basins: Recent advances*. Busby, C and Azor, A. Eds. Blackwell Publishing, 45–62. DOI: 10.1002/9781444347166.ch2

Gehrels, G., Giesler, D., Olsen, P., Kent, D., Marsh, A., Parker, W., Rasmussen, C., Mundil, R., Irmis, R., Geissman, J. and Lepre, C. 2020. LA-ICPMS U–Pb geochronology of detrital zircon grains from the Coconino, Moenkopi, and Chinle formations in the Petrified Forest National Park (Arizona). *Geochronology*, 2(2): 257–282. DOI: 10.5194/gchron-2-257-2020

Gow, C.E. 1981. Pachygenelus, Diarthrognathus and the double jaw articulation. *Palaeontologia a146fricana*, 24:15.

Haughton, S.H. 1924. The fauna and stratigraphy of the Stormberg Series. *Annals of the South African Museum*, 12(8): 323–497.

Herriott, T.M., Crowley, J.L., Schmitz, M.D., Wartes, M.A. and Gillis, R.J. 2019. Exploring the law of detrital zircon: LA-ICP-MS and CA-TIMS geochronology of Jurassic forearc strata, Cook Inlet, Alaska, USA. *Geology*, 47(11): 1044–1048. COI: 10.1130/G46312.1

Hofmann, M., Linnemann, U., Hoffmann, K.H., Gerdes, A., Eckelmann, K. and Gärtner, A. 2014. The Namuskluft and Dreigratberg sections in southern Namibia (Kalahari Craton, Gariep Belt): a geological history of Neoproterozoic rifting and recycling of cratonic crust during the dispersal of Rodinia until the amalgamation of Gondwana. *International Journal of Earth Sciences*, 103(5): 1187–1202. DOI: 10.1007/s00531-013-0949-6

Holzförster, F. 2007. Lithology and depositional environments of the Lower Jurassic Clarens Formation in the eastern Cape, South Africa. *South African Journal of Geology*, 110(4): 543–560. DOI: 10.2113/gssajg.110.4.543

Holzförster, F., Stollhofen, H. and Stanistreet, I.G., 1999. Lithostratigraphy and depositional environments in the Waterberg-Erongo area, central Namibia, and correlation with the main Karoo Basin, South Africa*. Journal of African Earth Sciences*, 29(1): 105–123. DOI: 10.1016/S0899-5362(99)00083-4

Ingersoll, R.V., Bullard, T.F., Ford, R.L., Grimm, J.P., Pickle, J.D. and Sares, S.W. 1984. The effect of grain size on detrital modes: a test of the Gazzi-Dickinson point-counting method*. Journal of Sedimentary Research,* 54(1): 103–116. DOI: 10.1306/212F83B9-2B24-11D7-8648000102C1865D

Jacobs, J., Pisarevsky, S., Thomas, R.J. and Becker, T. 2008. The Kalahari Craton during the assembly and dispersal of Rodinia. *Precambrian Research*, 160(1–2): 142–158. DOI: 10.1016/j.precamres.2007.04.022

Johnson, M.R. 1976. Stratigraphy and sedimentology of the Cape and Karoo Sequences in the eastern Cape Province. Unpublished doctoral thesis, Rhodes University, Grahamstown, South Africa, 336pp. Available: http://hdl.handle.net/10962/d1005617

Johnsson, M.J. and Basu, A. 1993. The system controlling the composition of clastic sediments. *Special Papers-Geological Society of America*, 1-1.

Jordan, T.A., Riley, T.R. and Siddoway, C.S. 2020. The geological history and evolution of West Antarctica. *Nature Reviews Earth and Environment*, 1(2): 117–133. DOI: 10.1038/s43017-019-0013-6

Jubb, R.A. 1973. Brief synthesis of present information on the geographical and stratigraphical distribution of fossil fish within the Stormberg Series, South Africa. *Palaeontologia africana,* 16: 17–23

Kitching, J.W. and Raath, M.A. 1984. Fossils from the Elliot and Clarens Formation (Karoo sequence) of the northeastern Cape, Orange Free State and Lesotho, and a suggested biozonation based on tetrapods. *Palaeontologia a147fricana*, 25: 111–125.

Knoll, F. 2005. The tetrapod fauna of the Upper Elliot and Clarens formations in the main Karoo Basin (South Africa and Lesotho). *Bulletin de la Société géologique de France*, 176(1): 81–91. DOI: 10.2113/176.1.81

Koen, G.M., 1955. Heavy minerals as an aid to the correlation of sediments of the Karroo system in the Northern part of the Union of South Africa. *South African Journal of Geology*, 58(1): 265–366.

Linol, B., de Wit, M.J., Barton, E., de Wit, M.M.J. and Guillocheau, F. 2016. U–Pb detrital zircon dates and source provenance analysis of Phanerozoic sequences of the Congo Basin, central Gondwana. *Gondwana Research*, 29(1): 208–219. DOI: 0.1016/j.gr.2014.11.009

Macey, P.H., Thomas, R.J., Minnaar, H.M., Gresse, P.G., Lambert, C.W., Groenewald, C.A., Miller, J. A., Indongo, J., Angombe, M., Shifotoka, G., Frei, D., Diener J.F.A., Kisters, A.F.M., Dhansay T., Smith, H., Doggart, S., Le Roux, P., Hartnady, M.I. and Tinguely, C. 2017. Origin and evolution of the ~1.9Ga Richtersveld Magmatic Arc, southwest Africa. *Precambrian Research*, 292: 417–451. DOI: 10.1016/j.precamres.2017.01.013

McPhee, B., Bordy, E.M., Sciscio, L. and Choiniere, J. 2017. The sauropodomorph biostratigraphy of the ElliotFormation of southern Africa: Tracking the evolution of Sauropodomorpha across the Triassic–Jurassic boundary. *Acta Palaeontologica Polonica*, 62(3): 441–465.

Meijs, L., 1960. Notes on the occurrence of petrified wood in Basutoland. *Basutoland Notes and Records*, 2: 20–26.

Minnaar, H. 2011. Composition and evolution of the proterozoic Vioolsdrif batholith (including the orange river group), Northern Cape province, South Africa. Unpublished doctoral thesis, University of the Free State. Available: http://hdl.handle.net/11660/2169

Morton, A.C. and Hallsworth, C. 2007. Stability of detrital heavy minerals during burial diagenesis. *Developments in Sedimentology*, 58: 215–245. DOI: 10.1016/S0070-4571(07)58007-6

Moulin, M., Fluteau, F., Courtillot, V., Marsh, J., Delpech, G., Quidelleur, X., Gérard, M. and Jay, A.E. 2011. An attempt to constrain the age, duration, and eruptive history of the Karoo flood basalt: Naudes Nek section (South Africa). *Journal of Geophysical Research: Solid Earth*, 116(B7). DOI: 10.1029/2011JB008210

Moulin, M., Fluteau, F., Courtillot, V., Marsh, J., Delpech, G., Quidelleur, X. and Gérard, M., 2017. Eruptive history of the Karoo lava flows and their impact on early Jurassic environmental change. *Journal of Geophysical Research: Solid Earth*, 122(2): 738–772. DOI: 10.1002/2016JB013354

Muhs, D.R. 2004. Mineralogical maturity in dunefields of North America, Africa and Australia. *Geomorphology*, 59(1-4): 247–269. DOI: 10.1016/j.geomorph.2003.07.020

Muir, R.A., Bordy, E.M., Mundil, R. and Frei, D. 2020. Recalibrating the breakup history of SW Gondwana: U–Pb radioisotopic age constraints from the southern Cape of South Africa. *Gondwana Research*, 84: 177–193. DOI: 10.1016/j.gr.2020.02.011

Nxumalo, V., 2020. Uranium Mineralisation and Provenance Analyses of the Karoo Supergroup in the Springbok Flats Coalfield, South Africa. Unpublished doctoral thesis, University of Johannesburg.

Olsen, P.E. and Galton, P.M. 1984. A review of the reptile and amphibian assemblages from the Stormberg of southern Africa, with special emphasis on the footprints and the age of the Stormberg. *Palaeontologia africana*, 25: 87–110.

Pankhurst, R.J., Riley, T.R., Fanning, C.M. and Kelley, S.P. 2000. Episodic silicic volcanism in Patagonia and the Antarctic Peninsula: chronology of magmatism associated with the break-up of Gondwana. *Journal of Petrology*, 41(5): 605-625. DOI: 10.1093/petrology/41.5.605

Pankhurst, R.J., Rapela, C.W., Fanning, C.M. and Márquez, M. 2006. Gondwanide continental collision and the origin of Patagonia. *Earth-Science Reviews*, 76(3–4): 235–257. DOI: 10.1016/j.earscirev.2006.02.001

Paton, C., Hellstrom, J., Paul, B., Woodhead, J. and Hergt, J. 2011. Iolite: Freeware for the visualisation and processing of mass spectrometric data. *Journal of Analytical Atomic Spectrometry*, 26(12): 2508–2518.

Petrus, J.A. and Kamber, B.S. 2012. VizualAge: A novel approach to laser ablation ICP-MS U-Pb geochronology data reduction. *Geostandards and Geoanalytical Research*, 36(3): 247–270. DOI: 10.1111/j.1751-908X.2012.00158.x

Pinto, V.M., Hartmann, L.A., Santos, J.O. and Mcnaughton, N.J. 2015. Zircon ages delimit the provenance of a sand extrudite from the Botucatu Formation in the Paraná volcanic province, Iraí, Brazil. *Anais da Academia Brasileira de Ciências*, 87: 1611–1622.

Pol, D., Ramezani, J., Gomez, K., Carballido, J.L., Carabajal, A.P., Rauhut, O.W.M., Escapa, I.H. and Cúneo, N.R. 2020. Extinction of herbivorous dinosaurs linked to Early Jurassic global warming event. *Proceedings of the Royal Society B*, 287(1939): 20202310. DOI: 0.1098/rspb.2020.2310

Rademan, Z. 2018. Radiometric dating and stratigraphic reassessment of the Elliot and Clarens formations; near Maphutseng and Moyeni, Kingdom of Lesotho, southern Africa.

Unpublished MSc dissertation, Stellenbosch University. Available: http://hdl.handle.net/10019.1/104888

Ramos, V.A., Vujovich, G., Martino, R. and Otamendi, J., 2010. Pampia: a large cratonic block missing in the Rodinia supercontinent. *Journal of Geodynamics*, 50(3–4): 243–25. DOI: 10.1016/j.jog.2010.01.019

Rapela, C.W., Pankhurst, R.J., Casquet, C., Baldo, E., Galindo, C., Fanning, C.M. and Dahlquist, J.M. 2010. The Western Sierras Pampeanas: Protracted Grenville-age history (1330–1030 Ma) of intra-oceanic arcs, subduction–accretion at continental-edge and AMCG intraplate magmatism. *Journal of South American Earth Sciences*, 29(1): 105–127. DOI: 10.1016/j.jsames.2009.08.004

Rino, S., Kon, Y., Sato, W., Maruyama, S., Santosh, M. and Zhao, D., 2008. The Grenvillian and Pan-African orogens: world's largest orogenies through geologic time, and their implications on the origin of superplume. *Gondwana Research*, 14(1–2): 51–72. DOI: 10.1016/j.gr.2008.01.001

Rossignol, C., Hallot, E., Bourquin, S., Poujol, M., Jolivet, M., Pellenard, P., Ducassou, C., Nalpas, T., Heilbronn, G., Yu, J. and Dabard, M.P. 2019. Using volcaniclastic rocks to constrain sedimentation ages: To what extent are volcanism and sedimentation synchronous?. *Sedimentary Geology*, 381: 46–64. DOI: 10.1016/j.sedgeo.2018.12.010

Spencer, C.J., Kirkland, C.L. and Taylor, R.J. 2016. Strategies towards statistically robust interpretations of in situ U–Pb zircon geochronology. *Geoscience Frontiers*, 7(4): 581–589. DOI: 10.1016/j.gsf.2015.11.006

Schneider, S., Hornung, J., Hinderer, M. and Garzanti, E. 2016. Petrography and geochemistry of modern river sediments in an equatorial environment (Rwenzori Mountains and Albertine rift, Uganda)—Implications for weathering and provenance. *Sedimentary Geology*, 336: 106–119. DOI: 10.1016/j.sedgeo.2016.02.006

Smith, R.M.H., Eriksson, P.G. and Botha, W.J. 1993. A review of the stratigraphy and sedimentary environments of the Karoo-aged basins of Southern Africa. *Journal of African Earth Sciences*, 16(1–2): 143–169.

Stagman, J.G. 1978. An outline of the geology of Rhodesia with contributions from N.M. Harrison, T.J. Broderick and V.R. Stocklmayer. *Bulletin, Geological Survey of Rhodesia*, 80, 126pp.

Stockley, G.M. 1947. Report on the Geology of Basutoland. *Morija Printing works*, Morija, 114 pp.

Svensen, H., Jamtveit, B., Planke, S., Chevallier, L., 2006. Structure and evolution of hydrothermal vent complexes in the Karoo Basin, South Africa. *Journal of the Geological Society*, 163, 671–682. DOI: 10.1144/1144-764905-037

Svensen, H., Corfu, F., Polteau, S., Hammer, Ø. And Planke, S. 2012. Rapid magma emplacement in the Karoo large Igneous Province. *Earth Planetary Science Letters*, 325–326: 1–9. DOI: 10.1016/j.epsl.2012.01.015

Tasch, P. 1984. Biostratigraphy and palaeontology of some conchostracan-bearing beds in southern Africa. *Palaeontologia africana*, 25: 61–85.

Thomspon, A.O. 1975. The Karoo Rocks in the Mazunga Area, Beitbridge District (No. 40). *Rhodesia Geological Survey*.

Tucker, R.T., Roberts, E.M., Hu, Y., Kemp, A.I. and Salisbury, S.W. 2013. Detrital zircon age constraints for the Winton Formation, Queensland: contextualizing Australia's Late Cretaceous dinosaur faunas. *Gondwana Research*, 24(2): 767–779. DOI: 10.1016/j.gr.2012.12.009

Van Dijk, D.E. and Eriksson, P.G. 2021. Bipedal leaping Jurassic vertebrates in Southern Africa: proposed new ichnotaxon and inferred palaeoenvironment. *Transactions of the Royal Society of South Africa*, 76(3): 235–245. DOI: 10.1080/0035919X.2021.1964104

Van Eeden, O.R. and Keyser, A.W. 1971. Fossielspore in die Holkranssandsteen op Pont Drift, Distrik Soutpansberg, Transvaal. *Annals of the Geological Survey of South Africa*, 9: 135–137.

Van Niekerk, H.S. 2006. The origin of the Kheis Terrane and its relationship with the Archean Kaapvaal Craton and the Grenvillian Namaqua Province in southern Africa. Unpublished doctoral thesis, University of Johannesburg.

Vermeesch, P. 2018. IsoplotR: A free and open toolbox for geochronology. *Geoscience Frontiers*, 9(5): 1479–1493. DOI: 10.1016/j.gsf.2018.04.001

Viglietti, P.A., Frei, D., Rubidge, B.S. and Smith, R.M. 2018. U-Pb detrital zircon dates and provenance data from the Beaufort Group (Karoo Supergroup) reflect sedimentary recycling and air-fall tuff deposition in the Permo-Triassic Karoo foreland basin. *Journal of African Earth Science*, 143: 59–66. DOI: 10.1016/j.jafrearsci.2017.11.006

Visser, J.N.J. 1984. A review of the Stormberg Group and Drakensberg volcanics in southern Africa. *Palaeontologia africana*, 25: 5–27.

Vorster, C. 2014. Laser Ablation ICP-MS Age Determination of Detrital Zircon Populations in the Phanerozoic Cape and Lower Karoo Supergroups (South Africa) and Correlatives in Argentina. Unpublished doctoral thesis, University of Johannesburg.

Weltje, G.J. and von Eynatten, H., 2004. Quantitative provenance analysis of sediments: review and outlook. *Sedimentary Geology*, 171(1–4): 1–11. DOI: 10.1016/j.sedgeo.2004.05.007

Zieger, J., Harazim, S., Hofmann, M., Gärtner, A., Gerdes, A., Marko, L. and Linnemann, U. 2020. Mesozoic deposits of SW Gondwana (Namibia): Unravelling Gondwanan sedimentary dispersion drivers by detrital zircon. *International Journal of Earth Sciences*, 109(5): 1683–1704. DOI: 10.1007/s00531-020-01864-2

Chapter 6. Conclusion

This study of the Clarens Formation of southern Africa contributes new insights into the development and evolution of an Early Jurassic aeolian desert system and the fluvio-lacustrine interactions within it. By reassessing the facies associations and their distribution throughout the Clarens Formation outcrop area, the study provides a better understanding of the small- to large-scale depositional processes that produced this sedimentary succession. Moreover, this study also presents the first-ever regional geochronological framework and detailed provenance history of the unit, utilising both petrographic and detrital zircon geochronology. These new depositional age constraints across the outcrop area assists in contextualising the history of the Clarens Formation within the evolution of southwestern Gondwana and the global climate trends in the Early Jurassic.

Complex fluvio-lacustrine processes within the broader aeolian system of the Clarens Formation can be ascribed to the development of three types of pluvial deposits, which were dependent on their spatial position within the sand sea setting and influenced by sediment availability and localised water-table fluctuations. Firstly, small ponds developed in dune hollows where high wind speeds and a high sediment availability allowed for migrating dunes to outpace water table rise. Such conditions are typically found in the erg centre, where sediment is abundantly available for wind transport. Both the second and third types of pluvial deposits show the development of large-scale lakes in which flooding is linked to ground water flow, however, the third type is different in that flooding is also associated with flood induced hyperconcentrated flows. The second and third types of pluvial deposits can be linked to a position closer to the erg margin, where a lower sediment availability permitted reworking of dunes that resulted in the expansion of interdunes. The thickness of these pluvial deposits types appears to be exceptional for such systems and along with the overall lack of desiccation features, suggest that these lacustrine systems were long-lived and supported thriving localised ecosystems.

The dominance of massive sandstones that characterises parts of the Clarens Formation is shown to reflect the development of transitional facies associations along a downwind erg margin. This was investigated by the application of grain size and other grain features from the known large-scale, cross-bedded sandstones that reflect migrating dunes. Comparing these known parameters to that of parameters expected from other processes, such as dust fall processes (loess) and mass movement processes, six facies types that can be shown to produce massive structures were classified. Given the strong west-to-east wind regime that was active during the Early Jurassic in southwestern Gondwana, these facies developed downwind of a vast desert system, and were the product of migrating dunes, sand sheets, sandy loess to loess deposited that developed along erg margins. Evidence for fluvial and lacustrine reworking of these primary products is also present. Overall, these would have formed by the combination of consistent long-term west-to-east winds and short-term suspension events, such as dust storms.

Overall, the facies of the Clarens Formation is dominated by both the Massive sandstones and the Aeolian Dune deposits. The former is particularly abundant in the upper and lower parts of the succession, while the latter significantly increases in abundance in the middle part, while aeolian sand sheet, ephemeral fluvial, lacustrine and debris flow deposits appear to be less common. This distribution confirms the tripartite zonation of the Clarens Formation linked to a wet-to-dry climate megacycle such that the lower zone represents small scale-dune fields present in the west of the basin with abundant downwind loess plains, while ephemeral fluvial processes entered the basin from the southern to eastern margins. An intensification in aridity resulted in an increased sediment availability that allowed for expansion of the erg, and migration of the erg margin towards the east.

In the upper zone, wet conditions emerged once again, resulting in erg shrinkage and establishment of loess plains with active ephemeral fluvial and lacustrine processes throughout.

Thickness trends throughout the Clarens Basin show a subtle north to south increase, while extreme thickness variations is particularly prevalent in the southern part of the basin. These thickness variations are ascribed to localised subsidence related to basement rheology and is supported by the extreme thickness of the pluvial facies situated in the south of the outcrop area. In addition, this interpretation is in line with a foresag basin model during terminal Karoo deposition.

Sediment source areas have been attributed to mostly the rocks that formed during the Damaran and Saldanian orogenic events are reflected in the dominant Pan-African zircon signals, while the high ZTR heavy mineral content, the consistent sandstone classification, the lack of a diverse heavy mineral suite and the detrital zircon signals that can be linked to several large-scale tectonic events, collectively suggest that the Clarens Formation detritus was largely composed of recycled material that was homogenised over southwestern Gondwana. Although evidence for primary sources can be identified, specific interpretations surrounding their source is masked by the overwhelming presence of recycled material. The only unique provenance was identified in the east of the basin, where ephemeral fluvial deposits indicate a source area situated to the east of the Kaapvaal Craton that was of metamorphic origin. Given the dominance of Grenvillian zircon signals, these were most likely sourced from the western Antarctic Haag Nunataks terrain. Early Jurassic zircon signals in the detrital samples suggests a primary source area towards the south and southwest of the Clarens basin. Their source has been interpreted to reflect volcanic ash plumes in Patagonia related to the Chon Aike Large Igneous Province that was windswept into the Clarens basin. In addition, the distribution, and maximum depositional ages, based on these Early Jurassic zircon signals, indicate that the three stratigraphic zones of the Clarens Formation can be linked to distinct depositional ages as the lower zone is late Sinemurian, the middle zone is early Pliensbachian, and the upper zone is late Pliensbachian. These depositional time intervals are in turn consistent with existing age constraints for the Clarens Formation. Furthermore, these zonal age constraints are also consistent with climatic trends on the Tethyan margin of Gondwana that indicate a wet phase for the late Sinemurian, a dry climatic phase for the early Pliensbachian and a humid phase for the late Pliensbachian. This, in turn, suggests that the climate trends observed in the Clarens Formation may have been linked to global Early Jurassic climate trends.

Although substantial strides have been made during this current investigation of the Clarens Formation, many questions have emerged. For this reason, the current study can act as a starting point for further investigations. Given the broad chronostratigraphic framework, future studies can focus on honing these zonal age constraints to better understand the basin dynamics that exists between the northern and southern parts of the basin and how these evolved through time. Moreover, a more detailed analysis of bounding surfaces and sets that are associated with the lacustrine deposits can allude to the development of these lakes within the aeolian setting of the Clarens Formation and how each type fits into the set and surface hierarchy. This may lead to further investigations related to the scales of the climatic cycles and megacycles and how these influenced the development of the informally defined zones of the Clarens Formation. Additionally, the improved understanding of how the depositional environment changed throughout the Early Jurassic may also provide an important context for studying palaeo-ecological development in the Sinemurian to Pliensbachian of southwestern Gondwana and how these responded to the global climatic changes.

Appendices:

Appendix 1: Co-ordinates of the study sites.

No. (from Figures)	Study site	Lat	Long
1	Spes Bona	29° 1'6.19"S	27°33'2.19"E
2	Moolmansberg	28°38'40.12"S	27°59'11.66"E
3	Witkop	28°22'57.83"S	27°54'6.21"E
4	Oorsprongsberg	28°23'4.14"S	28° 7'37.73"E
5	Clarens Municipal grounds	28°31'55.70"S	28°24'59.60"E
6	Nooitkondenk	28°28'31.29"S	28°28'11.44"E
7	Bergwoning	28°30'46.98"S	28°33'24.86"E
8	Makanyaneng	28°46'51.18"S	28°17'42.19"E
9	Cathedral Peak	28°57'24.09"S	29°14'12.49"E
10	Injisuthi	29° 6'33.87"S	29°26'17.40"E
11	Giant's Castle	29°16'51.81"S	29°16'51.81"S
12	Kamberg	29°23'57.72"S	29°40'22.40"E
13	Sani Pass	29°35'24.70"S	29°17'25.70"E
14	Ramatsediso's Nek	30° 3'30.87"S	28°55'30.91"E
15	Qachas nek	30° 2'36.03"S	28°40'58.74"E
16	Woodcliffe	30°59'51.65"S	28° 9'30.66"E
17	Talon	31° 9'45.15"S	27°55'48.71"E
18	Welgesind	31°17'3.66"S	26°30'16.52"E
19	Leeukop	31°16'11.46"S	26°50'3.88"E
20	Hillcleft	30°53'14.62"S	27°53'21.00"E
21	Belloch	30°42'45.17"S	27°41'29.27"
22	Malibe	30°15'17.42"S	27°56'48.71"E
23	Mt Moorosi	30°17'57.87"S	27°52'24.51"E
24	Mokhopa	30°19'49.73"S	27°36'42.50"E
25	Mohales Hoek	30°10'14.44"S	27°28'1.58"E
26	Hellspoort	29°51'32.23"S	27°25'34.65"E
27	Methinyeng	29°47'1.65"S	27°32'8.86"E
28	Abbebe	29°39'7.07"S	27°35'52.80"E
29	Koro Koro	29°29'45.70"S	27°40'0.29"E
30	Roma	29°29'2.03"S	27°44'31.08"E
31	Ha Ralejoe	29°25'25.08"S	27°41'53.66"E
32	Likosheng	29° 7'49.82"S	27°54'51.78"E
33	Fobani	29° 2'39.34"S	27°57'45.44"E
N/A	Fetcaniglen	30°45'24.88"S	27°44'59.32"E

Appendix 2: Palaeo-current measurements. B = bearing.

Location	B	Location	B	Location	B	Location	B
Ha Relajo	63	Belloch_3	90	Likosheng_1	136	korokoro_2	95
Ha Relajo	84	Welgesind	130	Likosheng_1	150	korokoro_2	110
Ha Relajo	130	Welgesind	120	Likosheng_1	142	Methinyeng	124
Ha Relajo	118	Welgesind	104	Likosheng_1	126	Methinyeng	156
Ha Relajo	141	Welgesind	78	Likosheng_1	119	Methinyeng	109
Ha Relajo	132	Welgesind	112	Likosheng_1	138	Methinyeng	73
Ha Relajo	140	Ramasnek_1	84	Likosheng_1	161	Mokhopa	72
Ha Relajo	126	Ramasnek_1	80	Likosheng_1	157	Witkop	50
Ha Relajo	97	Ramasnek_1	70	Likosheng_1	80	Witkop	60
Ha Relajo	117	Ramasnek_1	54	Likosheng_1	118	Witkop	105
Leeukop_1	158	Ramasnek_1	76	Likosheng_1	89	Staffordhill	140
Leeukop_1	150	Ramasnek_2	32	Likosheng_1	106	Staffordhill	52
Leeukop_1	138	Ramasnek_2	24	Likosheng_1	87	Staffordhill	161
Leeukop_1	138	Ramasnek_2	90	Likosheng_1	124	Staffordhill	149
Leeukop_1	146	Ramasnek_2	60	Likosheng_1	134	Staffordhill	104
Leeukop_1	118	Ramasnek_2	54	Likosheng_1	110	Staffordhill	98
Leeukop_1	94	Sanipass	84	Likosheng_1	129	Staffordhill	87
Leeukop_1	92	Sanipass	140	Likosheng_1	81	Belloch_1	154
Leeukop_1	70	Sanipass	142	Likosheng_1	98	Belloch_1	150
Leeukop_1	78	Sanipass	130	Likosheng_1	132	Belloch_3	121
Leeukop_1	68	Cathedral Peak	118	Likosheng_1	106	Belloch_3	139
Leeukop_1	110	Cathedral Peak	150	Likosheng_2	60	Belloch_3	137
Leeukop_1	84	Cathedral Peak	156	Likosheng_2	91	Belloch_3	124
Leeukop_1	78	Cathedral Peak	166	Likosheng_2	72	Belloch_2	280
Leeukop_1	72	Cathedral Peak	190	Likosheng_2	109	Belloch_2	281
Leeukop_1	74	Cathedral Peak	142	Likosheng_2	130	Belloch_2	275
Leeukop_1	88	Cathedral Peak	152	Likosheng_2	103	Belloch_2	220
Leeukop_1	74	Cathedral Peak	174	Likosheng_2	121	Belloch_2	240
Leeukop_2	72	Makanyaneng	102	Likosheng_2	117		
Leeukop_2	66	Makanyaneng	121	Likosheng_2	98		
Leeukop_2	62	Makanyaneng	145	Likosheng_2	97		
Leeukop_2	74	Makanyaneng	82	Likosheng_2	82		
Leeukop_2	76	Makanyaneng	103	LES3	126		
Talon	140	Makanyaneng	111	LES3	61		
Talon	120	Makanyaneng	122	LES3	132		
Talon	122	Makanyaneng	139	LES3	79		
Talon	112	Makanyaneng	120	LES3	92		
Talon	82	Makanyaneng	61	korokoro_1	128		
Talon	122	Makanyaneng	135	korokoro_1	64		
Talon	110	Makanyaneng	114	korokoro_2	108		
Talon	126	Makanyaneng	110	korokoro_2	106		
Talon	116	Likosheng_1	140	korokoro_2	91		

Appendix 3: Sedimentary logs with grain fabric orientations and R-value per thin section sample. For facies codes, see Table 4.1 in Chapter 4.

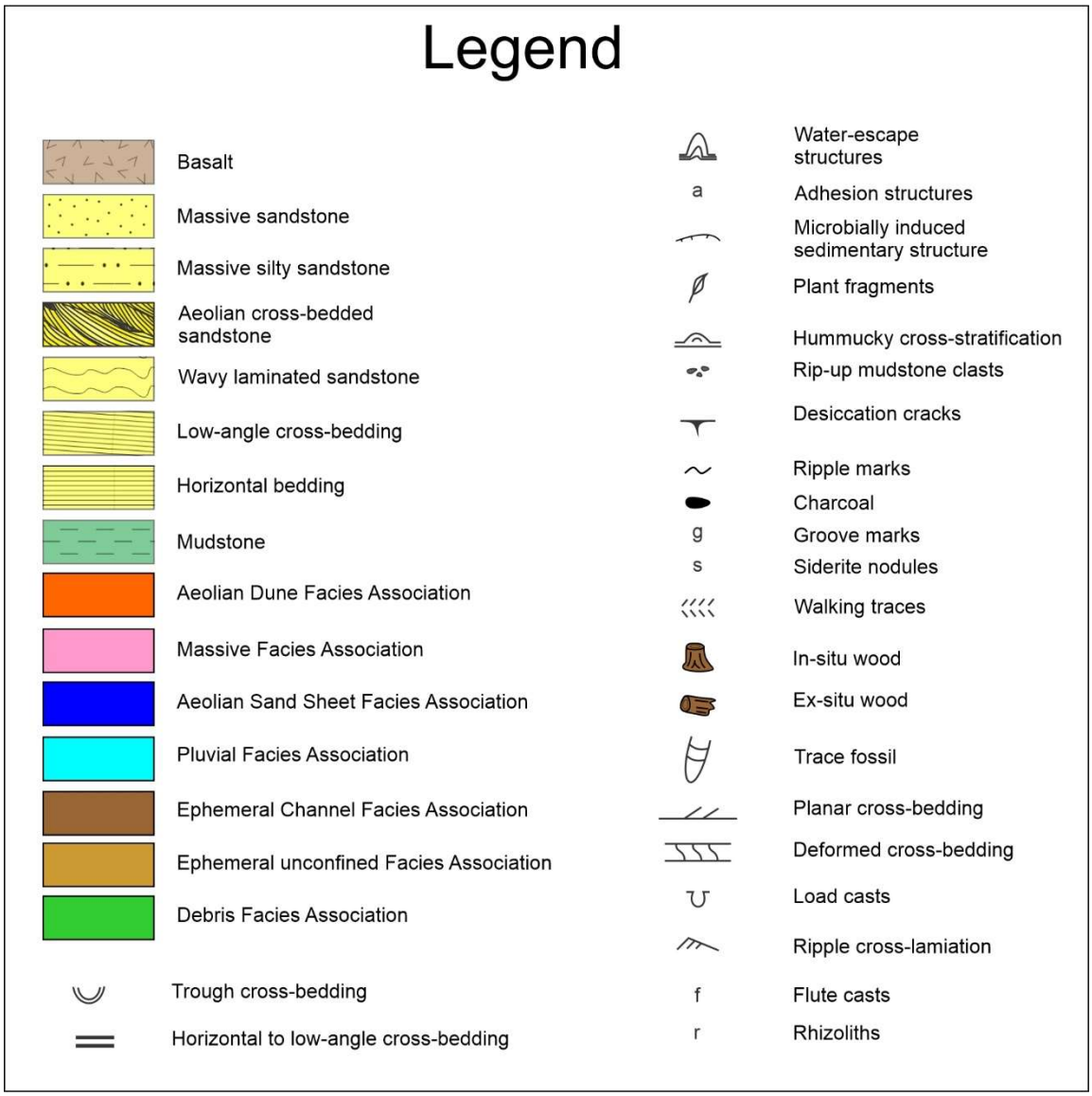

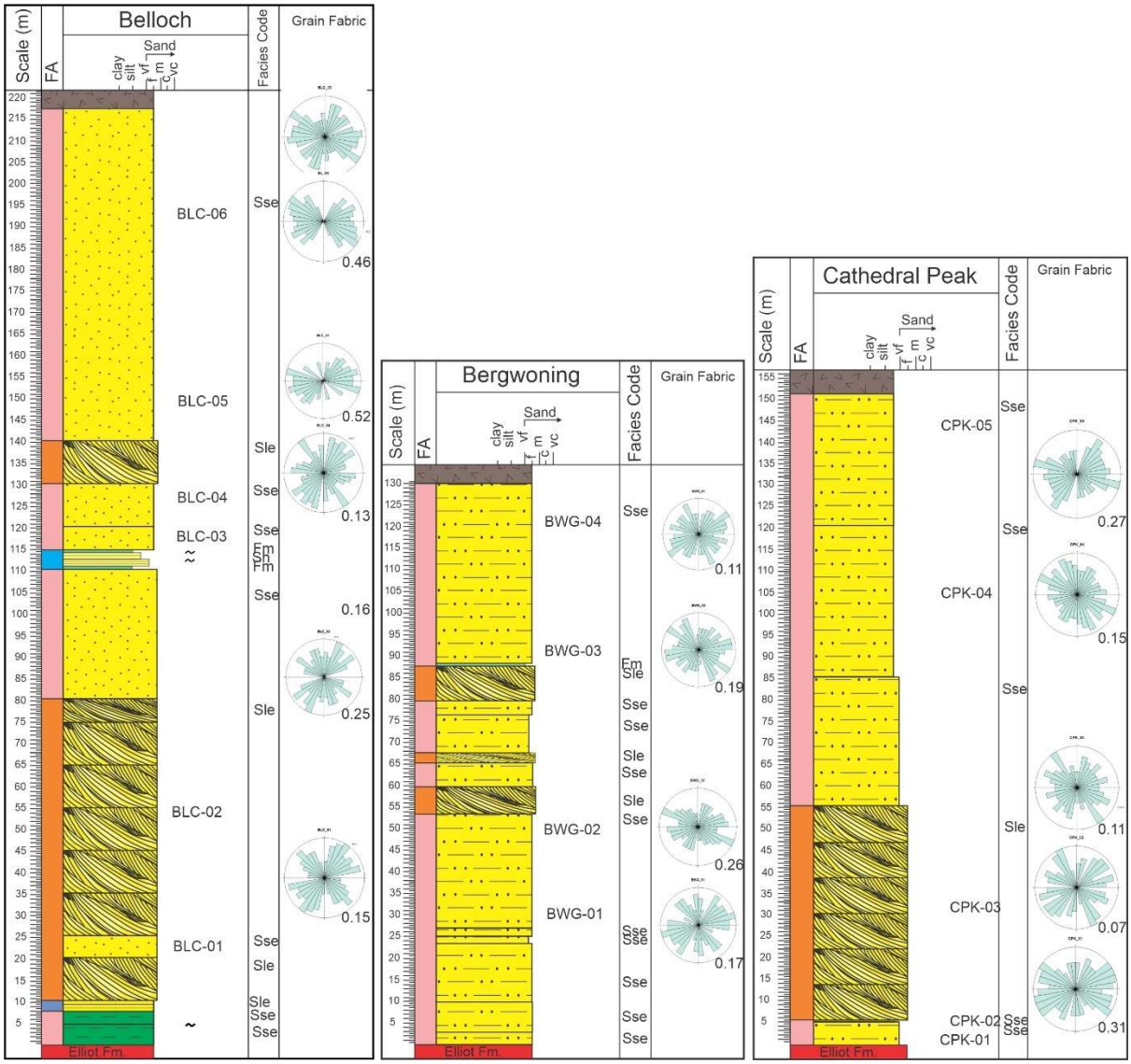
Belloch
Scale (m)
FA
clay
silt
Sand
vf
m
c
vc
Facies Code
Grain Fabric
BLC-06
BLC-05
BLC-04
BLC-03
BLC-02
BLC-01
Sse
Sle
Sse
Fm
Sse
Sle
Sse
Sle
Sse
Sse
0.46
0.52
0.13
0.16
0.25
0.15
Elliot Fm
Bergwoning
BWG-04
BWG-03
BWG-02
BWG-01
Sse
Fm
Sle
Sse
Sse
Sle
Sse
Sle
Sse
Sse
Sse
Sse
Sse
0.11
0.19
0.26
0.17
Elliot Fm
Cathedral Peak
CPK-05
CPK-04
CPK-03
CPK-02
CPK-01
Sse
Sse
Sse
Sle
Sse
Sse
0.27
0.15
0.11
0.07
0.31
Elliot Fm

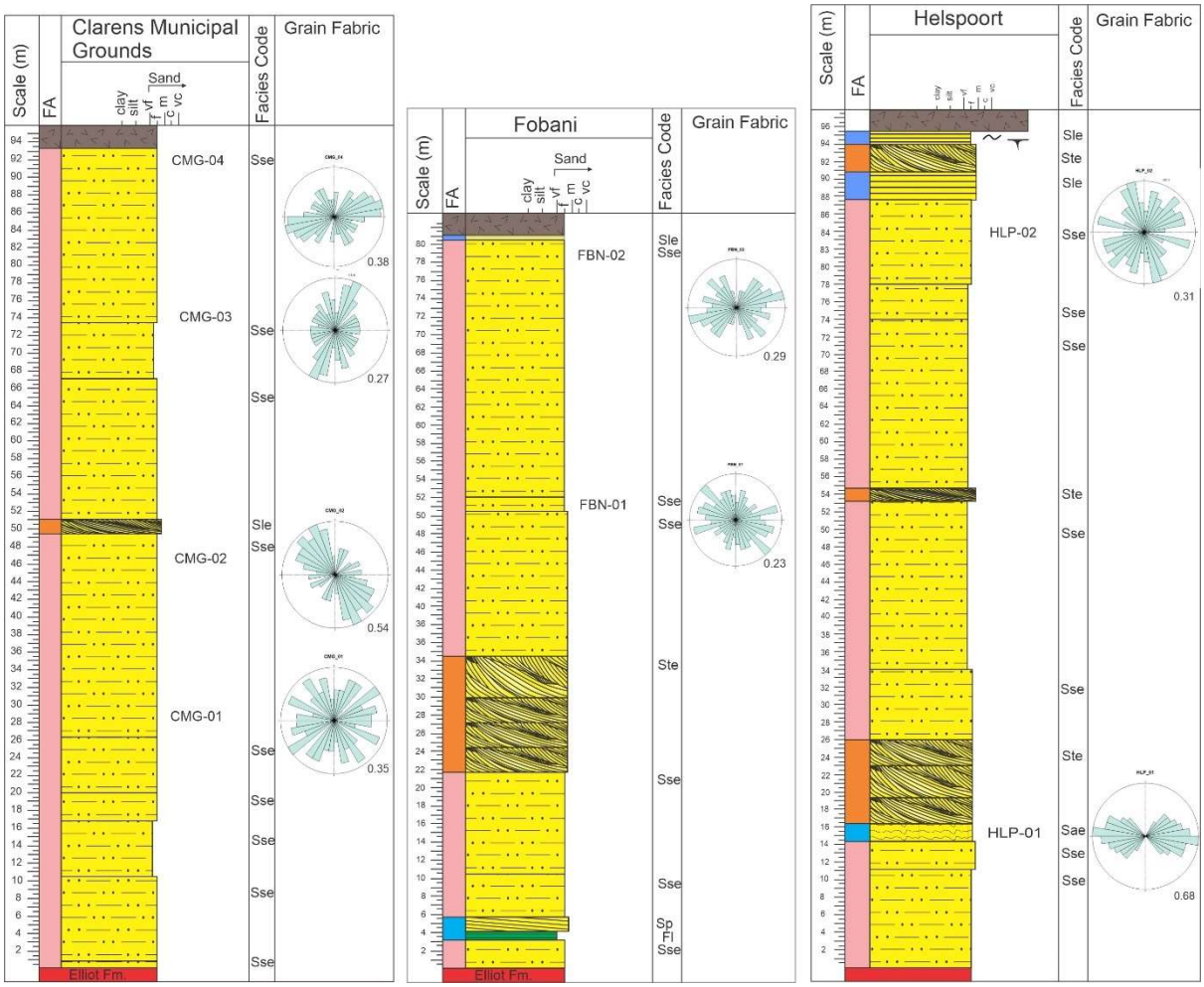
Clarens Municipal Grounds
Scale (m)
FA
Facies Code
Grain Fabric
Sand
clay
silt
vf
f
m
c
vc
CMG-04
CMG-03
CMG-02
CMG-01
Elliot Fm.
0.38
0.27
0.54
0.35
Fobani
FBN-02
FBN-01
0.29
0.23
Helspoort
HLP-02
HLP-01
0.31
0.68

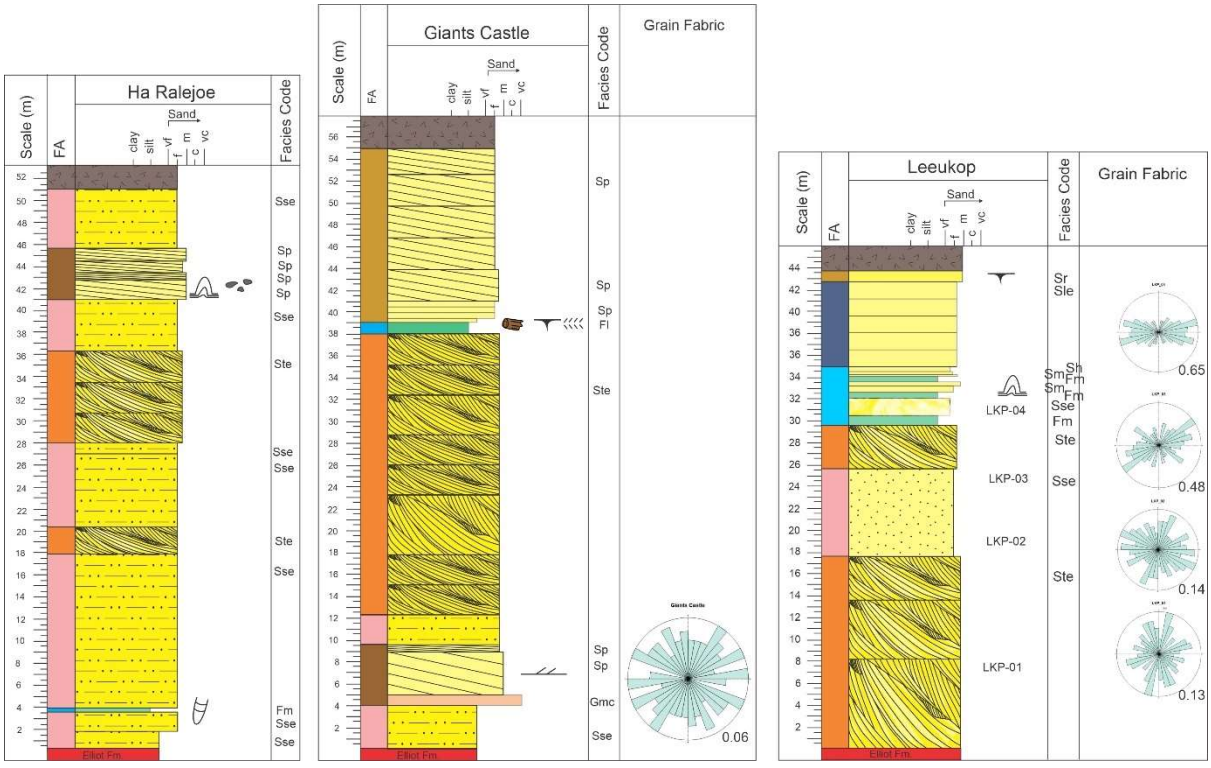
Ha Ralejoe
Giants Castle
Leeukop
LKP-04
LKP-03
LKP-02
LKP-01
0.06
0.65
0.48
0.14
0.13

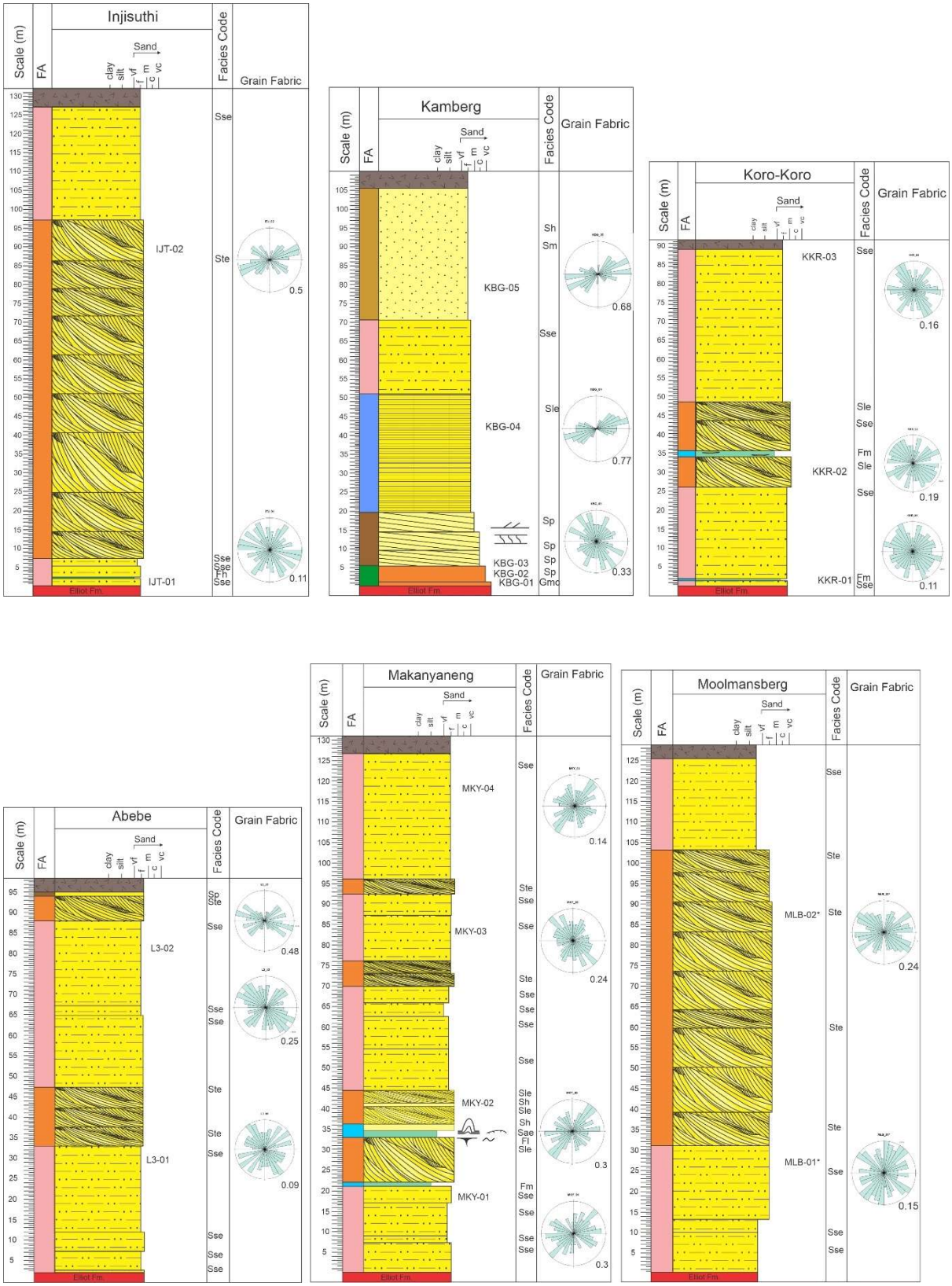
Injisuthi
Scale (m)
FA
Sand
clay
silt
vf
f
m
c
vc
Facies Code
Grain Fabric
IJT-02
IJT-01
Elliot Fm
Sse
Ste
Fm
0.5
0.11
Kamberg
KBG-05
KBG-04
KBG-03
KBG-02
KBG-01
Sh
Sm
Sle
Sp
Gmc
0.68
0.77
0.33
Koro-Koro
KKR-03
KKR-02
KKR-01
0.16
0.19
0.11
Abebe
L3-02
L3-01
0.48
0.25
0.09
Makanyaneng
MKY-04
MKY-03
MKY-02
MKY-01
0.14
0.24
0.3
0.3
Moolmansberg
MLB-02*
MLB-01*
0.24
0.15

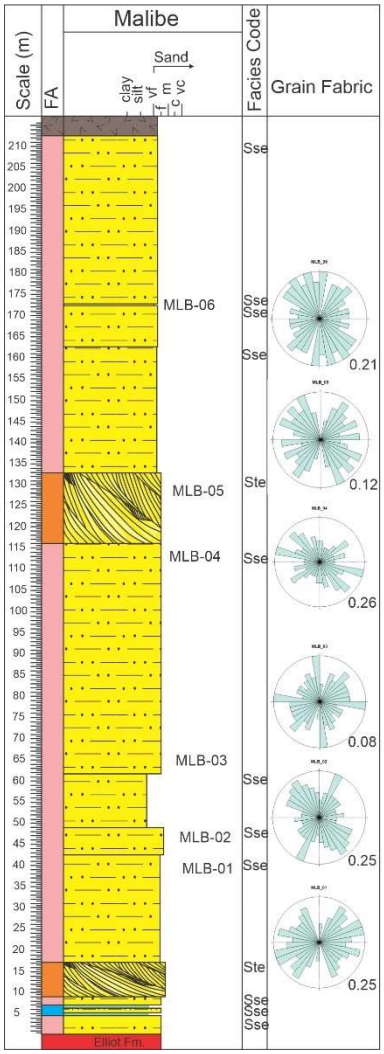
Malibe
Scale (m)
FA
Sand
clay
silt
vf
f
m
c
vc
Facies Code
Grain Fabric
MLB-06
MLB-05
MLB-04
MLB-03
MLB-02
MLB-01
Sse
Ste
0.21
0.12
0.26
0.08
0.25
0.25
Elliot Fm

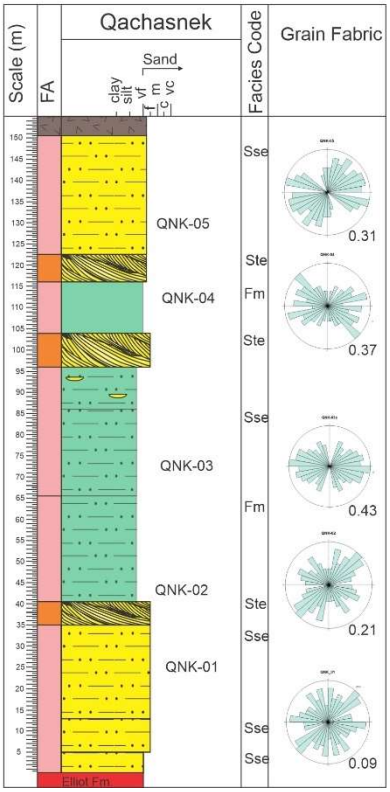
Qachasnek
Scale (m)
FA
Sand
clay
silt
vf
f
m
c
vc
Facies Code
Grain Fabric
QNK-05
QNK-04
QNK-03
QNK-02
QNK-01
Sse
Ste
Fm
0.31
0.37
0.43
0.21
0.09
Elliot Fm

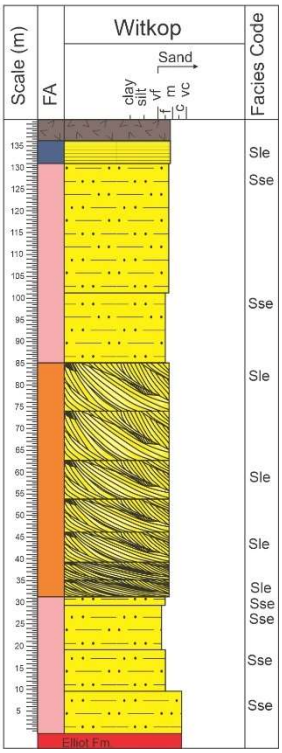
Witkop
Scale (m)
FA
Sand
clay
silt
vf
f
m
c
vc
Facies Code
Sle
Sse
Elliot Fm

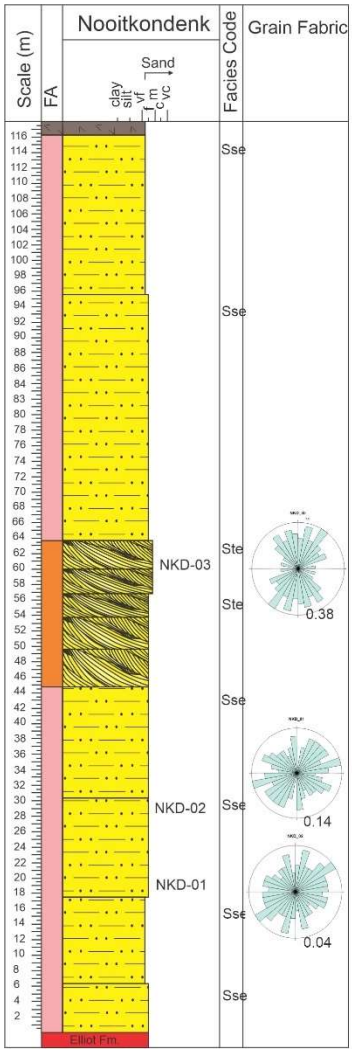
Nooitkondenk
Scale (m)
FA
Facies Code
Grain Fabric
Sand
clay
silt
vf
f
m
c
vc
NKD-03
NKD-02
NKD-01
Elliot Fm.
Sse
Ste
0.38
0.14
0.04

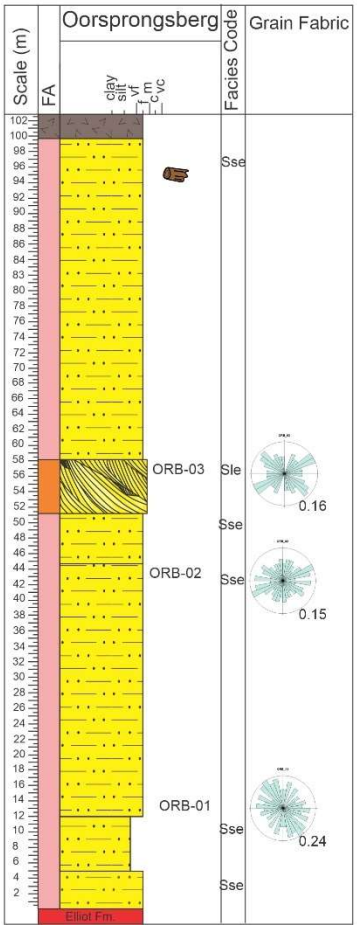
Oorsprongsberg
Scale (m)
FA
Facies Code
Grain Fabric
clay
silt
vf
f
m
c
vc
ORB-03
ORB-02
ORB-01
Elliot Fm.
Sse
Sle
0.16
0.15
0.24

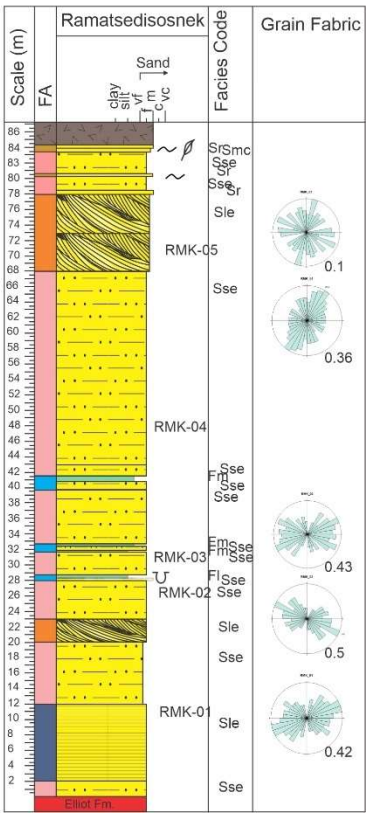
Ramatsedisosnek
Scale (m)
FA
Facies Code
Grain Fabric
Sand
clay
silt
vf
f
m
c
vc
RMK-05
RMK-04
RMK-03
RMK-02
RMK-01
Elliot Fm.
Sse
Sle
0.1
0.36
0.43
0.5
0.42

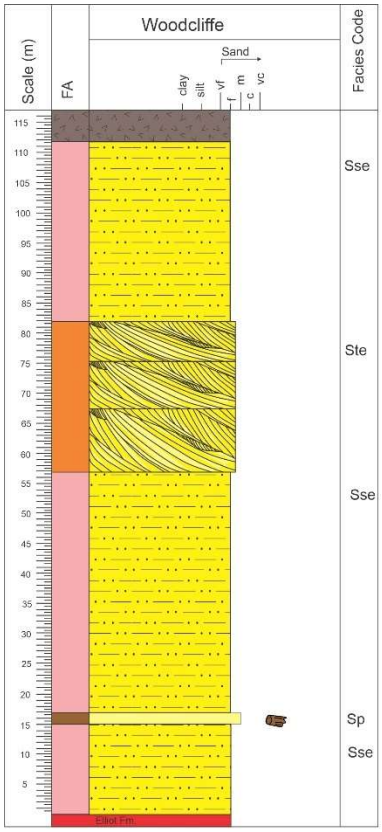
Woodcliffe
Scale (m)
FA
Sand
clay
silt
vf
f
m
c
vc
Facies Code
Sse
Ste
Sse
Sp
Sse
Elliot Fm

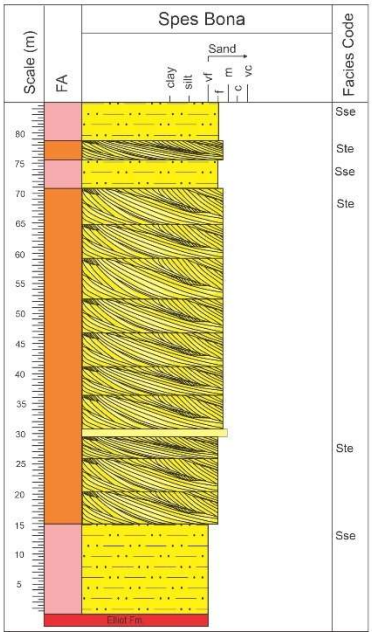
Spes Bona
Scale (m)
FA
Sand
clay
silt
vf
f
m
c
vc
Facies Code
Sse
Ste
Sse
Ste
Ste
Sse
Elliot Fm

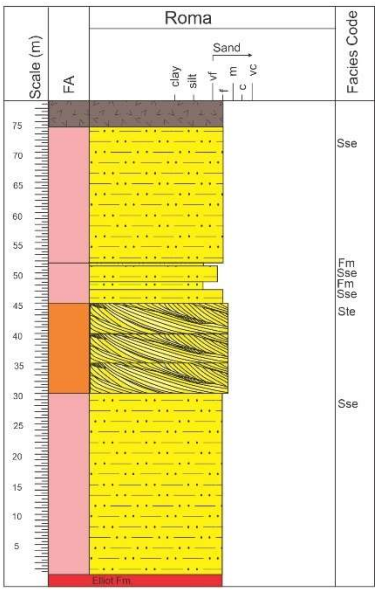
Roma
Scale (m)
FA
Sand
clay
silt
vf
f
m
c
vc
Facies Code
Sse
Fm
Sse
Fm
Sse
Ste
Sse
Elliot Fm

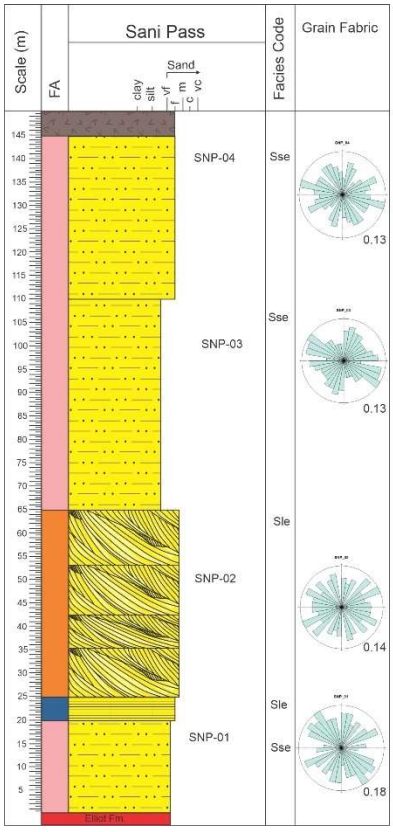
Sani Pass
Scale (m)
FA
Sand
clay
silt
vf
f
m
c
vc
Facies Code
Grain Fabric
SNP-04
SNP-03
SNP-02
SNP-01
Sse
Sse
Sle
Sle
Sse
0.13
0.13
0.14
0.18
Elliot Fm

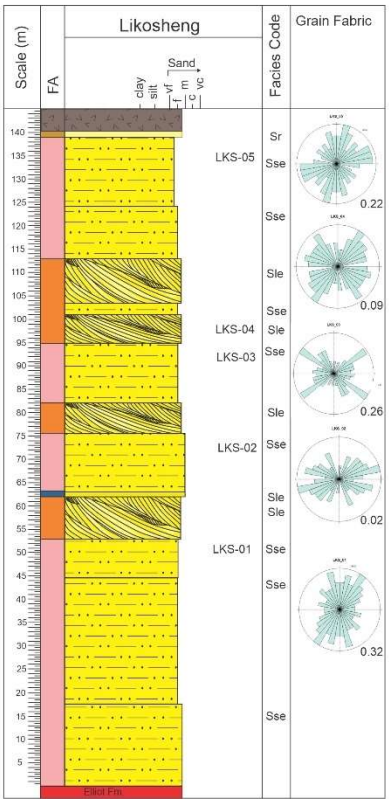
Likosheng
Scale (m)
FA
Sand
clay
silt
vf
f
m
c
vc
Facies Code
Grain Fabric
LKS-05
LKS-04
LKS-03
LKS-02
LKS-01
Sr
Sse
Sse
Sle
Sse
Sle
Sse
Sle
Sle
Sse
Sse
Sse
0.22
0.09
0.26
0.02
0.32
Elliot Fm

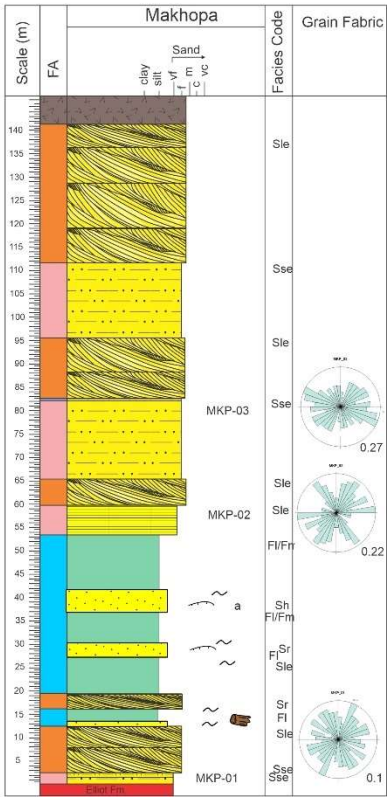
Makhopa
Scale (m)
FA
Sand
clay
silt
vf
f
m
c
vc
Facies Code
Grain Fabric
MKP-03
MKP-02
MKP-01
Sle
Sse
Sle
Sse
Sle
Fl/Fm
Sh
Fl/Fm
Sr
Fl
Sle
Sr
Fl
Sle
Sse
Sse
a
0.27
0.22
0.1
Elliot Fm

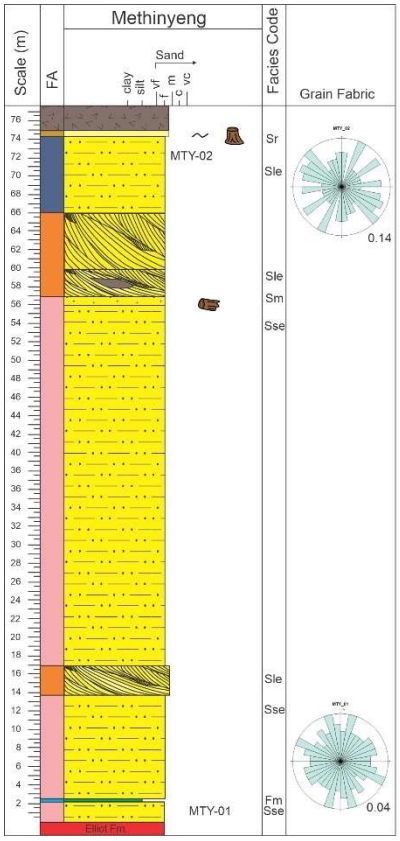
Methinyeng
Scale (m)
FA
Sand
clay
silt
vf
f
m
c
vc
Facies Code
Grain Fabric
MTY-02
MTY-01
Sr
Sle
Sle
Sm
Sse
Sle
Sse
Fm
Sse
0.14
0.04
Elliot Fm.

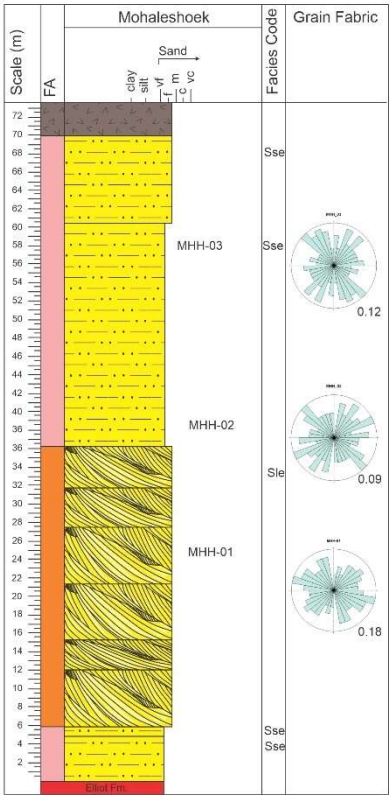
Mohaleshoek
Scale (m)
FA
Sand
clay
silt
vf
f
m
c
vc
Facies Code
Grain Fabric
MHH-03
MHH-02
MHH-01
Sse
Sse
Sle
Sse
Sse
0.12
0.09
0.18
Elliot Fm.

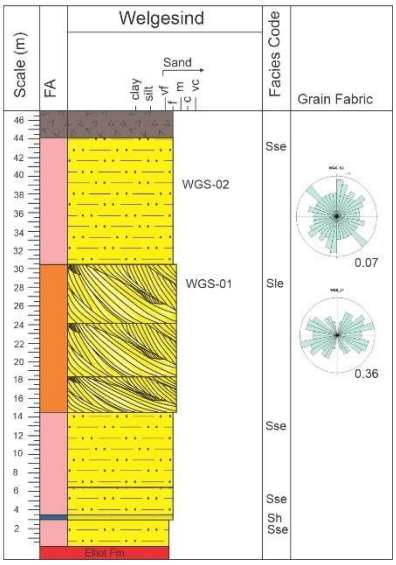
Welgesind
Scale (m)
FA
Sand
clay
silt
vf
f
m
c
vc
Facies Code
Grain Fabric
WGS-02
WGS-01
Sse
Sle
Sse
Sse
Sh
Sse
0.07
0.36
Elliot Fm.

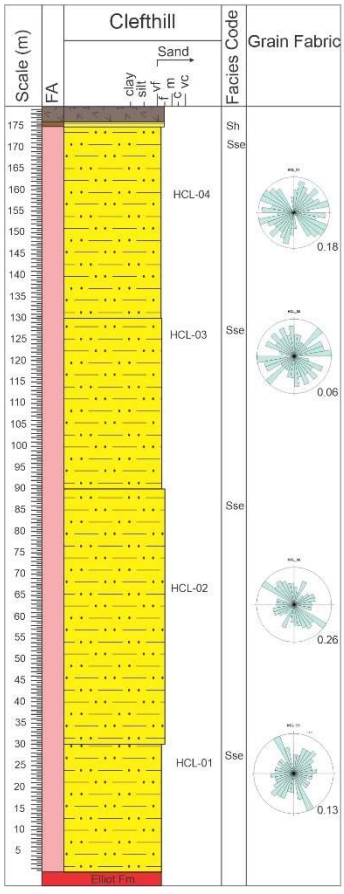
Clefthill
Scale (m)
FA
Sand
clay
silt
vf
f
m
c
vc
Facies Code
Grain Fabric
HCL-04
HCL-03
HCL-02
HCL-01
Sh
Sse
Sse
Sse
Sse
0.18
0.06
0.26
0.13
Elliot Fm.

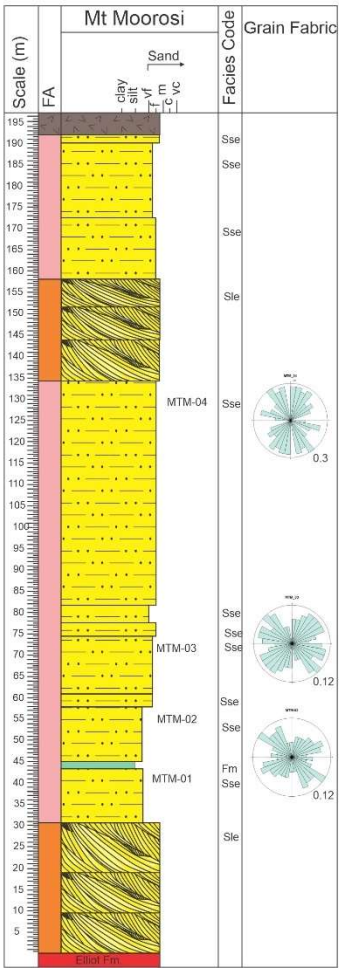
Mt Moorosi
Scale (m)
FA
Sand
clay
silt
vf
f
m
c
vc
Facies Code
Grain Fabric
MTM-04
MTM-03
MTM-02
MTM-01
Sse
Sse
Sse
Sle
Sse
Sse
Sse
Sse
Fm
Sse
Sle
0.3
0.12
0.12
Elliot Fm.

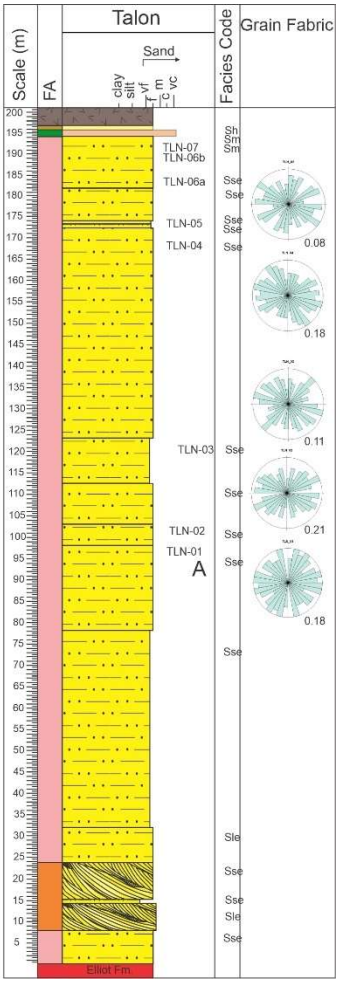
Talon
Scale (m)
FA
Sand
clay
silt
vf
f
m
c
vc
Facies Code
Grain Fabric
TLN-07
TLN-06b
TLN-06a
TLN-05
TLN-04
TLN-03
TLN-02
TLN-01
A
Sh
Sse
Sse
Sse
Sse
Sse
Sse
Sse
Sse
Sle
Sse
Sse
Sle
Sse
0.08
0.18
0.11
0.21
0.18
Elliot Fm.

Appendix 4: Re-interpretation of sedimentary logs from Beukes (1969). Note that sedimentary logs at study location of this current study are not re-interpreted. For facies codes, see Table 4.1 in Chapter 4.

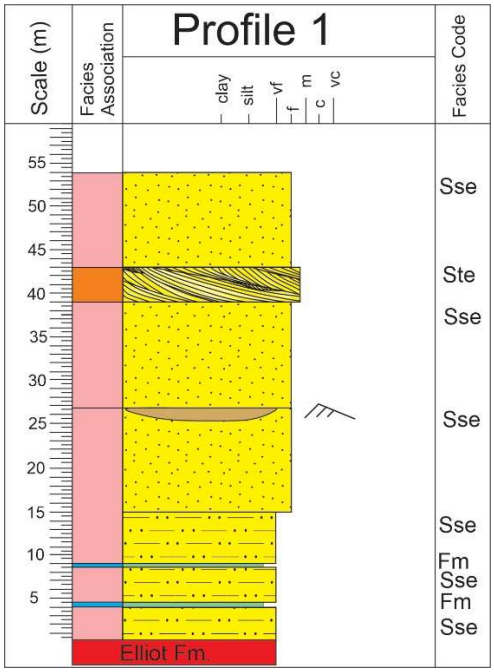

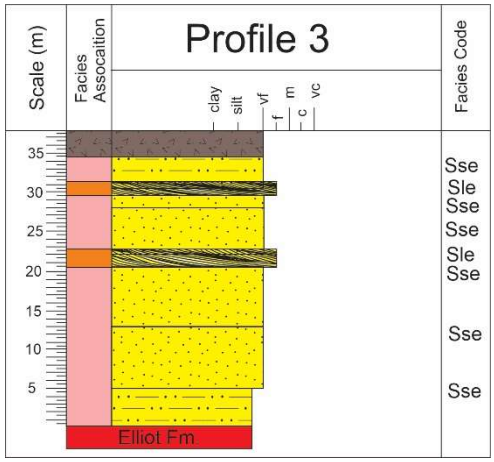

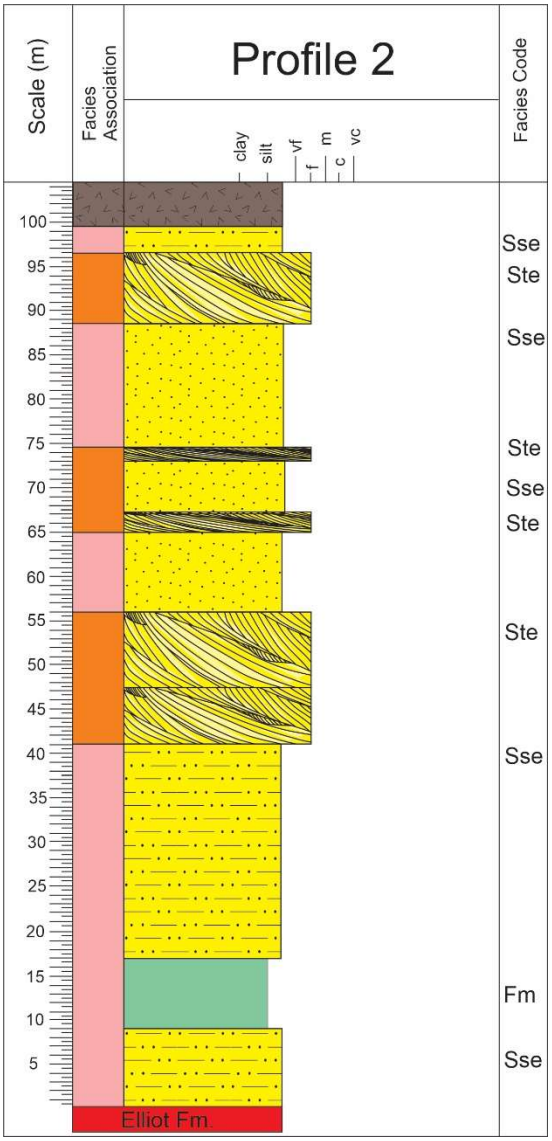

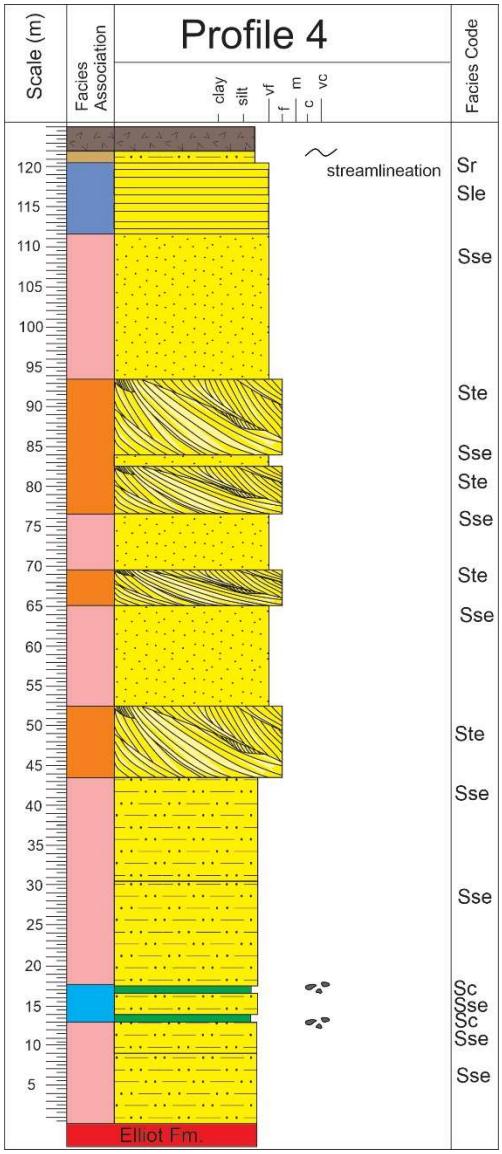
Profile 4
Scale (m)
Facies Association
clay
silt
vf
f
m
c
vc
Facies Code
streamlineation
Sr
Sle
Sse
Ste
Sse
Ste
Sse
Ste
Sse
Ste
Sse
Sse
Sc
Sse
Sc
Sse
Sse
Elliot Fm.

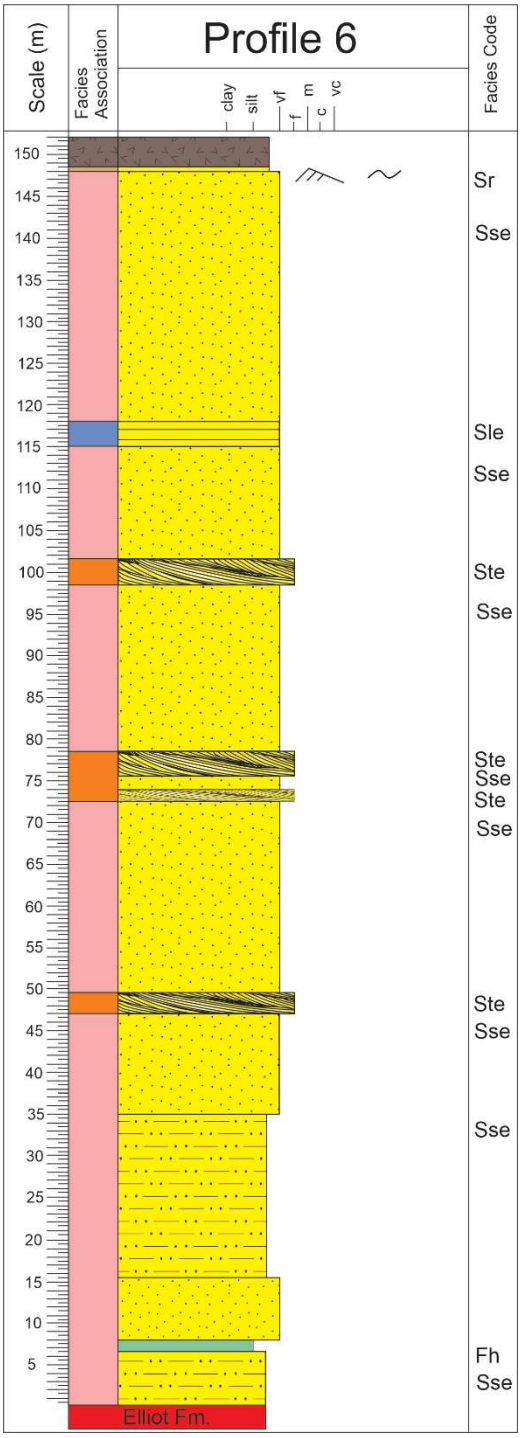
Profile 6
Scale (m)
Facies Association
clay
silt
vf
f
m
c
vc
Facies Code
Sr
Sse
Sle
Sse
Ste
Sse
Ste
Sse
Ste
Sse
Sse
Ste
Sse
Sse
Fh
Sse
Elliot Fm.

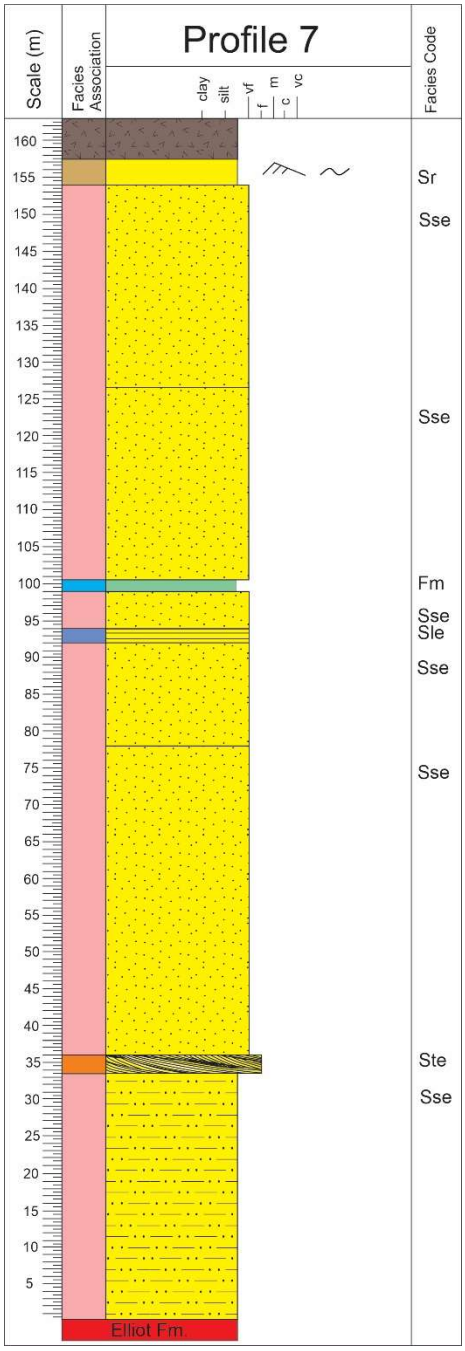
Profile 7
Scale (m)
Facies Association
clay
silt
vf
f
m
c
vc
Facies Code
Sr
Sse
Sse
Fm
Sse
Sle
Sse
Sse
Ste
Sse
Elliot Fm

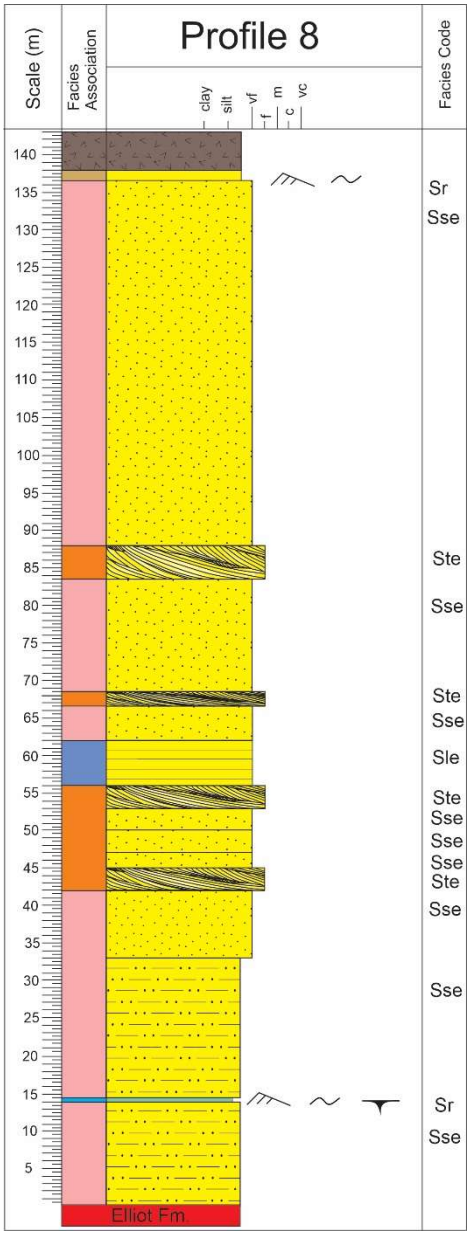
Profile 8
Scale (m)
Facies Association
clay
silt
vf
f
m
c
vc
Facies Code
Sr
Sse
Ste
Sse
Ste
Sse
Sle
Ste
Sse
Sse
Sse
Ste
Sse
Sse
Sr
Sse
Elliot Fm

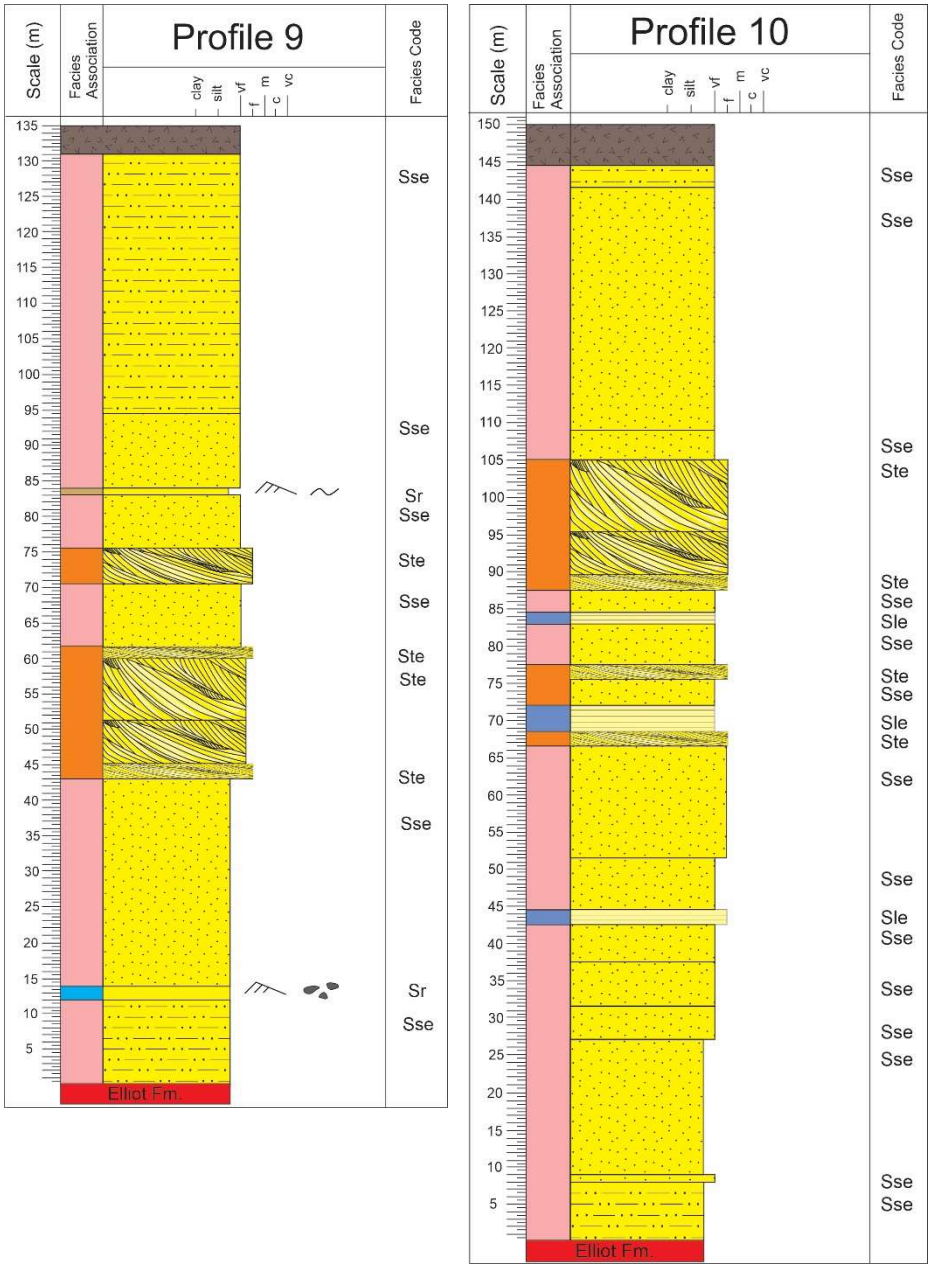
Profile 9
Scale (m)
Facies Association
clay
silt
vf
f
m
c
vc
Facies Code
135
130
125
120
115
110
105
100
95
90
85
80
75
70
65
60
55
50
45
40
35
30
25
20
15
10
5
Sse
Sse
Sr
Sse
Ste
Sse
Ste
Ste
Ste
Sse
Sr
Sse
Elliot Fm.
Profile 10
Scale (m)
Facies Association
clay
silt
vf
f
m
c
vc
Facies Code
150
145
140
135
130
125
120
115
110
105
100
95
90
85
80
75
70
65
60
55
50
45
40
35
30
25
20
15
10
5
Sse
Sse
Sse
Ste
Ste
Sse
Sle
Sse
Ste
Sse
Sle
Ste
Sse
Sse
Sle
Sse
Sse
Sse
Sse
Sse
Sse
Elliot Fm.

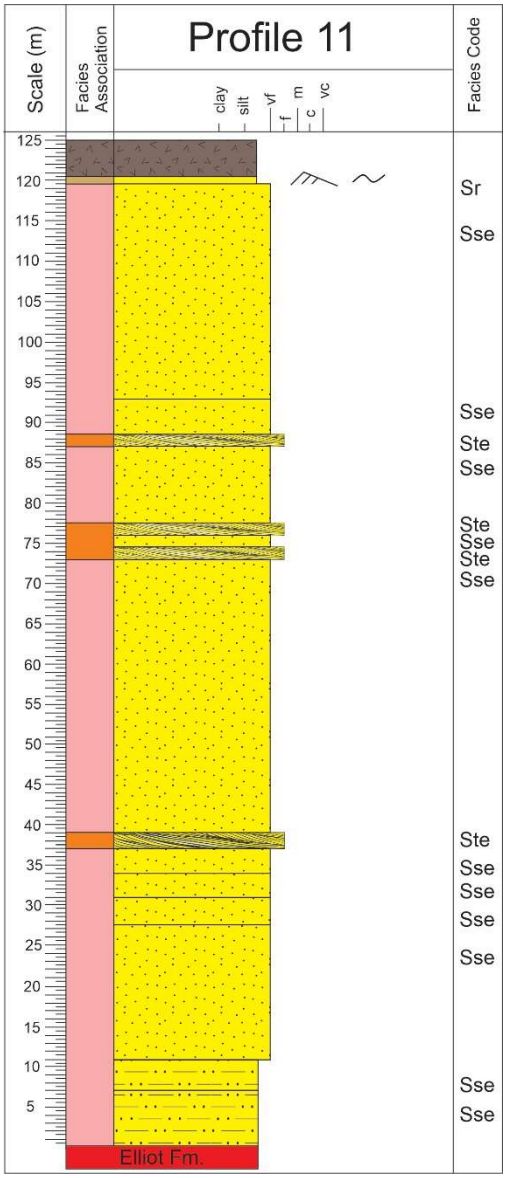
Profile 11
Scale (m)
Facies Association
clay
silt
vf
f
m
c
vc
Facies Code
125
120
115
110
105
100
95
90
85
80
75
70
65
60
55
50
45
40
35
30
25
20
15
10
5
Sr
Sse
Sse
Ste
Sse
Ste
Sse
Ste
Sse
Ste
Sse
Sse
Sse
Sse
Sse
Sse
Sse
Elliot Fm.

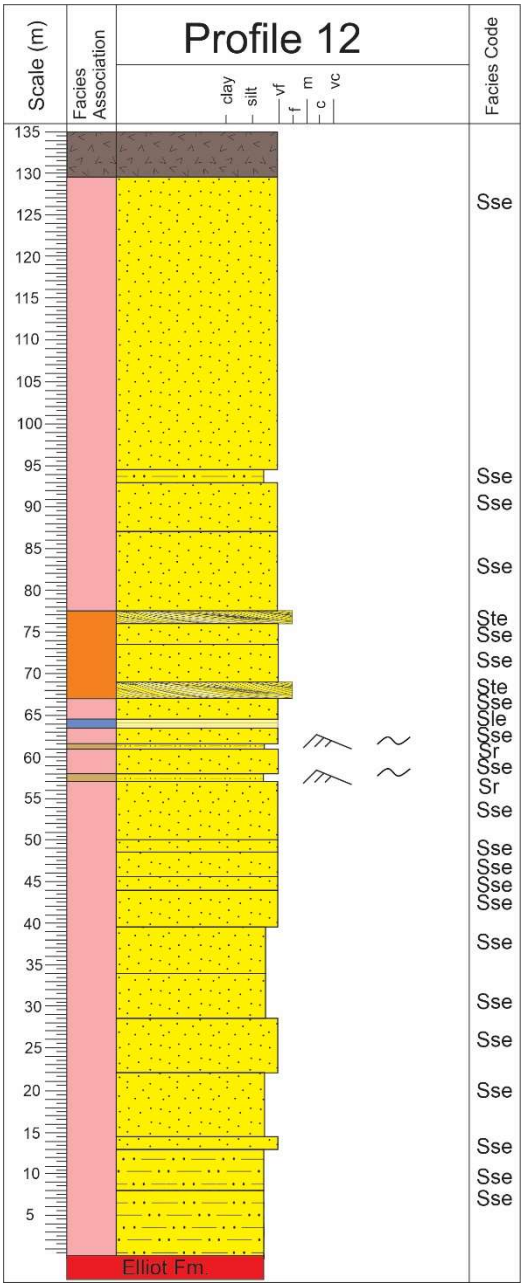
Profile 12
Scale (m)
Facies Association
clay
silt
vf
f
m
c
vc
Facies Code
135
130
125
120
115
110
105
100
95
90
85
80
75
70
65
60
55
50
45
40
35
30
25
20
15
10
5
Sse
Sse
Sse
Sse
Ste
Sse
Sse
Ste
Sse
Sle
Sse
Sr
Sse
Sr
Sse
Sse
Sse
Sse
Sse
Sse
Sse
Sse
Sse
Sse
Sse
Elliot Fm.

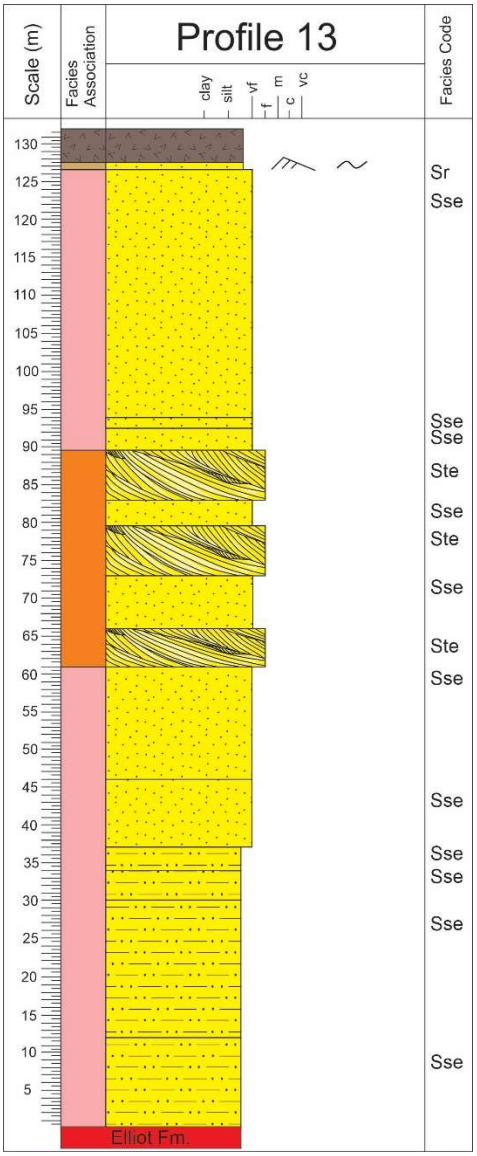
Profile 13
Scale (m)
Facies Association
clay
silt
vf
f
m
c
vc
Facies Code
Sr
Sse
Sse
Sse
Ste
Sse
Ste
Sse
Ste
Sse
Sse
Sse
Sse
Sse
Sse
Elliot Fm.

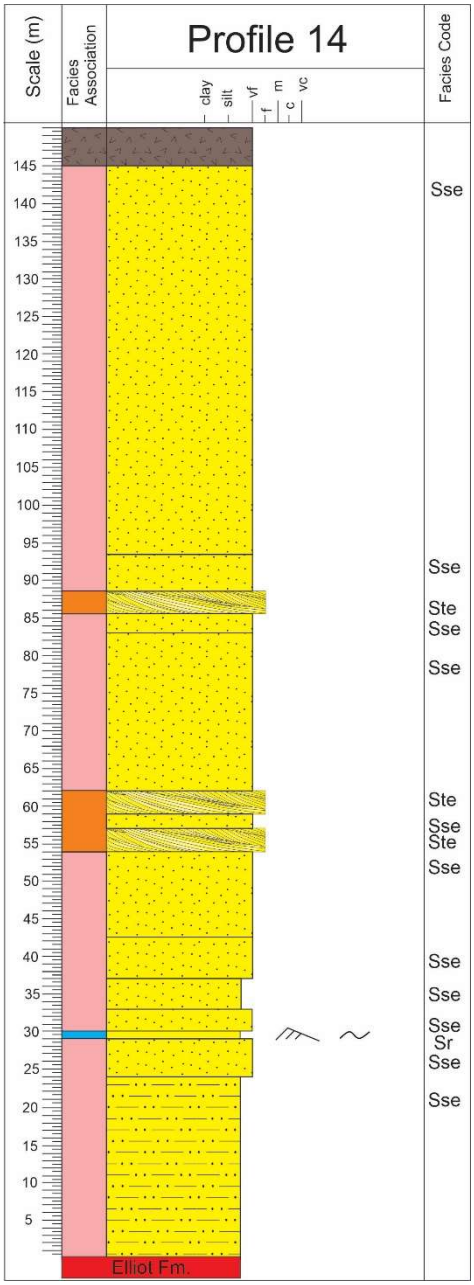
Profile 14
Scale (m)
Facies Association
clay
silt
vf
f
m
c
vc
Facies Code
Sse
Sse
Ste
Sse
Sse
Ste
Sse
Sse
Sse
Sse
Sse
Sr
Sse
Sse
Elliot Fm.

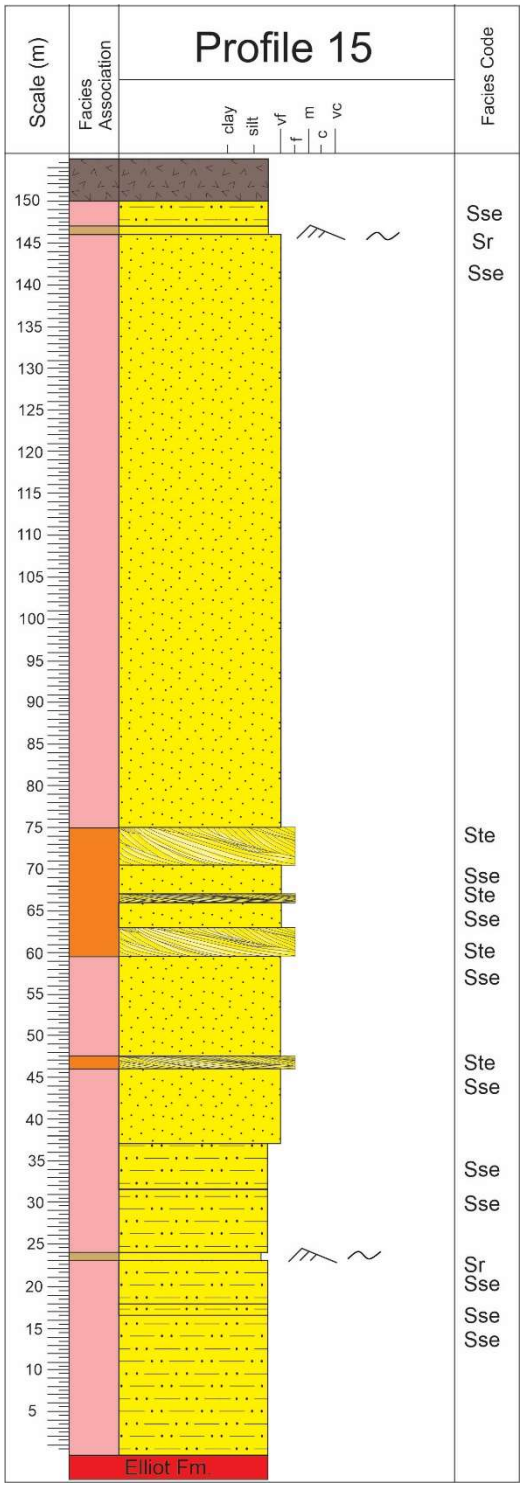
Profile 15
Scale (m)
Facies Association
clay
silt
vf
f
m
c
vc
Facies Code
150
145
140
135
130
125
120
115
110
105
100
95
90
85
80
75
70
65
60
55
50
45
40
35
30
25
20
15
10
5
Sse
Sr
Sse
Ste
Sse
Ste
Sse
Ste
Sse
Ste
Sse
Sse
Sse
Sr
Sse
Sse
Sse
Elliot Fm

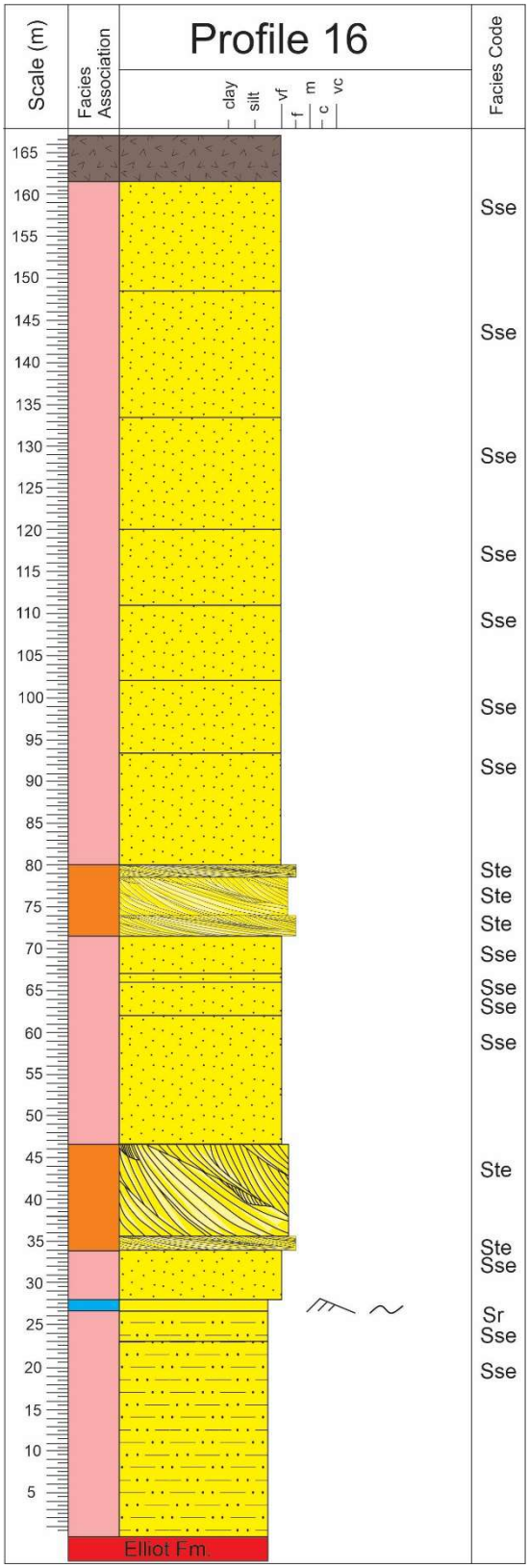
Profile 16
Scale (m)
Facies Association
clay
silt
vf
f
m
c
vc
Facies Code
165
160
155
150
145
140
135
130
125
120
115
110
105
100
95
90
85
80
75
70
65
60
55
50
45
40
35
30
25
20
15
10
5
Sse
Sse
Sse
Sse
Sse
Sse
Sse
Ste
Ste
Ste
Sse
Sse
Sse
Sse
Ste
Ste
Sse
Sr
Sse
Sse
Elliot Fm

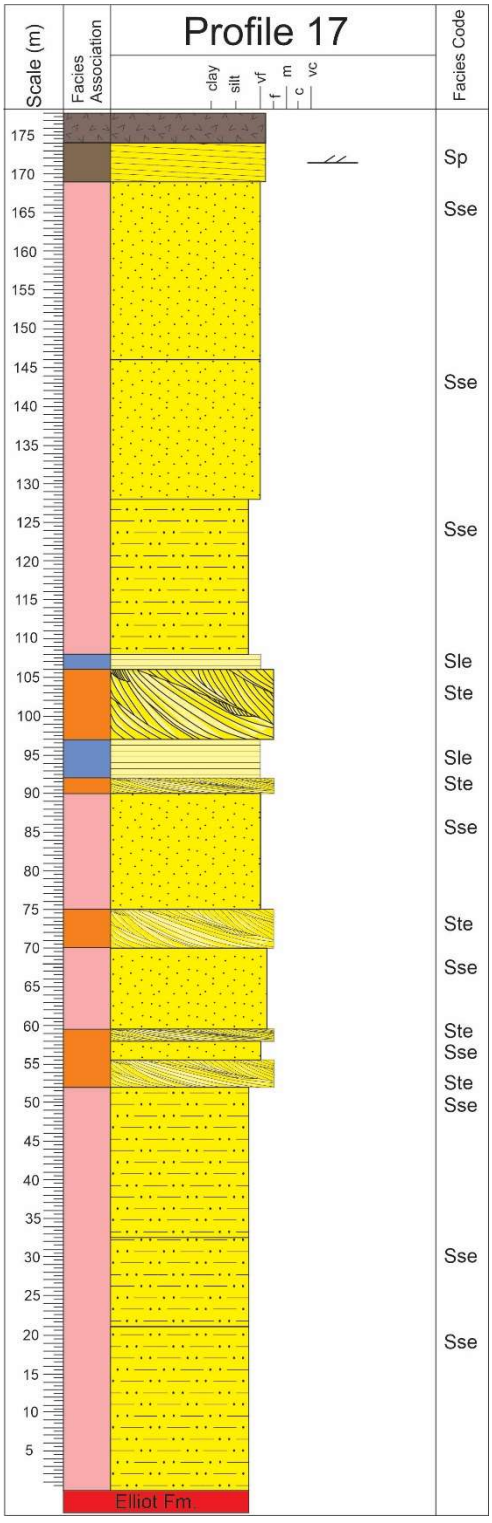
Profile 17
Scale (m)
Facies Association
clay
silt
vf
f
m
c
vc
Facies Code
175
170
165
160
155
150
145
140
135
130
125
120
115
110
105
100
95
90
85
80
75
70
65
60
55
50
45
40
35
30
25
20
15
10
5
Sp
Sse
Sse
Sse
Sle
Ste
Sle
Ste
Sse
Ste
Sse
Ste
Sse
Ste
Sse
Sse
Sse
Elliot Fm.

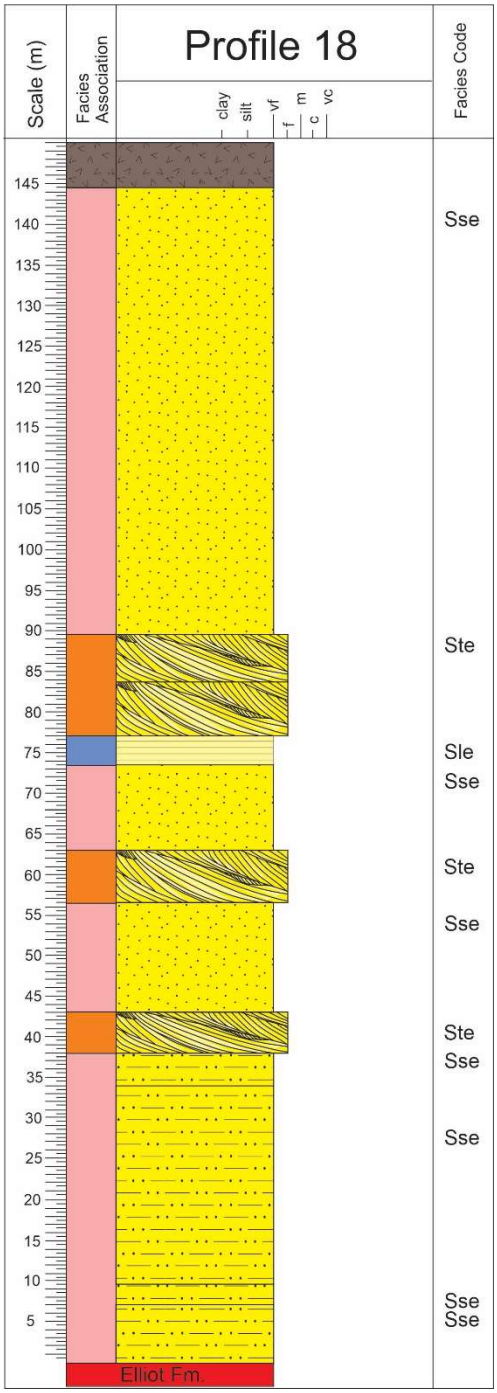
Profile 18
Scale (m)
Facies Association
clay
silt
vf
f
m
c
vc
Facies Code
145
140
135
130
125
120
115
110
105
100
95
90
85
80
75
70
65
60
55
50
45
40
35
30
25
20
15
10
5
Sse
Ste
Sle
Sse
Ste
Sse
Ste
Sse
Sse
Sse
Sse
Elliot Fm.

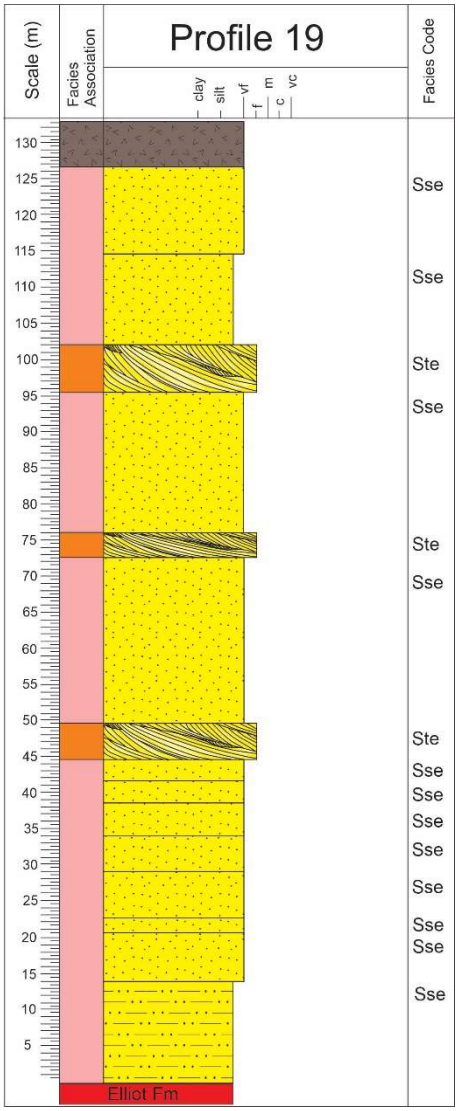
Profile 19
Scale (m)
Facies Association
clay
silt
vf
f
m
c
vc
Facies Code
130
125
120
115
110
105
100
95
90
85
80
75
70
65
60
55
50
45
40
35
30
25
20
15
10
5
Sse
Sse
Ste
Sse
Ste
Sse
Ste
Sse
Sse
Sse
Sse
Sse
Sse
Sse
Elliot Fm

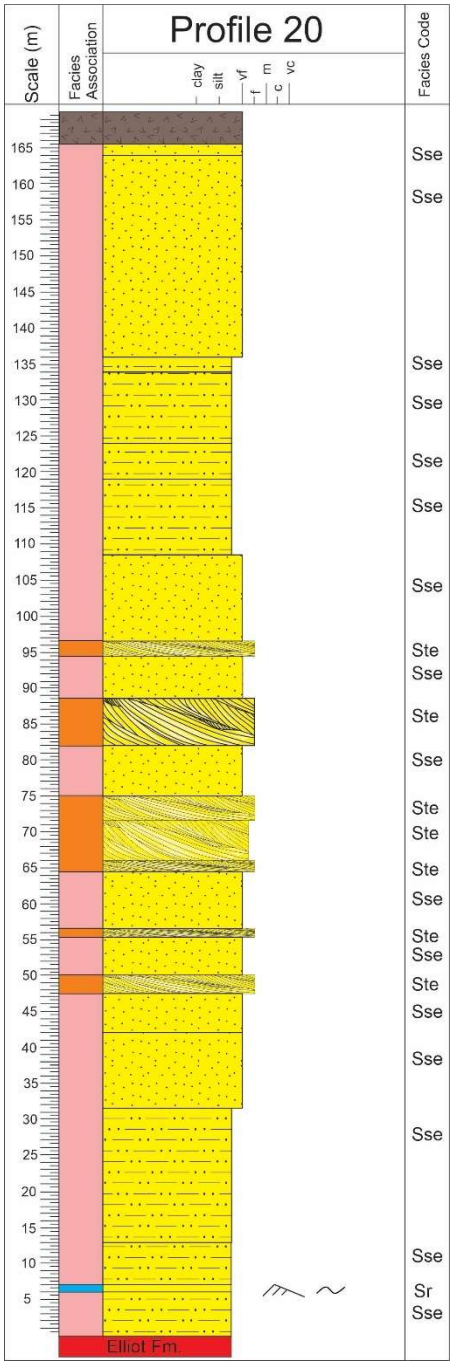
Profile 20
Scale (m)
Facies Association
clay
silt
vf
f
m
c
vc
Facies Code
165
160
155
150
145
140
135
130
125
120
115
110
105
100
95
90
85
80
75
70
65
60
55
50
45
40
35
30
25
20
15
10
5
Sse
Sse
Sse
Sse
Sse
Sse
Sse
Ste
Sse
Ste
Sse
Ste
Ste
Ste
Sse
Ste
Sse
Ste
Sse
Sse
Sse
Sse
Sr
Sse
Elliot Fm

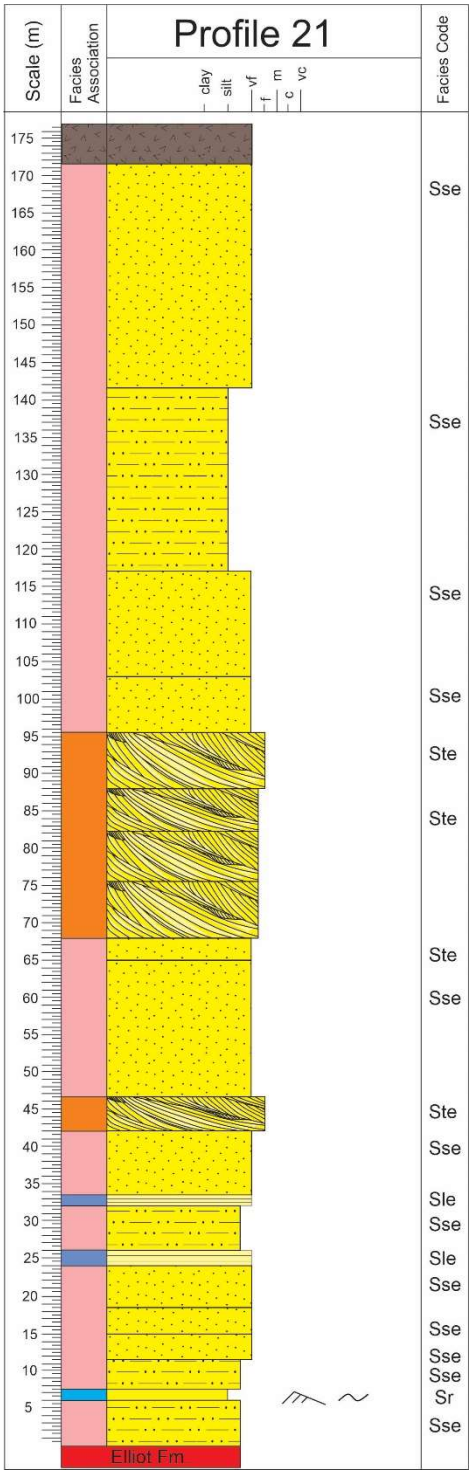
Profile 21
Scale (m)
Facies Association
clay
silt
vf
f
m
c
vc
Facies Code
175
170
165
160
155
150
145
140
135
130
125
120
115
110
105
100
95
90
85
80
75
70
65
60
55
50
45
40
35
30
25
20
15
10
5
Sse
Sse
Sse
Sse
Ste
Ste
Ste
Sse
Ste
Sse
Sle
Sse
Sle
Sse
Sse
Sse
Sse
Sr
Sse
Elliot Fm

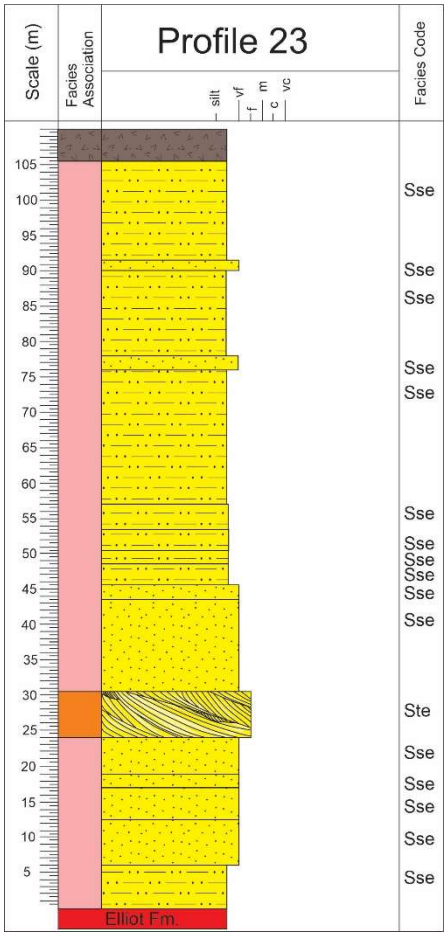
Profile 23
Scale (m)
Facies Association
silt
vf
f
m
c
vc
Facies Code
105
100
95
90
85
80
75
70
65
60
55
50
45
40
35
30
25
20
15
10
5
Sse
Sse
Sse
Sse
Sse
Sse
Sse
Sse
Sse
Sse
Sse
Ste
Sse
Sse
Sse
Sse
Sse
Elliot Fm.

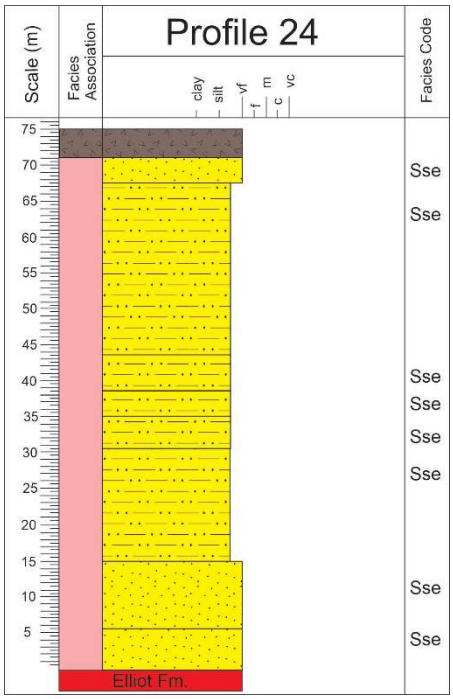
Profile 24
Scale (m)
Facies Association
clay
silt
vf
f
m
c
vc
Facies Code
75
70
65
60
55
50
45
40
35
30
25
20
15
10
5
Sse
Sse
Sse
Sse
Sse
Sse
Sse
Sse
Sse
Elliot Fm.

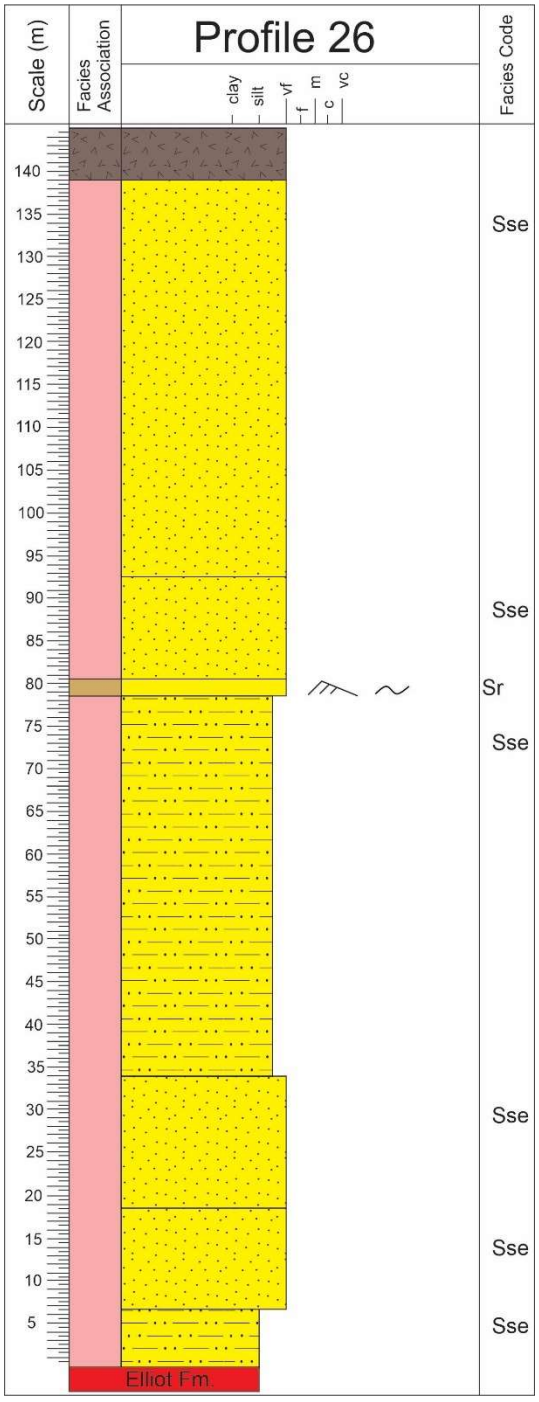
Profile 26
Scale (m)
Facies Association
clay
silt
vf
f
m
c
vc
Facies Code
140
135
130
125
120
115
110
105
100
95
90
85
80
75
70
65
60
55
50
45
40
35
30
25
20
15
10
5
Sse
Sse
Sr
Sse
Sse
Sse
Elliot Fm.

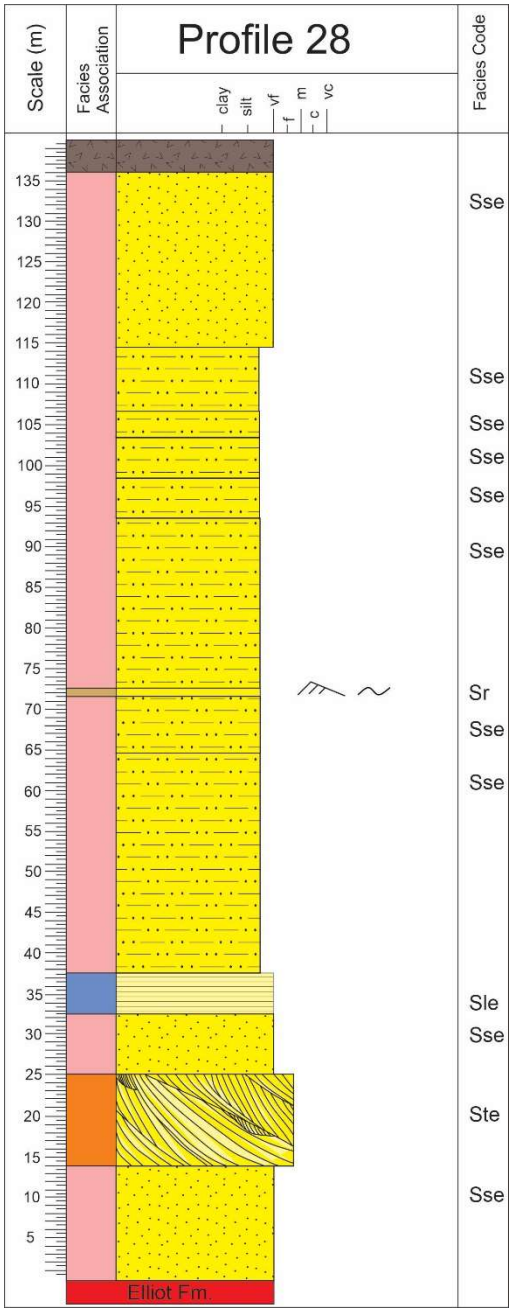
Profile 28
Scale (m)
Facies Association
clay
silt
vf
f
m
c
vc
Facies Code
135
130
125
120
115
110
105
100
95
90
85
80
75
70
65
60
55
50
45
40
35
30
25
20
15
10
5
Sse
Sse
Sse
Sse
Sse
Sr
Sse
Sse
Sle
Sse
Ste
Sse
Elliot Fm.

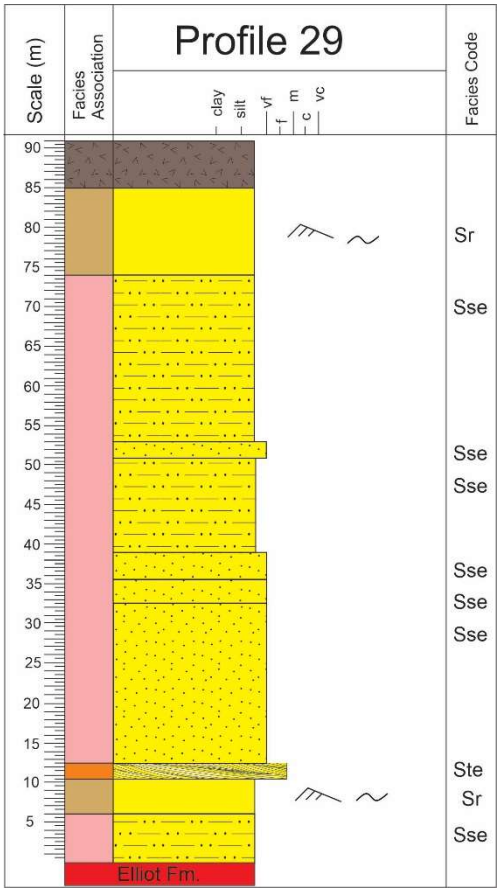
Profile 29
Scale (m)
Facies Association
clay
silt
vf
f
m
c
vc
Facies Code
90
85
80
75
70
65
60
55
50
45
40
35
30
25
20
15
10
5
Sr
Sse
Sse
Sse
Sse
Sse
Ste
Sr
Sse
Elliot Fm.

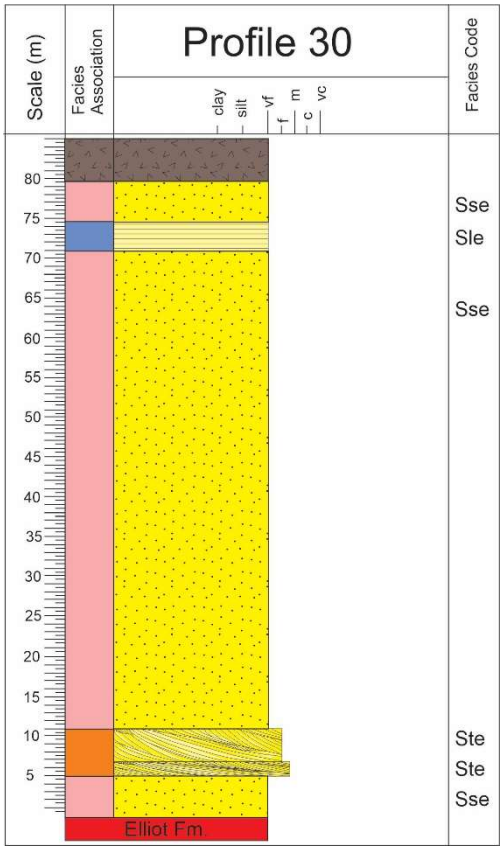
Profile 30
Scale (m)
Facies Association
clay
silt
vf
f
m
c
vc
Facies Code
80
75
70
65
60
55
50
45
40
35
30
25
20
15
10
5
Sse
Sle
Sse
Ste
Ste
Sse
Elliot Fm.

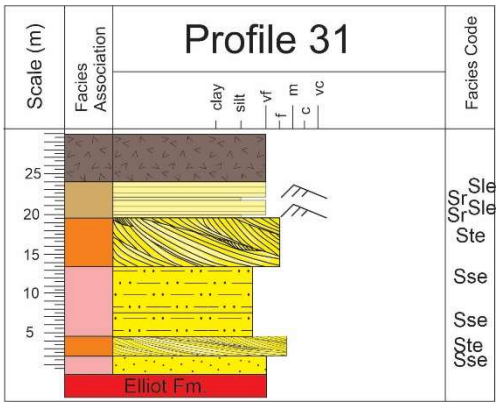
Profile 31
Scale (m)
Facies Association
clay
silt
vf
f
m
c
vc
Facies Code
25
20
15
10
5
Sr
Sr
Sle
Sle
Ste
Sse
Sse
Ste
Sse
Elliot Fm.

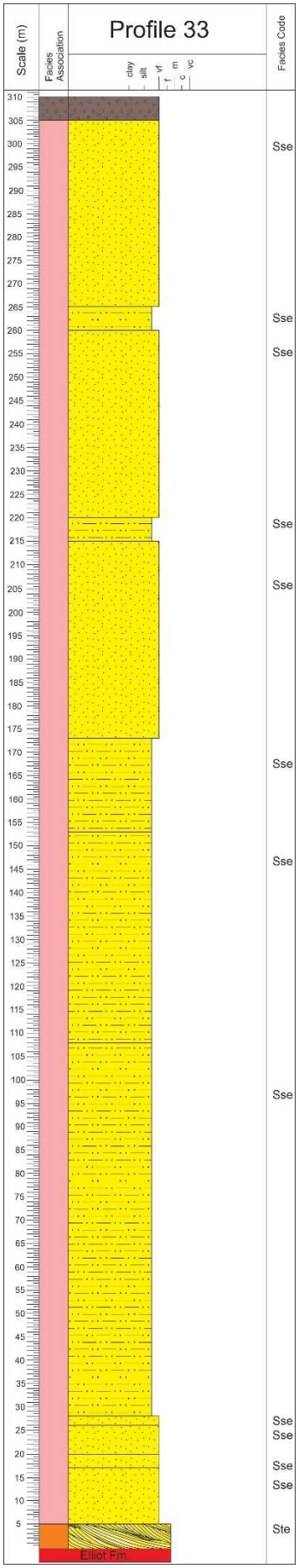
Profile 33
Scale (m)
Facies Association
clay
silt
vf
f
m
c
vc
Facies Code
Sse
Sse
Sse
Sse
Sse
Sse
Sse
Sse
Sse
Ste
Elliot Fm

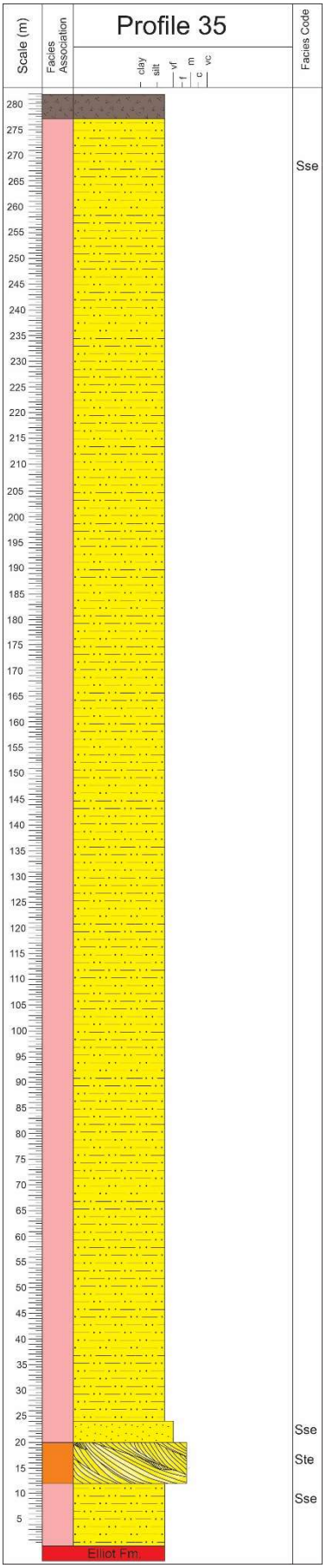
Profile 35
Scale (m)
Facies Association
clay
silt
vf
f
m
c
vc
Facies Code
Sse
Sse
Ste
Sse
Elliot Fm

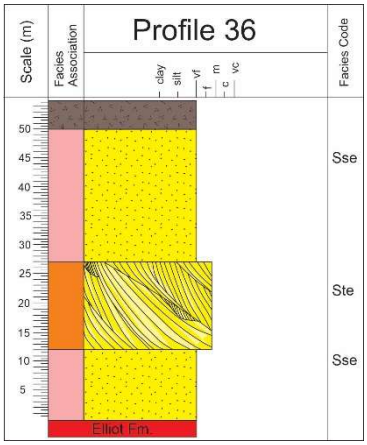
Profile 36
Scale (m)
Facies Association
Facies Code
clay
silt
vf
f
m
c
vc
50
45
40
35
30
25
20
15
10
5
Sse
Ste
Sse
Elliot Fm.

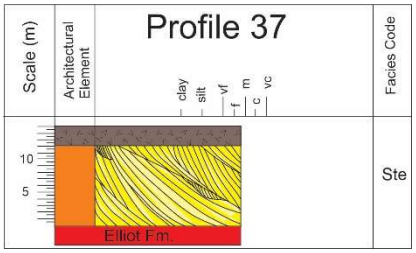
Profile 37
Scale (m)
Architectural Element
Facies Code
clay
silt
vf
f
m
c
vc
10
5
Ste
Elliot Fm.

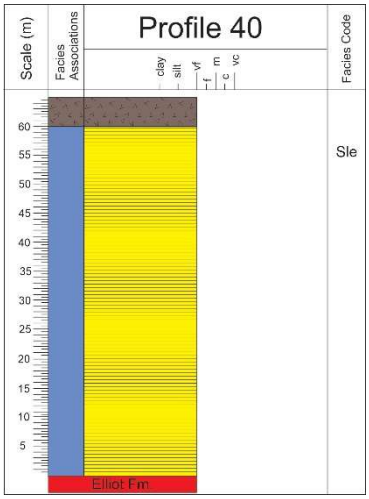
Profile 40
Scale (m)
Facies Associations
Facies Code
clay
silt
vf
f
m
c
vc
60
55
50
45
40
35
30
25
20
15
10
5
Sle
Elliot Fm.

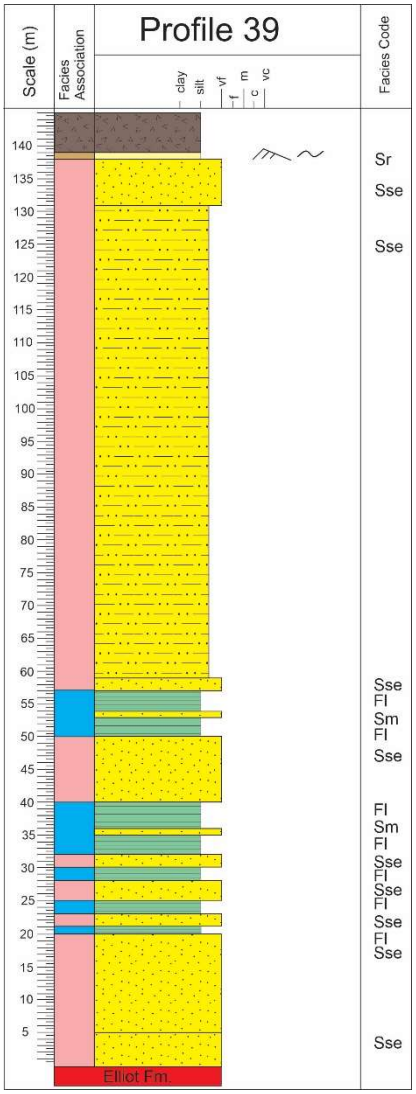
Profile 39
Scale (m)
Facies Association
Facies Code
clay
silt
vf
f
m
c
vc
140
135
130
125
120
115
110
105
100
95
90
85
80
75
70
65
60
55
50
45
40
35
30
25
20
15
10
5
Sr
Sse
Sse
Sse
Fl
Sm
Fl
Sse
Fl
Sm
Fl
Sse
Fl
Sse
Fl
Sse
Fl
Sse
Sse
Elliot Fm.

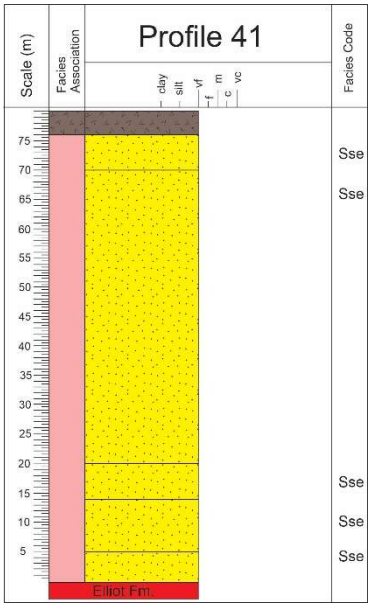
Profile 41
Scale (m)
Facies Association
Facies Code
clay
silt
vf
f
m
c
vc
75
70
65
60
55
50
45
40
35
30
25
20
15
10
5
Sse
Sse
Sse
Sse
Sse
Elliot Fm.

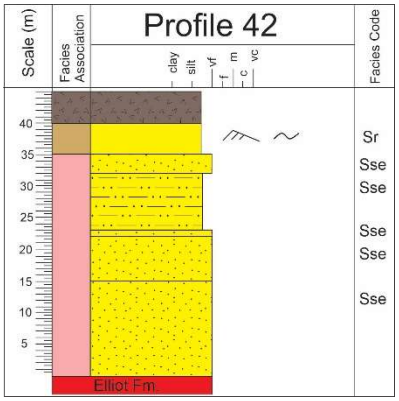
Profile 42
Scale (m)
Facies Association
clay
silt
vf
f
m
c
vc
Facies Code
40
35
30
25
20
15
10
5
Sr
Sse
Sse
Sse
Sse
Sse
Elliot Fm

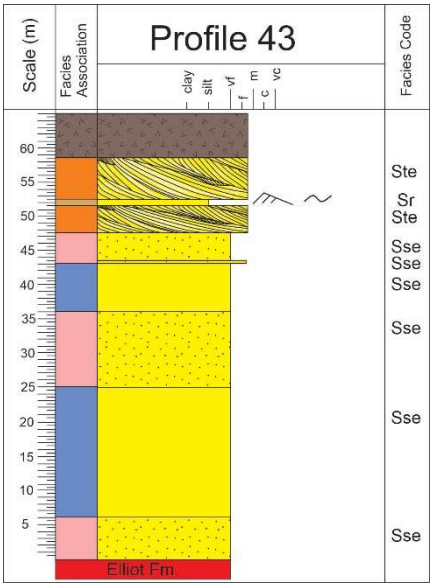
Profile 43
Scale (m)
Facies Association
clay
silt
vf
f
m
c
vc
Facies Code
60
55
50
45
40
35
30
25
20
15
10
5
Ste
Sr
Ste
Sse
Sse
Sse
Sse
Sse
Sse
Elliot Fm

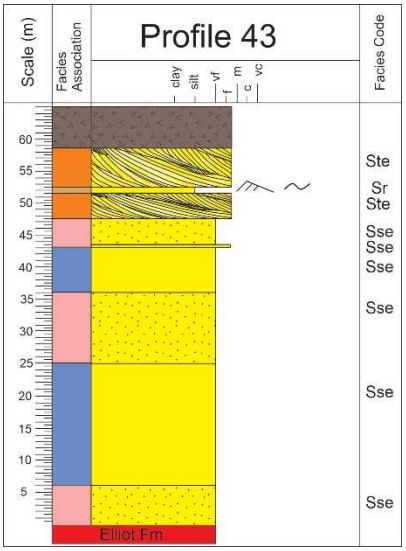
Profile 43
Scale (m)
Facies Association
clay
silt
vf
f
m
c
vc
Facies Code
60
55
50
45
40
35
30
25
20
15
10
5
Ste
Sr
Ste
Sse
Sse
Sse
Sse
Sse
Sse
Elliot Fm

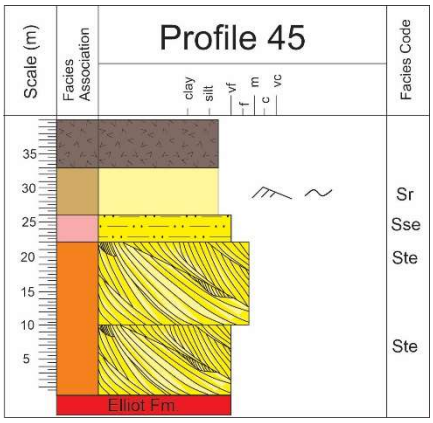
Profile 45
Scale (m)
Facies Association
clay
silt
vf
f
m
c
vc
Facies Code
35
30
25
20
15
10
5
Sr
Sse
Ste
Ste
Elliot Fm

Appendix 5: Re-interpretation of sedimentary logs of the Clarens Formation by Eriksson (1983).

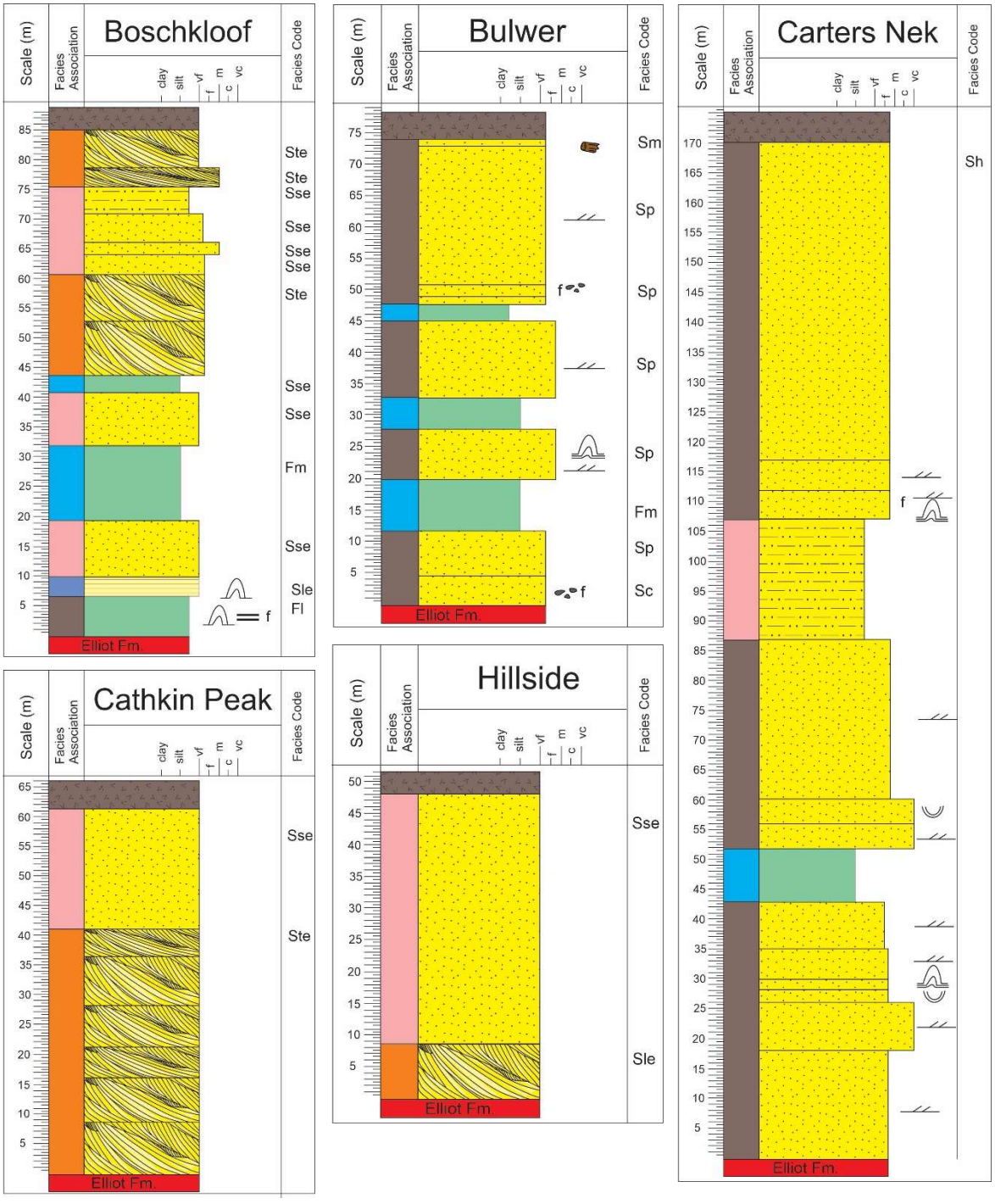

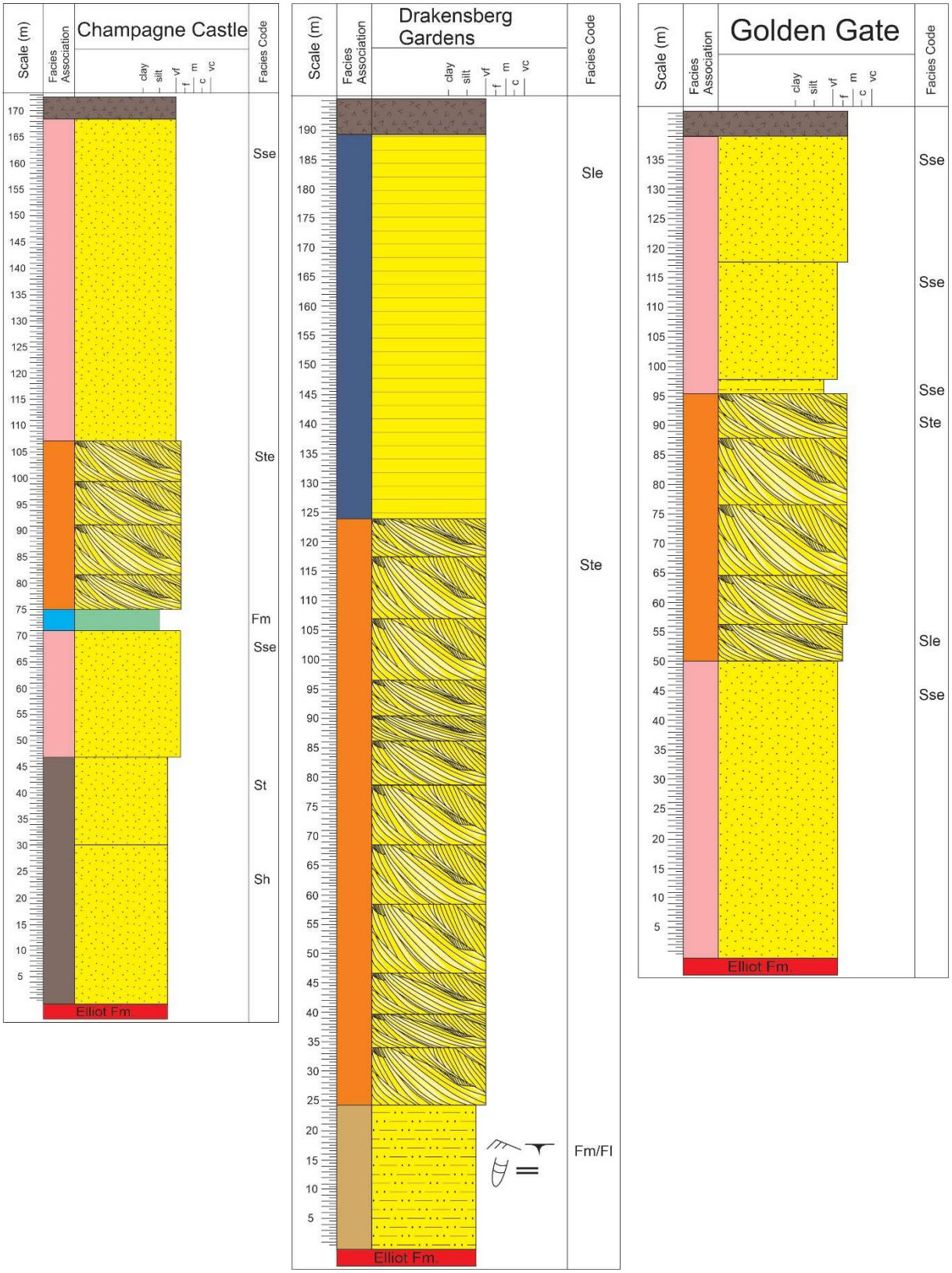
Champagne Castle
Scale (m)
Facies Association
clay
silt
vf
f
m
c
vc
Facies Code
Sse
Ste
Fm
Sse
St
Sh
Elliot Fm
Drakensberg Gardens
Sle
Ste
Fm/Fl
Elliot Fm.
Golden Gate
Sse
Sse
Sse
Ste
Sle
Sse
Elliot Fm

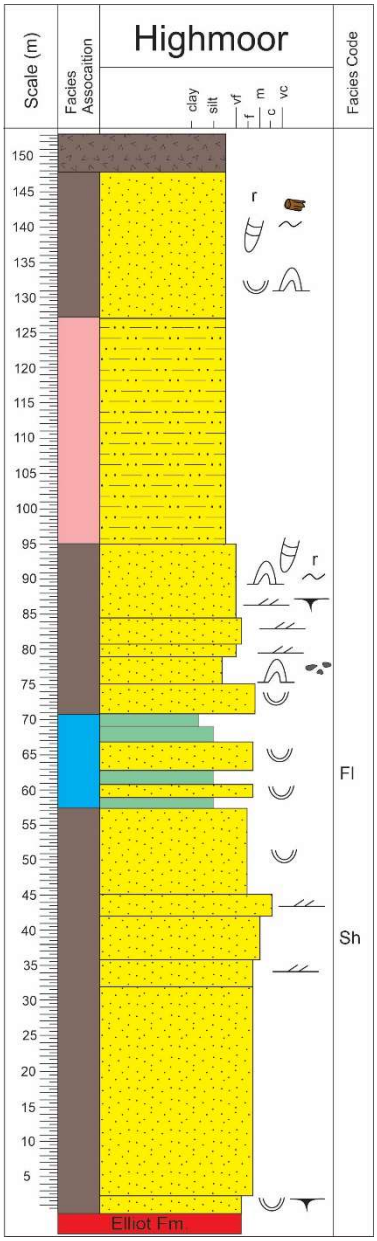
Highmoor
Scale (m)
Facies Association
Facies Code
clay
silt
vf
f
m
c
vc
Fl
Sh
Elliot Fm.

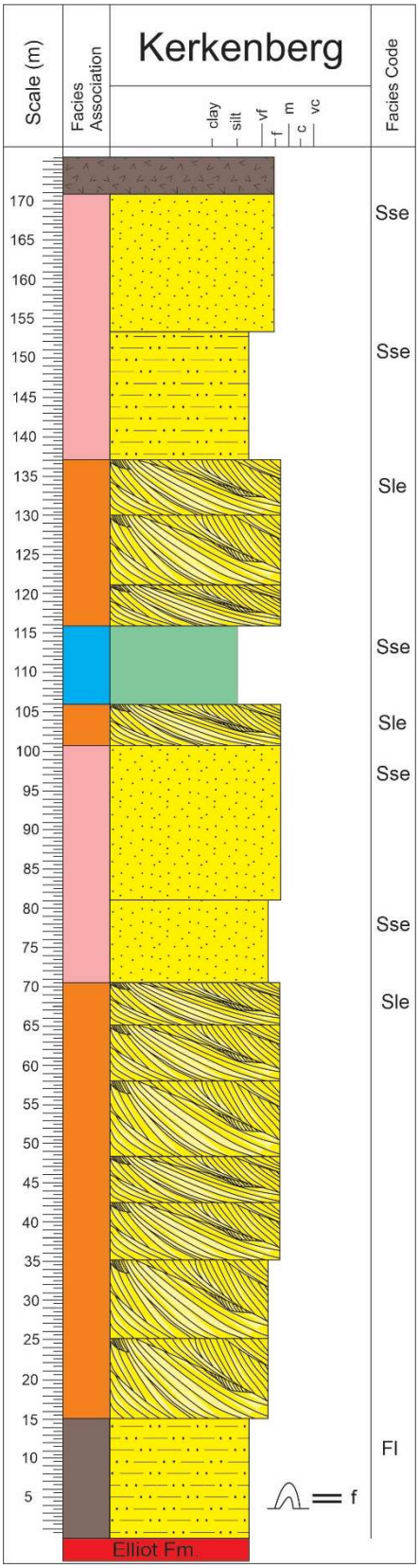
Kerkenberg
Scale (m)
Facies Association
Facies Code
clay
silt
vf
f
m
c
vc
Sse
Sse
Sle
Sse
Sle
Sse
Sse
Sle
Fl
f
Elliot Fm.

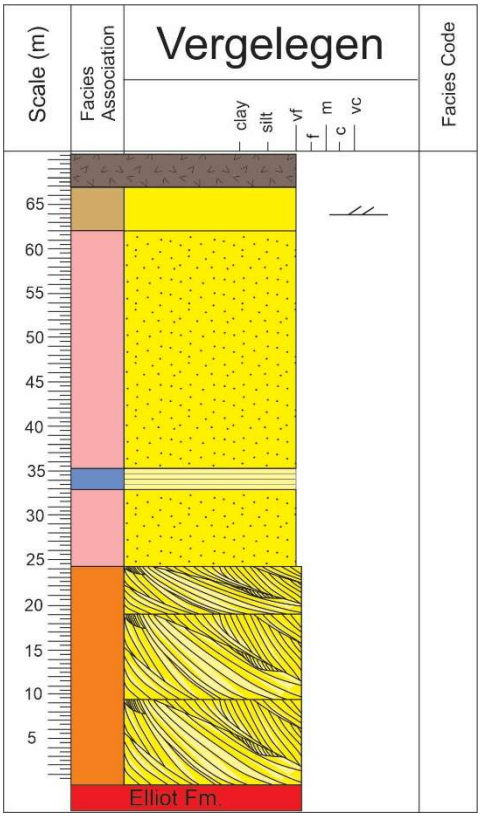
Vergelegen
Scale (m)
Facies Association
Facies Code
clay
silt
vf
f
m
c
vc
Elliot Fm.

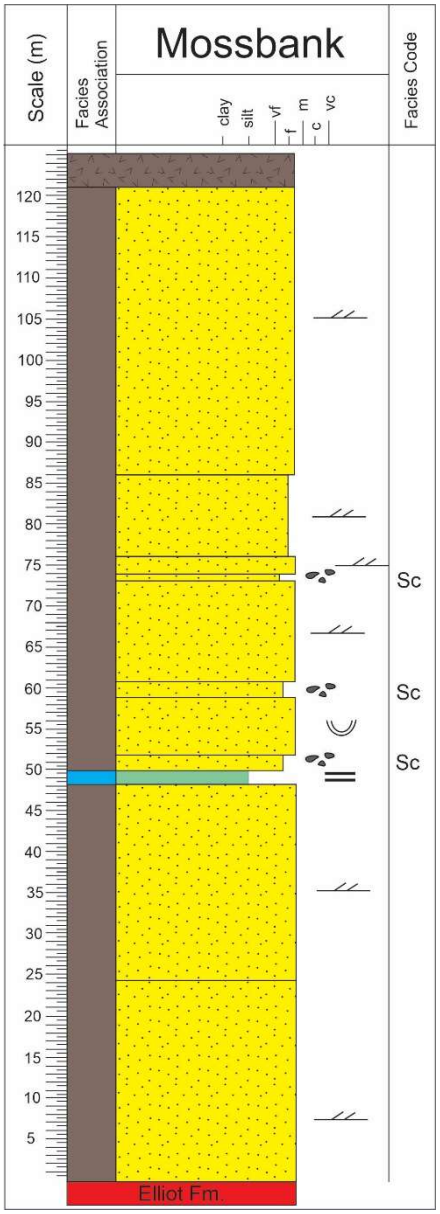
Scale (m)
Facies Association
Mossbank
clay
silt
vf
f
m
c
vc
Facies Code
Sc
Sc
Sc
Elliot Fm.

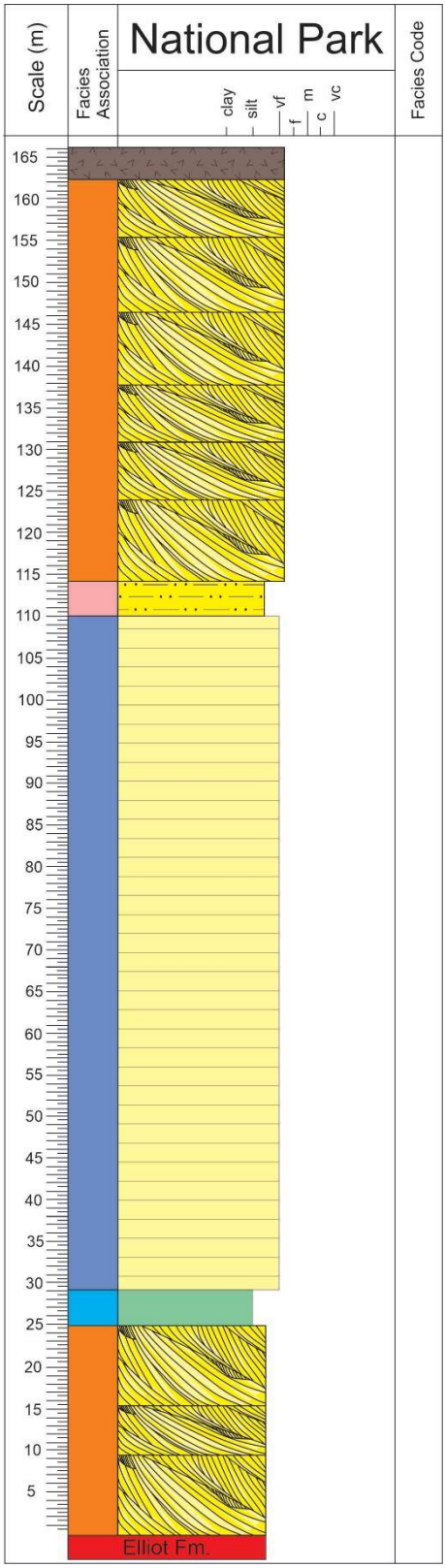
Scale (m)
Facies Association
National Park
clay
silt
vf
f
m
c
vc
Facies Code
Elliot Fm.

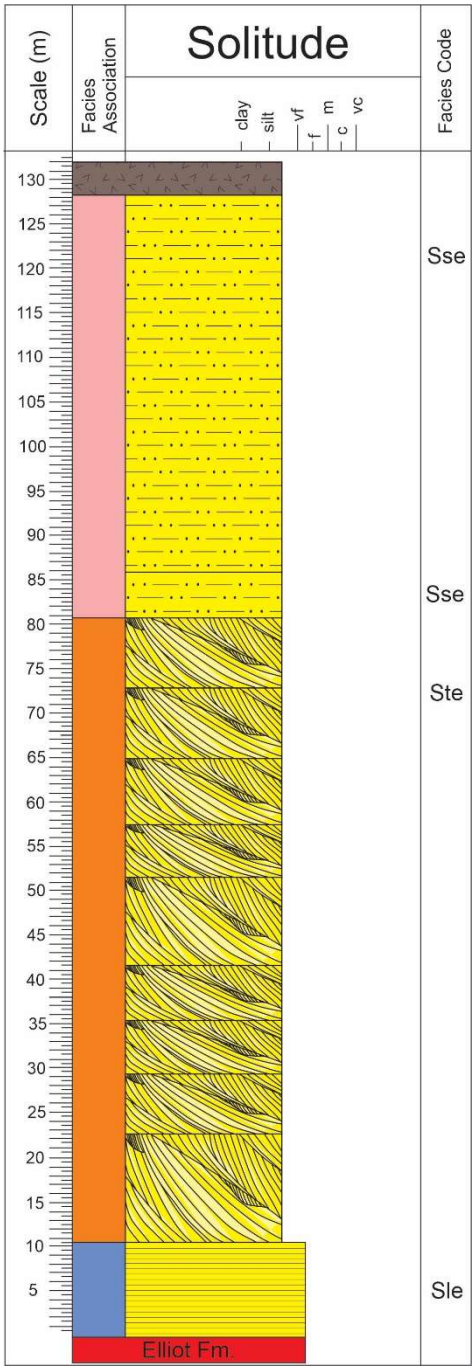
Scale (m)
Facies Association
Solitude
clay
silt
vf
f
m
c
vc
Facies Code
Sse
Sse
Ste
Sle
Elliot Fm.

Appendix 6: R thickness data input.

Location	x	y	Thickness (m)	Data_source
Moolmansberg	27.986572°	-28.644478°	126	Head_2020
Witkop	27.901725°	-28.382730°	136	Head_2020
Oorsprongsberg	28.127147°	-28.384483°	99	Head_2020
Nooitkondenk	28.469844°	-28.475358°	116	Head_2020
CMG	28.416556°	-28.532139°	93	Head_2020
Bergwoning	28.556906°	-28.513050°	130	Head_2020
CathPeak	29.236803°	-28.956692°	151	Head_2020
Injisuthi	29.438167°	-29.109408°	127	Head_2020
GiantsCastle	29.515600°	-29.281058°	53	Head_2020
Kamberg	29.672889°	-29.399367°	105	Head_2020
SaniPass	29.290472°	-29.590194°	145	Head_2020
RamatsedisosNek	28.925488°	-30.058306°	85	Head_2020
QachasNek	28.682982°	-30.043343°	150	Head_2020
Woodcliffe	28.158517°	-30.997681°	111	Head_2020
Talon	27.930197°	-31.162542°	197	Head_2020
Clefthill	27.889167°	-30.887394°	175	Head_2020
Belloch	27.691464°	-30.712547°	220	Head_2020
Welgesind	26.504589°	-31.284350°	44	Head_2020
Leeukop	26.834411°	-31.269850°	43	Head_2020
Malibe	27.946864°	-30.254839°	212	Head_2020
MtMoorosi	27.873475°	-30.299408°	192	Head_2020
Mokhopa	27.611806°	-30.330481°	140	Head_2020
Mohaleshoek	27.467106°	-30.170678°	70	Head_2020
Hellspoort	27.426292°	-29.858953°	96	Head_2020
Methinyeng	27.535794°	-29.783792°	75	Head_2020
Abebe	27.598000°	-29.651964°	95	Head_2020
KoroKoro	27.666747°	-29.496028°	89	Head_2020
Roma	27.741967°	-29.483897°	75	Head_2020
HaRalejoe	27.698239°	-29.423633°	51	Head_2020
Likosheng	27.914383°	-29.130506°	140	Head_2020
Fobani	27.962622°	-29.044261°	81	Head_2020
Makanyaneng	28.295053°	-28.780883°	127	Head_2020
Triploitania	27.592853°	-29.068715°	99	Beukes_1969
Wonderkop	27.707895°	-28.669673°	123	Beukes_1969
Witkop	27.901011°	-28.381969°	141	Beukes_1969
Beestekraal	27.967732°	-28.500216°	148	Beukes_1969
Dankbaarheid	28.196020°	-28.358921°	156	Beukes_1969
BellaVista	28.093219°	-28.453170°	138	Beukes_1969
Landkloof	28.052576°	-28.597303°	130	Beukes_1969
Broadlands	28.058206°	-28.712318°	146	Beukes_1969
Ornagia	28.333433°	-28.656335°	122	Beukes_1969
Saron	28.416818°	-28.533164°	127	Beukes_1969

Location	x	y	Thickness (m)	Data_source
Groenland	28.539803°	-28.513598°	128	Beukes_1969
Sandown	28.720889°	-28.504671°	145	Beukes_1969
Non-Pareil	28.531643°	-28.586873°	151	Beukes_1969
Vencedor	29.164700°	-28.239067°	162	Beukes_1969
Rensburg	29.253722°	-28.409576°	145	Beukes_1969
Retiefkop	29.113037°	-28.501850°	124	Beukes_1969
Witsieshoek	28.884404°	-28.677767°	166	Beukes_1969
Cavarn	28.974858°	-28.692669°	173	Beukes_1969
Wostijn	29.383615°	-29.047190°	101	Beukes_1969
Loteni	29.517933°	-29.429389°	70	Beukes_1969
DrakensbergGardens	29.184116°	-29.736091°	137	Beukes_1969
QachasNekB	28.690150°	-30.139379°	136	Beukes_1969
Lowel	28.355460°	-30.294592°	84	Beukes_1969
Pitseng	28.320514°	-30.750046°	79	Beukes_1969
Potberg	28.208161°	-30.931637°	23	Beukes_1969
Tushielaw	27.961035°	-30.792836°	200	Beukes_1969
Halseton	27.794677°	-30.705800°	305	Beukes_1969
Clantorf	27.843818°	-30.864274°	230	Beukes_1969
CarrigBawn	27.885817°	-31.093892°	277	Beukes_1969
ODPPass	27.516422°	-31.238037°	48	Beukes_1969
Geltchberg	27.492434°	-31.284214°	12	Beukes_1969
Vlakfontein	27.387984°	-31.322113°	83	Beukes_1969
Wolwekloof	27.307851°	-31.190371°	139	Beukes_1969
Alphawod	27.272303°	-31.090038°	60	Beukes_1969
Bamboeskloof	27.213717°	-30.746233°	76	Beukes_1969
KwaNojiki	27.515394°	-30.560023°	40	Beukes_1969
Thablesoba	27.554893°	-30.472186°	58	Beukes_1969
Pronkberg	26.869036°	-31.263016°	20	Beukes_1969
Spitkop	26.714614°	-31.190599°	33	Beukes_1969
Clarens	28.449870°	-28.517604°	100	Eriksson_1983
GoldenGate	28.620352°	-28.511067°	135	Eriksson_1983
Harrismith	29.179322°	-28.259046°	135	Eriksson_1983
Boschkloof	28.971974°	-28.528874°	80	Eriksson_1983
RoyalNatal	28.933126°	-28.680014°	140	Eriksson_1983
Cathkinpeak	29.390909°	-29.011900°	65	Eriksson_1983
ChampagneCastle	29.375914°	-29.052131°	167	Eriksson_1983
Highmoor	29.623780°	-29.316373°	155	Eriksson_1983
Kamberg	29.658158°	-29.396021°	115	Eriksson_1983
Vergelegen	29.444052°	-29.527676°	70	Eriksson_1983
CartersNek	29.689994°	-29.509632°	170	Eriksson_1983
Mossbank	29.698621°	-29.807014°	120	Eriksson_1983
Bulwer	29.746726°	-29.806178°	65	Eriksson_1983
ThabaNchu	26.883497°	-29.258251°	38	Robinson_1969
Kommissiepoort	27.265634°	-29.337371°	32	Robinson_1969
Charissma	27.558807°	-28.846188°	79	Robinson_1969

Location	x	y	Thickness (m)	Data_source
Donside	28.098660°	-28.751625°	97	Robinson_1969
Bethlehemstar	28.199624°	-28.551406°	165	Robinson_1969
Spitskrans	28.423077°	-28.349937°	65	Robinson_1969
GlenLyon	28.417855°	-28.618249°	140	Robinson_1969
Boesmansnek	29.141020°	-29.830099°	231	Robinson_1969
StBernard	29.086994°	-29.992172°	196	Robinson_1969
Pitseng	28.309959°	-30.756050°	36	Robinson_1969
NaudesNek	28.206441°	-30.905215°	36	Robinson_1969
Rockwater	28.200226°	-31.149451°	31	Robinson_1969
Barklypass	27.823563°	-31.247507°	85	Robinson_1969
Kranzkloof	26.410313°	-31.315205°	22	Robinson_1969
Bitterplaat	26.972199°	-31.203546°	30	Robinson_1969
Klipfontein	27.015705°	-30.957440°	15	Robinson_1969
Meerwyk	26.693242°	-30.939464°	52	Robinson_1969
Hoogwater	26.586903°	-30.778968°	5	Robinson_1969
Herchel	27.180923°	-30.633398°	18	Robinson_1969
Vechtkop	27.180590°	-30.279653°	30	Robinson_1969
Brakfontein	26.938927°	-30.279459°	40	Robinson_1969
Genovia	27.253566°	-30.031490°	69	Robinson_1969
Joang	28.224734°	-28.977169°	152	Stockley_1947
Thaba Phatsoa	28.113738°	-29.008719°	198	Stockley_1947
Mamathe	27.843894°	-29.134422°	122	Stockley_1947
Thakampholo	27.935339°	-29.120114°	61	Stockley_1947
Mofoka's Store	27.610328°	-29.526056°	152	Stockley_1947
Khatleng	27.549250°	-29.675628°	174	Stockley_1947
Thabaneng	27.524903°	-29.809172°	76	Stockley_1947
Thabana Morena	27.446789°	-29.861725°	122	Stockley_1947
Thaba Tsoeu	27.485769°	-30.078081°	183	Stockley_1947
Moyeni/Leloaleng	27.670908°	-30.390008°	67	Stockley_1947
Masitisi mission	27.648000°	-30.410417°	88	Stockley_1947
Dilly Dilly	27.691306°	-30.508139°	122	Stockley_1947
Kubung	28.016685°	-30.104824°	213	Stockley_1947
Au	28.587026°	-30.077258°	165	Stockley_1947
Kabi	27.766757°	-30.327239°	31	Stockley_1947
Tosing	27.909818°	-30.326267°	110	Stockley_1947
Ralebone	27.989220°	-30.408910°	238	Stockley_1947
Nmatatiele	28.800096°	-30.105259°	0	Du Toit
WtFletcher	28.219773°	-30.667478°	0	Du Toit
WElliot	27.492456°	-31.354170°	0	Du Toit

Appendix 7: R script for thickness estimation.

```
data(CT) ### locatios and thicknesses for est - thickness in m

data(CG) ### Qgis grid over Clarens basin

data(CTK) ### location and thicknesses for est - thickness in km

data(CGN) ### Qgis updated grid at 0.5by0.5 deg

data(CGU) #### Qgis updated grid at 0.5by0.5 deg 10 March

coordinates (Thicknes)<- c("x","y")### convert to spatial data

coordinates (Thicknes)<- c("left","top")### convert to spatial data

###plot of thickness relative to the max measurement

plot(Thickness, asp=1, cex=4*Thickness$thickness/max(Thickness$thickness), pch=1)

###

gridded(CG) <- T ### set to grid

hist(CT$thickness, breaks=20) ### histogram

### Data spatial info####

(gamma <- 0.5 * (CT$thickness[1] - CT$thickness[2])^2) ###semi_variance

dim(coordinates(CT))

head(coordinates(CT)[,1])

head(coordinates(CT)[,2])

coordinates(CT)[1,]

coordinates(CT)[2,]

coordinates(CT)[1,1]

(sep <- sqrt((coordinates(CT)[1, 1] - coordinates(CT)[2,1])^2 + (coordinates(CT)[1, 2] -
coordinates(CT)[2,2])^2)) ###Data separation

###Variography###

(v<- variogram(thickness.1~1, CT, cutoff=2.0, width=0.2))  ###semi_variogram

print(plot(v, plot.numbers=T))

vm<- vgm(psill=0.09, model="Sph", range=1.0, nugget=0.03 )

print(plot(v, pl=T, model = vm))

(vmf<- fit.variogram(v, vm))

k40 <- krige(thickness.1~1, locations = CT, newdata=CG, model=vmf) ###run OK
```

```
print(spplot(k40, "var1.pred", main = "OK prediction, Thickness",asp = 1, col.regions =
bpy.colors(64)))

###Code for first attempt at OK###

(v<- variogram(thickness~1, CT, cutoff=1.5, width=0.1))

print(plot(v, plot.numbers=T))

(vmf<- fit.variogram(v, vm))

print(plot(v, pl=T, model=vm))

vm<- vgm(psill=3000, model="Sph", range=0.8, nugget=800)

(vmf<- fit.variogram(v, vm))

k40<- krige(thickness~1, locations=CT, newdata=CG, model=vmf)

print(spplot(k40, "var1.pred", main = "OK prediction, Thickness",asp = 1, col.regions =
bpy.colors(64)))

###second attempt at km scale####

(v<- variogram(thickness~1, CTK, cutoff=1, width=0.1))

vm<- vgm(psill=0.003, model="Sph", range=0.8, nugget=0.0007)

print(plot(v, pl=T, model = vm))

(vmf<- fit.variogram(v, vm))

k40 <- krige(thickness~1, locations = CTK, newdata=CG, model=vmf)

print(spplot(k40, "var1.pred", main = "OK prediction, Thickness",asp = 1, col.regions =
bpy.colors(64)))

##########

### Neighbourhood (search radius) that could reflect local subsidence vs regional

k40 <- krige(thickness~1, locations = CT, newdata=CG, model=vmf, maxdist = 0.8)

print(spplot(k40, "var1.pred", main = "OK prediction, Thickness",asp = 1, col.regions =
bpy.colors(64)))

###New grid OK ###

(v<- variogram(thickness~1, CT, cutoff=1.5, width=0.1))

print(plot(v, plot.numbers=T))

vm<- vgm(psill=3000, model="Sph", range=0.8, nugget=700)

print(plot(v, pl=T, model = vm))

(vmf<- fit.variogram(v, vm))

k40 <- krige(thickness~1, locations = CT, newdata=CGN, model=vmf)
```

```
print(spplot(k40, "var1.pred", main = "OK prediction, Thickness",asp = 1, col.regions =
bpy.colors(64)))

### New grid OK with 1 deg search neigbourhood ###

k40 <- krige(thickness~1, locations = CT, newdata=CGN, model=vmf, maxdist=1.0)

print(spplot(k40, "var1.pred", main = "OK prediction, Thickness",asp = 1, col.regions =
bpy.colors(64)))

### New grid OK with 0.5 deg search neigbourhood (rough range limit) ###

k40 <- krige(thickness~1, locations = CT, newdata=CGN, model=vmf, maxdist=0.5)

print(spplot(k40, "var1.pred", main = "OK prediction, Thickness",asp = 1, col.regions =
bpy.colors(64)))

#########

###Test at manual vm at 0.8 search neighbourhood ###

k40 <- krige(thickness~1, locations = CT, newdata=CGN, model=vm, maxdist=0.8)

print(spplot(k40, "var1.pred", main = "OK prediction, Thickness",asp = 1, col.regions =
bpy.colors(64)))

vm

###model psill range

###1   Nug   700   0.0

###2   Sph  3000   0.8

### new vm ###

vm

### model psill range

###1   Nug   500   0.0

###2   Sph  3300   0.5


vm<- vgm(psill=3300, model="Sph", range=0.5, nugget=500)

print(plot(v, pl=T, model = vm))

k40 <- krige(thickness~1, locations = CT, newdata=CGU, model=vm, maxdist=0.5)

print(spplot(k40, "var1.pred", main = "OK prediction, Thickness",asp = 1, col.regions =
bpy.colors(64)))
```

Appendix 8: Semi-variogram used in the Ordinary Kriging estimation of thickness.

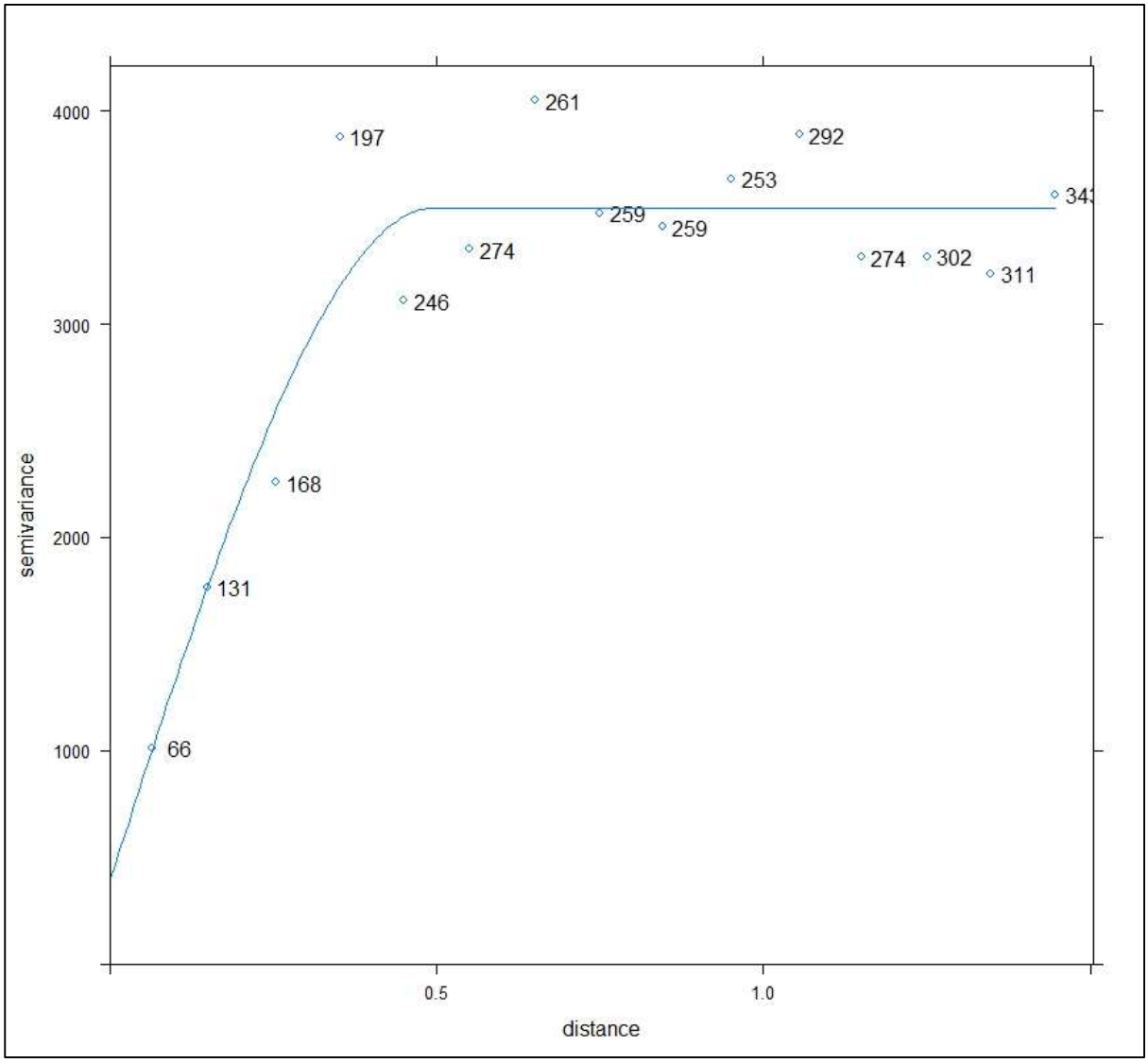

Appendix 9: Sandstone classification.

Sample	no	Qt	Qm	Qp	Ft	L	Classification
MLB-01*	1	270	259	11	25	5	quartzose
MLB-02*	2	269	259	10	23	6	quartzose
MLB-03*	3	275	267	8	22	3	quartzose
NKD-01	4	276	264	12	21	3	quartzose
NKD_02	5	273	264	9	21	5	quartzose
NKD-03	6	267	256	11	24	8	quartzose
CMG-01	7	275	267	8	15	7	quartzose
CMG-02	8	284	273	11	12	4	pure quartzose
CMG-03	9	269	259	10	23	8	quartzose
CMG-04	10	270	263	7	22	5	quartzose
BWG-01	11	270	264	6	25	3	quartzose
BWG-02	12	271	266	5	23	4	quartzose
BWG-03	13	267	259	8	30	3	Quarts-rich feldspatho-quartzose
BWG-04	14	263	257	6	28	7	quartzose
ORB-01	15	273	267	6	22	5	quartzose
zORB-02	16	271	263	8	23	6	quartzose
ORB-03	17	272	259	13	22	4	quartzose
LKP-01	18	274	264	10	23	3	quartzose
LKP-02	19	265	252	13	29	4	quartzose
LKP-03	20	272	264	8	25	2	quartzose
LKP-04	21	270	261	9	24	6	quartzose
TLN-01	22	258	252	6	28	6	quartzose
TLN-03	24	263	244	19	22	6	quartzose
TLN-04	25	269	246	23	22	7	quartzose
TLN-05	26	257	234	23	18	7	quartzose
TLN-06A	27	262	235	27	29	4	quartzose
BLC-01	30	273	253	20	22	3	quartzose
BLC-02	31	269	251	18	26	5	quartzose
BLC-03	32	267	253	14	27	4	quartzose
BLC-04	33	275	258	17	19	3	quartzose
BLC-05	34	269	256	13	23	7	quartzose
BLC-06	35	268	253	15	26	5	quartzose
HCL-01	36	270	255	15	24	5	quartzose
HCL-02	37	267	257	10	27	5	quartzose
HCL-03	38	272	259	13	19	6	quartzose
HCL-04	39	270	258	12	21	4	quartzose
WGS-01	40	268	251	17	20	10	quartzose
WGS-02	41	279	257	22	17	4	quartzose
WCF-01	43	271	258	13	14	12	quartzose
SNP-01	44	276	264	12	18	4	quartzose
SNP-02	45	268	262	6	27	5	quartzose
SNP-03	46	270	262	8	27	3	quartzose
SNP-04	47	274	254	20	23	3	quartzose
DBG-01	48	280	272	8	18	2	quartzose
DBG-02	49	276	271	5	23	1	quartzose
RNK-01	50	269	264	5	26	5	quartzose
RNK-02	51	273	268	5	20	5	quartzose
RNK-03	52	276	271	5	21	3	quartzose
RNK-04	53	277	257	20	19	3	quartzose
RNK-05	54	270	258	12	25	5	quartzose
RNK-06	55	284	280	4	14	2	quartzose
GCL-01	56	275	270	5	22	3	quartzose
RNL-01	57	276	271	5	20	4	quartzose
RNL-02	58	267	260	7	27	6	quartzose
KBG-01	59	263	257	6	28	7	quartzose

KBG-02	60	234	202	32	33	10	quartzose
KBG-03	61	271	239	32	23	1	quartzose
KBG-04	62	276	235	41	18	0	quartzose
KBG-05	63	280	266	14	19	1	quartzose
IJT-01	64	275	270	5	20	5	quartzose
IJT-02	65	276	272	4	20	3	quartzose
CPK-01	66	276	268	8	23	0	quartzose
CPK-02	67	271	268	3	27	2	quartzose
CPK-03	68	268	255	13	27	4	quartzose
CPK-04	69	269	261	8	30	1	Quarts-rich feldspatho-quartzose
CPK-05	70	269	260	9	27	3	quartzose
MKY-01	71	279	271	8	20	1	quartzose
MKY-02	72	271	259	12	25	2	quartzose
MKY-03	73	276	269	7	21	2	quartzose
MKY-04	74	274	266	8	22	4	quartzose
FBN-01	75	271	264	7	24	3	quartzose
FBN-02	76	272	263	9	23	4	quartzose
LKS-01	77	269	260	9	28	2	quartzose
LKS-02	78	272	263	9	23	4	quartzose
LKS-03	79	276	264	12	18	4	quartzose
LKS-04	80	279	266	13	14	3	quartzose
LKS-05	81	282	278	4	16	2	quartzose
ABB-01	82	278	271	7	19	2	quartzose
ABB-02	83	272	265	7	25	3	quartzose
ABB-03	84	278	270	8	18	4	quartzose
KKR-01	85	276	255	21	21	2	quartzose
KKR-02	86	286	269	17	9	3	pure quartzose
KKR-03	87	273	268	5	24	2	quartzose
MTY-01	88	279	260	19	17	2	quartzose
MTY-02	89	276	265	11	20	4	quartzose
MTY-03	90	271	268	3	21	5	quartzose
MTY-04	91	271	266	5	25	4	quartzose
HLP-01	92	274	253	21	24	2	quartzose
HLP-03	94	277	268	9	20	2	quartzose
MHH-02	96	278	264	14	20	2	quartzose
MHH-03	97	276	265	11	16	5	quartzose
MKP-01	98	282	268	14	17	1	quartzose
MKP-02	99	273	267	6	26	1	quartzose
MKP-03	100	279	268	11	18	3	quartzose
MTM-03	103	275	269	6	21	4	quartzose
MLB-01	105	282	271	11	18	0	quartzose
MLB-02	106	272	252	20	24	3	quartzose
MLB-03	107	275	271	4	22	2	quartzose
MLB-04	108	274	268	6	24	2	quartzose
MLB-06	110	279	268	11	17	3	quartzose

Appendix 10: U-(Th)-Pb dating method, School of Geosciences, University of the Witwatersrand, South Africa – Metadata table for 2019 data run prepared by Laura Bracciali.

LA ICP-MS (laser ablation inductively coupled plasma mass spectrometry) U-Pb measurements were carried out in the Earthlab at the University of the Witwatersrand (Johannesburg, South Africa) employing an Applied Spectra (AS) RESOlution 193 nm ArF excimer laser system coupled to a Thermo Scientific Element XR magnetic sector-field ICP-MS. The U-Pb measurements were performed in low resolution and electrostatic scanning (E-scan) modes. U-Pb data and metadata are tabulated in Supplementary Tables 1-2.

At the start of each analytical session the mass spectrometer was tuned by ablating a line scan on the NIST610 glass. The torch position, lenses and gas flows were tuned while measuring ^{206}Pb, ^{238}U and $^{238}U^{16}O$ to get stable signals and maximum sensitivity for ^{206}Pb and ^{238}U, while maintaining low oxide rates ($ThO^{+}/Th < 0.2$ %) and Th/U ratio > 0.9.

The laser sampling protocol employed a 24 m static spot and a fluence of 2.5 J/cm^2 and took place in a SE-155 dual-volume ablation cell using a continuous flow of He gas combined with Argon (incorporated into the cell funnel) and a small volume of N_2 (added after the cell) to enhance signal stability and sensitivity, respectively.

The laser and ICP-MS software packages were synchronized in order to allow automated execution of the analyses. Each analytical session included up to 400 measurements.

Before the gas blank measurement, each spot was pre-ablated by firing two laser shots to remove common Pb from the surface that may have been introduced during the sample preparation.

During each analytical session the zircon reference materials GJ-1 (Jackson et al., 2004), Plešovice (Sláma et al., 2008) and 91500 (Wiedenbeck et al., 1995) were measured between groups of 12 unknowns. Zircon GJ-1 was used as a matrix-matched primary reference material to correct for mass discrimination on measured isotope ratios in unknown samples and simultaneous correction for instrumental drift. The GJ-1 isotopic ratios used for the correction are those reported by Horstwood et al. (2016). Plešovice and 91500 were used as secondary reference materials to validate the results and assess the quality of the data for each analytical session.

Data reduction was performed with the software package Iolite v.3.5 (Paton et al., 2011), combined with VizualAge (Petrus and Kamber, 2012). An exponential model of laser-induced elemental fractionation (LIEF) obtained by combining the isotopic ratios of the primary reference material from the entire session is used to correct for time-dependent down-hole elemental fractionation in the unknowns, under the assumption of same fractionation behaviour in the reference material and the unknowns. After correction for LIEF and drift and normalization to the main reference material (performed in Iolite), uncertainty components for systematic errors are propagated by quadratic addition according to the recommendations of Horstwood et al. (2016). All absolute ages and uncertainties were calculated with Isoplot v. 4.15 (Ludwig 2012).

Laboratory & Sample Preparation	
Laboratory name	Earthlab, School of Geosciences, University of the Witwatersrand
Sample type / mineral	Detrital / Zircons
Sample preparation	Conventional mineral separation, 1 inch resin mount, 1 µm polish to finish
Imaging	CL, ZEISS Merlin SEM, 11 nA, 10kV, 10 mm working distance at the Central Analytical Facilities, Stellenbosch University
Laser ablation system	
Make, Model & type	AS RESOlution SE Excimer laser
Ablation cell & volume	Laurin Technic S-155 dual-volume cell
Laser wavelength	193 nm
Pulse width	5–7 ns
Fluence	2.7 J/cm^{-2}
Repetition rate	7 Hz
Spot size	24 µm
Sampling mode / pattern	Static spot ablation
Carrier gas	mixed He-Ar atmosphere in the cell, with addition of N_2 (5.5 ml/min) after the cell
Pre-ablation surface cleaning	2 pulses, same spot size as during ablation
Ablation duration	29 s
Wash-out delay	7 s
Cell carrier gas flow	0.35 l/min He
ICP-MS Instrument	
Make, Model & type	Thermo Scientific Element XR ICP-MS
Sample introduction	Ablation aerosol via conventional tubing
RF power	1350 W
Make-up gas flow	1.0 l/min Ar
Detection system	Combination of a single Faraday collector with a SEM (Secondary Electron Multiplier)
Masses measured	202, 204, 206, 207, 208, 232, 238. All masses measured in pulse counting mode, except for ^{238}U (analog mode).
Integration time per peak (segment duration)	7, 14, 15, 18, 8, 8, 13 ms, respectively
Total integration time per output datapoint	0.1 s
Sensitivity	0.3% U
Dead time	25 ns
Data Processing	
Gas blank	12 s on peak prior to each measurement
Calibration strategy	GJ-1 used as primary reference material, Plešovice and 91500 used as secondary reference materials
Reference Material info	GJ-1 (Jackson et al. 2004; revised isotopic ratios from Horstwood et al. 2016); Plešovice (Slama et al. 2008); 91500 (Wiedenbeck et al. 1995)
Data processing package used / Correction for LIEF	Iolite reduction software package v.3.5 with VizualAge; LIEF modelled within each analytical session on the basis of combined analyses of the main reference material; LIEF correction assumes reference material and samples behave identically. All ages and uncertainties calculated with Isoplot v. 4.15 (Ludwig 2012)
Mass discrimination	Reference material-sample bracketing with ^{207}Pb/^{206}Pb and ^{206}Pb/^{238}U normalized to zircon GJ-1
Common-Pb correction	No common Pb correction applied to the data
Uncertainty level & propagation	Decay constant uncertainties, ratio uncertainty of primary reference material and long-term excess variance of secondary reference material are propagated by quadratic addition. Age uncertainties are quoted at the 2s absolute level.
Quality control / Validation	Plešovice: Wtd avg ^{206}Pb/^{238}U age = 338.6 ± 0.5 Ma (95% conf, MSWD = 1.5, n = 68); 91500: Wtd avg ^{206}Pb/^{238}U age = 1067.2 ± 2.1 Ma (95% conf, MSWD = 1.1; n = 41).

References

Horstwood, M.S.A., Košler, J., Gehrels, G., Jackson, S.E., McLean, N.M., Paton, C., Pearson, N.J., Sircombe, K., Sylvester, P., Vermeesch, P., Bowring, J .F., Condon, D.J., Schoene, B. 2016. Community-Derived Standards for LA-ICP-MS U-(Th-)Pb Geochronology – Uncertainty Propagation, Age Interpretation and Data Reporting. *Geostandards and Geoanalytical Research*, 40 (3): 301–332.

Jackson, S.E., Pearson, N.J., Griffin, W.L. Belousova, E.A. 2004. The application of laser ablation-inductively coupled plasma-mass spectrometry to in situ U-Pb zircon geochronology, *Chemical Geology,* 211: 47–69.

Ludwig, K.R. 2012. Isoplot Version 3.75–4.15: a Geochronological Toolkit for Microsoft Excel. *Berkeley Geochronological Center Special Publication*, 5.

Paton, C., Hellstrom, J., Paul, B., Woodhead, J., Hergt, J. 2011. Iolite: freeware for the visualisation and processing of mass spectrometric data. *Journal of Analytical Atomic Spectrometry*, 26: 2508–2518.

Petrus, J.A., Kamber, B.S. 2012. VizualAge: A Novel Approach to Laser Ablation ICP-MS U-Pb Geochronology Data Reduction. *Geostandards and Geoanalytical Research*, 36: 247-270.

Sláma, J., Košler, J., Condon, D.J., Crowley, J.L., Gerdes, A., Hanchar, J.M., Horstwood, M.S.A., Morris, G.A., Nasdala, L., Norberg, N., Schaltegger, U., Schoene, B., Tubrett, M.N., Whitehouse, M.J. 2008. Plešovice zircon – a new natural reference material for U-Pb and Hf isotopic microanalysis. *Chemical Geology*, 241: 1–35.

Wiedenbeck, M.A.P. C., Alle, P., Corfu, F.Y., Griffin, W.L., Meier, M., Oberli, F.V., Quadt, A.V., Roddick, J.C. and Spiegel, W. 1995. Three natural zircon standards for U-Th-Pb, Lu-Hf, trace element and REE analyses. *Geostandards newsletter*, 19(1): 1-23.

Appendix 11: Analytical Protocols using LA-SF-ICPMS at Wits for 2020 data run Prepared by Robert Bolhar.

Prior to laser ablation analysis zircons and other accessory minerals need to be separated and mounted in epoxy to be examined by backscattered (BSE) and cathodo-luminescence (CL) imaging for selecting locations for analysis and to avoid cracks and inclusions.

U-Pb zircon: Instrumentation and Data Acquisition

U-Th-Pb measurements were carried out in the Earthlab at the University of the Witwatersrand, employing an Applied Spectra/Australian Scientific Instruments (ASI) Resolution 193 nm ArF excimer system coupled to a Thermo Scientific Fisher sector-field ICPMS (Element XR). The U-Th-Pb measurements were performed in low resolution and electrostatic scanning (E-scan) modes. Data were acquired by single spot analysis (24 μm), using a laser repetition rate of 8 Hz and a fluence of 2.5 Jcm^{-2}. Total signal acquisition time was 30 sec, allowing data processing and preparation for the next analysis, and comprising 5 sec of pre- and post-ablation (gas blank) and 20 sec of ablation measurements. Laser sampling took place in a SE155 dual-volume ablation cell (Laurin Technic, Canberra, Australia) using a mixed He-Ar atmosphere and a small volume of N_2 to enhance signal stability and sensitivity. The following gas flows were applied: He (450 ml/min), Ar (1000 ml/min) and N_2 (5 ml/min), respectively. Zircon standard GJ1 (Jackson et al., 2004) served for calibration, and Rak17 (Webb et al. 2019), 91500 (Wiedenbeck et al., 1995) and Plešovice (Sláma et al., 2008) zircon certified reference materials (CMRs) were analyzed as unknows to evaluate accuracy and precision. The LA-ICPMS system was tuned during line scans using NIST 612 glass for maximum sensitivity for ^{238}U and ^{206}Pb, while maintaining oxide levels (ThO^+/Th) < 0.2 % and the Th/U ratio >0.95. Typically, the primary calibration standard analysed at the beginning and end of a sequence, and 20 analyses of unknowns were followed by analyses of one primary calibration standard and secondary standards for quality control purposes. Prior to each spot analysis surface material was removed using 2 laser pulses. The following masses were measured (6 samples per peak): ^{202}Hg, $^{204}(Pb+Hg)$, ^{206}Pb, ^{207}Pb, ^{208}Pb, ^{232}Th, ^{235}U, and ^{238}U. Magnet settling time was 0.001 sec, and sample times ranged from 0.0005 sec ($^{202,204}Hg$) to 0.0045 sec (^{207}Pb). All isotopes were measured in pulse counting mode, except for ^{238}U and ^{232}Th ("triple", including counting or analogue). A summary of instrument settings is provided in table 1.

U-Pb data reduction using iolite

Data reduction was performed using the iolite extension (http://www.iolite.org. au) to the software Igor Pro (http://www.wavemetrics.com), proceeding in a series of sequential steps, including data import, selection of integrations, baseline subtraction, drift and down-hole fractionation, calibration and error propagation (Paton et al., 2010, 2011). Additionally, the data reduction scheme (DRS) VizualAge (Petrus and Kamber, 2012; http://www.japetrus.net/va) was applied to more carefully select integrations in order to minimize discordance and to avoid common Pb.

U-Th-Pb data presentation and calculation of ages

Graphic presentation and calculation of Concordia ages was carried out using the software ISOPLOT-R (Vermeesch, 2018). Uncertainties on individual and mean/regressed ages are 2SE (standard error, absolute).

Table 1: Operating conditions and data acquisation for U-Pb zircon

ICP-MS		
Instrument	magnetic sector	
Manufacturer	Thermo Scientific Instruments	
Model	Element XR	
RF power [W]		1450
Gas Flows		
Cooling (Ar [l/min]	16	
Auxiliary (Ar) [l/min]	1.0	
Sample (Ar) [l/min]	1.0	
Carrier (He) [l/min]	0.45	
N [l/min]	0.005	
Laser		
Instrument	ArF excimer	
Manufacturer	Australian Scientific Instruments	
Model	Resolution SE155	
Wavelength [nm]	193	
Spot size [microns]	24	
Repetition Rate [Hz]	8	
Laser Fluence [J/cm2]	2.5	
Data Acquisition		
Resolution Mode	Low	
Protocol	Time-resolved	
Scan Mode	E-scan	
Scanned Masses	202, 204, 206, 207, 208, 232, 235, 238	
Settling Times	0.001	
Sample Times	0.001-0.0045	
Samples Per Peak	6	
Detection Mode	Counting for all isotopes except 238 and 232 (triple)	
Detector Deadtime [n sec]	25	
Background (gas blank) [sec]	two times 5	
Ablation Time [sec]	20	
Standards		
Calibration (primary)	zircon GJ1	
Internal	na	
Control (secondary)	Rak17, Plesovice, 91500	
Data Reduction		
Software	iolite, in-built into Igor Pro	
Data Reduction Scheme(s)	VizualAge	

References

Jackson, S.E., Pearson, N.J., Griffin, W.L. and Belousova, E A. 2004. The application of laser ablation-inductively coupled plasma-mass spectrometry to in situ U–Pb zircon geochronology. *Chemical Geology*, *211*(1-2): 47-69.

Petrus, J.A. and Kamber, B.S. 2012. VizualAge: A novel approach to laser ablation ICP-MS U-Pb geochronology data reduction. Geostandards and Geoanalytical Research, *36*(3): 247-270.

Paton, C., Woodhead, J.D., Hellstrom, J.C., Hergt, J.M., Greig, A. and Maas, R. 2010. Improved laser ablation U-Pb zircon geochronology through robust downhole fractionation correction. *Geochemistry, Geophysics, Geosystems*, *11*(3).

Paton, C., Hellstrom, J., Paul, B., Woodhead, J., and Hergt, J. 2011. Iolite: Freeware for the visualisation and processing of mass spectrometric data. *Journal of Analytical Atomic Spectrometry*, *26*(12): 2508-2518.

Sláma, J., Košler, J., Condon, D.J., Crowley, J.L., Gerdes, A., Hanchar, J.M., Horstwood, M.S., Morris, G.A., Nasdala, L., Norberg, N. and Schaltegger, U. 2008. Plešovice zircon—a new natural reference material for U–Pb and Hf isotopic microanalysis. *Chemical Geology*, 249(1-2): 1-35.

Vermeesch, P. 2018. IsoplotR: a free and open toolbox for geochronology. *Geoscience Frontiers*, 9(5): 1479-1493.

Webb, P., Wiedenbeck, M., Glodny, J. 2019. An International Proficiency Test for U-Pb Geochronology Laboratories — *Report on the 2019 Round of G-Chron based on Palaeozoic Zircon Rak-17* (Distribution: September 2019)

Wiedenbeck, M.A.P. C., Alle, P., Corfu, F.Y., Griffin, W.L., Meier, M., Oberli, F.V., Quadt, A.V., Roddick, J.C. and Spiegel, W. 1995. Three natural zircon standards for U-Th-Pb, Lu-Hf, trace element and REE analyses. *Geostandards newsletter*, 19(1): 1-23.

Appendix 12: Wetherill concordia diagrams for the 21 detrital zircon samples of the Clarens Formation.

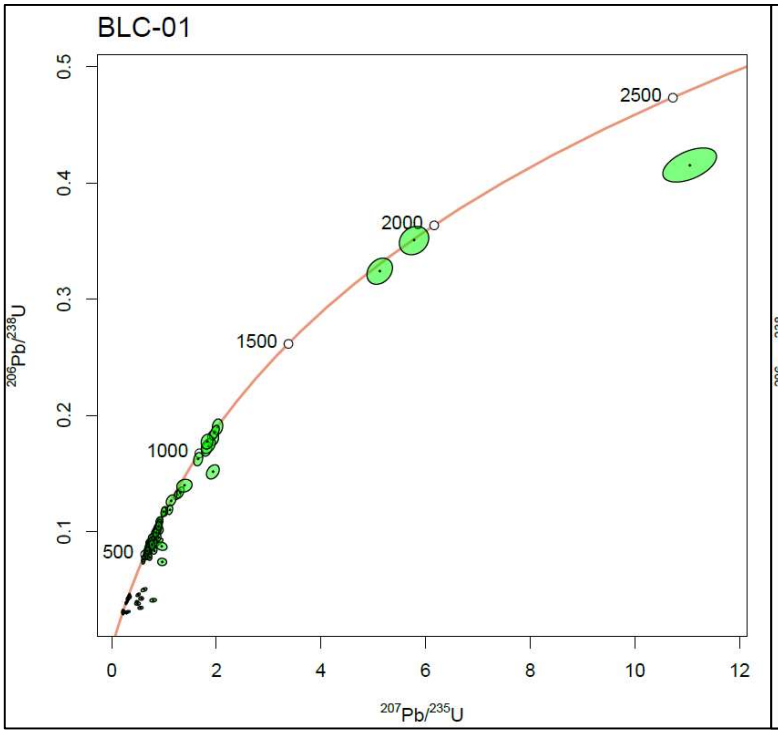

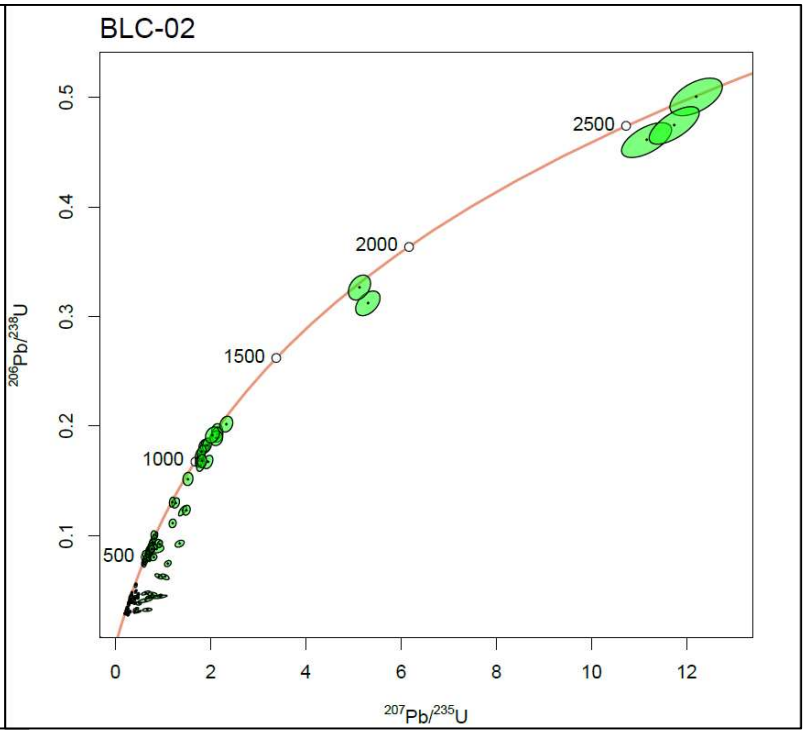

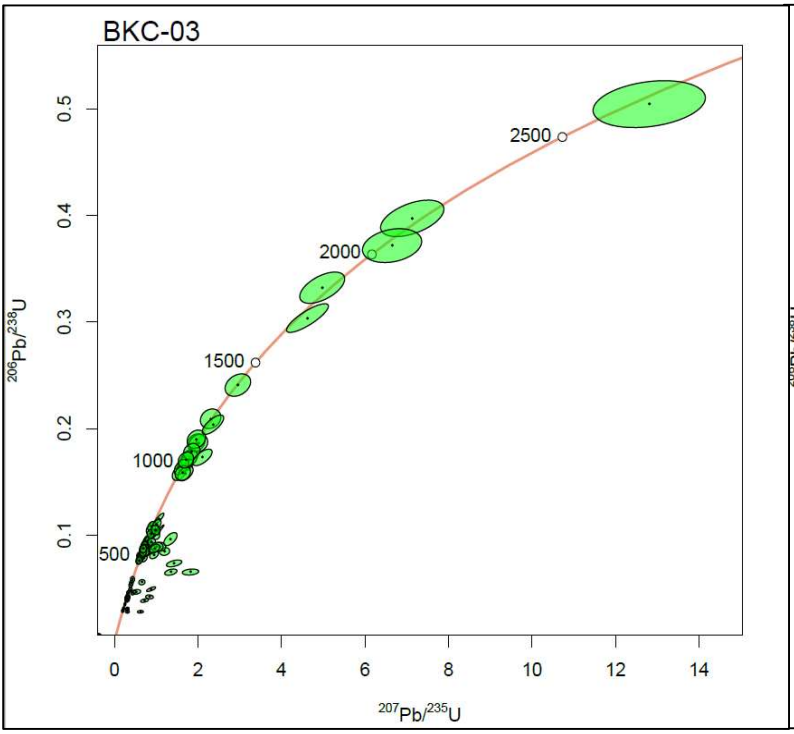

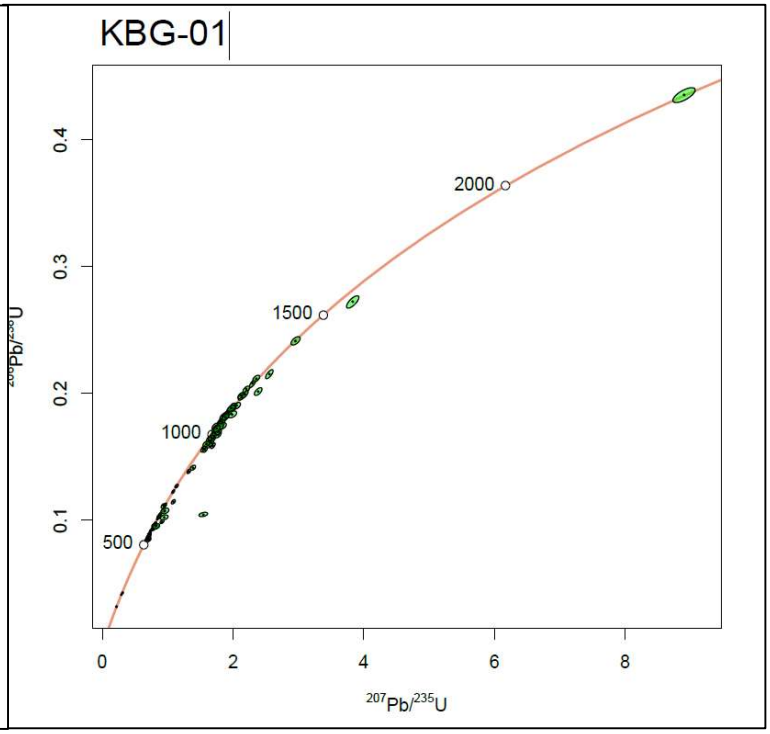

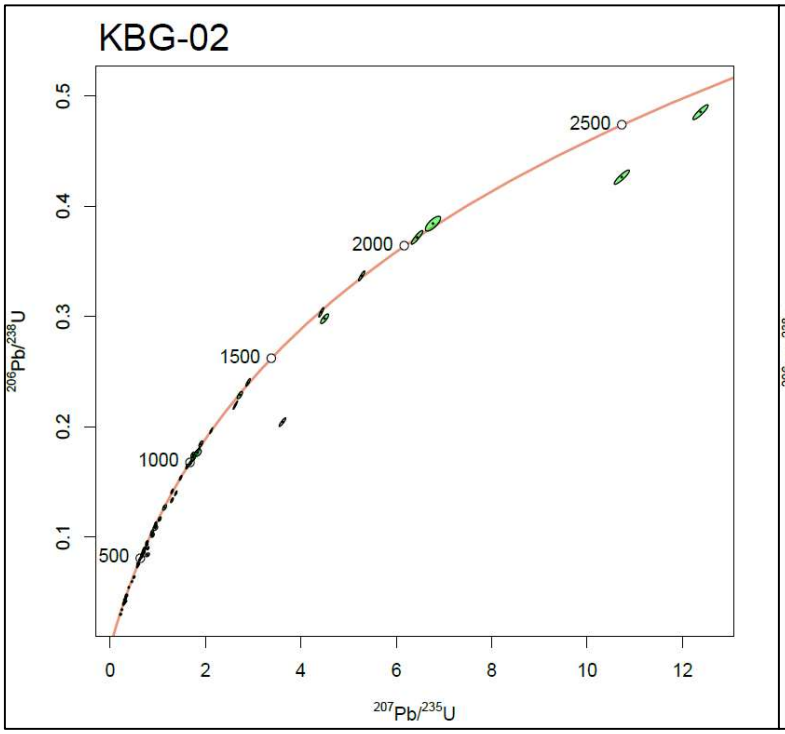
KBG-02
500
1000
1500
2000
2500
0.1
0.2
0.3
0.4
0.5
0
2
4
6
8
10
12
$^{206}Pb/^{238}U$
$^{207}Pb/^{235}U$

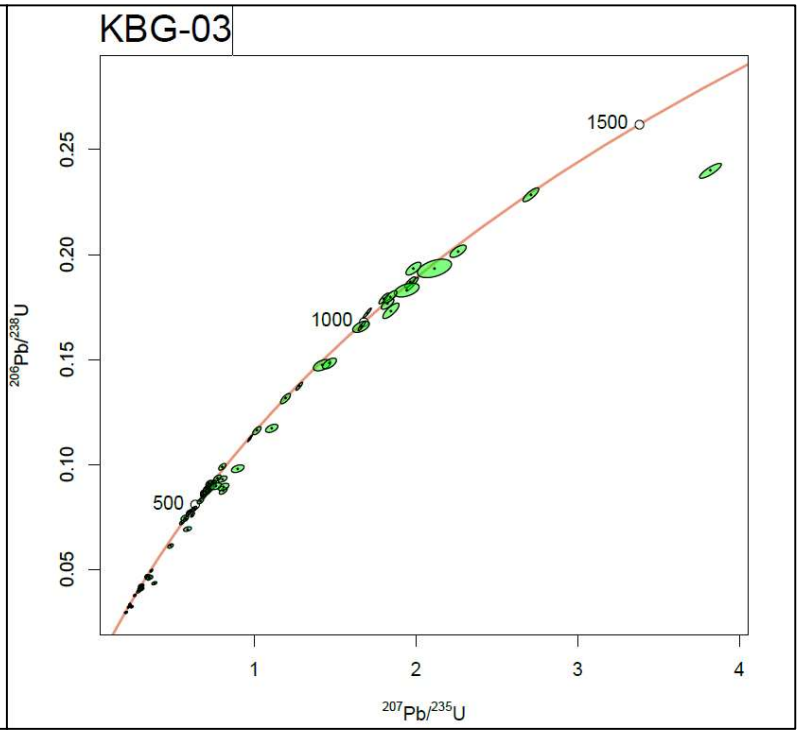
KBG-03
500
1000
1500
0.05
0.10
0.15
0.20
0.25
1
2
3
4
$^{206}Pb/^{238}U$
$^{207}Pb/^{235}U$

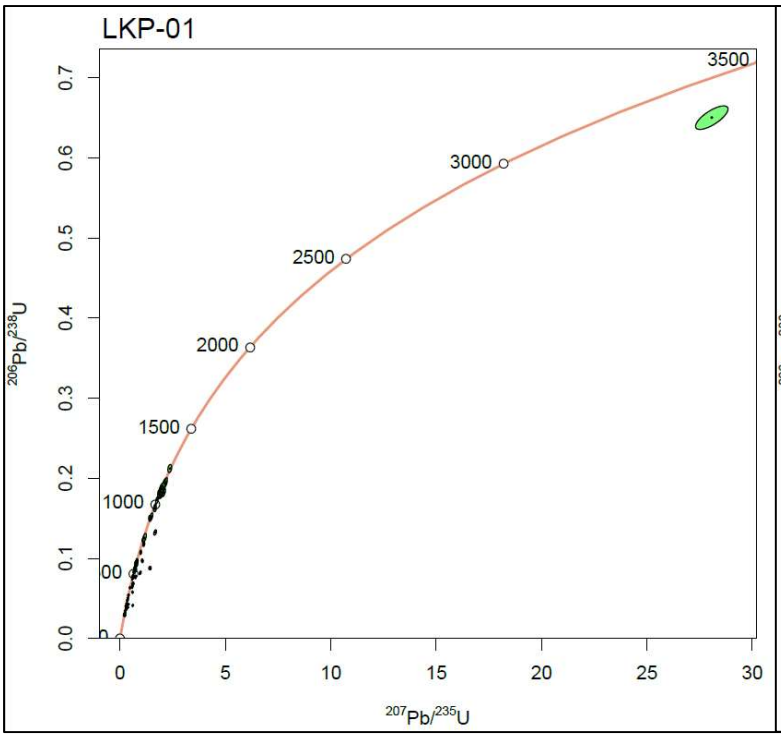
LKP-01
00
1000
1500
2000
2500
3000
3500
0.0
0.1
0.2
0.3
0.4
0.5
0.6
0.7
0
5
10
15
20
25
30
$^{206}Pb/^{238}U$
$^{207}Pb/^{235}U$

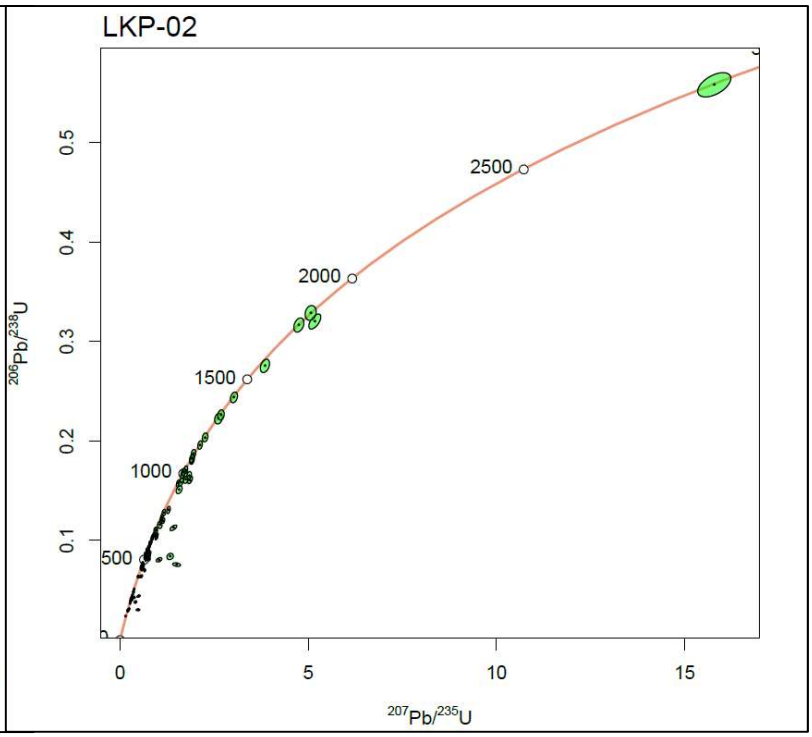
LKP-02
500
1000
1500
2000
2500
0.1
0.2
0.3
0.4
0.5
0
5
10
15
$^{206}Pb/^{238}U$
$^{207}Pb/^{235}U$

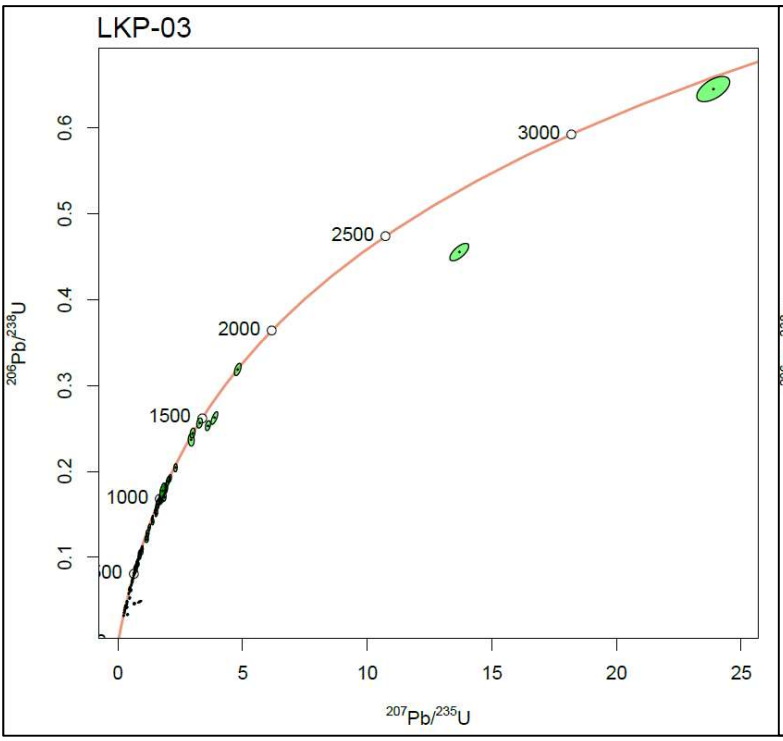
LKP-03
3000
2500
2000
1500
1000
500
0.1
0.2
0.3
0.4
0.5
0.6
0
5
10
15
20
25
$^{206}Pb/^{238}U$
$^{207}Pb/^{235}U$

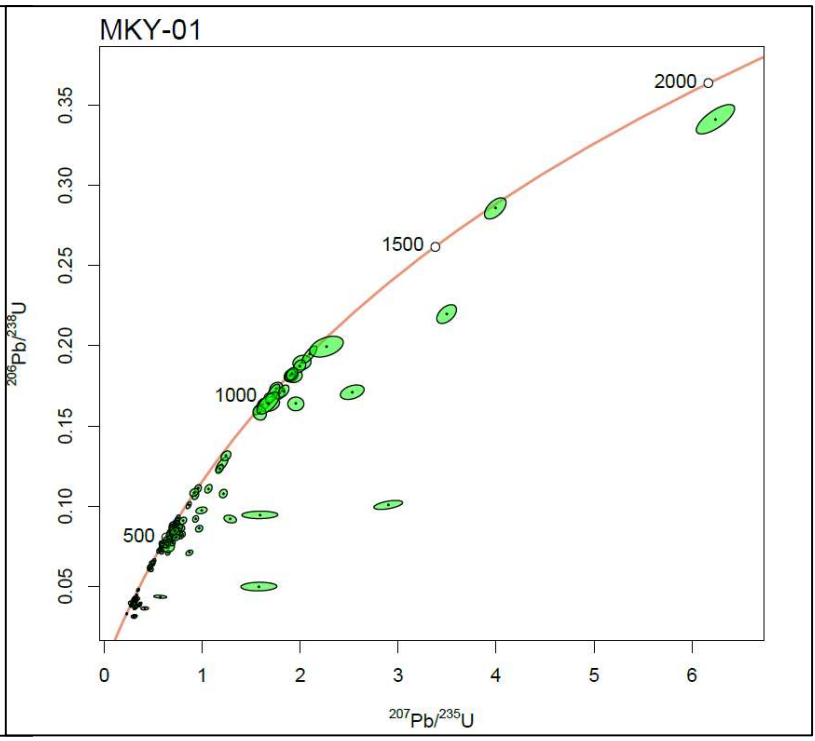
MKY-01
2000
1500
1000
500
0.05
0.10
0.15
0.20
0.25
0.30
0.35
0
1
2
3
4
5
6
$^{206}Pb/^{238}U$
$^{207}Pb/^{235}U$

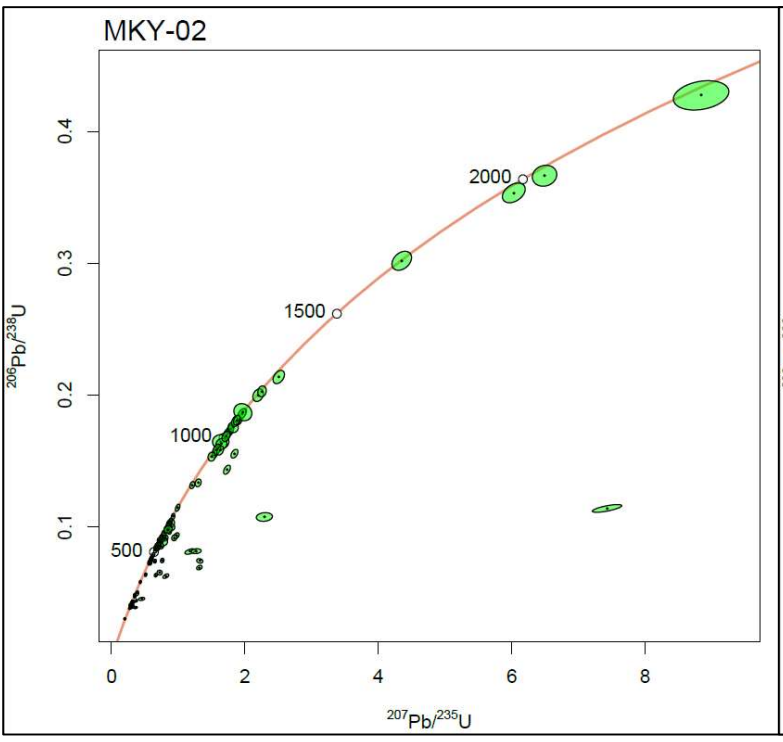
MKY-02
2000
1500
1000
500
0.1
0.2
0.3
0.4
0
2
4
6
8
$^{206}Pb/^{238}U$
$^{207}Pb/^{235}U$

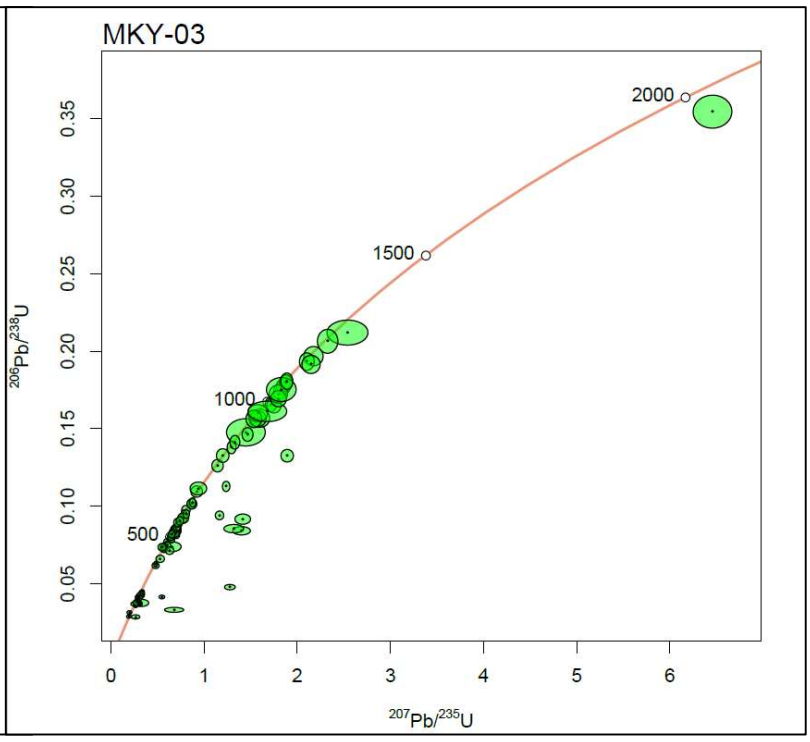
MKY-03
2000
1500
1000
500
0.05
0.10
0.15
0.20
0.25
0.30
0.35
0
1
2
3
4
5
6
$^{206}Pb/^{238}U$
$^{207}Pb/^{235}U$

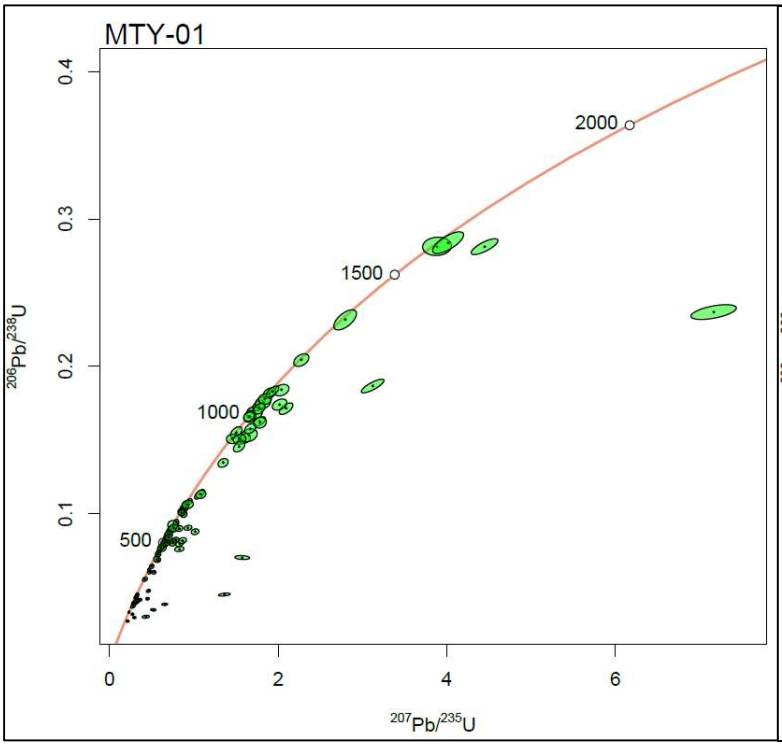
MTY-01
2000
1500
1000
500
0.4
0.3
0.2
0.1
0
2
4
6
$^{206}Pb/^{238}U$
$^{207}Pb/^{235}U$

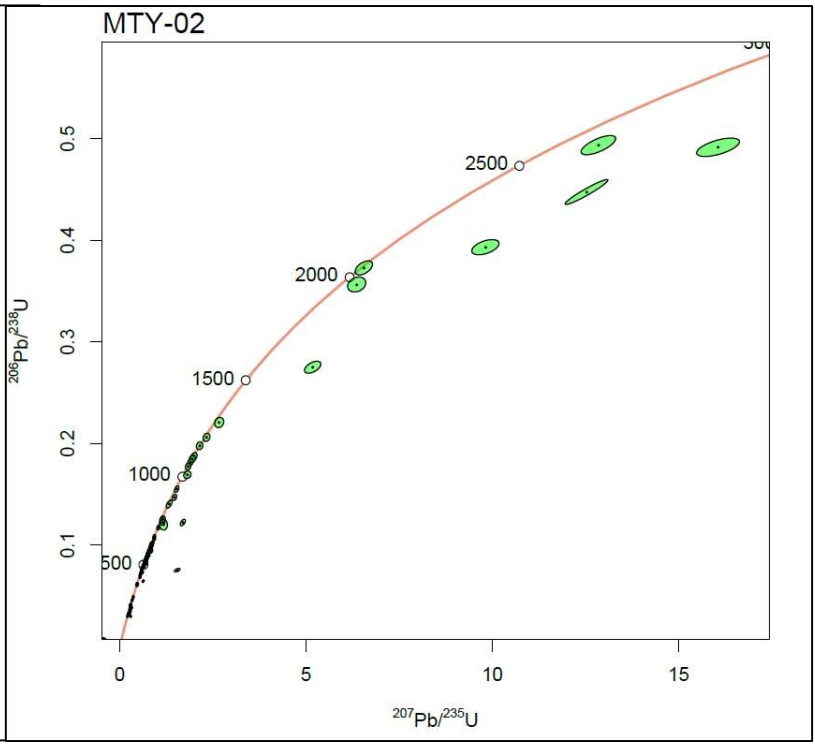
MTY-02
2500
2000
1500
1000
500
0.5
0.4
0.3
0.2
0.1
0
5
10
15
$^{206}Pb/^{238}U$
$^{207}Pb/^{235}U$

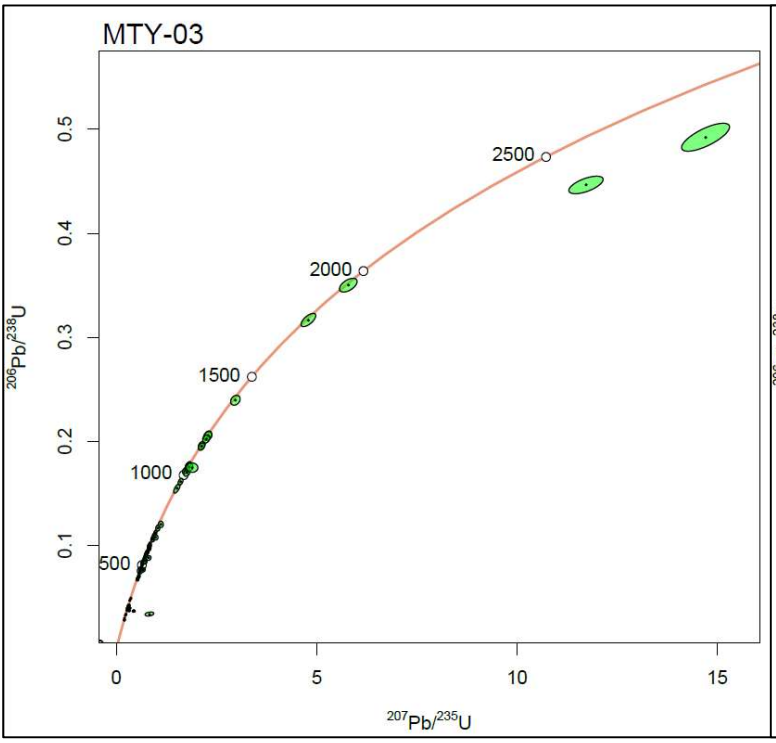
MTY-03
2500
2000
1500
1000
500
0.5
0.4
0.3
0.2
0.1
0
5
10
15
$^{206}Pb/^{238}U$
$^{207}Pb/^{235}U$

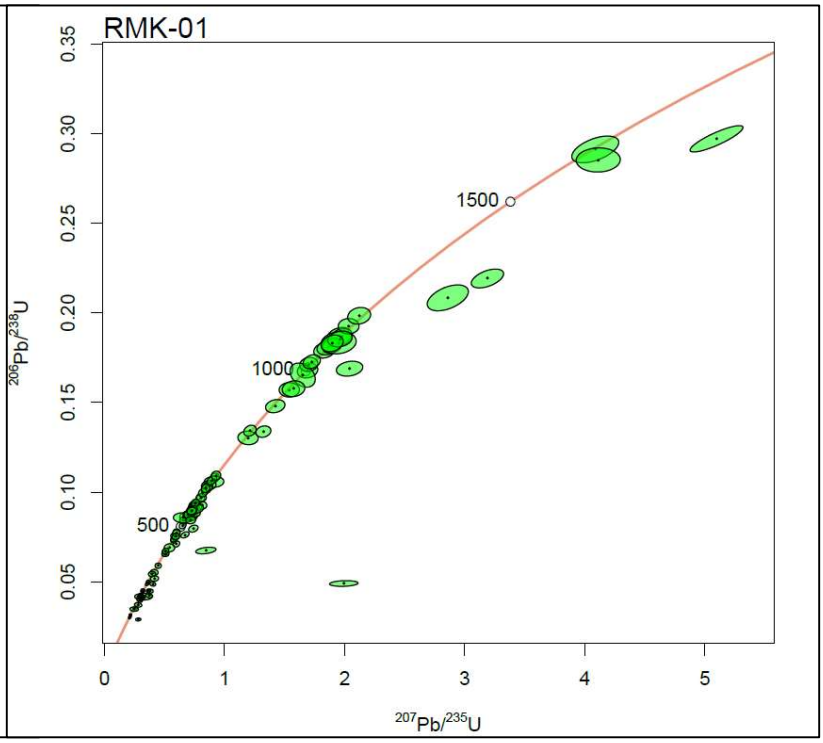
RMK-01
1500
1000
500
0.35
0.30
0.25
0.20
0.15
0.10
0.05
0
1
2
3
4
5
$^{206}Pb/^{238}U$
$^{207}Pb/^{235}U$

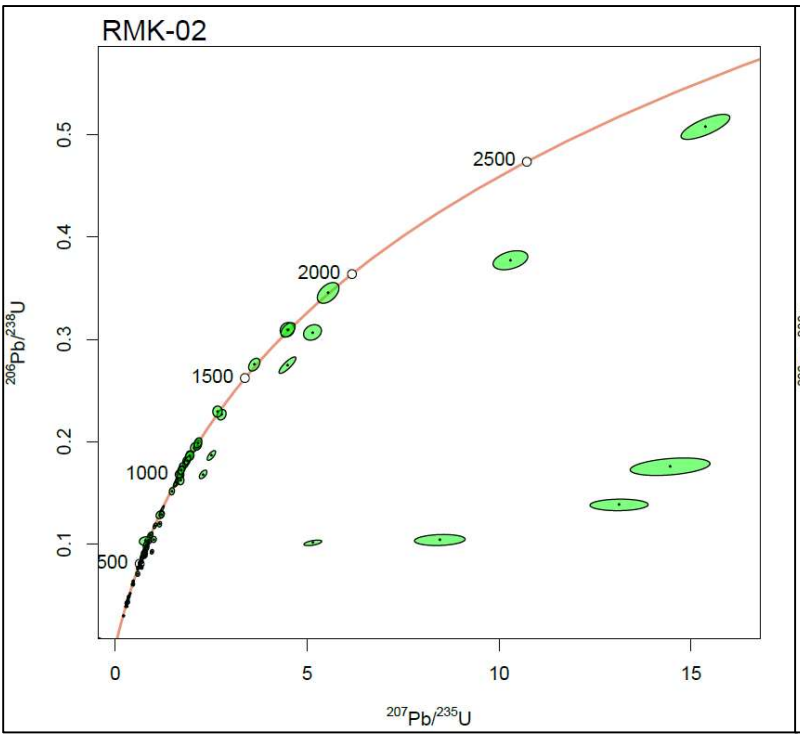
RMK-02
500
1000
1500
2000
2500
0.1
0.2
0.3
0.4
0.5
0
5
10
15
$^{206}Pb/^{238}U$
$^{207}Pb/^{235}U$

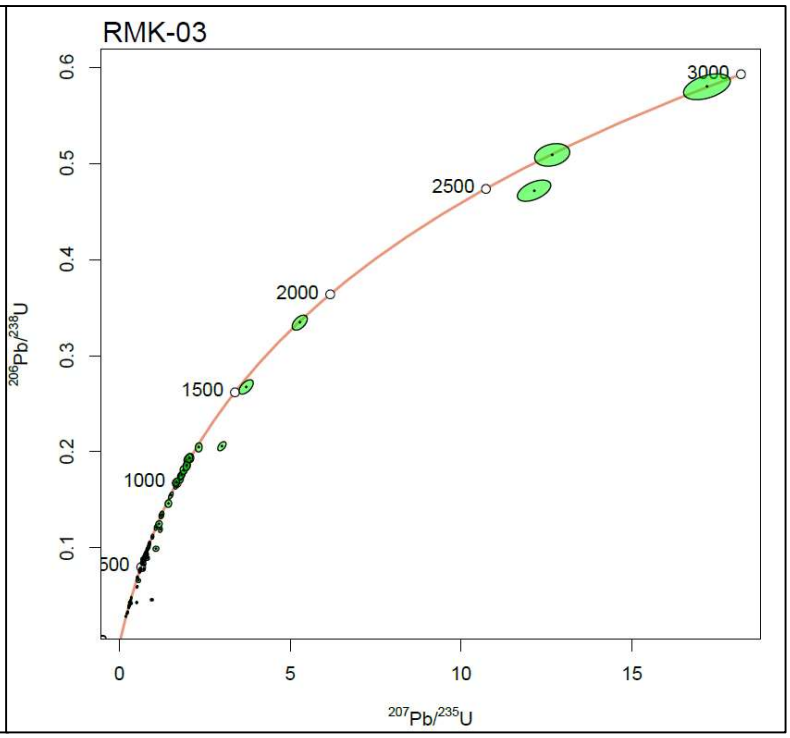
RMK-03
500
1000
1500
2000
2500
3000
0.1
0.2
0.3
0.4
0.5
0.6
0
5
10
15
$^{206}Pb/^{238}U$
$^{207}Pb/^{235}U$

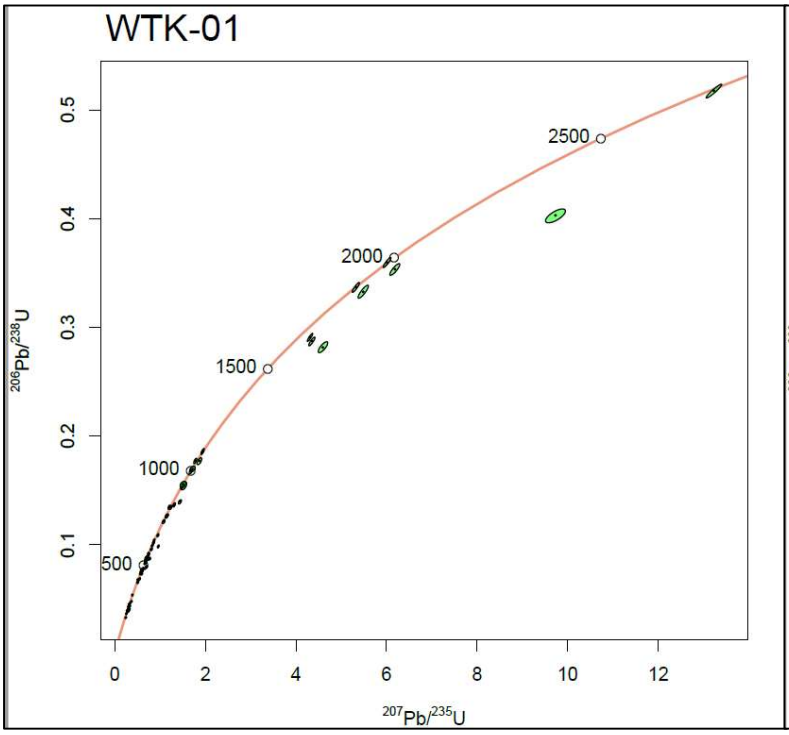
WTK-01
500
1000
1500
2000
2500
0.1
0.2
0.3
0.4
0.5
0
2
4
6
8
10
12
$^{206}Pb/^{238}U$
$^{207}Pb/^{235}U$

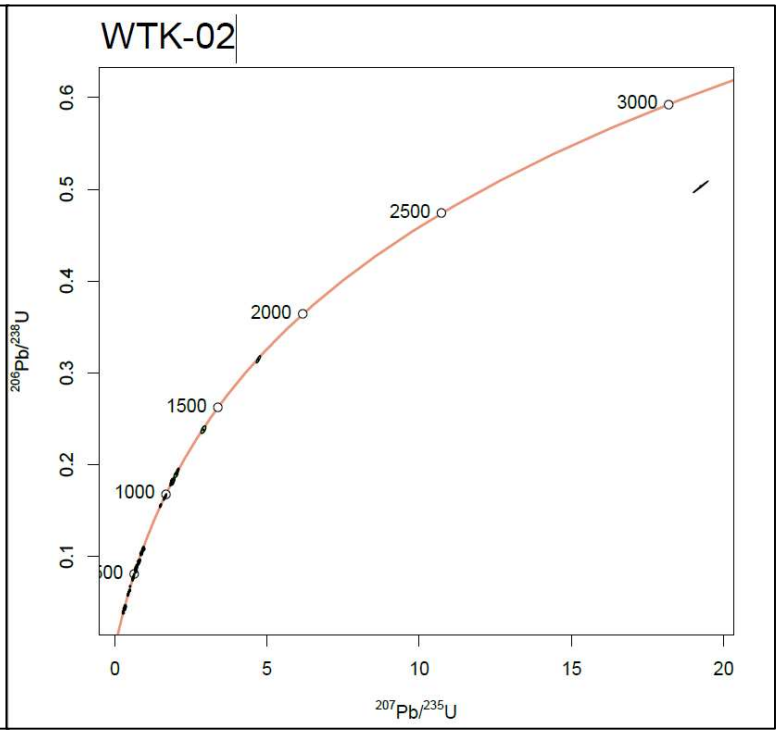
WTK-02
500
1000
1500
2000
2500
3000
0.1
0.2
0.3
0.4
0.5
0.6
0
5
10
15
20
$^{206}Pb/^{238}U$
$^{207}Pb/^{235}U$

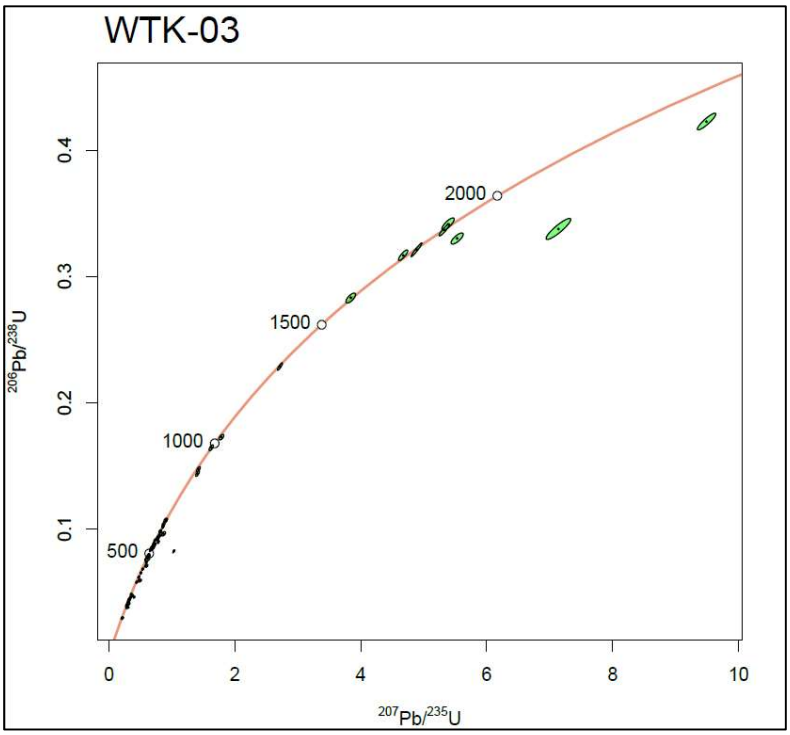
WTK-03
2000
1500
1000
500
0.1
0.2
0.3
0.4
0
2
4
6
8
10
$^{206}Pb/^{238}U$
$^{207}Pb/^{235}U$

Appendix 13: Concordant textural zones on a single zircon.

Sample-core/rim	Core texture date	2s	Rim texture date	2s
BLC-01-43/44	198.8	5.6	191.4	5.4
BLC-01-78/79	639.8	18	662.1	18
BLC-01-94/95	506.6	14	517.1	14
BLC-02-11/12	1155.0	30	504.0	30
BLC-02-91/92	2610.0	20.0	2612.0	14.0
BLC-03-5/6	576.4	20	527.6	18
BLC-03-30/31	2105.0	200	2100.3	190
BLC-03-33/34	497.8	17	998.3	33
KBG-01-20/21	936.7	12.3	598.7	6.5
KBG-01-34/35	979.5	11.1	657.0	8.1
KBG-01-40/41	1662.6	21.8	1397.7	28.1
KBG-01-45/46	979.5	11.6	523.2	5.9
KBG-01-60/61	630.4	5.8	526.4	6.5
KBG-01-75/76	1052.3	43.3	1011.2	30.6
KBG-01-85/86	1041.5	17.2	1044.2	27.2
KBG-02-31/32	245.8	3.6	254.6	3.5
KBG-02-37/38	843.0	10.2	623.8	9.4
KBG-02-80/81	1081.8	24.7	1110.8	67.8
KBG-03-4/5	554.7	6.5	562.0	6.5
KBG-03-17/18	561.7	5.9	534.4	6.5
KBG-03-43/44	607.8	7.6	546.0	7.1
KBG-03-52/53	708.1	9.2	538.0	7.1
KBG-03-56/57	475.4	6.0	480.5	5.6
LKP-01-36/37	258.8	5.1	264.4	5.5
LKP-01-55/56	510.4	9.7	522.2	9.7
MTY-02-1/2	241.2	4.2	232.2	3.6
MTY-02-24/25	291.5	4.7	380.2	6.4
RMK-01-56/57	986.0	30	622.3	12
RMK-01-60/61	554.0	11	521.2	9.4
RMK-01-82/83	194.8	3.6	199.7	3.7
RMK-01-108/107	1103.0	53	1115.0	59
RMK-02-6/7	1728.0	39	1713.0	39
RMK-03-8/9	261.0	5.1	257.8	5
RMK-03-11/12	1100.0	55	1051.0	56
RMK-03-40/41	1024.0	50	577.9	11
RMK-03-58/59	251.7	5.6	264.6	5.5
WTK-01-1/2	272.9	3.5	263.0	3.4
WTK-01-20/21	1871.2	14.0	1802.0	16.3
WTK-01-28/29	826.0	9.1	1008.7	25.6
WTK-01-59/60	539.0	6.5	526.8	5.5
WTK-01-70/71	473.7	6.0	469.2	7.2
WTK-01-103/104	923.9	16.7	483.4	5.8
WTK-02-40/41	286.8	3.6	287.5	3.9
WTK-02-42/43	461.9	5.1	265.0	3.2
WTK-02-83/84	637.8	7.0	641.5	6.4
WTK-02-91/92	634.5	7.0	669.1	7.5
WTK-03-4/5	981.7	10.5	493.4	5.9
WTK-03-7/8	293.1	3.9	271.2	2.8
WTK-03-19/20	1812.6	18.0	1748.1	16.3
WTK-03-35/36	1868.9	23.7	1872.0	15.8
WTK-03-38/39	654.1	6.4	656.5	6.4
WTK-03-65/66	280.7	3.8	287.9	3.6
WTK-03-84/85	541.5	6.5	474.6	7.8

Clarens Formation zircon datasets and supplementary materials are available on the following link:

https://figshare.com/s/6788ee86634ce85c9009